NASA CR- 165,390

A Reproduced Copy

OF

NASA CR- 165,390

NASA CR-165390
NOR-81-127

FINAL REPORT

EXPERIMENTAL INVESTIGATION OF TANGENTIAL BLOWING FOR CONTROL OF THE STRONG SHOCK BOUNDARY LAYER INTERACTION ON INLET RAMPS

Myles F. Schwendemann

Northrop Corporation

Hawthorne, California

Prepared for

Lewis Research Center

Under Contract NAS2-9281

June
1981

1 Report No	2 Government Accession No	3 Recipient's Catalog No
NASA CR-165390		

4 Title and Subtitle	5 Report Date
Experimental Investigation of Tangential Blowing for Control of the Strong Shock Boundary Layer Interaction on Inlet Ramps	June 1981
	6 Performing Organization Code
7 Author(s)	8 Performing Organization Report No
Myles F. Schwendemann	NOR-81-127
	10 Work Unit No
9 Performing Organization Name and Address	11 Contract or Grant No
Northrop Corporation Aircraft Division One Northrop Avenue Hawthorne, CA 90250	NAS2-9281
	13 Type of Report and Period Covered
12 Sponsoring Agency Name and Address	Contractor Report
National Aeronautics and Space Administration Washington, D. C. 20546	14 Sponsoring Agency Code

15 Supplementary Notes

Final Report, Project Manager, Bobby W. Sanders, Propulsion Systems Division, NASA Lewis Research Center, Cleveland, Ohio 44135

16 Abstract

A 0.165-scale isolated inlet model was tested in the NASA Lewis Research Center 8-ft by 6-ft Supersonic Wind Tunnel. Ramp boundary layer control was provided by tangential blowing from a row of holes in an aft-facing step set into the ramp surface. Testing was performed at Mach numbers from 1.36 to 1.96 using both cold and heated air in the blowing system. Stable inlet flow was achieved at all Mach numbers. Blowing hole geometry was found to be significant at 96%. Blowing air temperature was found to have only a small effect on system performance. High blowing levels were required at the most severe test conditions.

17 Key Words (Suggested by Author(s))	18 Distribution Statement
Air induction systems; Air inlets; Inlet flow; Supersonic inlets, Boundary layer control; Blowing	Unclassified - unlimited

19 Security Classif (of this report)	20 Security Classif (of this page)	21 No of Pages	22 Price*
Unclassified	Unclassified	188	

* For sale by the National Technical Information Service Springfield Virginia 22161

TABLE OF CONTENTS

SUMMARY

The use of tangential blowing from a row of holes in an aft facing step was found to provide good control of the ramp boundary layer normal shock interaction on a fixed geometry inlet over a wide range of inlet mass flow ratios. Ramp Mach numbers of 1.36 to 1.96 were investigated. Blowing geometry had a significant effect on system performance at the highest Mach number. The use of high temperature air in the blowing system had only a small effect on system performance. The required blowing rates were significantly high for the most severe test conditions.

INTRODUCTION

Fixed geometry, external compression inlets often provide the optimal air induction system for transonic, tactical fighter aircraft. The low ramp angles typically employed yield both a high ramp Mach number and a lengthy ramp in order to avoid ingestion of the shear layer produced by the intersection of the ramp shock with the terminal normal shock. As a result, the terminal shock of these simple two-shock inlets may be of considerable strength at maximum supersonic speed and the ramp boundary layer may be relatively thick. Some form of boundary layer control is required or the terminal shock-ramp boundary layer interaction will lead to high distortion levels at the compressor face as a result of boundary layer separation or inlet buzz.

Ramp boundary layer control is often accomplished by means of distributed suction on the ramp surface. This type of system has been investigated by Wong (ref. 1), among others, and is capable of controlling the boundary layer interaction for normal shock strengths to Mach 2.0 (2.0M). These suction or bleed systems, however, may pose difficult problems of vehicle integration, requiring a large internal volume within the ramp to remove the low energy flow bled from the boundary layer, division into cells to prevent recirculation, and suitable locations for dumping or disposing of the bleed flow. These requirements may add considerably to the structural weight and complexity of the inlet system, and may limit the choice of ramp angle, inlet geometry, and inlet location available to the designer.

Accordingly, an investigation of the use of tangential blowing for control of the normal shock-ramp boundary layer

interaction was begun, also by Wong (refs. 2 and 3). These early tests utilized a series of jets produced by a row of holes in an aft facing step to energize the ramp boundary layer ahead of the normal shock and were successful in inhibiting separation and maintaining stable inlet flow for normal shocks of up to 1.75M. Attempts to control stronger shocks of up to 2.0M were unsuccessful in spite of greatly increased blowing levels; and attempts to utilize high temperature air in the blowing system produced confusing results because the parameters successfully used to correlate the performance of systems employing unheated air failed to predict the required blowing levels.

The failure of the blowing systems to control the 2.0M shock was tentatively attributed to expansion of the high pressure, blowing jet plume into the ramp flow creating an oblique shock-boundary layer interaction ahead of the blowing system, see figure 1. The effect of increased step height, allowing plume expansion without interference with the oncoming ramp flow, is one focus of this investigation.

The second objective of the current investigation is the effect of blowing air temperature on system performance. The bulk of published data for all types of blowing systems involve the use of blowing air having the same total temperature as that of the freestream flow, whereas air obtained from compressor bleed will be of higher temperature. The blowing parameter used in the investigation by Wong (refs. 2 and 3) was that suggested by Kelly (ref. 4), and is detailed in figure 2. This parameter CMMCRD which includes the difference between the blowing velocity and ramp velocity will be referred to as "the relative blowing coefficient" in this report. Note that the velocity difference is a much stronger function of temperature than the blowing velocity for typical ramp conditions and that if this parameter successfully correlates blowing performance

regardless of blowing air temperature, the use of high temperature blowing air allows greatly reduced blowing flows, relative to cold flow, while maintaining effective control of the shock boundary layer interaction.

The effect of blowing geometry on the effectiveness of hot air blowing is explored in this report and an alternate blowing parameter CMMCD is examined.

APPARATUS AND PROCEDURE

Model

Ramp blowing systems were incorporated into a simple, 0.165 scale isolated inlet model to allow testing under controlled conditions reasonably free of configuration peculiar effects. Blowing configurations consisted of a line of uniformly spaced holes exiting from an aft facing step recessed into a flat horizontal ramp. The rectangular inlet had a height to width ratio of 0.64 and was followed by a straight centerline diffuser and a metering section. The general arrangement of the model can be seen in the photographs of figures 3, 4, and 5.

The ramp, cowl, and blowing slot are shown in figures 6 and 7. The ramp surface was parallel to the duct centerline, and the ramp width was 26 percent greater than the cowl highlight. The upper corners of the inlet cowl had an internal radius of 0.635 centimeters (0.25 inches). The lower corners were square and transitioned to the 0.635 centimeter radius just forward of the throat instrumentation plane by means of a linear fillet. Limited testing was performed using an alternate shortened cowl which moved the highlight plane 2.54 centimeters (1.0 inches) aft of the baseline position, increasing the distance between the fixed blowing station and the cowl.

The blowing configurations and configuration codes are shown in figure 8. Configurations 21, 22, and 23 had the same nominal total exit area but had varied hole spacing to hole diameter ratios. Configuration 24 had the same spacing ratio as configuration 21 but was larger, having an exit area 77 percent greater. All configurations had the same step height to nozzle diameter ratio but had differing base area to exit area ratios. Configuration 24 when tested with the shortened cowl is identified as configuration 26.

The blowing jets exited from an aft facing step located 0.667 throat heights in front of the baseline cowl position. The blowing extended over 86.7 percent of the ramp width and exceeded the capture width by 9 percent. The blowing nozzles were aligned with the surface aft of the blowing step which slanted upward to merge with the ramp surface just forward of the baseline cowl position. The blowing holes were manufactured by an EDM process and had a nominal length to diameter ratio of 2:1.

The cowl was followed by a "throat section" of constant cross-section for a length of 1.5 throat heights. This section was 7.62 centimeters high (3.00 inches) by 11.811 centimeters (4.65 inches) wide with a 0.635 centimeter (0.25 inches) corner radius.

The "throat section"was followed by a straight line diffuser transitioning to a circular section, 13.72 centimeters (5.40 inches) in diameter, over a distance of 58.42 centimeters (23.00 inches), 2.5 centimeters (0.988 inches) in front of the compressor face instrumentation plane. At the entrance, the diffuser was merged to the constant "throat" section by a 3.81 centimeter (1.5 inch) radius on the upper and lower surfaces. The diffuser length to outlet diameter ratio was 4.26 and its area ratio was 1.65.

The circular compressor face plane, 13.72 centimeters in diameter (5.40 inches), was followed by a short transition to a metering and control tube 14.12 centimeters (5.56 inches) in diameter with a length of 27.91 centimeters (10.99 inches). A flared skirt and conical plug were used to vary the duct mass flow.

The overall duct area distribution is shown in figure 9.

Instrumentation

The model was equipped with fifteen ramp static ports. Eighty-two total pressure measurements were obtained from three rakes mounted in the inlet throat and from a forty probe compressor face array. Compressor face instrumentation also included eight dynamic pressure transducers and eleven thermocouples.

The ramp static pressure instrumentation, shown in figure 10, consisted of three symmetrical lines of ports on the ramp surface and a single port offset to the far left. A single tap on the ramp centerline was placed immediately aft of the blowing station.

The throat instrumentation plane contained three full height total pressure rakes and three static ports on both the upper and lower surface, see figure 11. The rake consisted of 0.1016 centimeter (.040 inch) tubing reinforced with a .0254 centimeter (0.01 inch) sheathing about the rake to strengthen the assembly. The total thickness of the rake structure was approximately 0.152 centimeters (0.060 inch). The probes extended approximately 0.254 centimeters (0.1 inch) forward of the support.

Additional static ports were located at the entrance to the diffuser 11.43 centimeters (4.5 inches) aft of the baseline highlight, and in the diffuser 19.05 centimeters (7.5 inches) and 26.67 centimeters (10.5 inches) aft of the highlight. The locations of these ports are shown in figure 12.

The compressor face array consisted of forty total pressures, eight dynamic total pressures, and eleven thermocouples, see figure 13. The dynamic probes were of the Hoflinger type and were used to obtain RMS pressure fluctuation levels. These data were filtered above 650 Hz. The chromel-alumel thermocouples were unshielded, twisted junctions.

Main duct mass flow was controlled and measured by means of a cylindrical metering tube terminating in a flared skirt. A conical plug was moved into and out of the flared skirt to vary duct flow. The metering exit was choked during this test. The duct mass flow was obtained from tube static pressure, plug position, and a calibration obtained for an earlier system of the same design, reported in reference 5.

Blowing mass flow was monitored by means of a choked venturi-type flowmeter. Conditions in the ramp blowing plenum were obtained from a single pressure transducer and a single chromel-alumel thermocouple.

Total and static pressures on the model were monitored by means of scanivalves.

Test Facility

The model was tested in the Lewis Research Center 8-Ft. by 6-Ft. Supersonic Wind Tunnel described in reference 6. The tunnel was operated in the Propulsion Cycle mode. Typical run conditions for this test are given in table I.

The model was sting-mounted on the tunnel centerline. A limited pitch capability was available to maintain a zero ramp angle and a yaw capability of five degrees was available. When yawed, the inlet cowl moved off the tunnel centerline.

Blowing air was supplied to the model using the Variable Pressure Air System. The maximum temperature available from the heater was 644 deg K (1160 deg R). The air was supplied to the model by means of insulated lines yielding a maximum temperature of 593 deg K (1067 deg R) at the flowmeter located alongside the main duct.

Data were recorded using the Lewis Research Center CADDE II data system.

Test Procedure

A standard test sequence was followed in acquiring the data:

1) Tunnel and blowing conditions were established with the inlet operating at critical or near critical mass-flow rates.

2) Inlet flow was reduced using a fixed schedule, moving the cowl shock wave forward until "buzz" or unstable flow was encountered.

3) Stable flow was re-established by increasing inlet flow.

4) A final data point was taken at a near "buzz" condition.

Occasionally, intermittent "buzz" occurred during the final data scan. When this was detected, the point was repeated at a slightly lower mass flow.

Buzz was determined by observation of a dual-oscilloscope display of two of the eight dynamic transducers in the compressor face array. At the higher test Mach numbers, the onset of inlet instability was clearly defined. However, at the lowest test Mach number 1.36 M, only a gradual increase in the fluctuating level of the unsteady pressure was apparent and a definite "buzz point" was not established.

Corrections to Data

Discharge coefficients for the blowing holes were found to vary with temperature when the tunnel was in operation but not under static, wind-off test conditions. It was concluded that this behavior was most probably due to errors in the plenum temperature measurement. A correction has been applied to the plenum temperature data used in this report. Details of this correction may be found in Appendix A.

RESULTS AND DISCUSSION

The blowing boundary layer control system was capable of providing stable inlet flow at all test Mach numbers. A more detailed discussion of the blowing system characteristics is given below. The basic inlet performance data from which these results were derived are presented in figures 47 through 54.

Test results are presented in terms of throat rake pitot pressure distributions, ramp surface pressure distributions, inlet stability boundaries, and inlet performance parameters. The ramp surface pressure distributions show the static to freestream total pressure ratios along the ramp centerline and vertical dashed lines topped by symbols indicating the predicted normal shock location estimated by means of reference 7 with modification for three-dimensional effects. The inlet stability boundaries indicate the minimum mass flow ratio at which stable operation was achieved as well as regions of operation where separated flow was observed at the throat instrumentation plane. Test results are presented in terms of the external mass flow ratio MFRX, an estimate of the amount of oncoming freestream flow captured by the inlet. This parameter is further defined in Appendix B. Solid symbols indicate data taken in buzz.

Comparison of Blowing Parameters

Earlier tests of ramp blowing systems reported in references 2 and 3 used the relative blowing coefficient CMMCRD, defined in figure 2, as a blowing parameter. This parameter had proved useful in correlating the results of cold flow blowing tests but was not successful in predicting the results for tests using hot flow. A much higher value of relative blowing coefficient was required to achieve similar results when hot air rather than cold air was used in the blowing

system, giving the impression that hot air blowing was less effective than cold air blowing. The comparisons of hot and cold air blowing shown in figures 14, 15, 16 and 17 agree with these earlier results, but clearly indicate that the absolute blowing coefficient CMMCD, also defined in figure 2, provides much better correlation of boundary layer control effects on inlet performance than does the relative blowing coefficient. The inlet performance is similar, but not identical, at approximately equal values of absolute blowing coefficient, but not at equal values of relative blowing coefficient for both hot and cold air blowing. This conclusion is also supported by the calculations presented in Appendix D. Accordingly, the remainder of the report will use the absolute blowing coefficient as the primary correlating parameter.

Blowing System Performance At 1.96M

At 1.96M, a significant configuration effect was observed. As shown in figure 18, configurations 23 and 24 were capable of providing stable, buzz-free inlet operation over a significantly larger range of inlet mass flows than configuration 21. All configurations tested at this Mach number, however, showed separated flow at the throat rake instrumentation plane over much of the range of operation. Basic inlet performance data are presented in figure 47 for Mach 1.96.

The more limited inlet mass flow range for configuration 21 is clearly evident in the comparison of inlet performance for the three configurations, shown in figure 19. The behavior of configurations 21 and 24 at this Mach number was anticipated as previous testing, reported in reference 3, had led to the blowing plume expansion hypothesis illustrated in figure 1. The geometric data of figure 8 show that while the blowing step height to blowing hole diameter ratio is approximately the same for all configurations, configuration 24 has a larger exit area. The larger exit area allows configuration 24 to operate

at lower pressure ratios than configuration 21 while maintaining the same blowing coefficient. Thus, with increasing blowing coefficient, the plume of configuration 21 will expand above the ramp surface while that of configuration 24 remains below the step height until a much higher level is reached. Therefore, configuration 21 should produce ramp flow interference and configuration 24 should not. However, the ramp pressures for configuration 21 shown in figure 20, do not show the expected upstream influence of the blowing jet even at the highest blowing level allowed by the test setup, and indicate little apparent effect of the blowing jet on surface pressures for the critical flow condition when the normal shock pressure rise was not present on the external ramp surface. The lack of evidence of upstream influence of the blowing jet, as well as the apparent small influence of the blowing jet on the external flow, tends to contradict the underexpanded plume explanation for the improved performance of configuration 24. Even when the blowing rate for configuration 24 was increased to nearly twice that required for control over the full range of mass flow ratios, making its blowing jet plume expansion tendencies similar to that of configuration 21, no degradation of flow resulted, although a complex flow pattern was produced at lower mass flow ratios, see figure 21. Configuration 23, which had the same exit area and blowing step height ratio as configuration 21, performed over the same inlet mass flow ratio range as configuration 24. If the underexpanded plume hypothesis were valid, configuration 23 should have performed more like configuration 21 than configuration 24. The fact that the opposite occurred further contradicts this explanation of the blowing system performance. Both successful configurations had a larger blowing hole size, a larger blowing step, and a larger blowing step base-area-to-fully-expanded-plume-area ratio than the more limited configuration 21.

Configuration 21 is unique in the test results at this Mach number in that significant asymmetries were present in the ramp flow, see figure 22. For all other conditions and configurations, near two-dimensional or laterally symmetric flow was present. Although the ramp pressure distribution for configuration 24 which operated over a full range of mass flow ratios was quite similar to that of configuration 21, see figures 20 and 23, the flow showed little asymmetry and became attached as the mass flow was lowered below the level at which configuration 21 failed. The degree of separation at the throat station was also apparently decreasing at the time of flow breakdown for configuration 21. The behavior of configuration 23 was similar to that of configuration 24 as shown by a comparison of the ramp pressure levels of figures 23 and 24. Clearly lacking for all three configurations is the presence of a distinct normal shock pressure rise. Instead a plateau pressure appeared which varied little with mass flow ratio or shock position. The pressure rise was less than the nominal inviscid normal shock value of 0.59 and more nearly approximated a strong oblique shock value, suggesting the establishment of a separated subsonic flow region extending from the inlet face to the blowing station. With the exception of the flow asymmetry for configuration 21, the ramp pressures of all three configurations behaved similarly prior to flow breakdown.

At higher blowing coefficients, figure 19, the turbulence and distortion parameters for the three configurations were also similar prior to the onset of flow instability although configurations 23 and 24 did show better pressure recovery. A comparison of the three configurations at a lower blowing level, figure 25, where all operated over the same mass flow range, again shows similar trends in distortion and turbulence. Configuration 24 shows a clear advantage in pressure recovery followed by configurations 23 and 21. The recovery for configuration 21 was exaggerated by a 0.25 degree ramp angle increase due to model position variation.

The similar behavior of all three configurations prior to breakdown suggests that the difference in performance may be due to slightly better mixing characteristics of the blowing geometries of configurations 23 and 24 allowing the flow to become attached before the shock location proceeded to the blowing station. This may be due to the greater base-area-to fully-expanded-jet-area ratios of configurations 23 and 24, or to their common large blowing hole size.

Blowing System Performance At 1.76M

At 1.76M, all four configurations were capable of providing stable inlet operation over a full range of mass flow ratios, corresponding to normal shock locations from the cowl to the blowing station. Throat rake separation was limited to the lowest blowing coefficients tested and a well defined normal shock pressure rise was present in the ramp surface pressures. Basic inlet performance data are presented in figures 48 and 49 for 1.76M.

As shown in figure 26, all configurations were capable of providing stable inlet operation over approximately the same range of mass flow ratios, configuration 23 requiring a larger blowing coefficient than the other configurations to achieve the same performance. A more detailed comparison is shown in figure 27, the performance of the configurations being similar at higher blowing coefficients, but differing at lower blowing coefficients. At the higher blowing coefficients the ramp pressure distributions showed a distinct normal shock pressure rise at this Mach number, see figure 28. As the blowing coefficient was lowered into the levels allowing only control over a partial range of mass flow ratios the ramp pressure rise, also shown in figure 28, became less distinct and more smeared. Occasionally even at high blowing levels the ramp flow would lapse from a sharp distinct normal shock pressure rise to a smeared pressure rise. This was the cause

of the "blip" in rms pressure at a mass flow ratio of 0.67 shown in figure 27. As seen in figure 29, this blip was reflected both in the ramp pressure levels and at the throat rake as a loss of the blowing flow excess, see data at MFRX of 0.67. Similar behavior was exhibited by all the configurations tested for absolute blowing coefficients of 20 to 30, sometimes at the higher end of this blowing range and at other times only at the lower end. This behavior was more common for configuration 22, however.

At elevated blowing temperatures, the data of figure 30 indicate an effect on the system performance requiring a blowing level increase of approximately five to ten percent above cold flow levels to maintain the same stability range. Note that the minimum blowing levels for hot flow, figure 30, were above those at which throat rake separation was noted for cold flow, figure 26. The relative performance of the configurations was approximately the same as for cold flow except for configuration 22 which suffered degraded performance.

Blowing System Performance At 1.56M

At 1.56M, all configurations were capable of providing control over the same full range of mass flow ratios, corresponding to normal shock locations from the inlet highlight to the blowing station. A distinct normal shock pressure rise was indicated by the ramp surface pressures at all blowing coefficients tested but the pressure rise was somewhat more gradual at the lowest blowing levels. Throat rake pressures showed separation only at the lowest blowing levels. Basic inlet performance data are presented in figures 50 and 51.

A comparison of the inlet stability boundaries for cold and hot blowing flow, shown in figures 31 and 32 respectively, indicates that slightly higher blowing levels were required when heated air was used in the blowing system than when cold

air was used. The lack of an indicated separated flow regime for the hot data is not significant as the minimum levels tested were slightly higher than the minimum cold flow levels at which separation occurred.

Qualitative differences again occurred among the configurations with configuration 21 showing the best performance and configuration 24 the poorest. Reference to the geometric data of figure 8 indicates that the configurations having the smaller blowing holes and blowing step height were favored. The differences between the configurations are further illustrated in figure 33. Although the blowing coefficients for the four configurations are only approximately equal, a definite difference between the configurations is apparent. Additionally, both configurations 23 and 24 showed a small degree of separation at the throat rakes while configurations 21 and 22 did not.

Blowing System Performance At 1.36M

At 1.36M, it is difficult to draw sharp distinctions among the various configurations due to the difficulties in defining the onset of inlet instability that were discussed in the section on test procedure. These difficulties may have been due in part to the decreased level of the "buzz" pressure fluctuations relative to other inlet turbulence but were also due to a difference in behavior of the inlet system at this lower Mach number. At the higher Mach numbers, any indication of the ramp pressure rise ahead of the blowing station was accompanied by the onset of inlet instability and massive throat separation. However, as shown in figure 34, at this Mach number the pressure rise passed upstream of the blowing station without indication of separation at the throat station. This characteristic may have made the buzz point less distinct than at higher Mach numbers. The data presented in figure 52 do tend to indicate that the relative performance of the

various configurations may be similar to that at 1.56M, the smaller scale blowing configurations having the best performance. Note also that the maximum inlet flow rates at this Mach number were limited by throat rake blockage, and that the maximum mass flow ratio was less than the critical level, an effect also seen in figure 52.

Inlet Performance With The Short Cowl

Configuration 24 was tested with a short cowl as configuration 26. With the cowl relocated to X/Hth of -0.3333, the ramp was effectively lengthened and the blowing station moved away from the cowl allowing a lower mass flow ratio prior to the shock reaching the blowing station. Stable flow was achieved over a very wide range of mass flow ratios. At the highest blowing rate tested at 1.76M, stable flow persisted at the lowest mass flow ratio allowed by the plug limits. However, at the higher mass flow ratios, the oscilloscope output of the compressor face dynamic probes showed an unsteady pressure component having the "buzz" frequency but of a lower magnitude than normally associated with unstable operation. This component vanished as the mass flow ratio was lowered. This trend is visible in the rms levels of the inlet performance data in figures 53 and 54. The throat rake data indicate separated flow for these high mass flow conditions, and attached flow at lower mass flow ratios. The inlet stability curves of figures 35 and 36 show these regions of throat separation as well as a comparison with the stability limits for configuration 24. The short cowl configuration shows a lower limiting mass flow ratio than the standard cowl even for those blowing levels where the inlet mass flow range for the standard cowl was not limited by the shock passing the blowing station. However, at these lower blowing levels the onset of the smeared pressure rise often preceded the estimated shock location, and a comparison of ramp pressures for these two configurations indicates that the flow breakdown occurred for

similar ramp pressure rise distributions, see figures 37 and 38; the blowing performance at minimum mass flow ratio was therefore dependent on both shock standoff distance from the cowl, and shock distance from the blowing station.

Effect of Blowing Air Temperature

The use of heated air in the blowing system was found to have little effect on inlet performance when compared at equal values of absolute blowing coefficient, CMMCD. As shown in figures 14 through 17, similar inlet performance occurred for the hot and cold air tests at similar values of CMMCD. Note that when the results are compared using the relative blowing coefficient of references 2 and 3, CMMCRD, strong effects seem apparent. The majority of data show even better correlation than these few examples; more typical data are shown in figures 39 and 40.

The most significant temperature effects were noted for configuration 22 at 1.76M. The inlet operating range showed a definite degradation due to the use of high temperature air at the lower blowing levels, see figures 41 and 42, but the performance parameters were similar prior to flow breakdown. This temperature effect is also reflected in the ramp pressure distributions shown in figure 43, where the pressure rise is less distinct for the hot flow case. At 1.56M, the use of heated air had a smaller effect on configuration 22, and inlet performance was similar to that of the other configurations.

Comparison of the stability data of figures 26, 30, 31, and 32 also shows that the performance varied little with blowing air temperature. These curves do indicate that a slightly higher value of blowing coefficient was required to achieve the same stability range when hot air rather than cold air was used. The difference is small, about 5 percent with the exception of configuration 22, and may lie within the accuracy of the test technique.

Effect of Sideslip

Limited data were taken for all configurations at five degrees of sideslip at 1.76M and 1.56M. This amount of sideslip typically had little effect on inlet performance. An example of these data is shown in figure 44. Definite asymmetries were produced on the ramp surface and at the throat plane as shown in figure 45.

An exception to this general effect occurred for configuration 21. As shown in figure 46, the mass flow range over which stable flow was achieved was significantly increased when sideslip was present.

Required Blowing Rates

The blowing flow needed to maintain stable inlet flow for normal shock positions from the cowl to the blowing station varied with Mach number. The necessary blowing flow increased with Mach number and with shock standoff distance from the cowl. Under the most severe conditions the blowing flow became a significant portion of the total inlet flow. For cold flow and the standard cowl, the required blowing mass flow increased from 2.2 percent of capture flow at 1.56M to 5.5 percent at 1.96M. The use of heated air in the blowing system reduced the required blowing flow in inverse proportion to the square root of the blowing temperature ratio. At a temperature ratio (TRC) of 1.6, required blowing mass flows were approximately 79 percent of cold flow levels.

Repeatability

In general repeatability of the data was excellent. However, several events occurred within the test matrix which indicate that the behavior of the inlet system may be locally sensitive under certain operating conditions. The occurrence

of intermediate ramp flow separation for configuration 22 at 1.76M has been discussed previously. This resulted in the "blip" in rms pressure shown in figure 27. A similar event is shown in figure 16 for configuration 23 at a lower blowing level. These spikes in rms levels may well indicate a tendency towards flow breakdown at intermediate normal shock positions, and may be related to the effects of temperature on configuration 22 at 1.76M, either through actual flow breakdown or possibly through interpretation of the rms spike as incipient "buzz" during the test. Unusual results also occurred for configuration 21 at lower blowing coefficients. As shown in figure 50, a blowing coefficient reduction of 9.7 to 9.0 resulted in an increased mass flow range.

RESULTS AND CONCLUSIONS

1) Tangential blowing was found to be capable of controlling the ramp boundary layer-normal shock interaction for shock strengths of up to 2.0M.

2) The use of hot air in the blowing system was found to have only a small effect on blowing system performance.

3) A blowing parameter based on the absolute value of the blowing velocity was found to provide good correlation of test results using both hot and cold air in the blowing system. A parameter, used in prior investigations, based on the relative difference of the blowing flow and ramp flow velocities was found to be a poor correlator.

4) Significant differences in preferred blowing hole geometries occurred at different ramp Mach numbers. At the highest Mach number where large amounts of blowing and high pressure ratios were required, larger blowing hole sizes and larger blowing step base area ratios gave significantly better performance than the smaller scale holes preferred at lower Mach numbers.

5) Small amounts of sideslip or ramp crossflow had little effect on system performance.

REFERENCES

1. Wong, W. F.. The Application of Boundary Layer Suction to Suppress Strong Shock-Induced Separation In Supersonic Inlets. AIAA paper 74-1063, 1974.

2. Wong, W. F. and Hall, G. R.. Suppression of Strong Shock Boundary Layer Interaction In Supersonic Inlets By Boundary Layer Blowing. AIAA paper 75-1209, October 1975.

3. Wong, W. F.. Application of Boundary Layer Blowing to Suppress Strong Shock Induced Separation In Supersonic Inlets. AIAA paper 77-174, January 1977.

4. Kelly, M. W.. Analysis of Some Parameters Used In Correlating Blowing Type Boundary Layer Control Data. NACA RM A56F12, September 1956.

5. Calibration of the Northrop Ligh Weight Fighter (YF-17) 0.2 Scale Inlet Model Left Flowmeter. AEDC Project No. PA261, 16T/S Projects Branch Memo, 31 July 1973.

6. Swallow, R. J. and Aiello, R. A.. NASA Lewis 8- by 6-Foot Supersonic Wind Tunnel. NASA TM X-71542, 1974.

7. Moeckel, W. E.: Approximate Methods For Predicting Form and Location Of Detached Shock Waves Ahead of Plane or Axially Symmetric Bodies. NACA TN1921, 1949.

MACH NUMBER	MO	-	1.961	1.766	1.563	1.364
FREESTREAM TOTAL PRESSURE	HO	KN/M^2	167.8	156.2	138.6	124.0
		psia	24.34	22.66	20.10	17.99
FREESTREAM TOTAL TEMPERATURE	TTO	deg-K	353.0	342.0	327.5	316.5
		deg-R	635.4	615.6	589.5	569.7
ESTIMATED BOUNDARY LAYER MOMENTUM THICKNESS AT BLOWING STATION	θ_1	cm	0.0139	0.0143	0.0149	0.0155
		in	0.00546	0.00565	0.00588	0.00612

TABLE I. TYPICAL TEST CONDITIONS

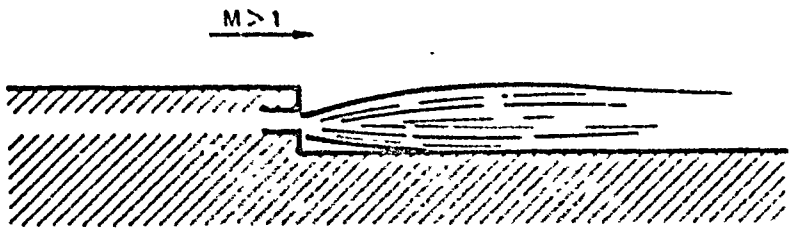

a) BLOWING PLUME DOES NOT INTERFERE WITH RAMP FLOW

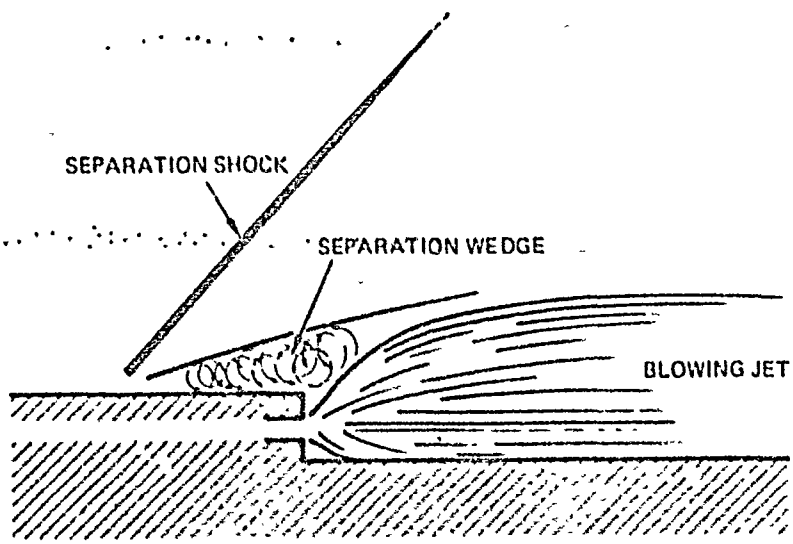

b) A HIGHLY UNDEREXPANDED JET CAUSES UPSTREAM INTERFERENCE

FIGURE 1. ASSUMED EFFECT OF BLOWING STEP HEIGHT

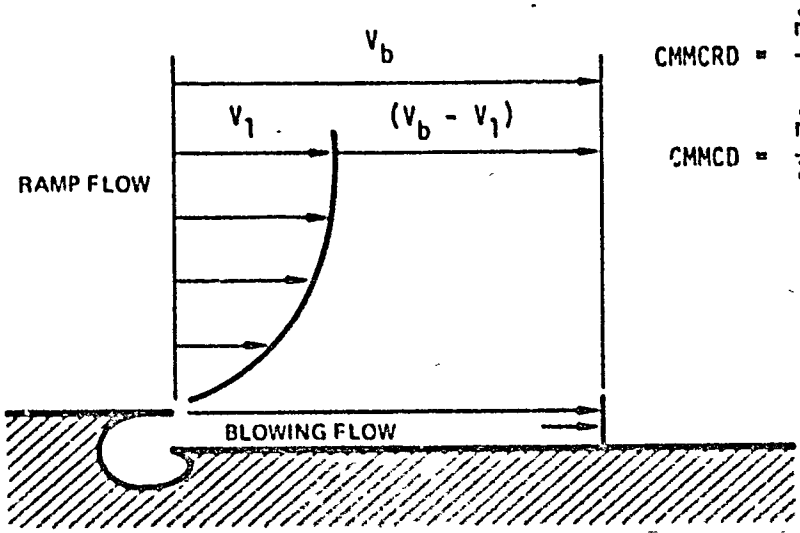

a) DEFINITION OF BLOWING COEFFICIENTS

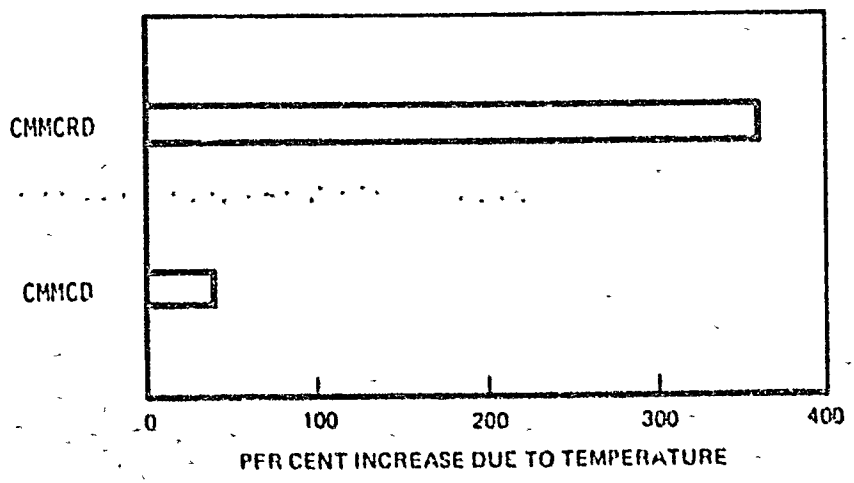

b) EFFECT OF AN INCREASE OF TOTAL TEMPERATURE RATIO FROM 1 TO 2 AT 1.7GM. CONSTANT WEIGHT FLOW

FIGURE 2. RELATIVE AND ABSOLUTE BLOWING COEFFICIENTS

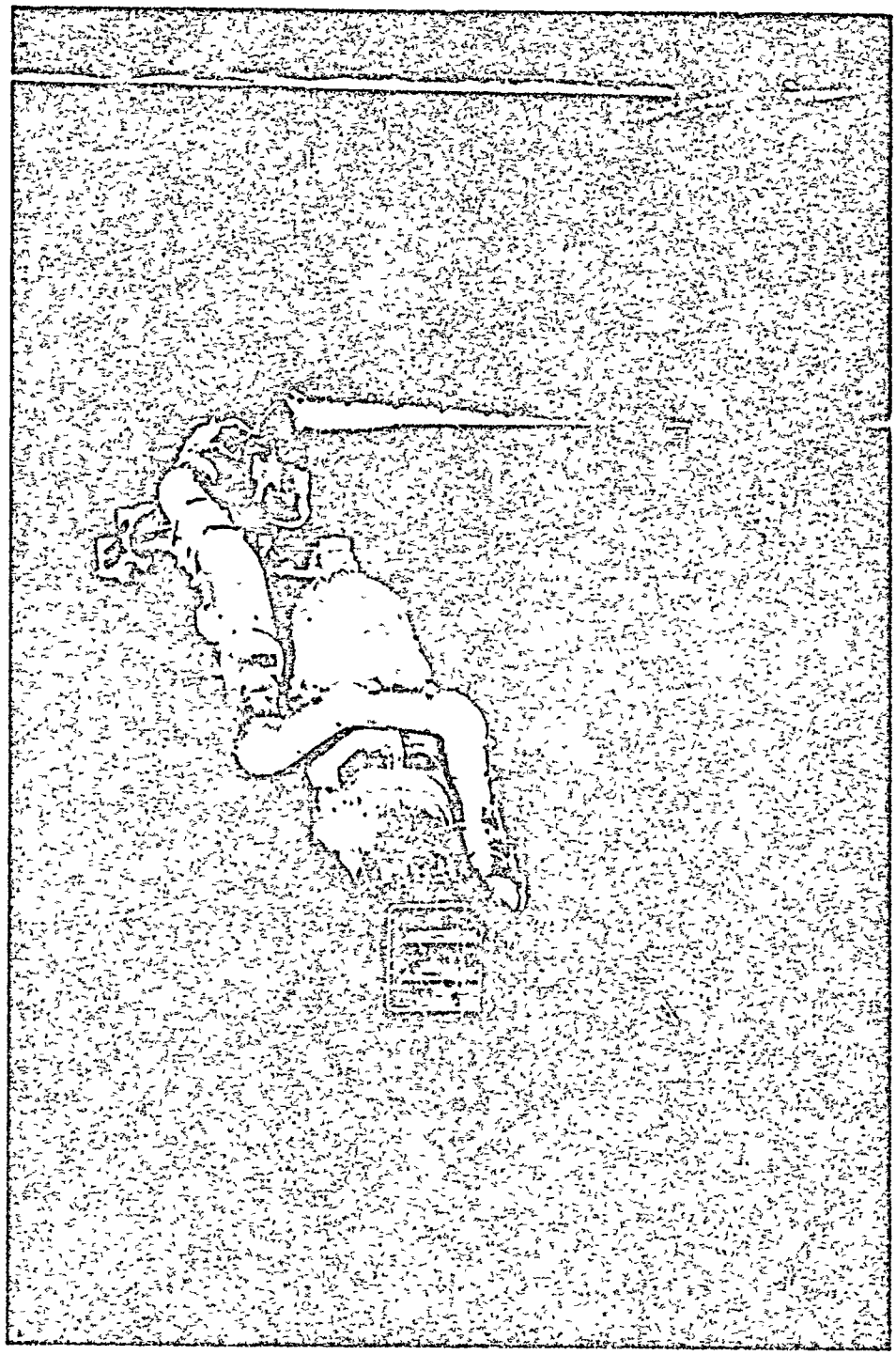

81-01653

FIGURE 3. MODEL INSTALLATION IN THE 8-FT BY 6-FT SUPERSONIC WIND TUNNEL

ORIGINAL PAGE
BLACK AND WHITE PHOTOGRAPH

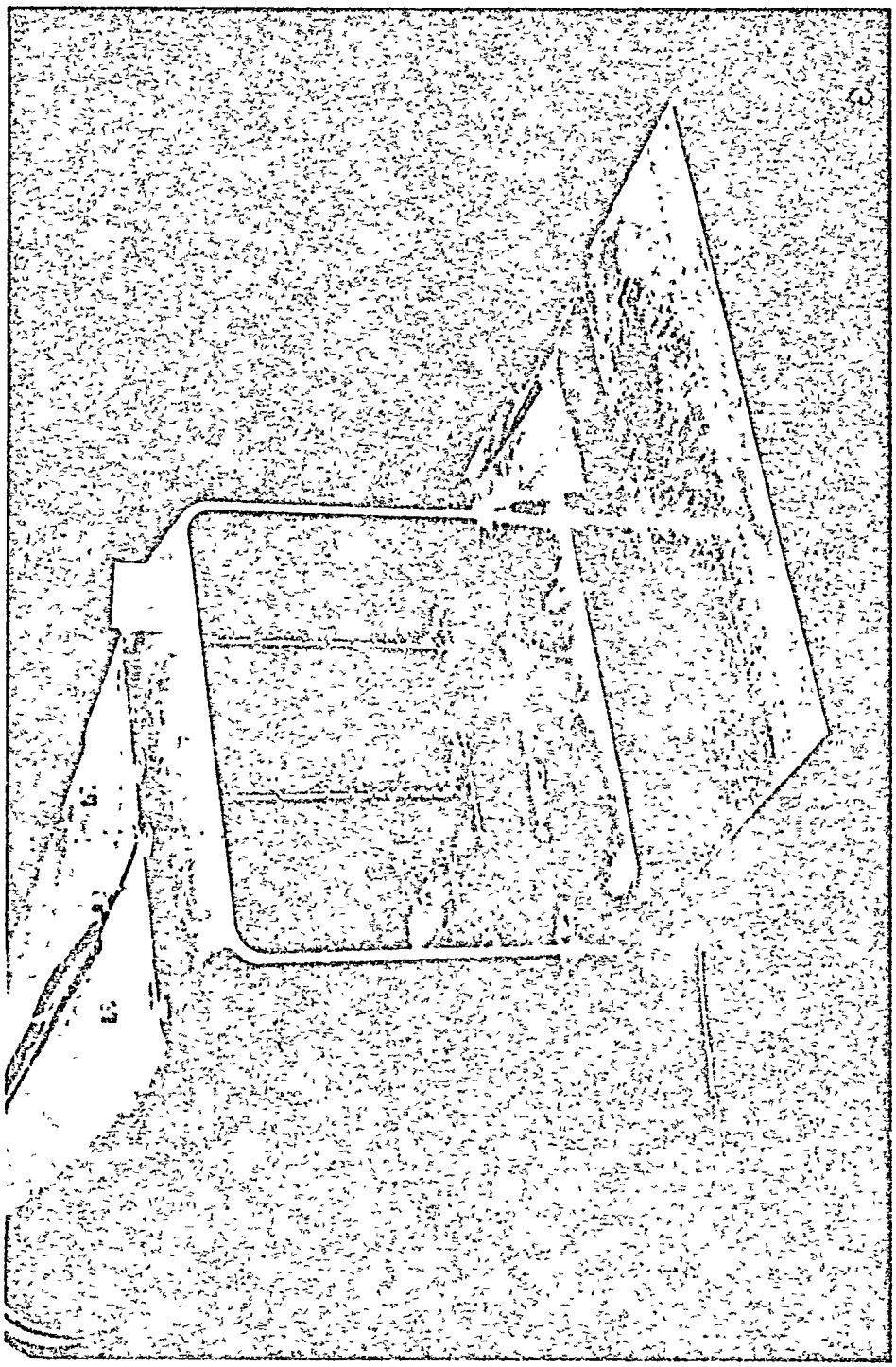

FIGURE 4. INLET COWL AND RAMP

ORIGINAL PAGE
BLACK AND WHITE PHOTOGRAPH

FIGURE 5. AFT FACING BLOWING STEP – CONFIGURATION 24

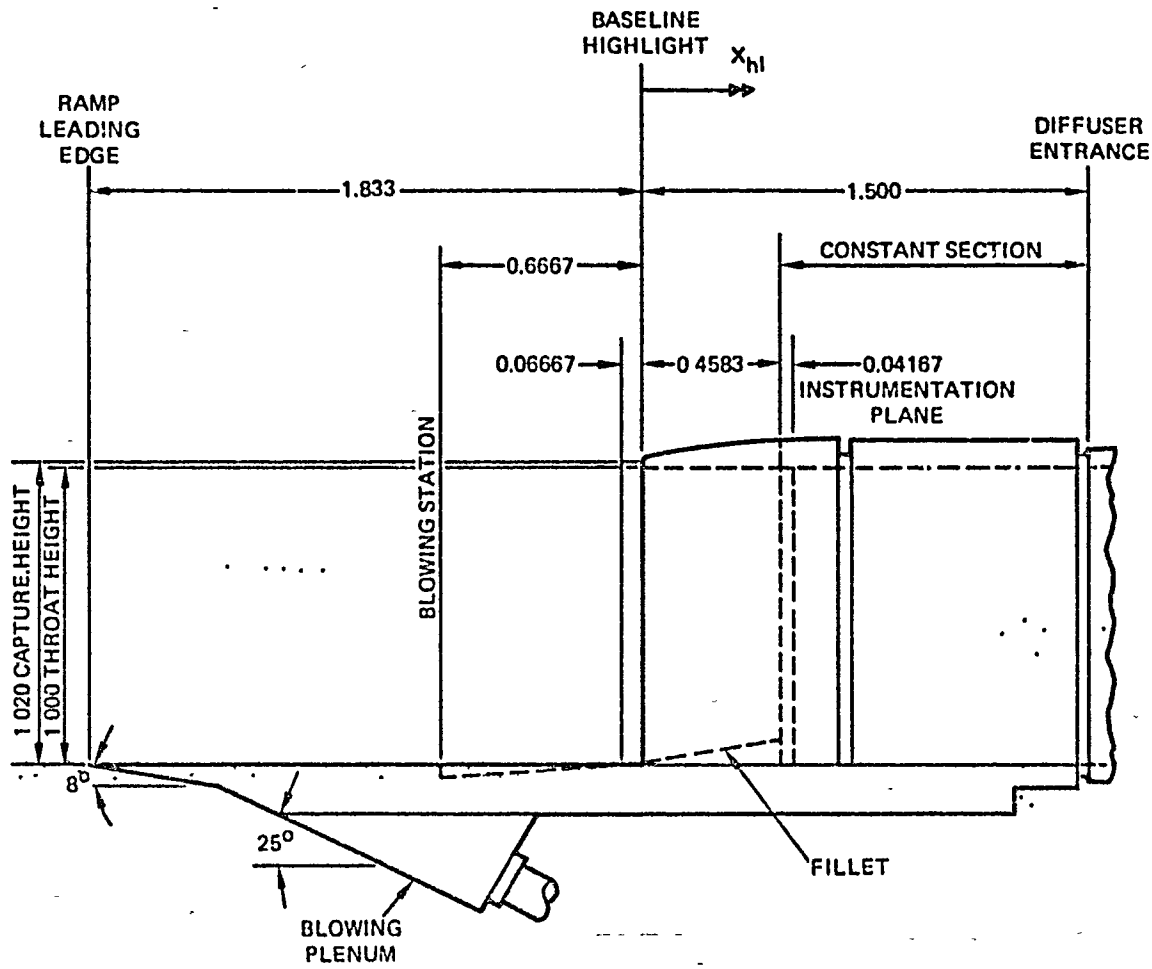

NOTE: ALL DIMENSIONS ARE EXPRESSED IN TERMS OF THE INLET THROAT HEIGHT, H_{th} = 7.62 CM (3.00 IN)

FIGURE 6. INLET RAMP AND COWL – SIDE VIEW

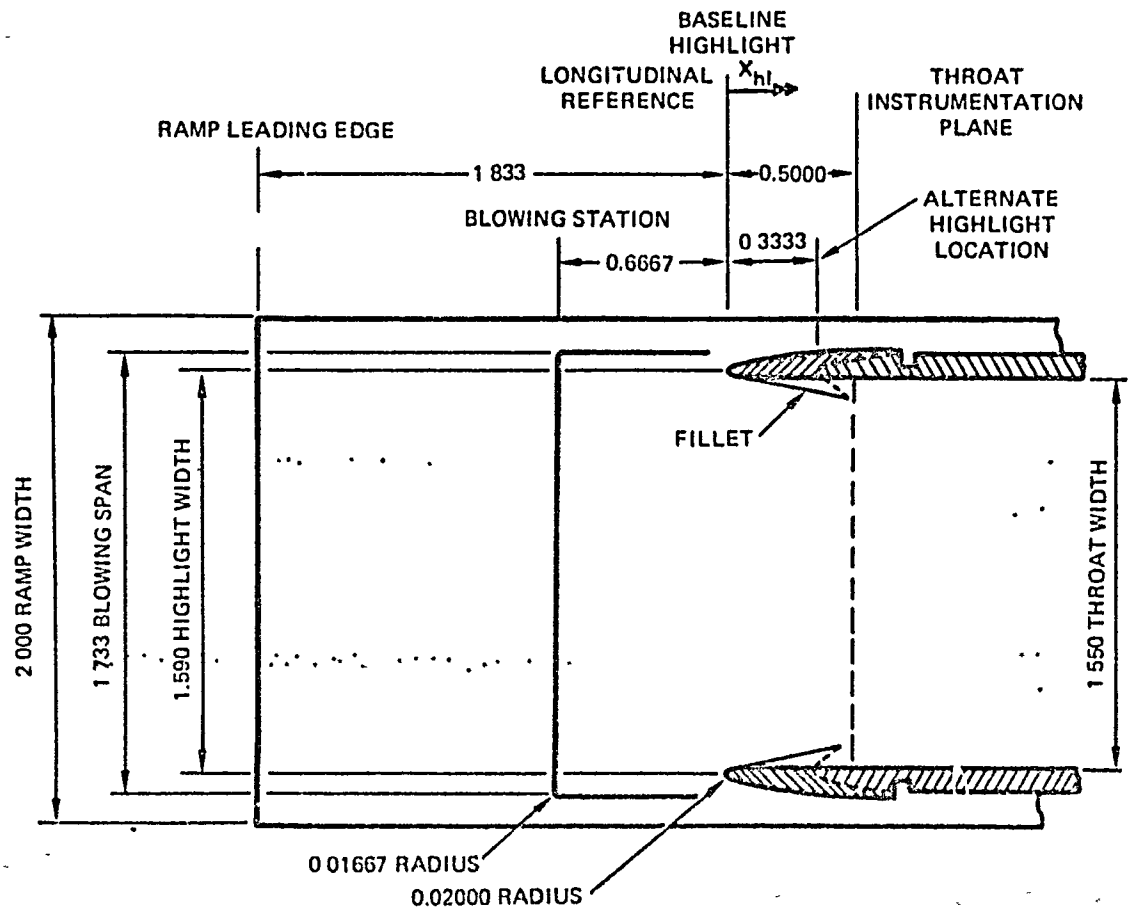

NOTE: ALL DIMENSIONS ARE EXPRESSED IN TERMS OF THE INLET THROAT HEIGHT, Hth = 7.62 CM (3 00 IN.)

FIGURE 7. INLET RAMP AND COWL – TOP VIEW

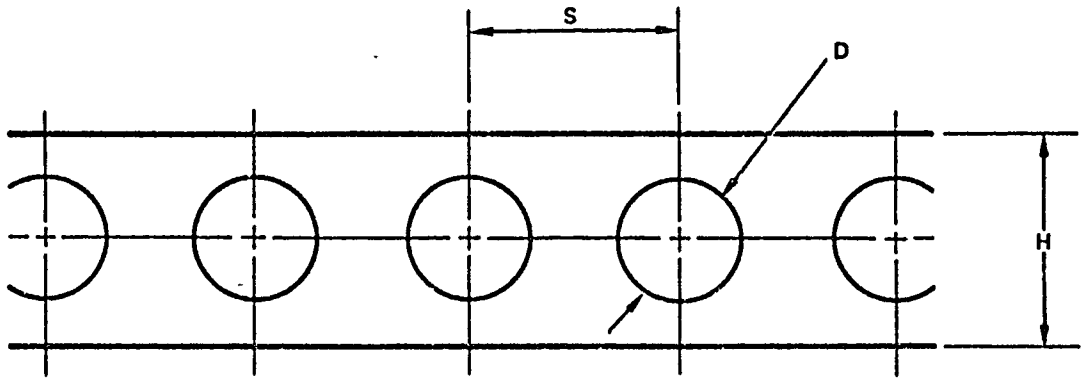

CONF	HOLE DIAMETER		BLOWING AREA		SPACING RATIO	HEIGHT RATIO	BASE AREA RATIO
CODE	D		A_b		$\frac{S}{D}$	$\frac{H}{D}$	$\frac{H \cdot S}{A_b}$
–	CM	IN	CM^2	IN^2	–	–	–
21	0 061	0 024	0.49	0 076	1.292	2.21	3 63
22	0 079	0 031	0.48	0 074	1.710	2 35	5.13
23	0 099	0.039	0 48	0 074	2.154	2.26	6.19
24, 26*	0 102	0 040	0.85	0.131	1.250	2.15	3.42

* WHEN TESTED WITH THE SHORT COWL

FIGURE 8. BLOWING NOZZLE HOLE CONFIGURATIONS

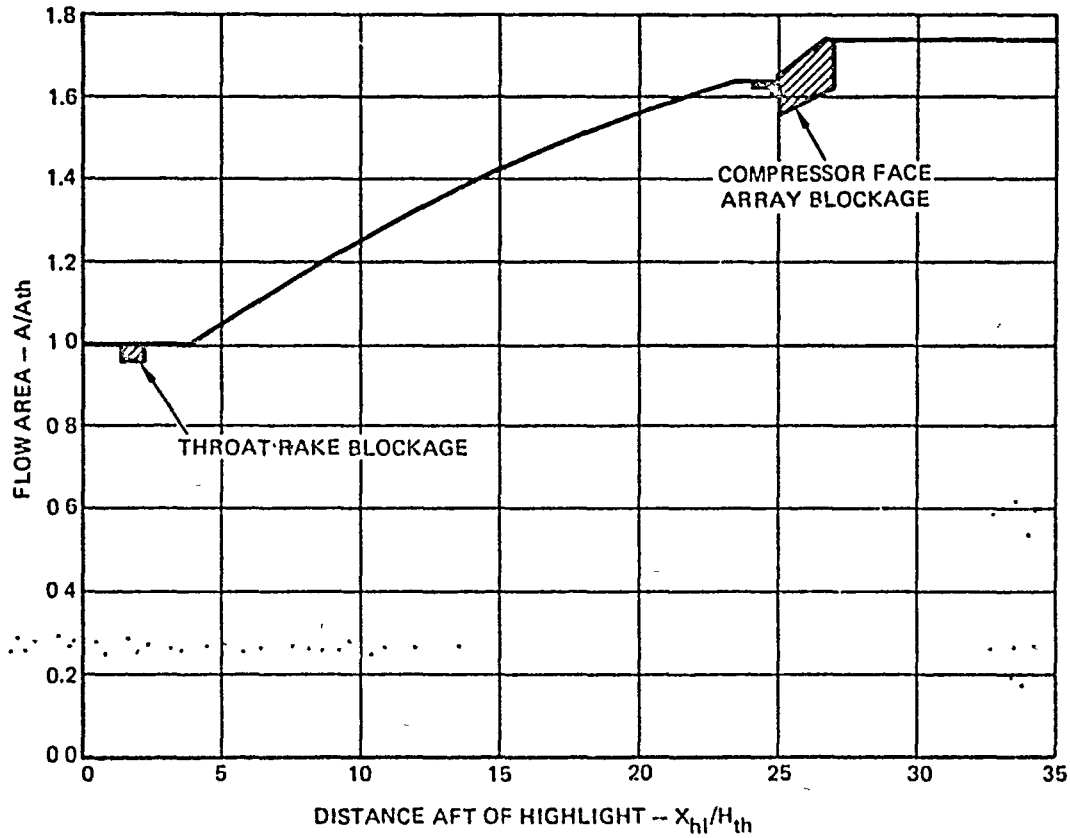

FIGURE 9. INLET FLOW AREA DISTRIBUTION

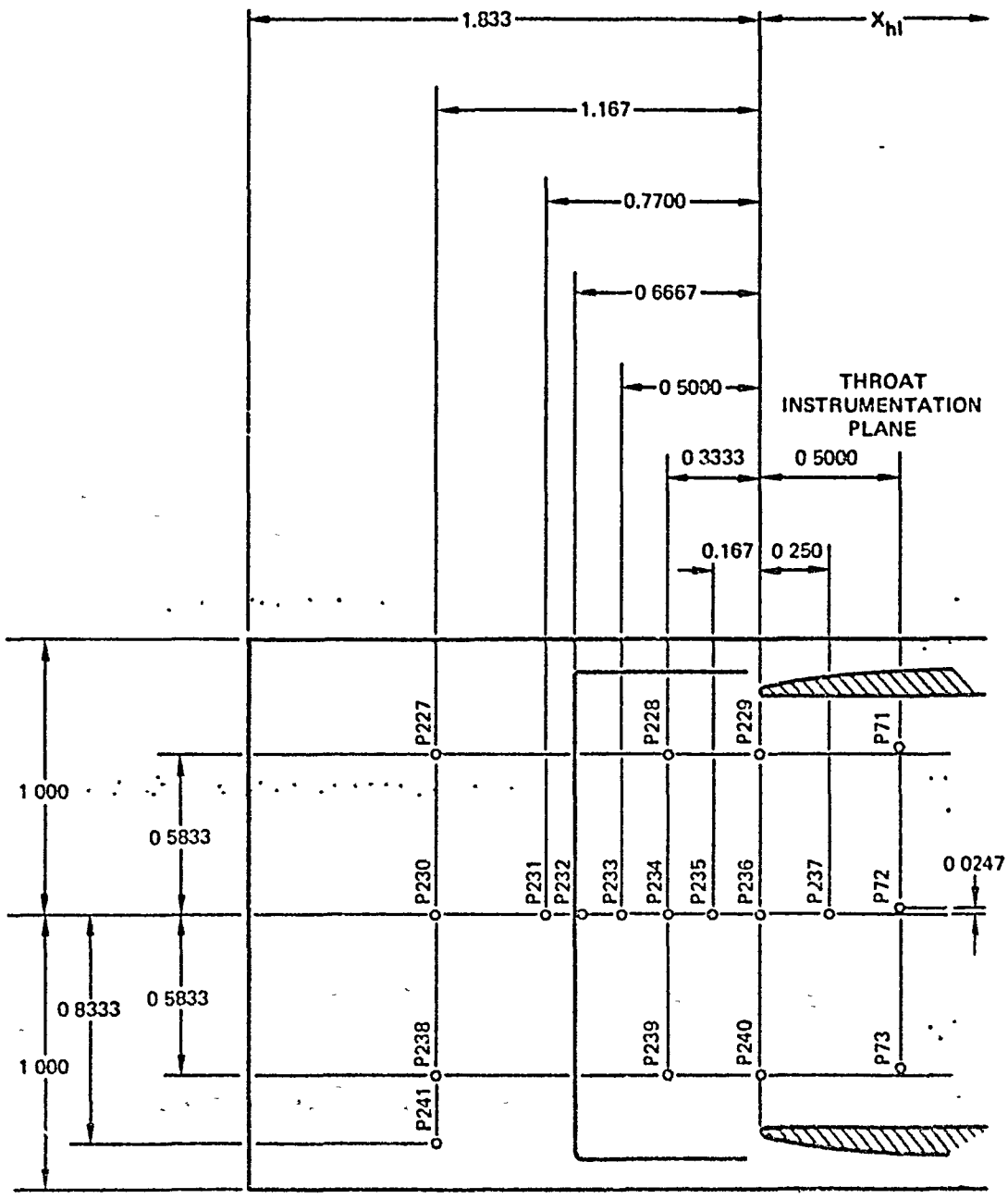

NOTE: ALL DIMENSIONS ARE EXPRESSED IN TERMS OF THE INLET THROAT HEIGHT, H_{th} = 7.62 CM (3.00 IN)

FIGURE 10. RAMP PRESSURE PORT LOCATIONS

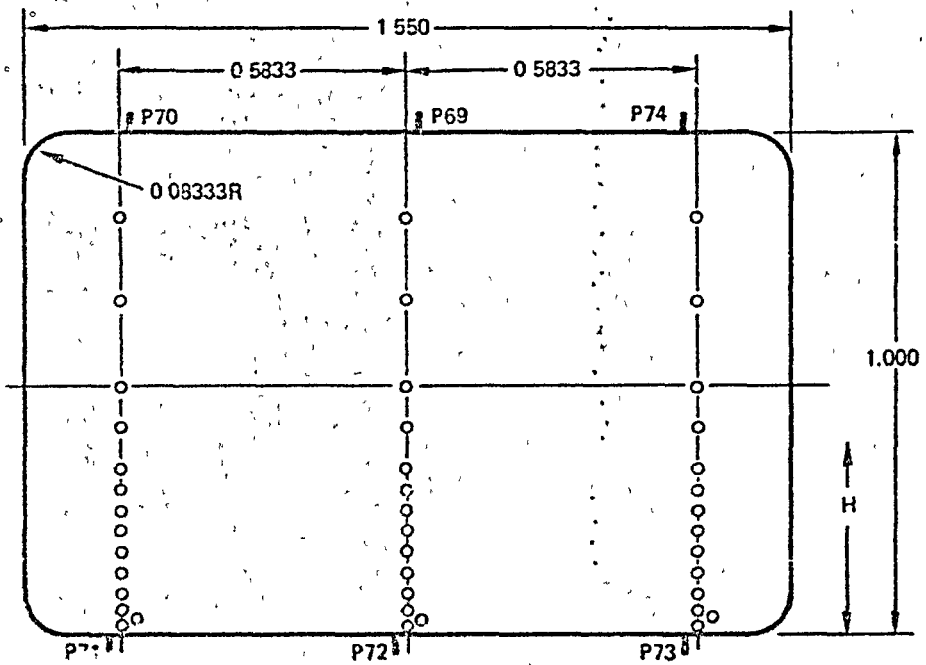

NOTE: ALL DIMENSIONS ARE EXPRESSED IN TERMS OF THROAT HEIGHT, H_{th} = 7.62 CM (3 00 IN)

H/H_{th}	RT	CL	LT
	4 445Y	0 000Y	-4 445Y
0 000	P71*	P72*	P73*
0 017	P75	P89	P103
0.033	P76+	P90+	P104+
0 050	P77	P91	P105
0 083	P78	P92	P106
0 125	P79	P93	P107
0.167	P80	P94	P108
0 208	P81	P95	P109
0 250	P82	P96	P110
0 292	P83	P97	P111
0.333	P84	P98	P112
0 417	P85	P99	P113
0 500	P86	P100	P114
0 667	P87	P101	P115
0 833	P88	P102	P116
1 000	P70*	P69*	P74*

+0 229 CM (0 09 IN) TOTAL HEAD PROBE OFFSET
*0 188 CM (0 074 IN) STATIC PORT OFFSET

ORIGINAL PAGE IS
OF POOR QUALITY

FIGURE 11. THROAT PLANE PRESSURE INSTRUMENTATION

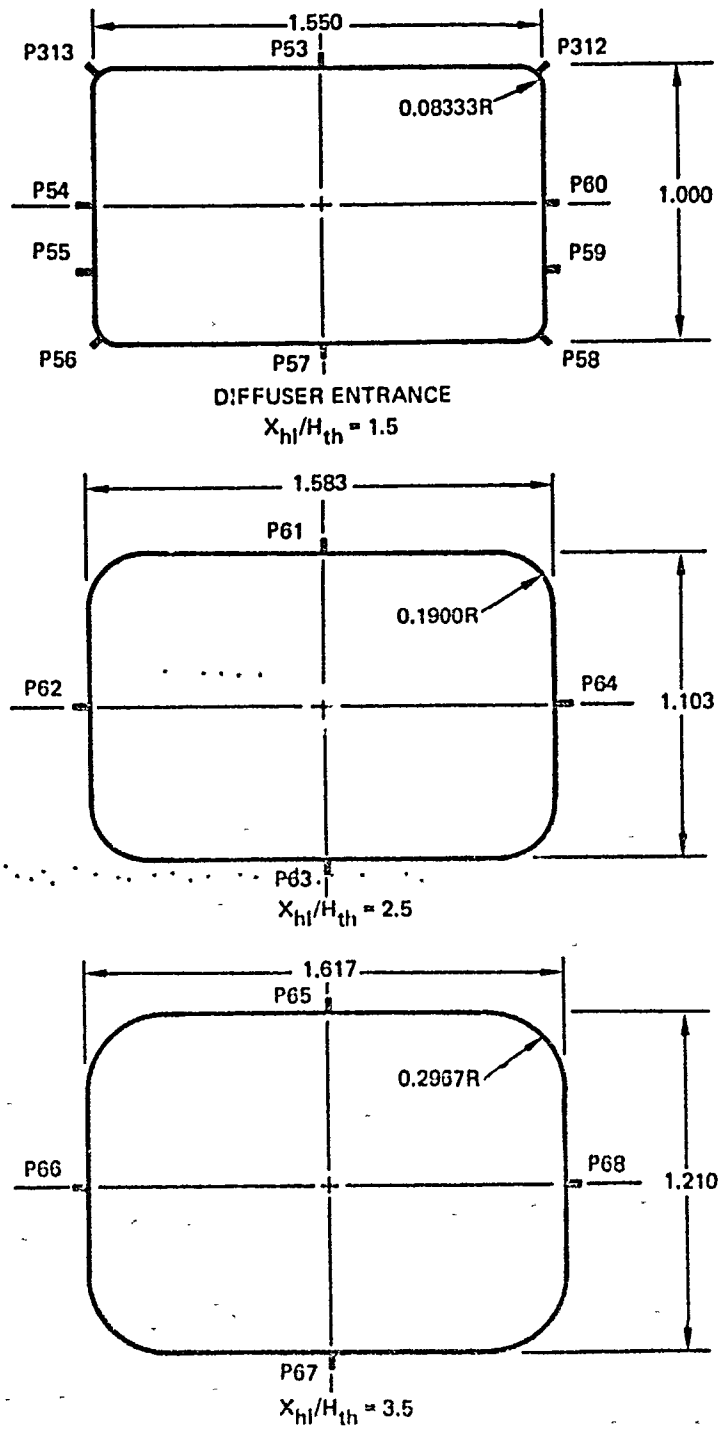

NOTE:
ALL DIMENSIONS ARE EXPRESSED IN THROAT HEIGHT, H_{th} = 7.62 CM (3 00 IN)

FIGURE 12. DUCT PRESSURE INSTRUMENTATION

ORIGINAL PAGE IS
OF POOR QUALITY

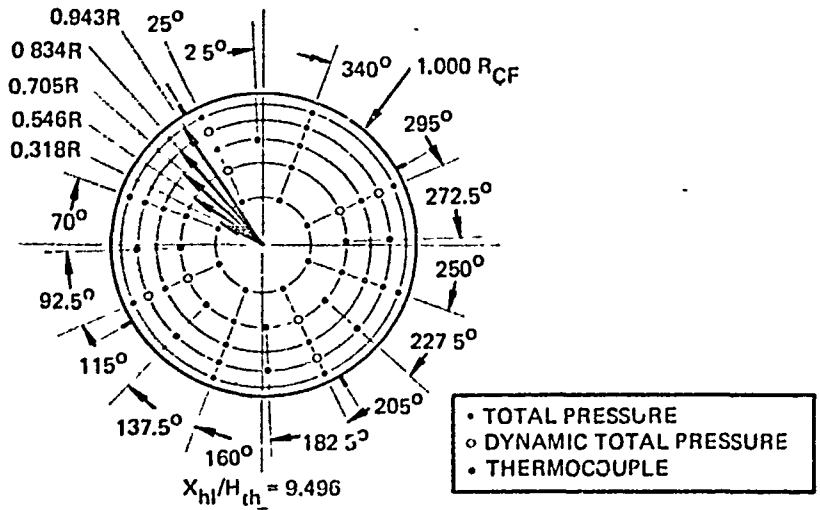

NOTE. ALL RADII ARE EXPRESSED IN TERMS OF THE COMPRESSOR FACE RATIOS, R_{CF} = 6.858 CM (2 7 IN)

TOTAL PRESSURE PROBES

	RAKE	6	5	4	3	2	1	8	7
RING	$\frac{R}{RCF}$	25°	70°	115°	160°	205°	250°	295°	340°
1	0 318	P26	P21	P16	P11	P6	P1	P36	P31
2	0 546	P27	P22	P17	P12	P7	P2	P37	P32
3	0.705	P28	P23	P18	P13	P8	P3	P38	P33
4	0 834	P29	P24	P19	P14	P9	P4	P39	P34
5	0 943	P30	P25	P20	P15	P10	P5	P40	P35

STATIC PRESSURE PORTS

RING	$\frac{R}{RCF}$	30°		120°		210°		300°	
STATIC	1 000	P41		P42		P43		P44	

CrAl TEMPERATURE PROBES

	RAKE	6T	5T	4T	3T	2T	1T
RING	$\frac{R}{RCF}$	2.5°	92 5°	137.5°	182 5°	227.5°	272 5°
2	0 546		T19	T17	T15	T13	T11
3	0.705	T21					
4	0 834		T20	T18	T16	T14	T12

FIGURE 13. COMPRESSOR FACE INSTRUMENTATION ARRAY

ORIGINAL PAGE IS
OF POOR QUALITY

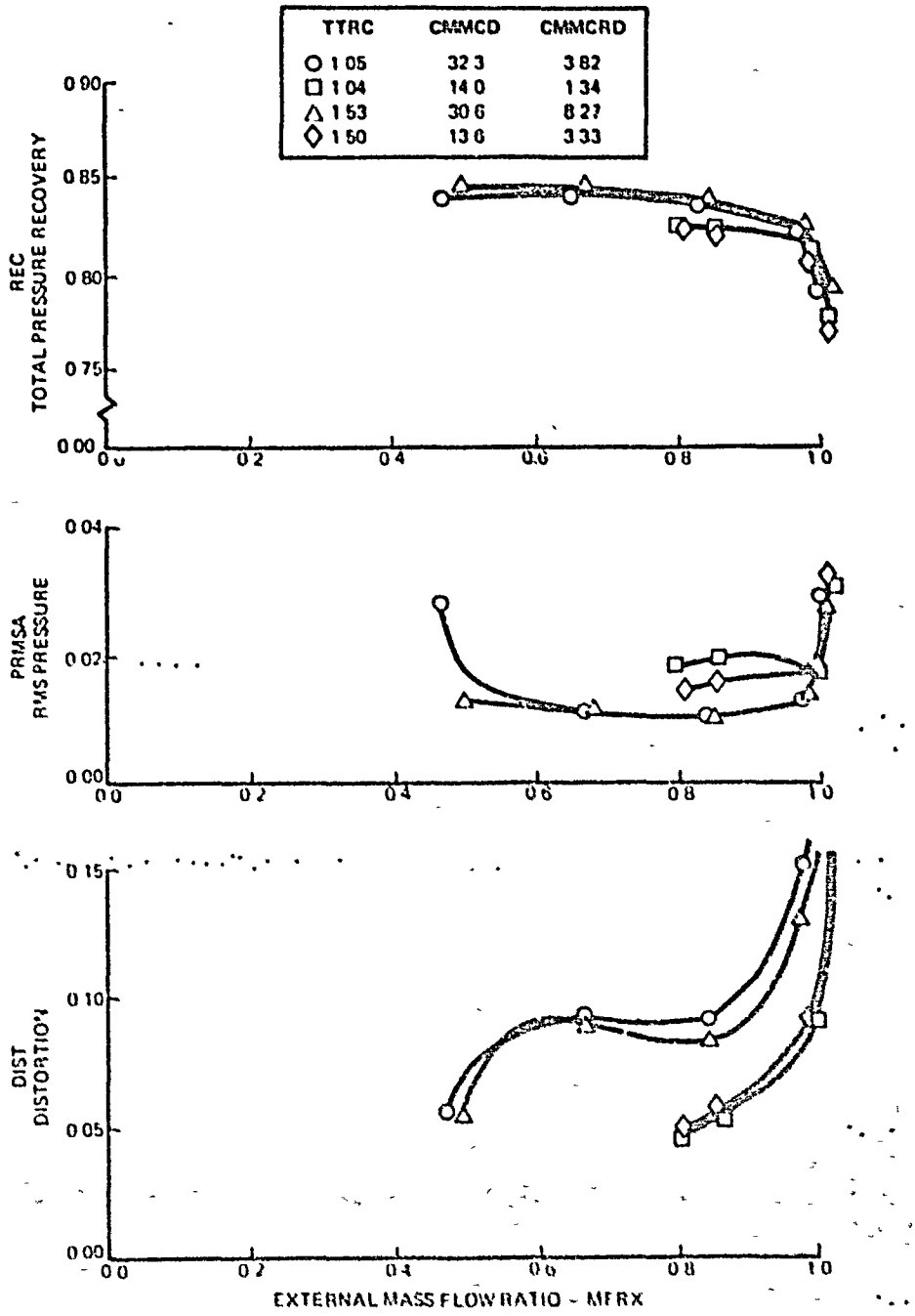

FIGURE 14. COMPARISON OF BLOWING PARAMETERS FOR CONFIGURATION 21 AT 1.76M

ORIGINAL PAGE 13
OF POOR QUALITY

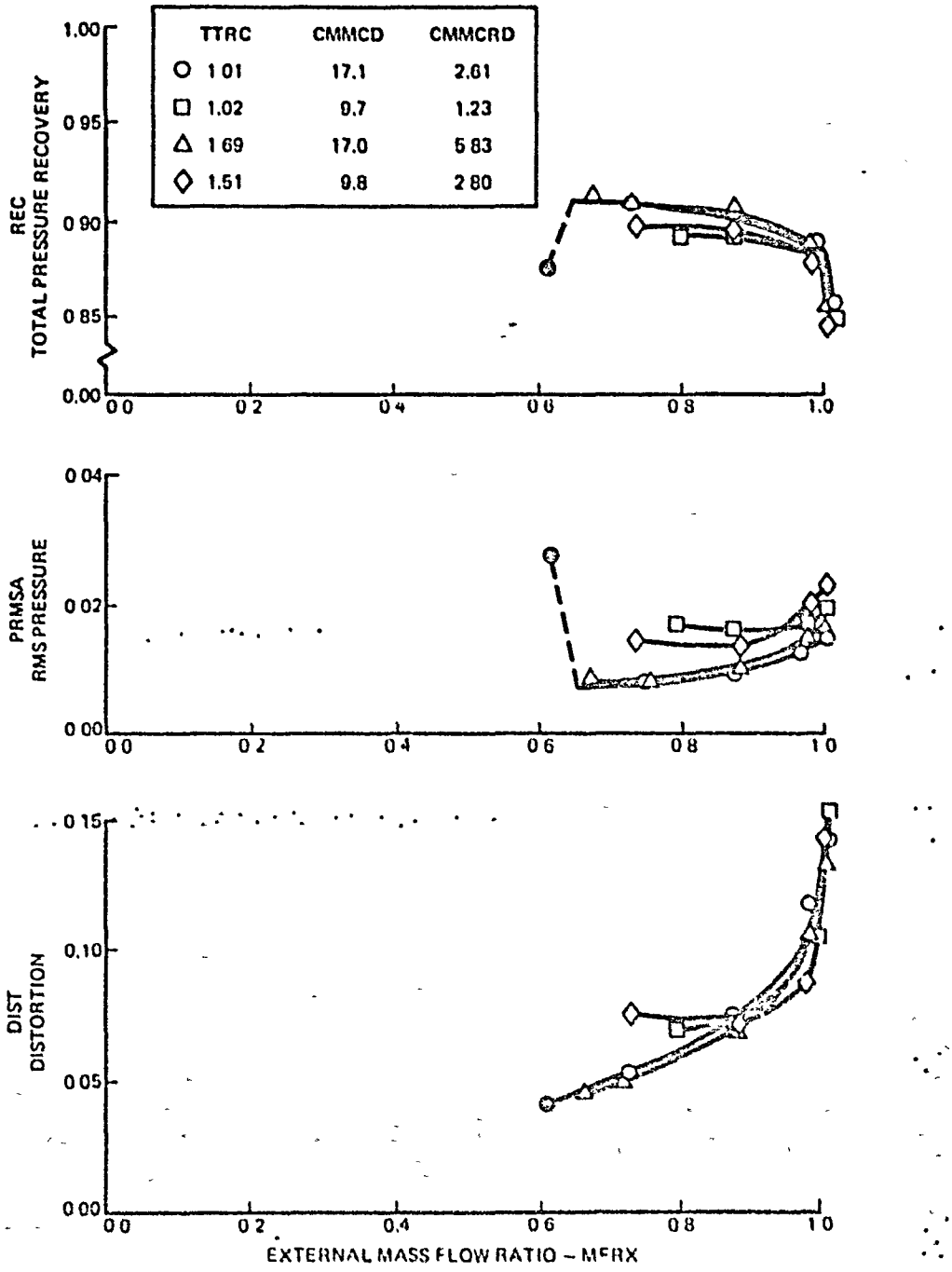

FIGURE 15. COMPARISON OF BLOWING PARAMETERS FOR CONFIGURATION 21 AT 1.56M

ORIGINAL PAGE IS
OF POOR QUALITY

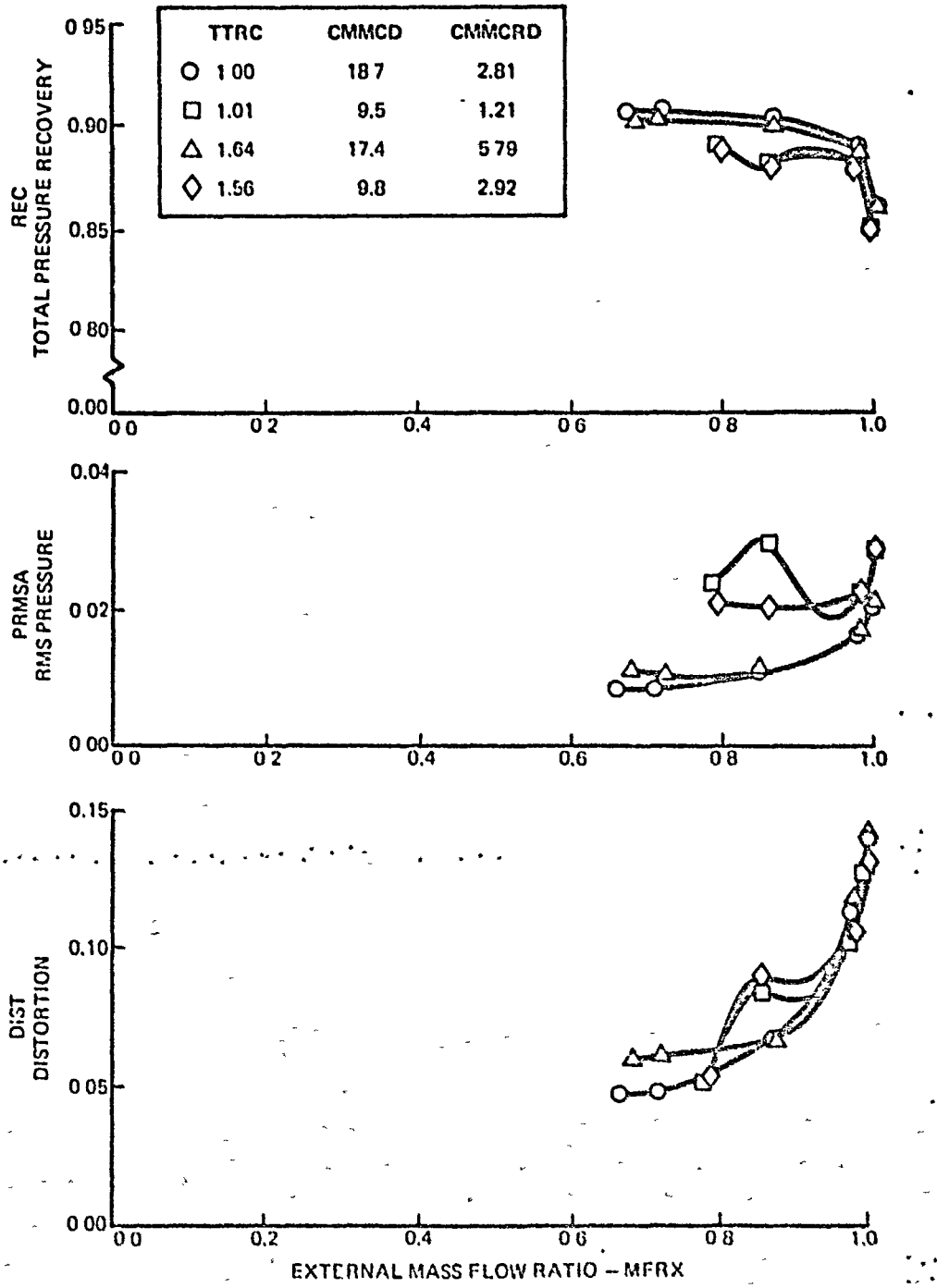

FIGURE 16. A COMPARISON OF BLOWING PARAMETERS FOR CONFIGURATION 23 AT 1.56M

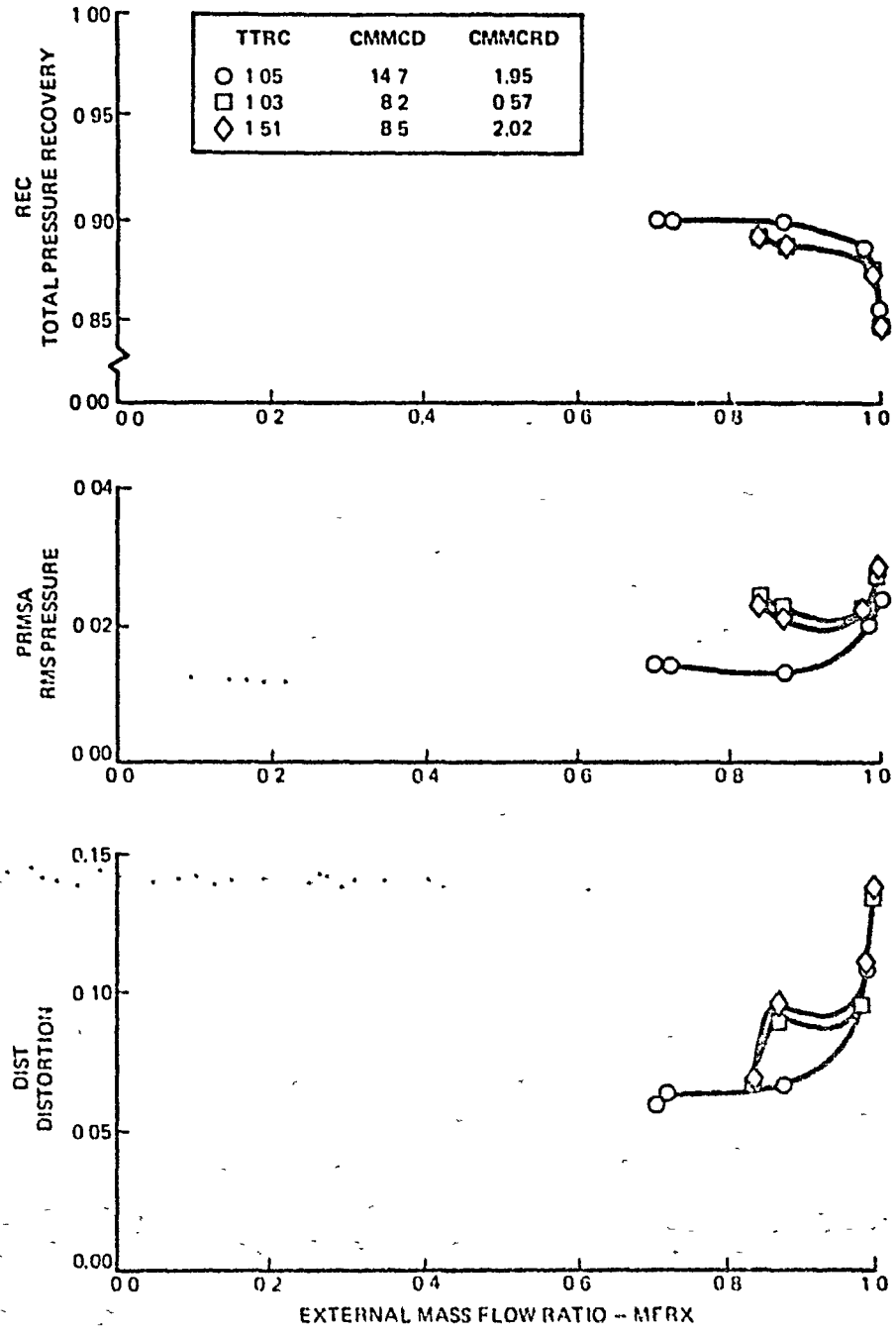

FIGURE 17. A COMPARISON OF BLOWING PARAMETERS FOR CONFIGURATION 24 AT 1.56M

ORIGINAL PAGE IS
OF POOR QUALITY

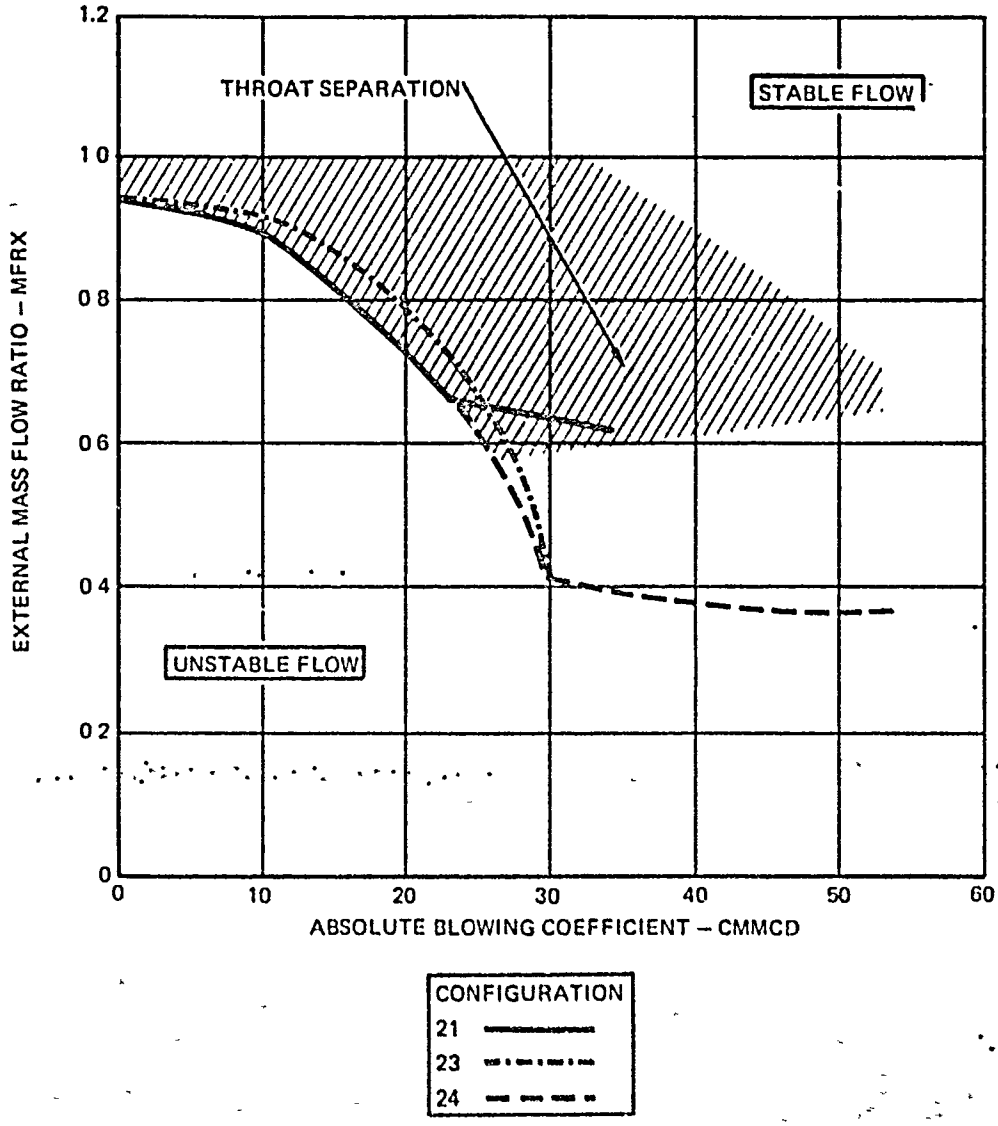

FIGURE 18. INLET STABILITY AT 1.96M, COLD FLOW

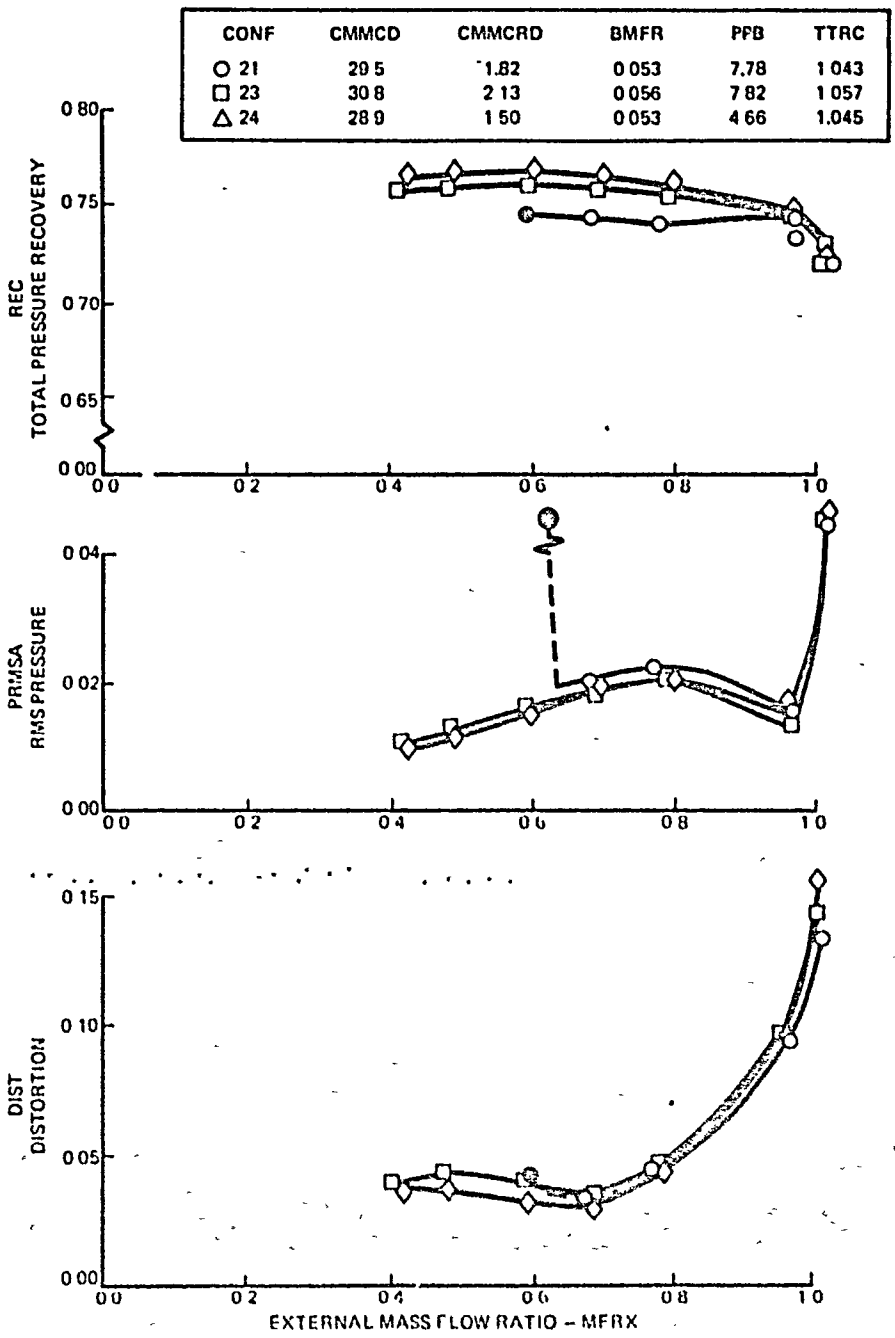

FIGURE 19. EFFECT OF BLOWING CONFIGURATION AT 1.96M – FLOW BREAKDOWN FOR CONFIGURATION 21

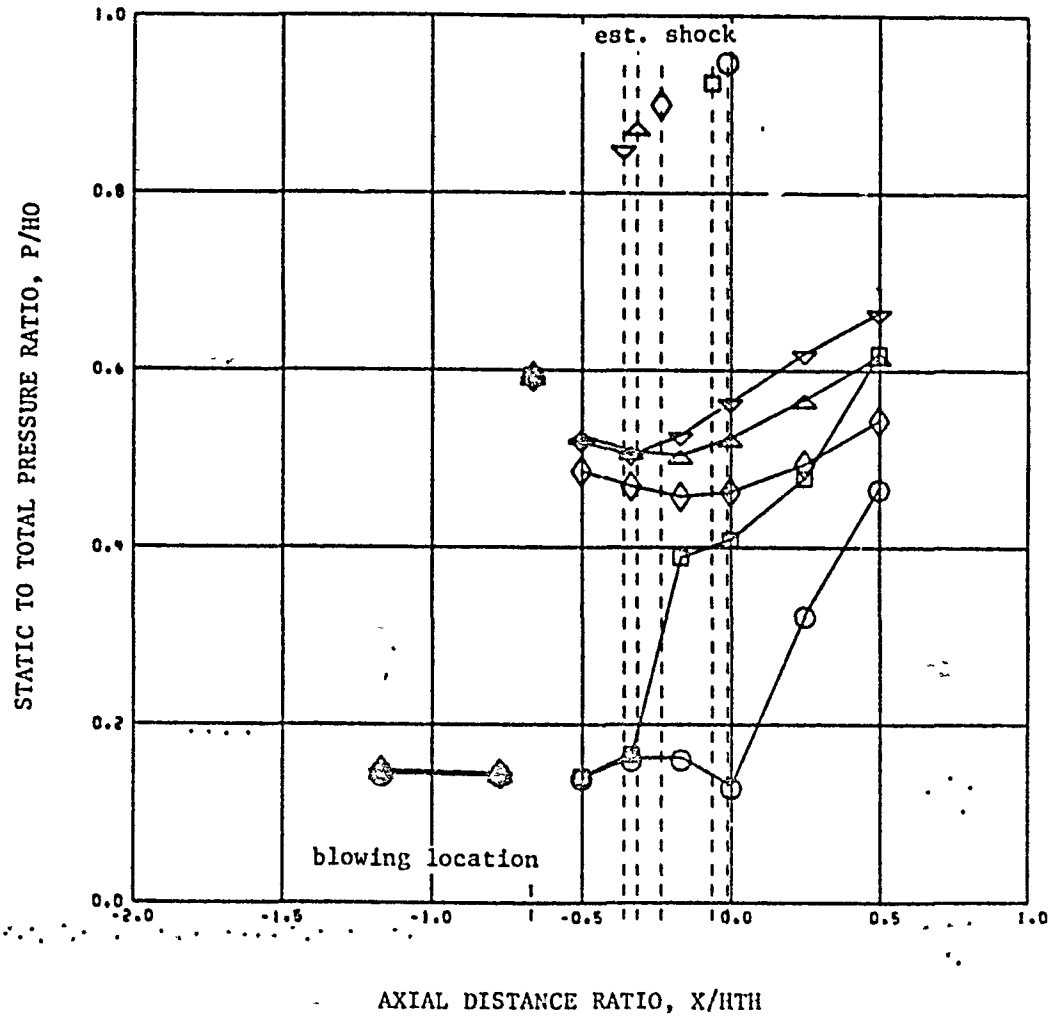

SYM	MFRX
○	1.021
□	0.968
◇	0.778
△	0.682
▽	0.596

FIGURE 20. RAMP PRESSURE DISTRIBUTION FOR CONFIGURATION 21 AT 1.96M, CMMCD = 33.7

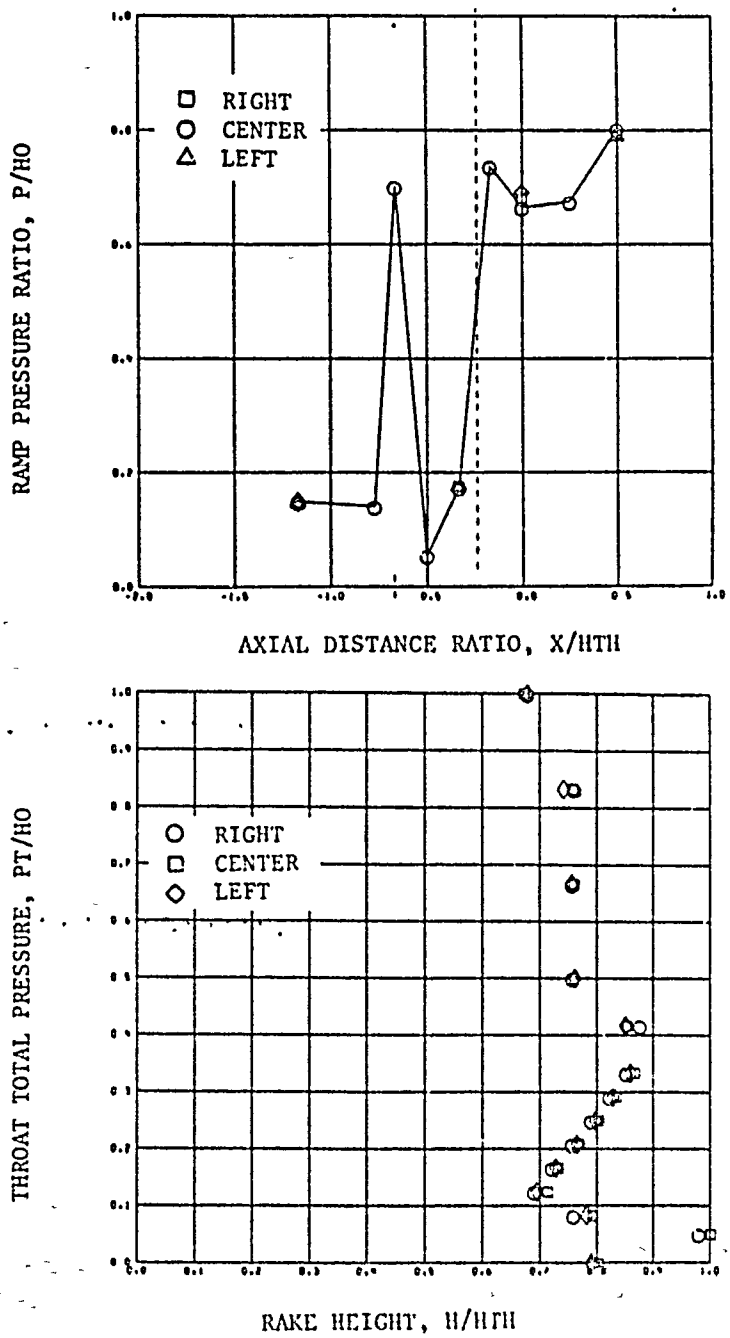

FIGURE 21. INLET FLOW CONDITIONS FOR CONFIGURATION 24 AT VERY HIGH BLOWING RATES, 1.96M, CEMCD=52.9, MFRX=0.77

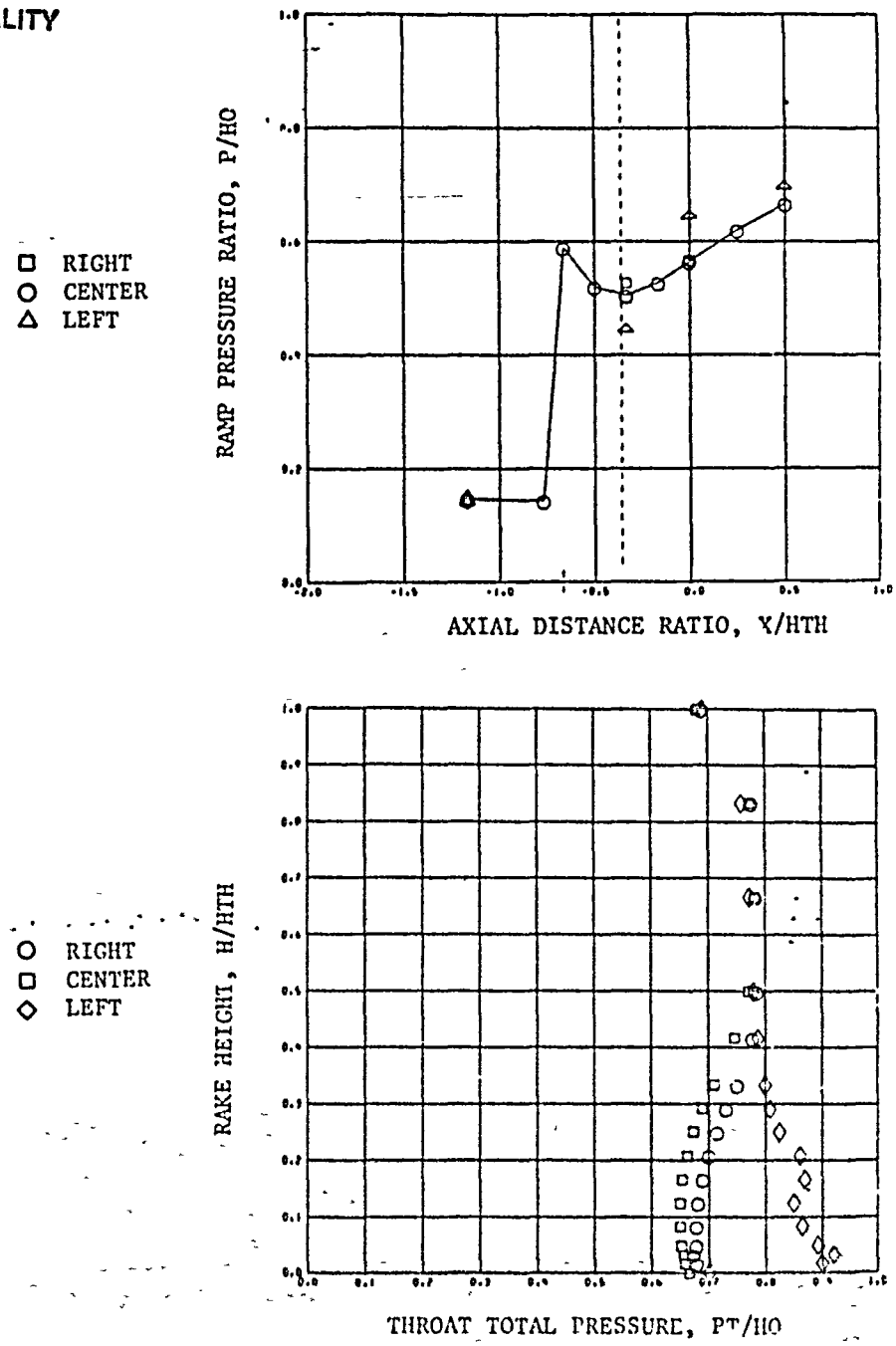

FIGURE 22. INLET FLOW ASYMMETRY FOR CONFIGURATION 21 AT 1.96M, CMMCD = 33.7, COLD FLOW, MFRX = 0.626

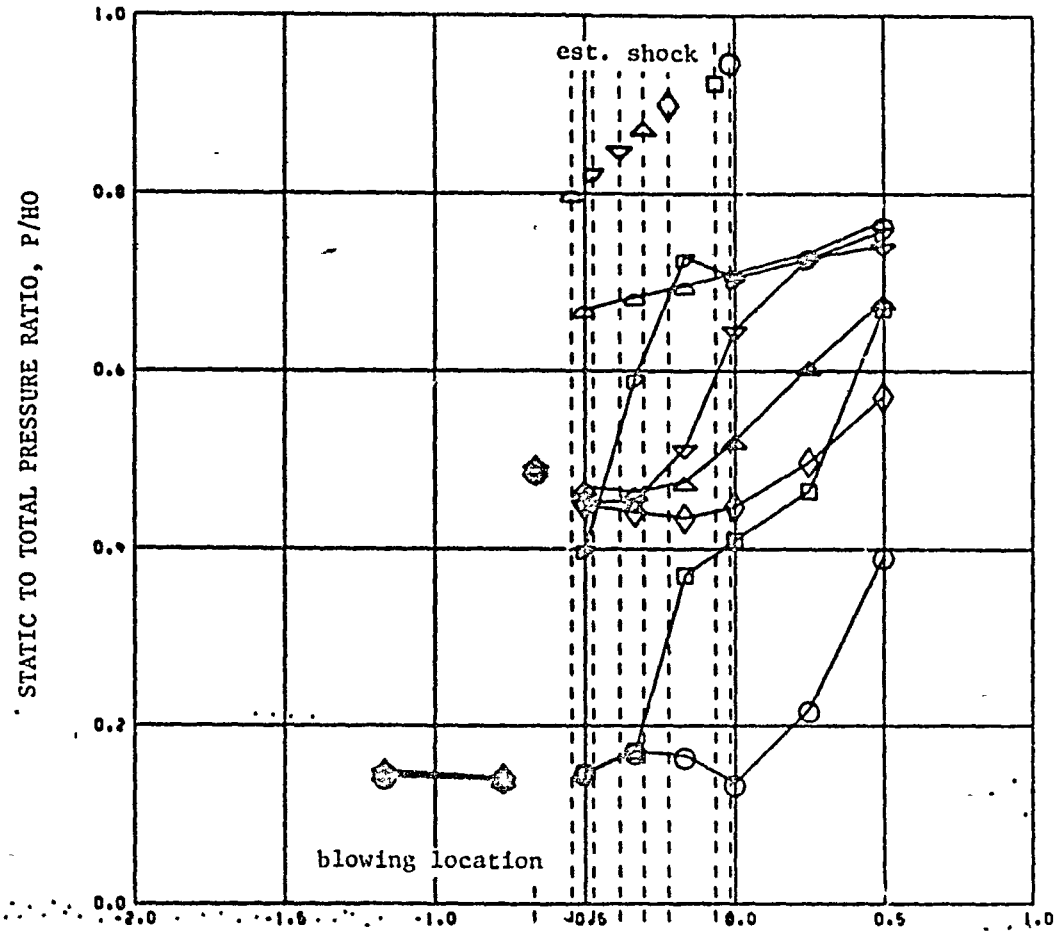

SYM	MFRX
○	1.018
□	0.964
◇	0.788
△	0.691
▽	0.597
▷	0.484
▷	0.394

FIGURE 23. RAMP PRESSURE DISTRIBUTION FOR CONFIGURATION 24 AT 1.96M, CMMCD = 36.4

ORIGINAL PAGE IS
OF POOR QUALITY

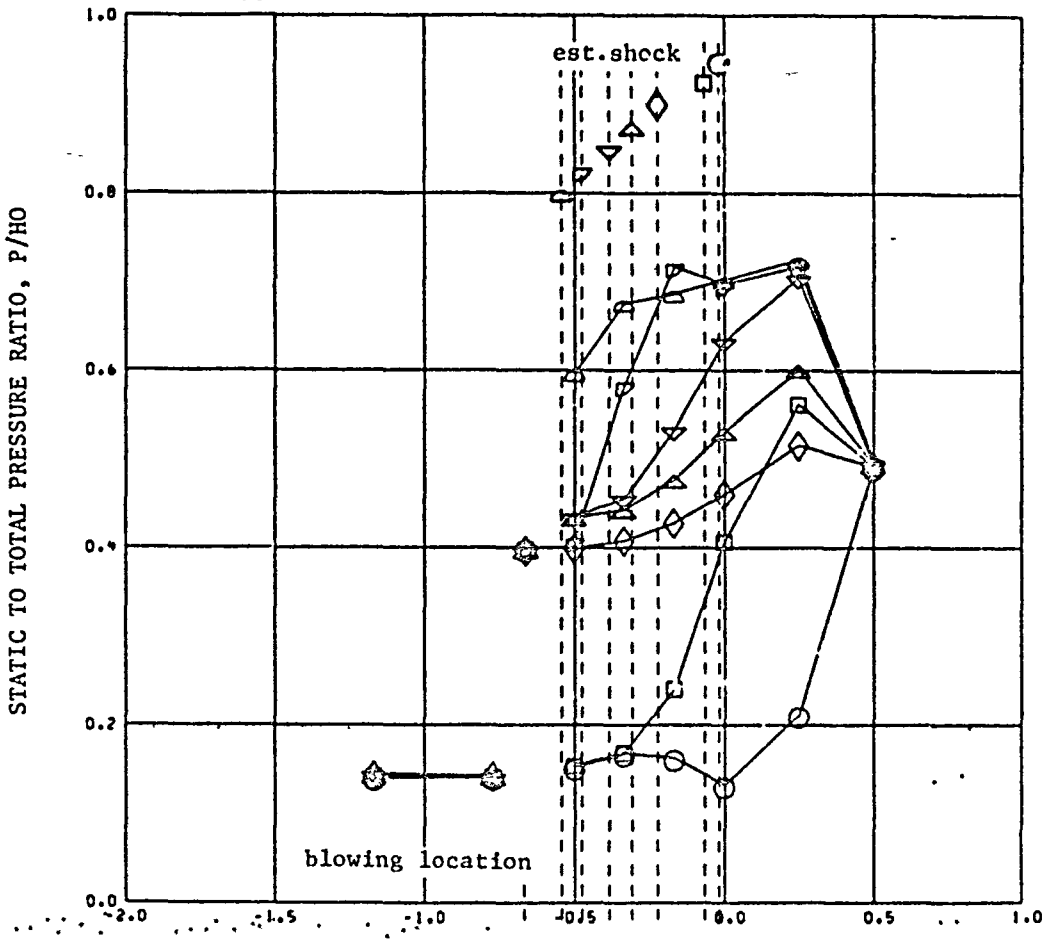

AXIAL DISTANCE RATIO, X/HTH

SYM	MFRX
○	1.016
□	0.964
◇	0.788
△	0.689
▽	0.595
▷	0.483
⬭	0.395

FIGURE 24. RAMP PRRESURE DISTRIBUTION FOR CONFIGURATION 23 AT 1.96M, CMMCD = 34.2

ORIGINAL PAGE IS
OF POOR QUALITY

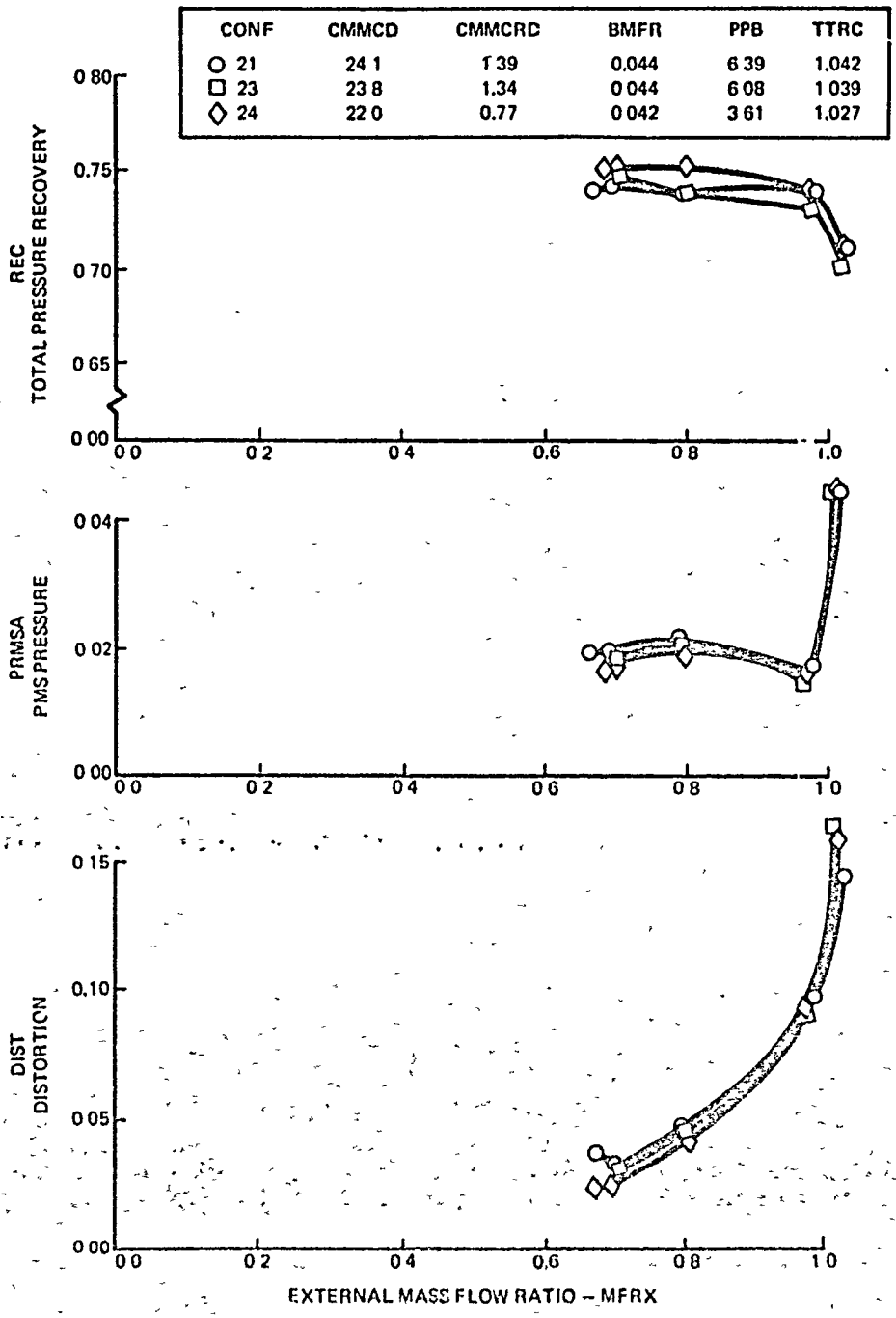

FIGURE 25. EFFECT OF BLOWING CONFIGURATION AT 1.96M – PARTIAL RANGE CONTROL FOR ALL CONFIGURATIONS

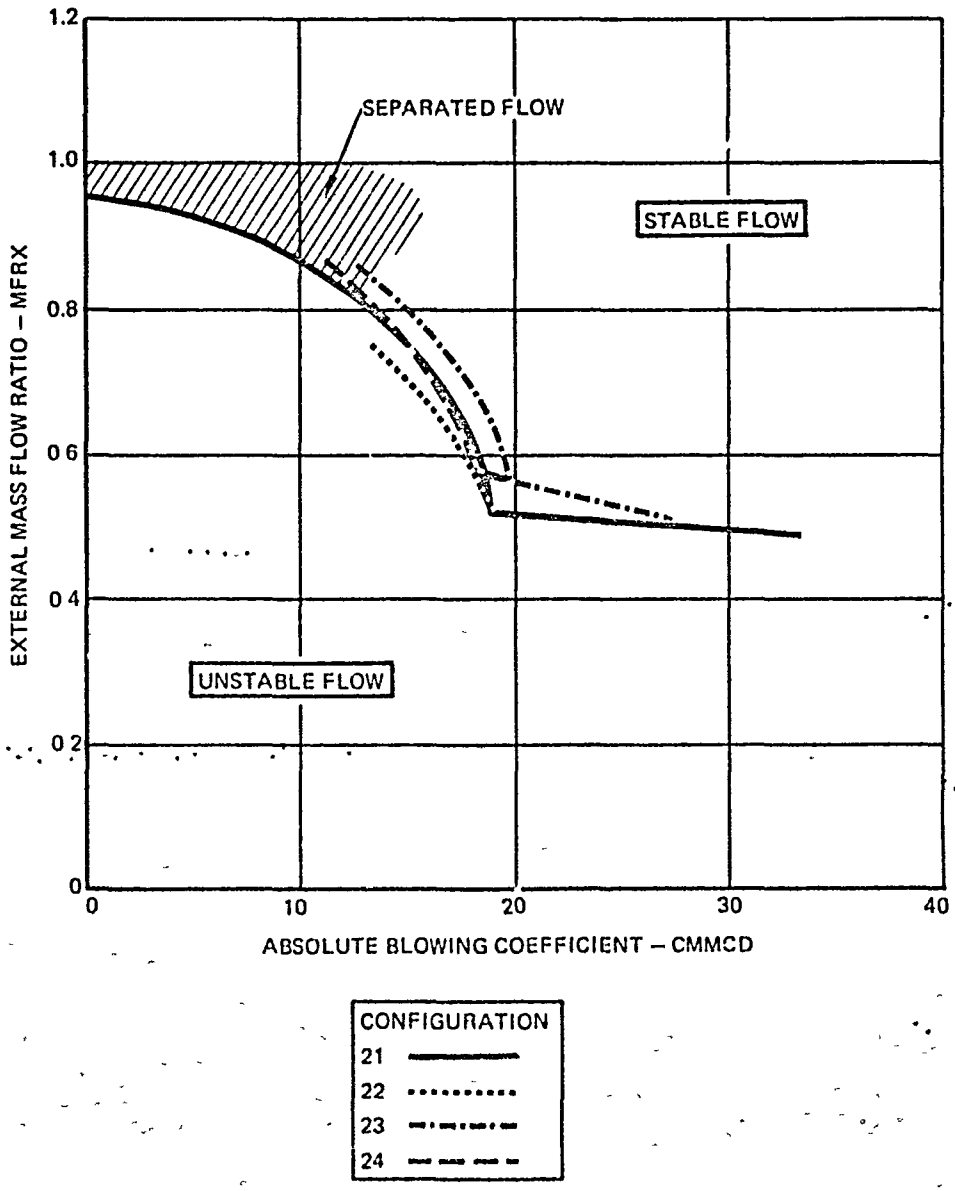

FIGURE 26. INLET STABILITY AT 1.76M, COLD FLOW

CONF	CMMCD	CMMCRD	BMFR	PPB	TTRC
○ 21	17.3	1.78	0.032	5 40	1.043
△ 22	14.9	1 40	0 027	4.47	1 030
□ 23	16.7	1.68	C030	4.94	1.037
◇ 24	15 6	1.22	0 029	3.01	1.047

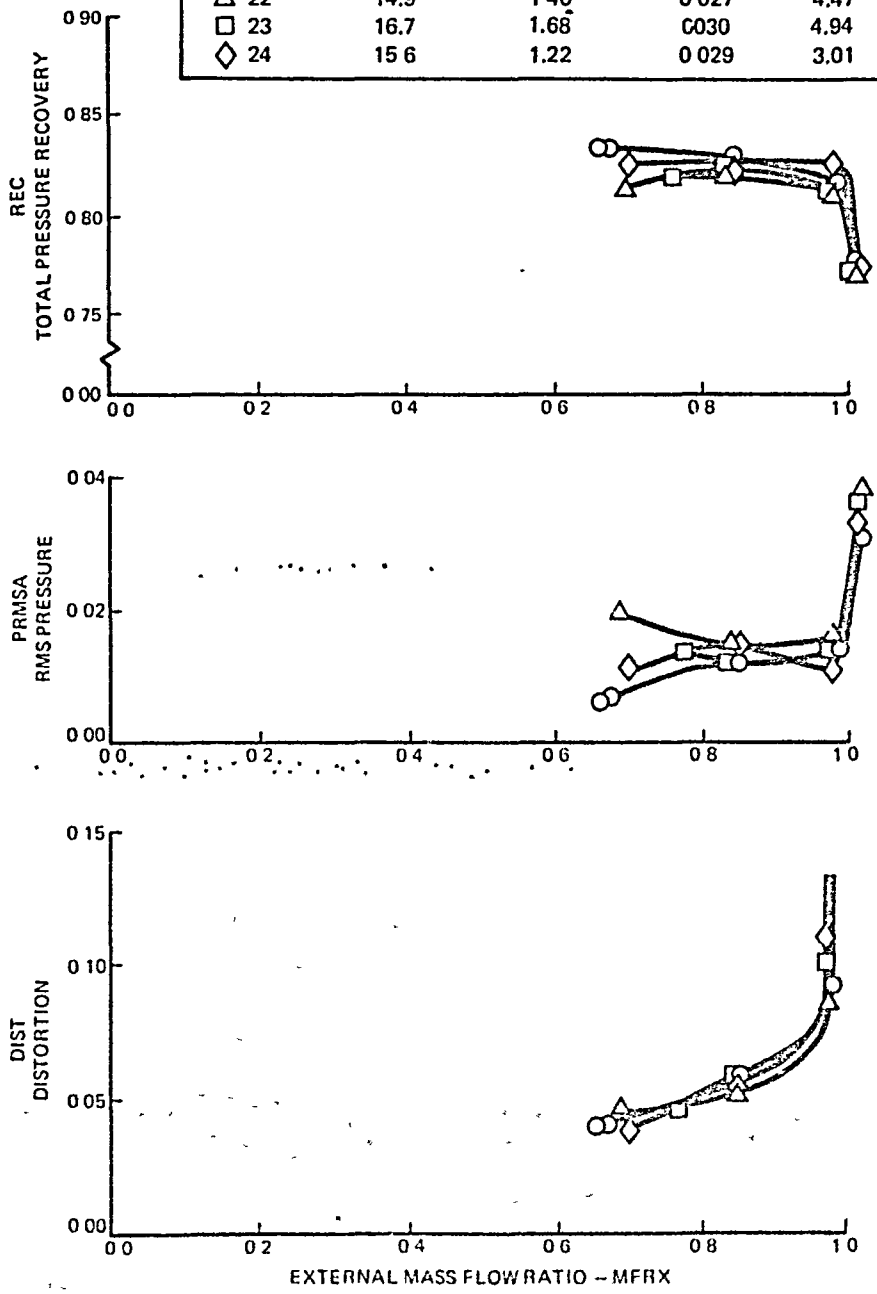

FIGURE 27. EFFECT OF BLOWING CONFIGURATION AT 1.76M, COLD FLOW

ORIGINAL PAGE IS
OF POOR QUALITY

CONF	CMMCD	CMMCRD	BMFR	PPB	TTRC
○ 21	24.7	2.94	0 044	7.42	1.058
△ 22	26 2	2.94	0 047	7.73	1.039
□ 23	26.8	3.01	0.048	7.76	1.040
◇ 24	25.6	2.36	0 047	4.74	1.029

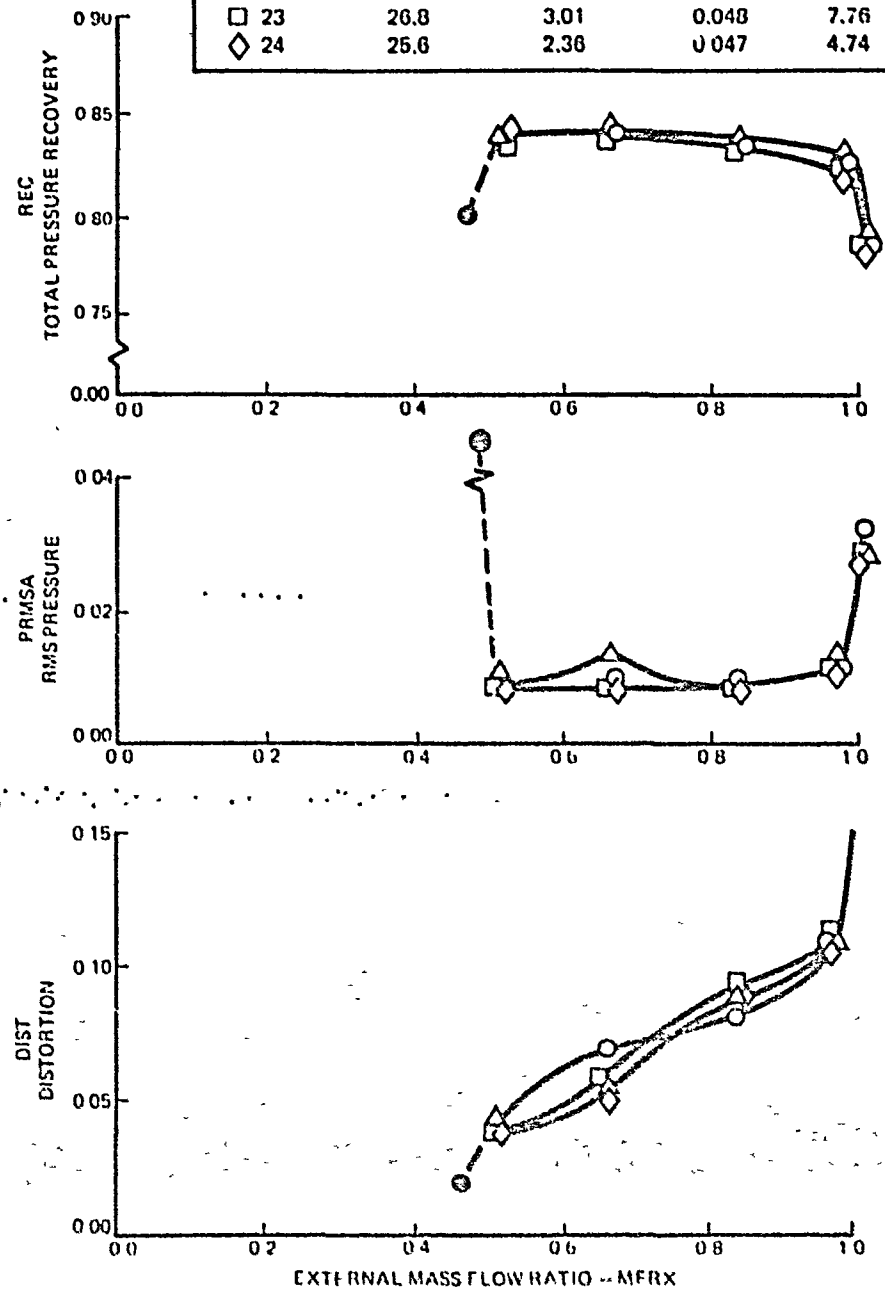

FIGURE 27 CONCLUDED.

ORIGINAL PAGE IS
OF POOR QUALITY

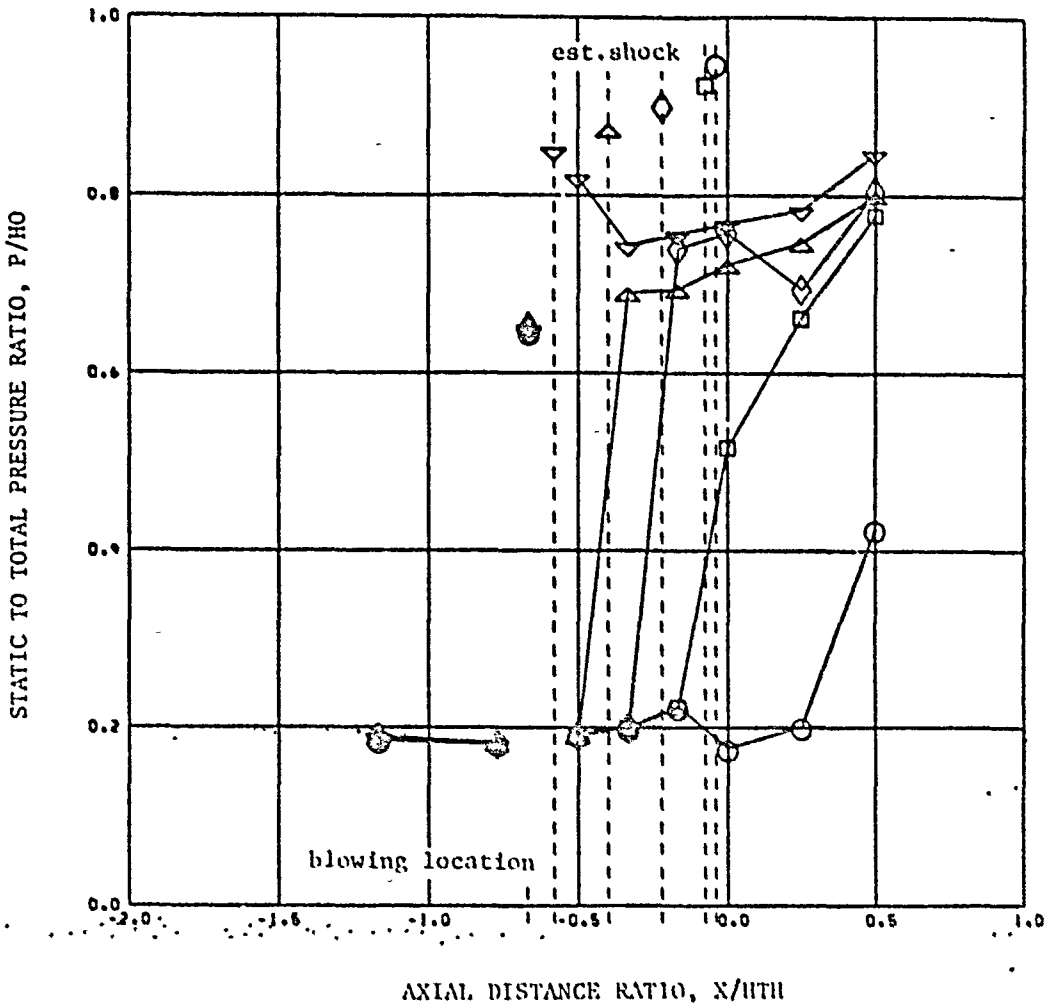

SYM	MFRX
○	1.001
□	0.968
◇	0.832
△	0.658
▽	0.470

FIGURE 28. EFFECT OF BLOWING LEVEL ON SHOCK PRESSURE RISE AT 1.76M, CONFIGURATION 21, CMMCD = 32.1, COLD FLOW

ORIGINAL PAGE IS
OF POOR QUALITY

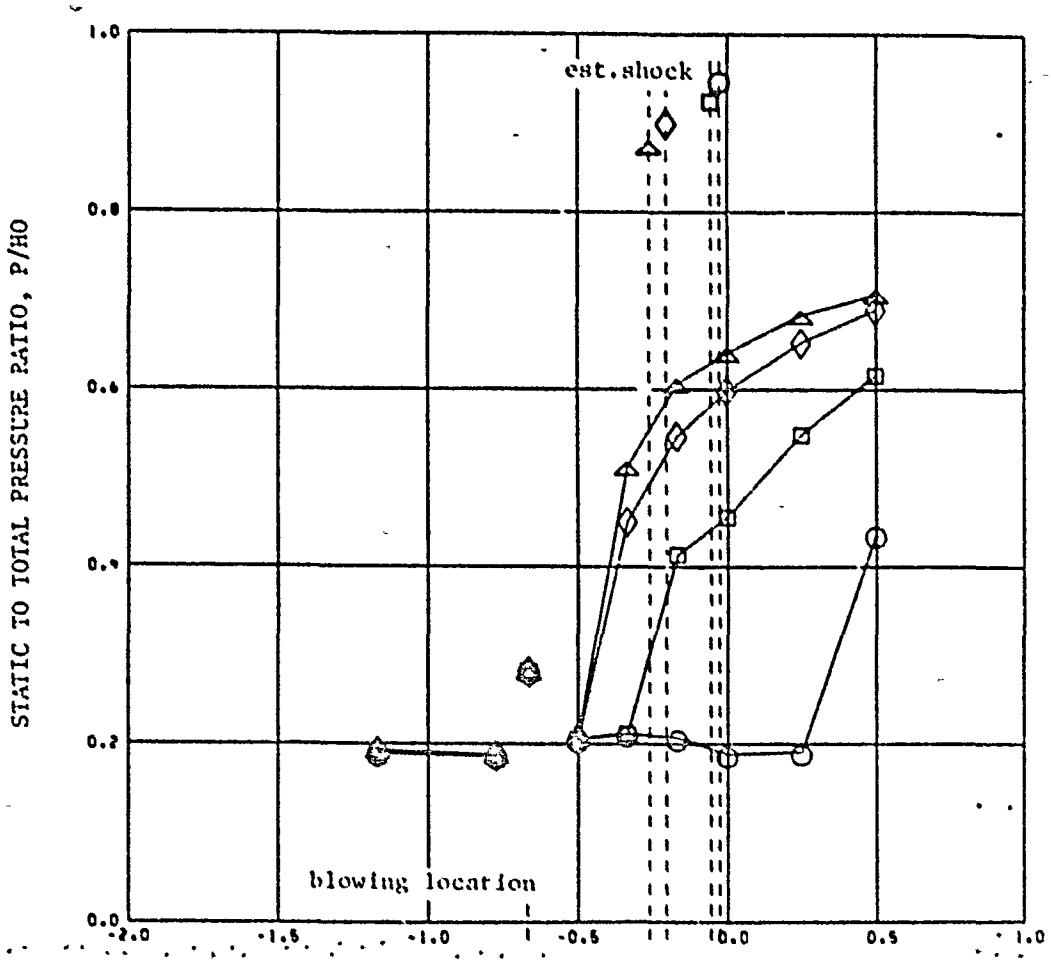

SYM	MFRX
○	1.013
□	0.987
◇	0.849
△	0.795

FIGURE 28 CONCLUDED. CONFIGURATION 21, 1.76M, CMMCD = 14.0, COLD FLOW

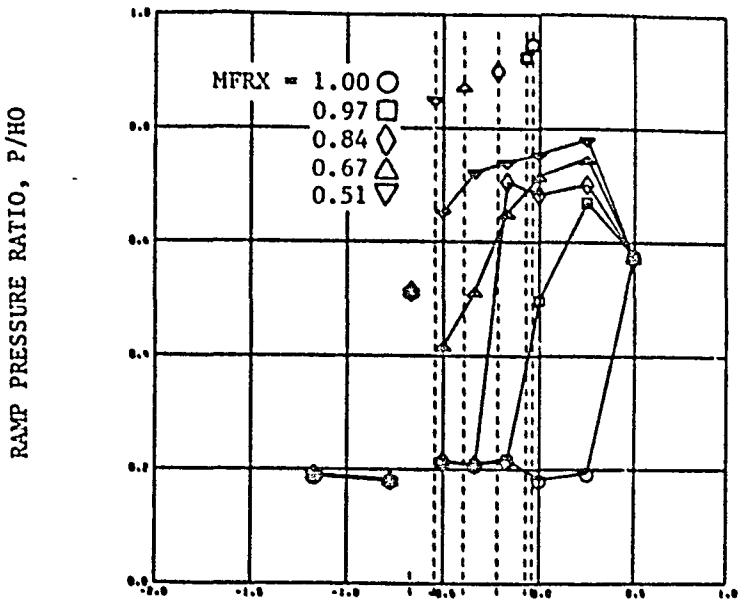

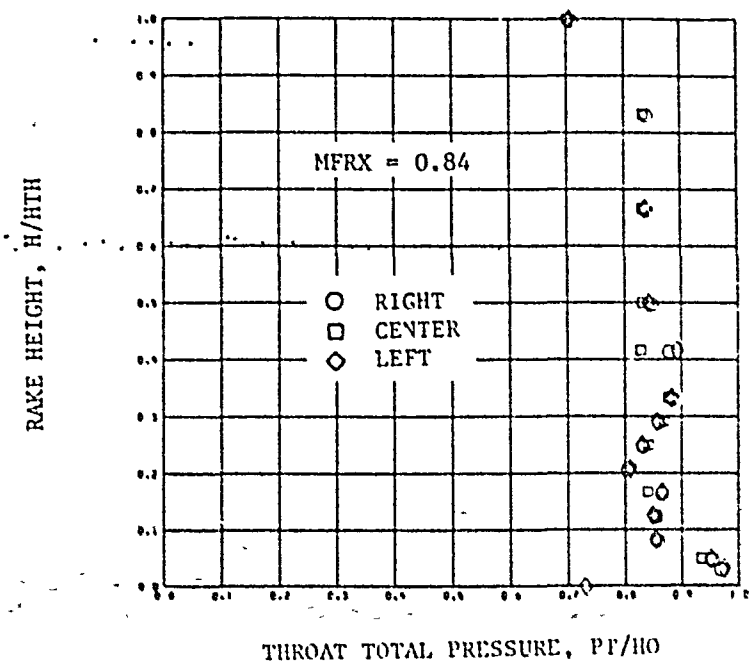

FIGURE 29. RAMP FLOW CHARACTERISTICS FOR CONFIGURATION 22 AT 1.76M CMMCD = 26.2

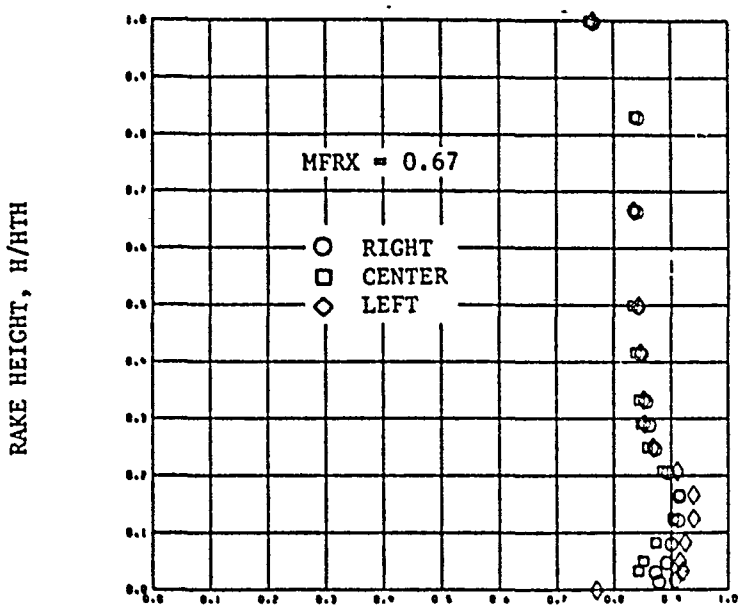

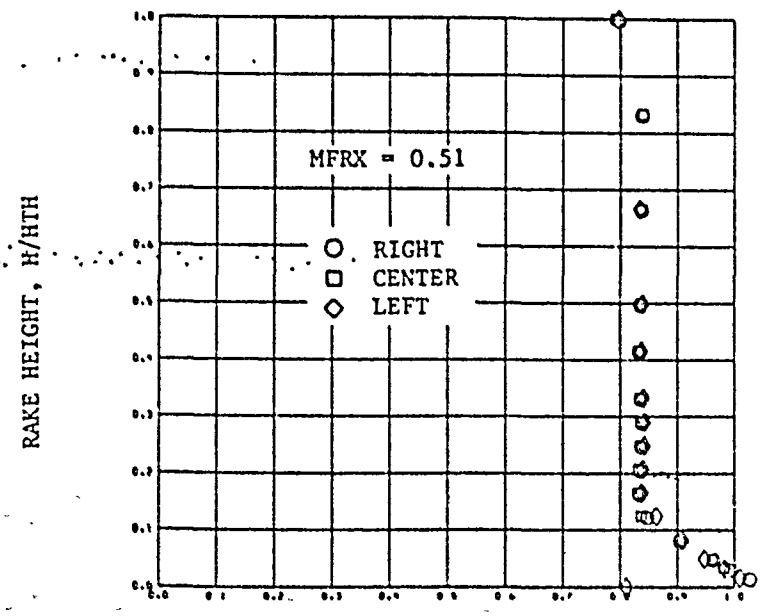

FIGURE 29. CONCLUDED

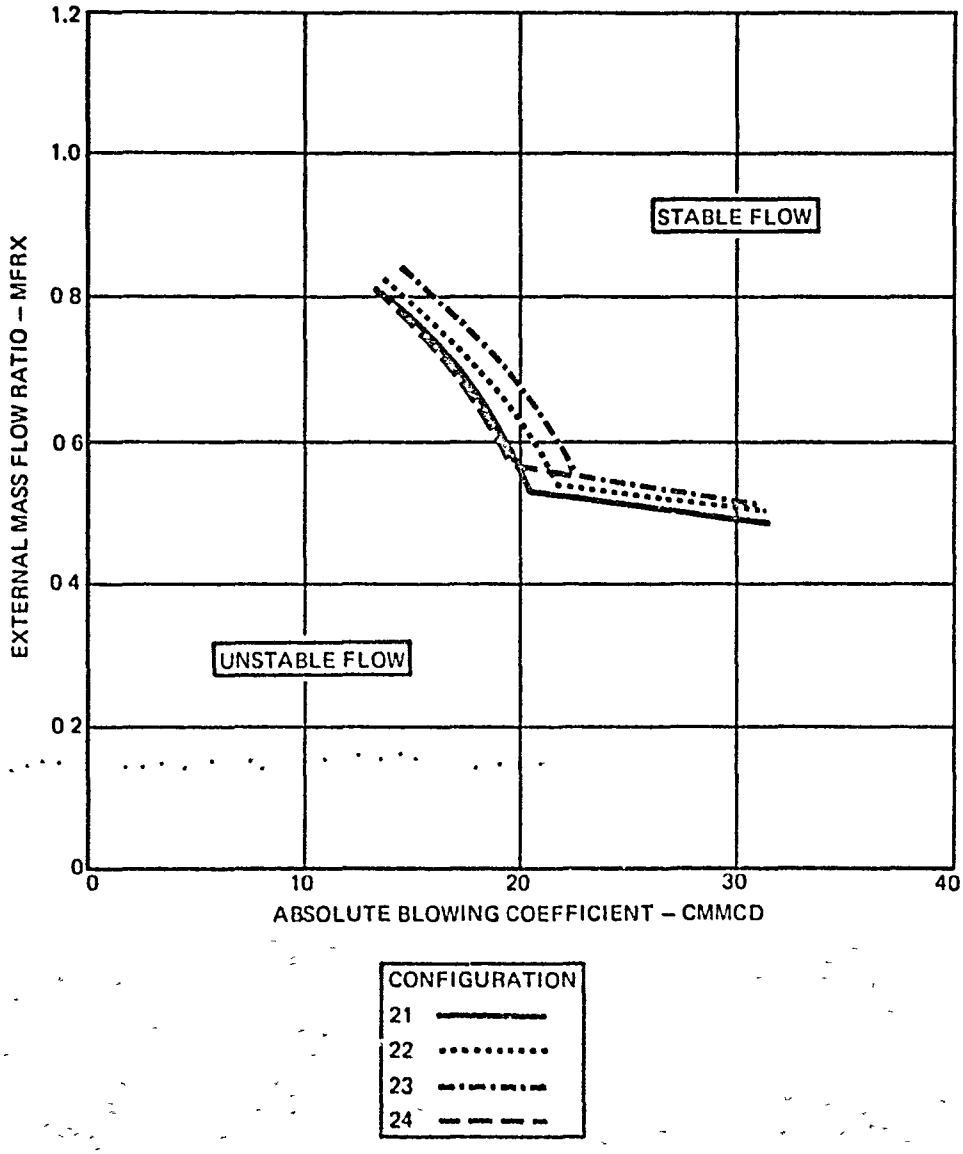

FIGURE 30. INLET STABILITY AT 1.76M, HOT FLOW

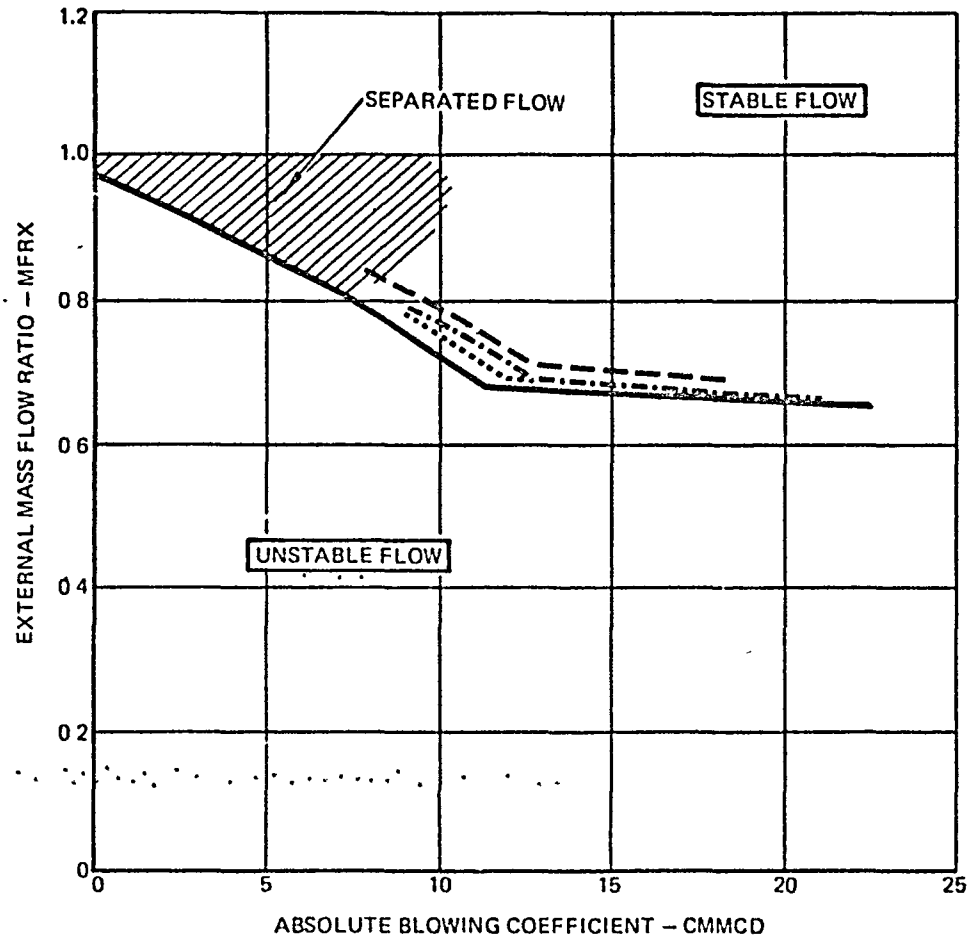

FIGURE 31. INLET STABILITY AT 1.56M, COLD FLOW

ORIGINAL PAGE IS
OF POOR QUALITY

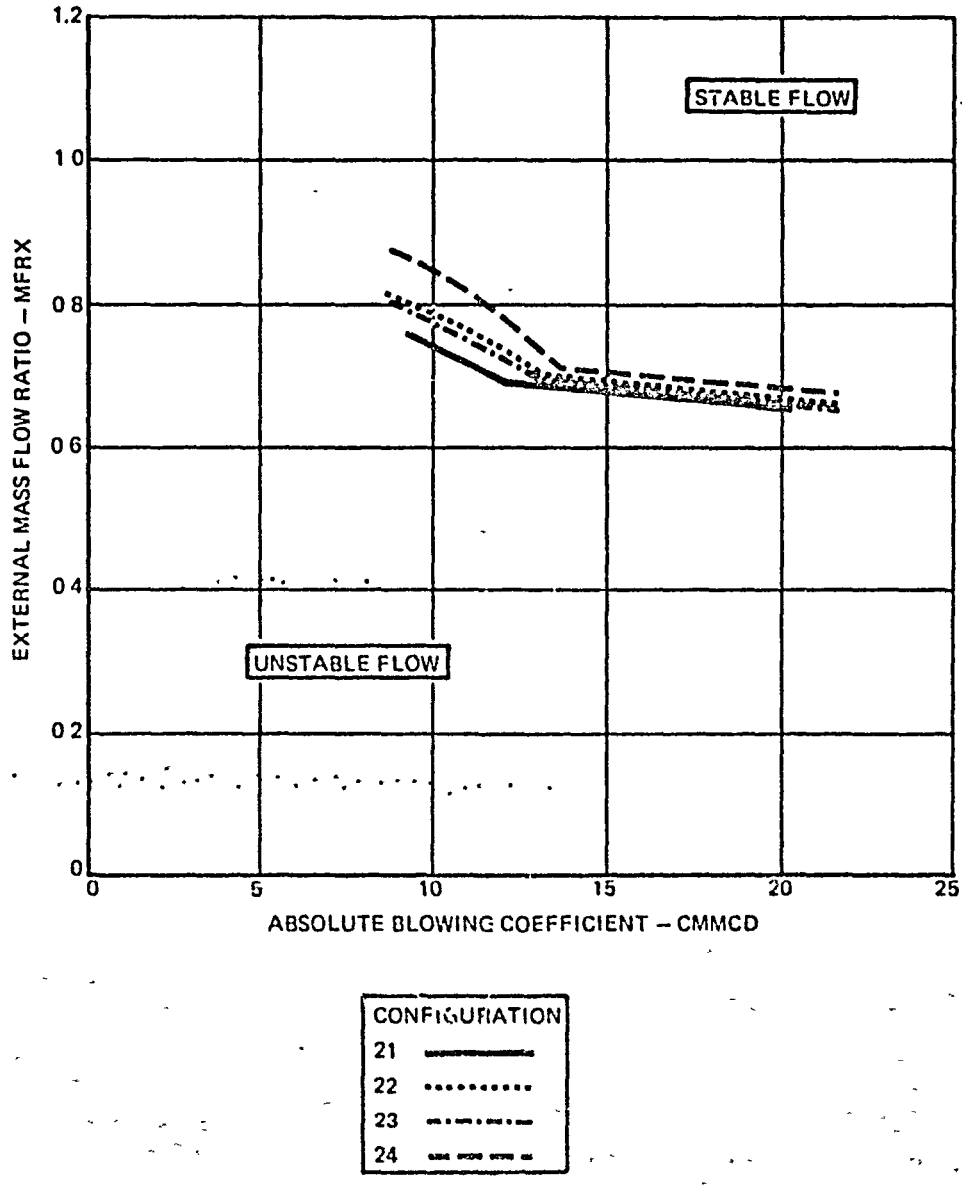

FIGURE 32. INLET STABILITY AT 1.56M, HOT FLOW

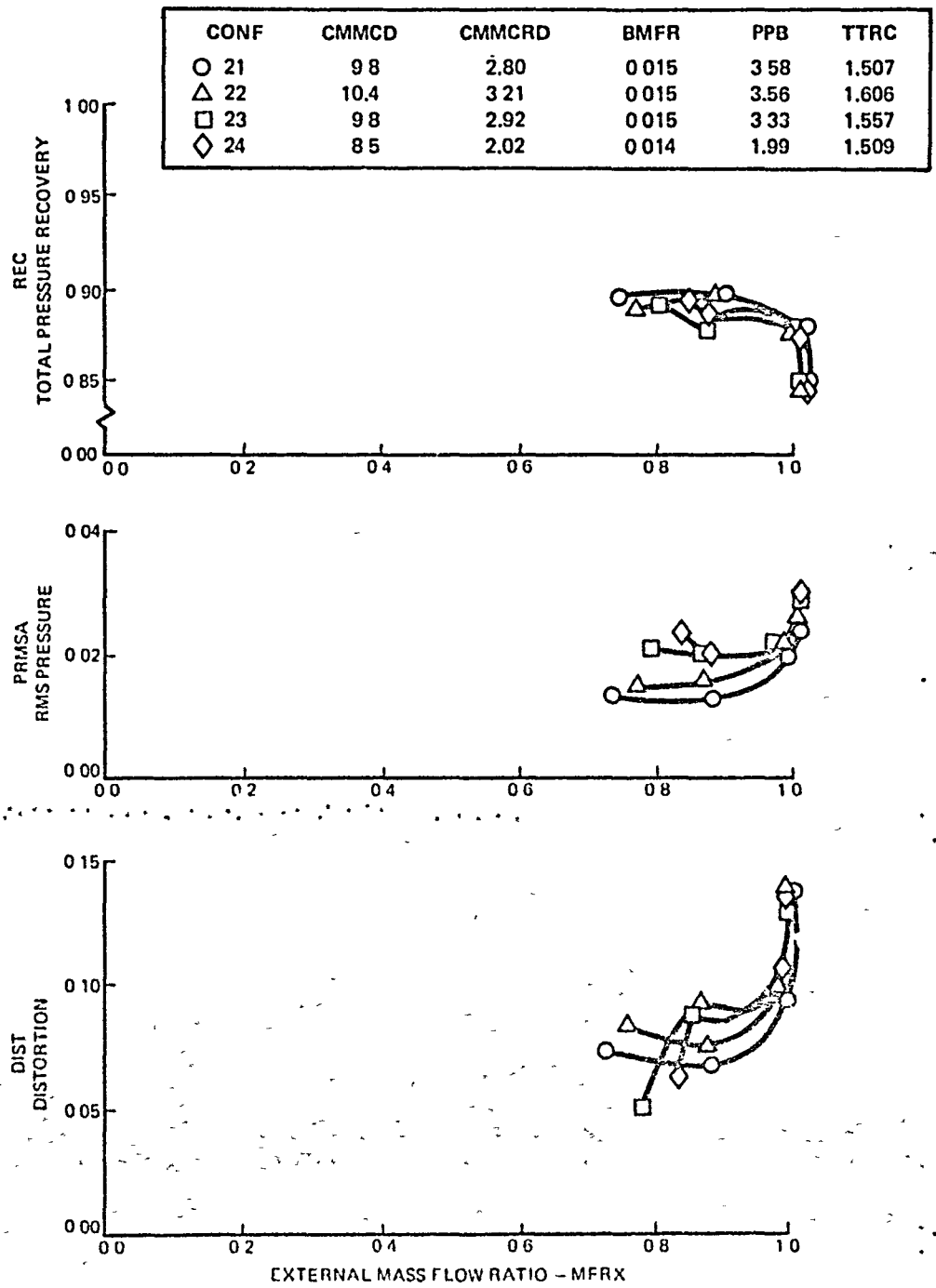

FIGURE 33. EFFECT OF BLOWING CONFIGURATION AT 1.56M, HOT FLOW

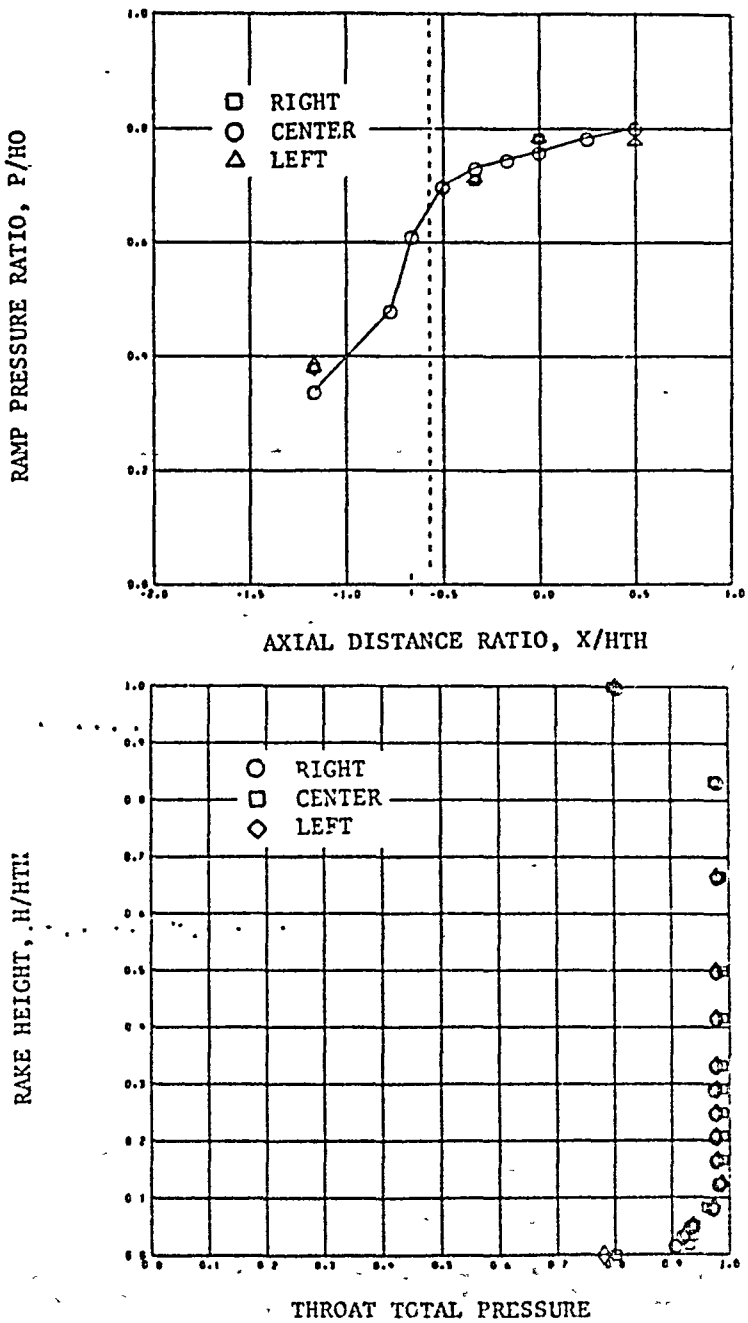

FIGURE 34. ATTACHED FLOW WITH PRESSURE RISE AHEAD OF BLOWING STATION AT 1.36M, CONFIGURATION 21, CMMCD = 11.0, MFRX = 0.78

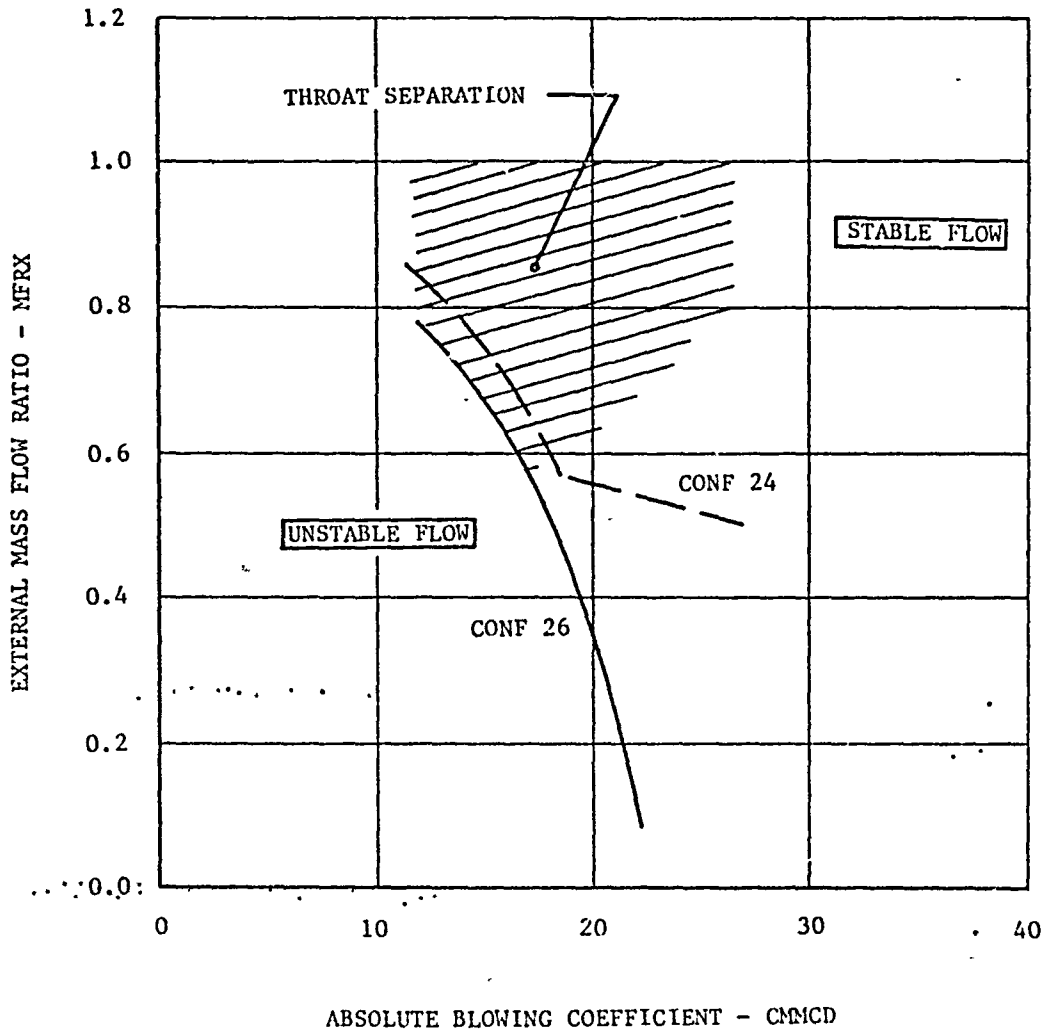

FIGURE 35. INLET STABILITY WITH SHORT COWL, CONFIGURATION 26, AT 1.76M, COLD FLOW

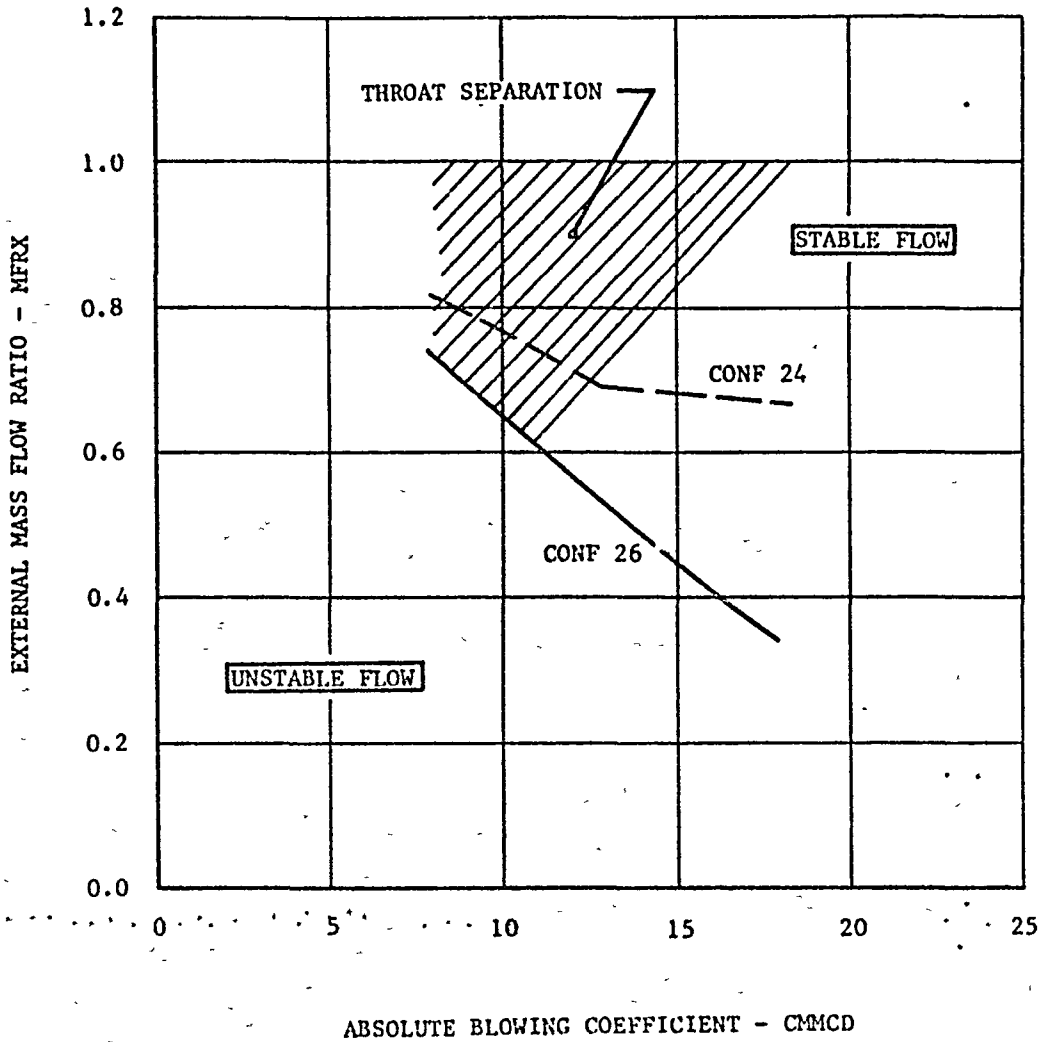

FIGURE 36. INLET STABILITY WITH SHORT COWL, CONFIGURATION 26, AT 1.56M, COLD FLOW

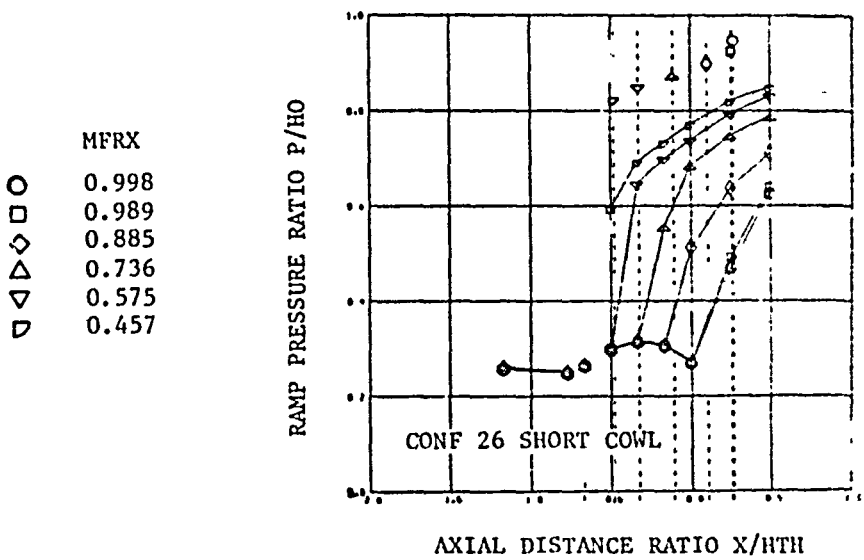

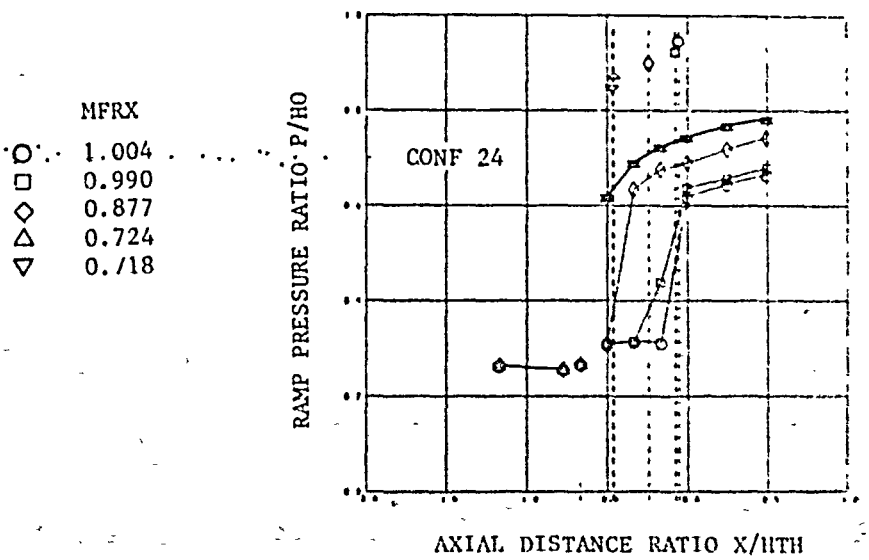

FIGURE 37. RAMP PRESSURES PRIOR TO FLOW BREAKDOWN AT 1.56M
CONFIGURATIONS 24 AND 26, CMMCD = 14.7

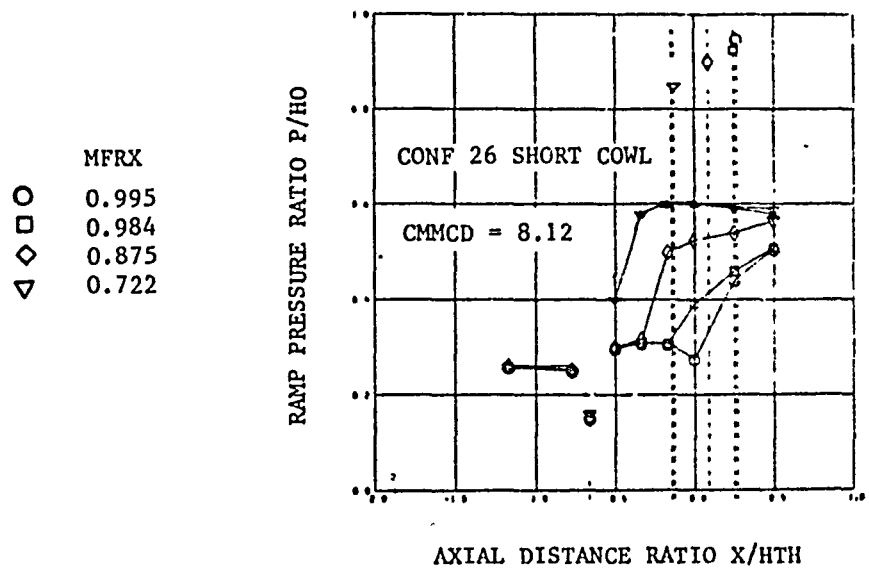

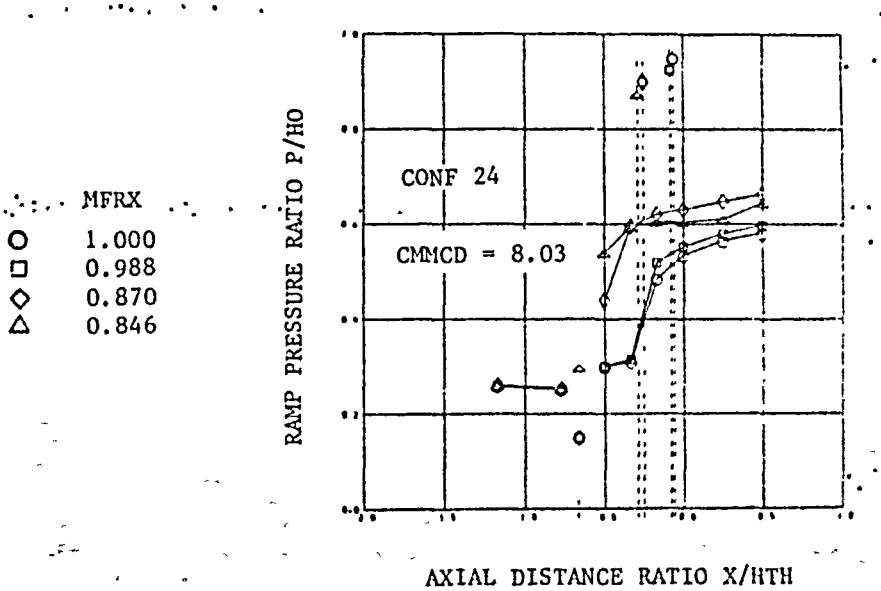

FIGURE 38. RAMP PRESSURES PRIOR TO FLOW BREAKDOWN AT 1.56M
CONFIGURATIONS 24 AND 26, CMMCD = 8.0

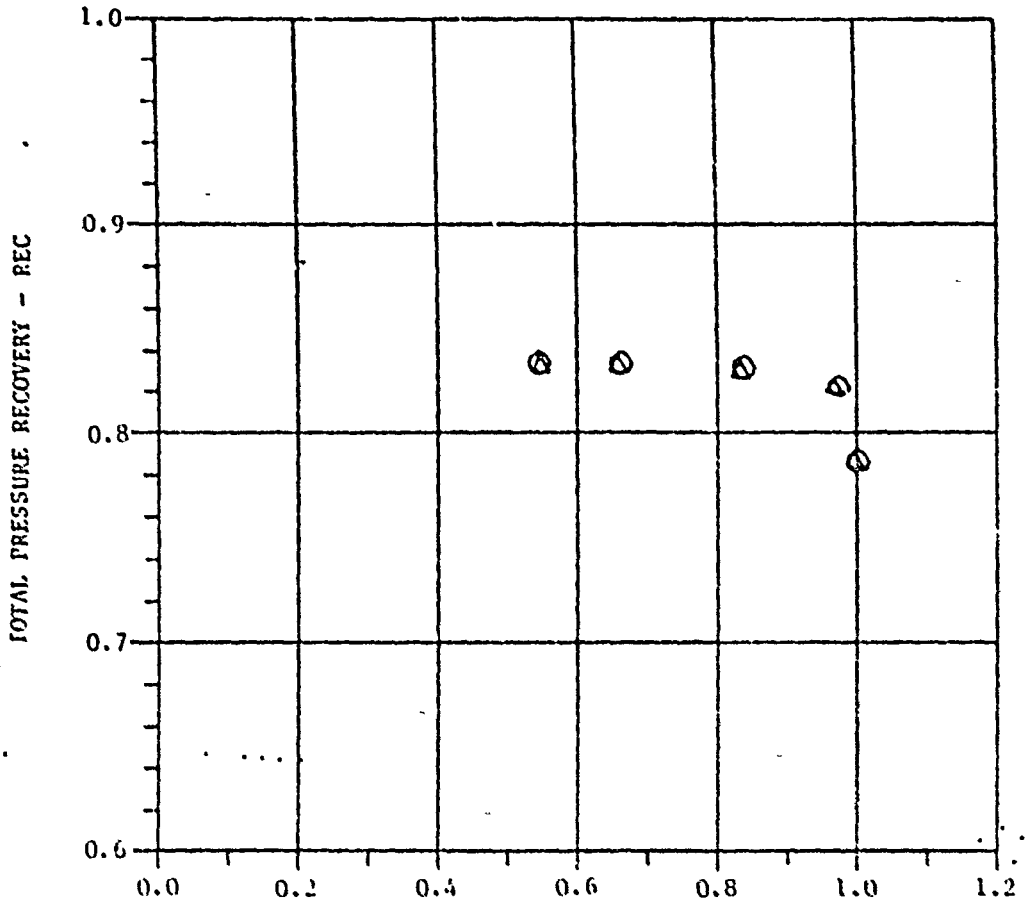

MACH • 1.77 CONF • 83

SYM	CRRCD	CRRCRD	BMFR	PFB	TTRC
○	80.7	8.38	0.041	6.60	1.084
△	84.6	6.09	0.035	7.80	1.092

FIGURE 39. EFFECT OF BLOWING AIR TEMPERATURE ON CONFIGURATION 23 AT 1.77M, HIGH BLOWING LEVEL

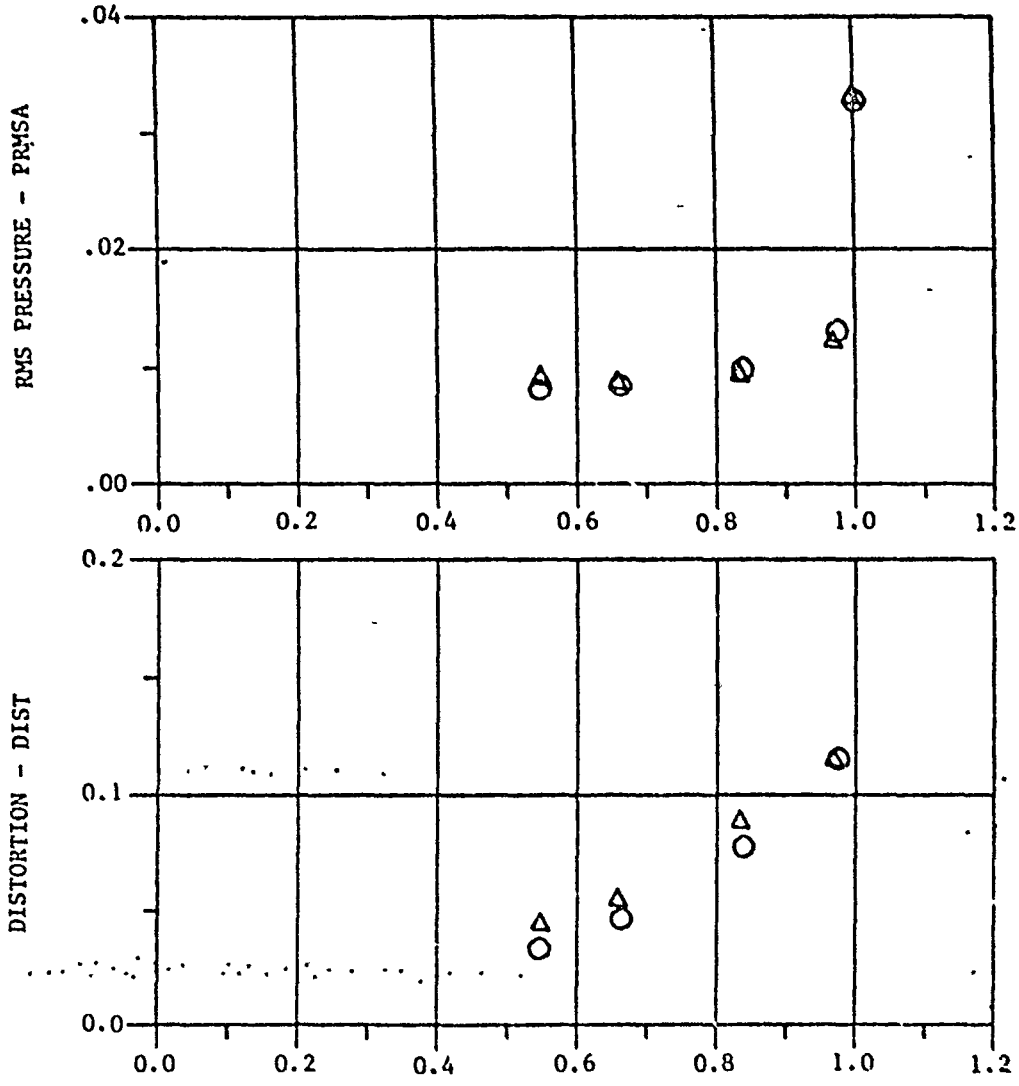

SYM	CORCD	CORCRD	DMFR	PPB	TTRC
○	88.7	0.33	0.041	6.62	1.004
△	84.6	0.09	0.035	7.80	1.008

FIGURE 39. CONCLUDED

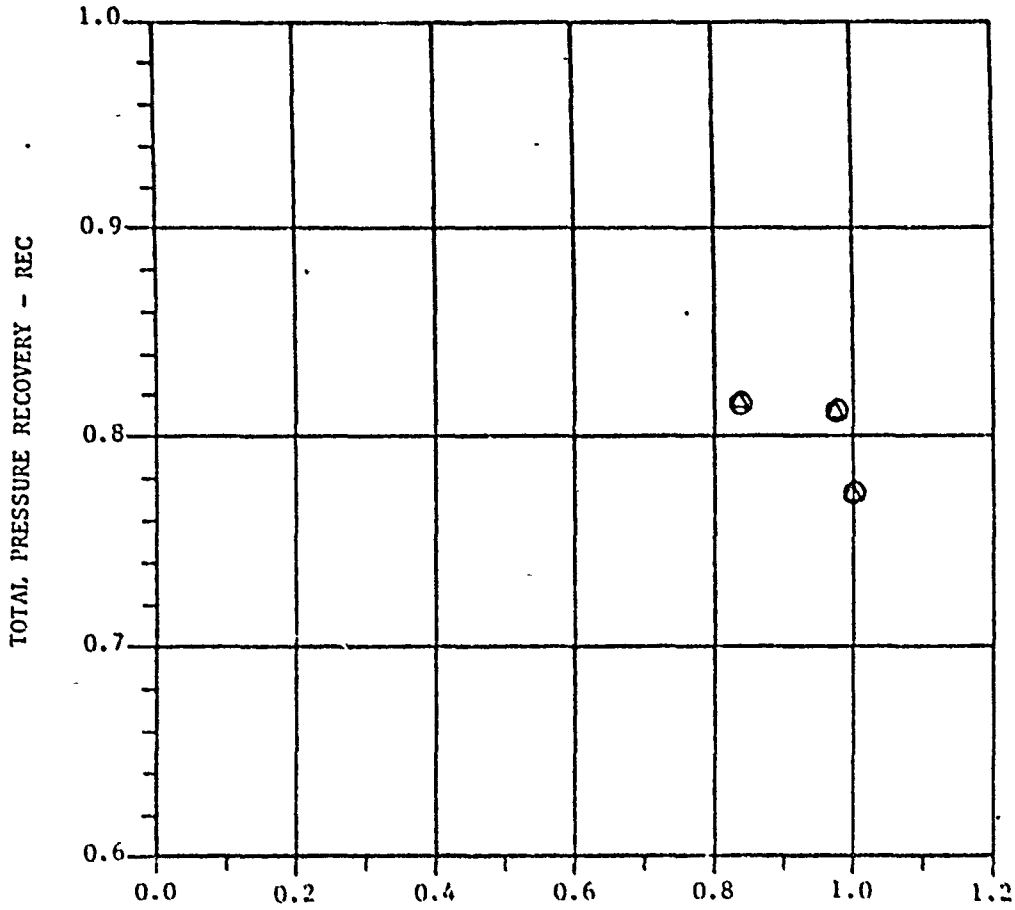

MACH = 1.77 CONF = 83

SYM	CRNCD	CRNCRD	BMFR	PPB	TTRC
○	13.6	1.89	0.000	4.04	1.049
△	14.7	3.89	0.033	4.49	1.096

FIGURE 40. EFFECT OF BLOWING AIR TEMPERATURE ON CONFIGURATION 23 AT 1.77M, LOW BLOWING LEVEL

ORIGINAL PAGE IS
OF POOR QUALITY

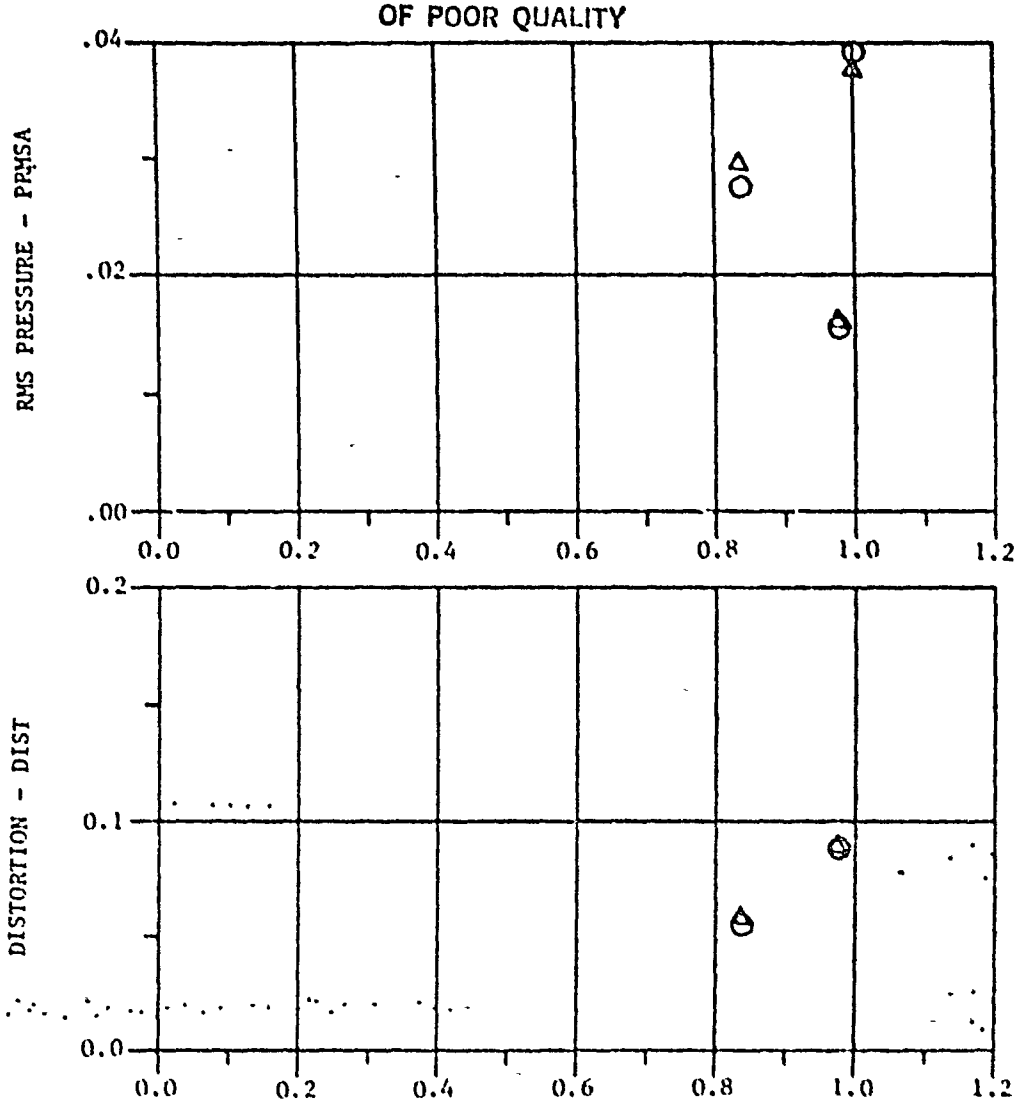

EXTERNAL MASS FLOW RATIO - MFRX

SYM	CRNCD	CRNCRD	DNFR	PPB	TTRC
○	13.0	1.85	0.008	4.04	1.040
△	14.7	3.69	0.003	4.40	1.038

FIGURE 40. CONCLUDED

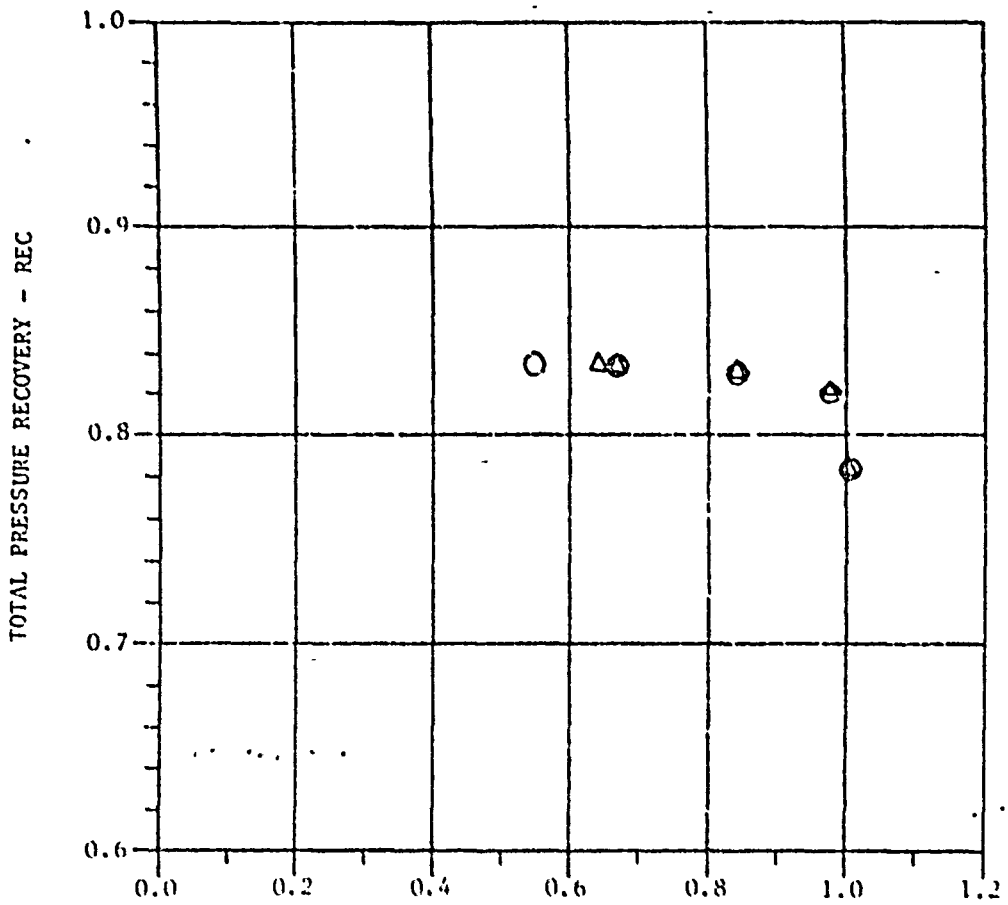

MACH = 1.76 CONF = 22

SYM	CMMCD	CMMCRD	DMFR	PPB	TTRC
○	18.8	1.83	0.034	5.55	1.035
△	19.0	5.35	0.038	5.82	1.030

FIGURE 41. EFFECT OF BLOWING AIR TEMPERATURE ON CONFIGURATION 22 AT 1.76M, CMMCD = 19

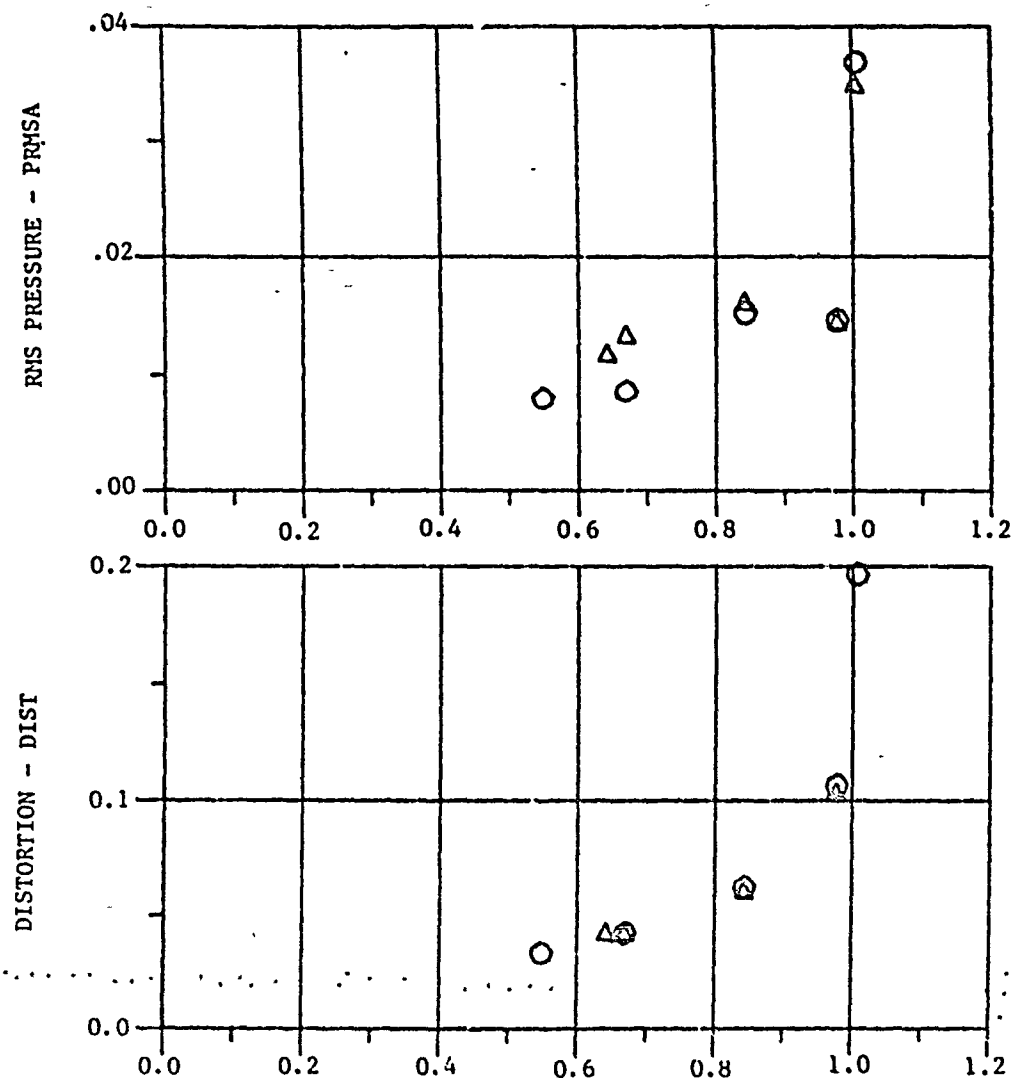

SYM	CORCD	CORCRD	DRFR	PPB	TTRC
○	10.6	1.83	0.034	5.66	1.635
△	10.6	5.35	0.039	5.03	1.609

FIGURE 41. CONCLUDED

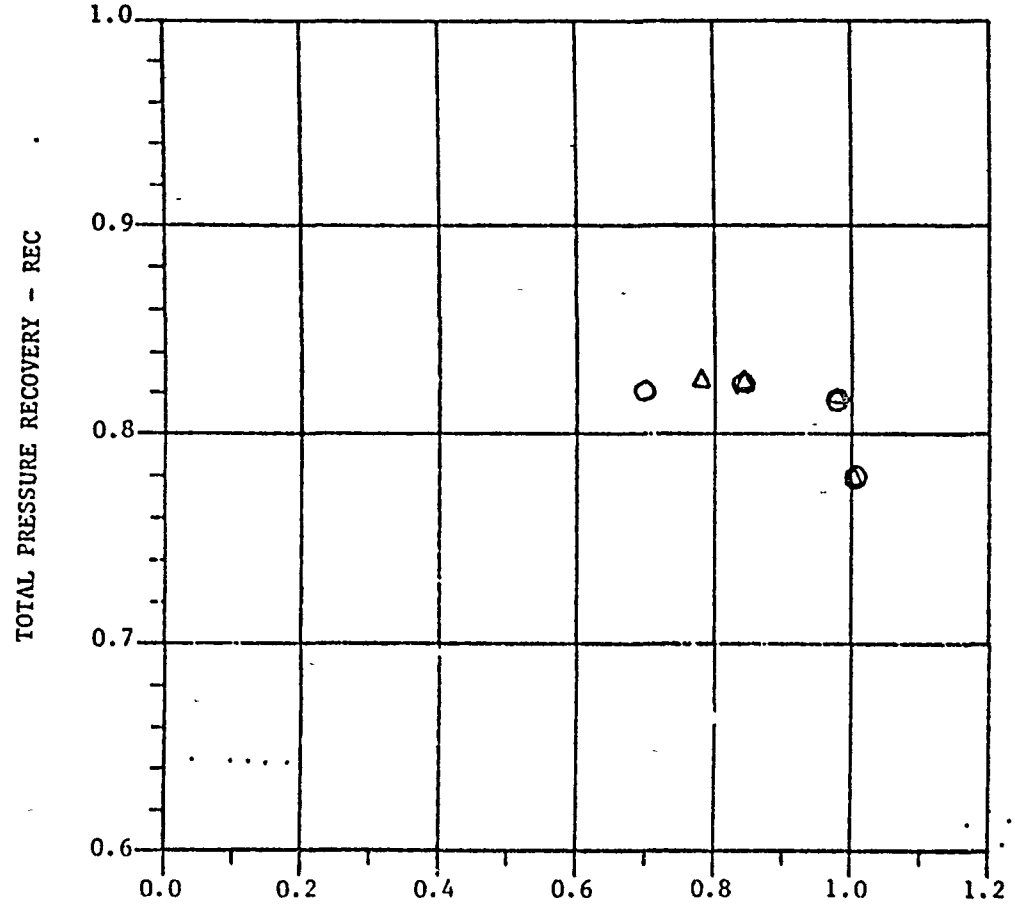

MACH = 1.76 CONF = 22

SYM	CMMCD	CMMCRD	BRFR	PPB	TTRC
○	14.9	1.49	0.687	4.47	1.030
△	14.8	3.88	0.683	4.46	1.558

FIGURE 42. EFFECT OF BLOWING AIR TEMPERATURE ON CONFIGURATION 22 AT 1.76M, CMMCD = 15

ORIGINAL PAGE IS
OF POOR QUALITY

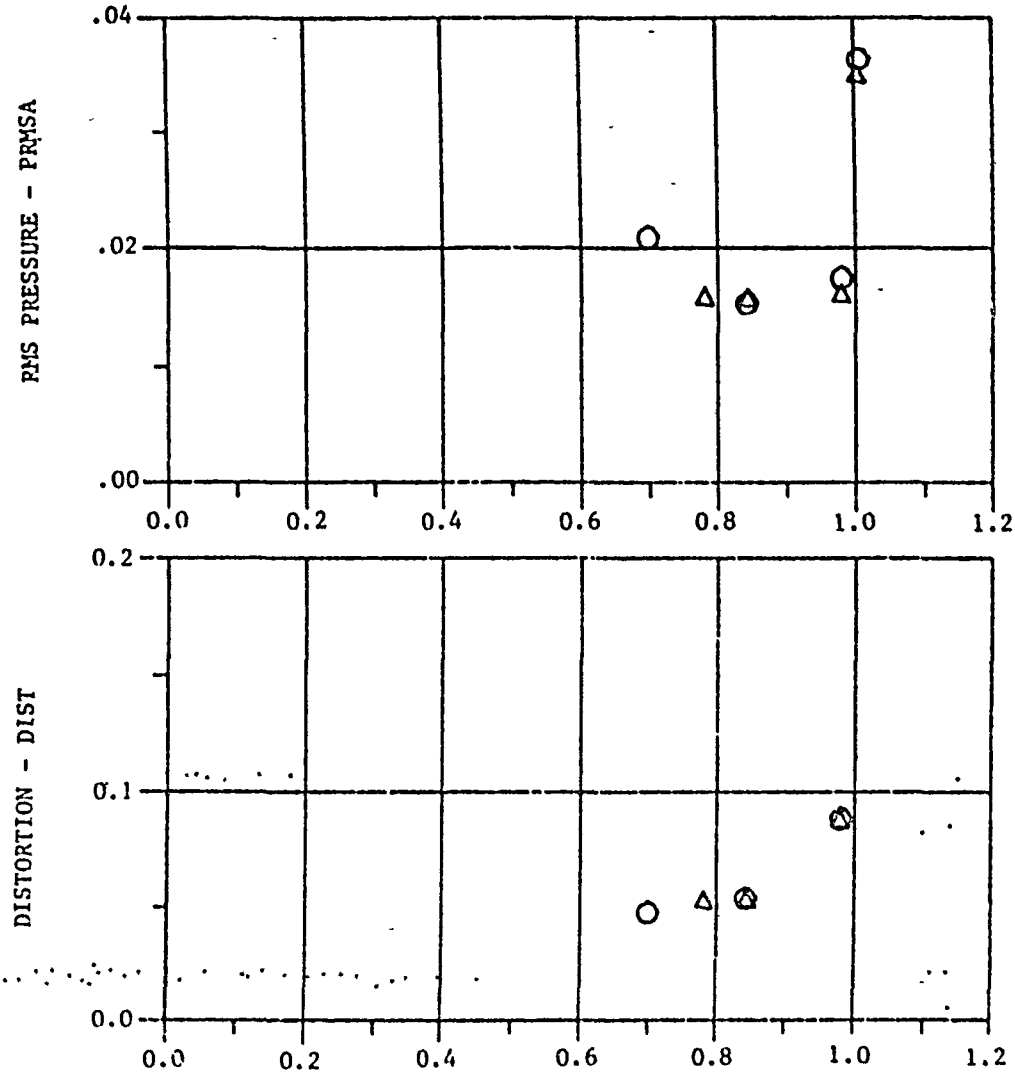

SYM	CNFGD	CNFGRD	DIFR	PPB	TTRC
○	14.9	1.48	0.037	4.47	1.039
△	14.0	3.68	0.038	4.46	1.068

FIGURE 42. CONCLUDED

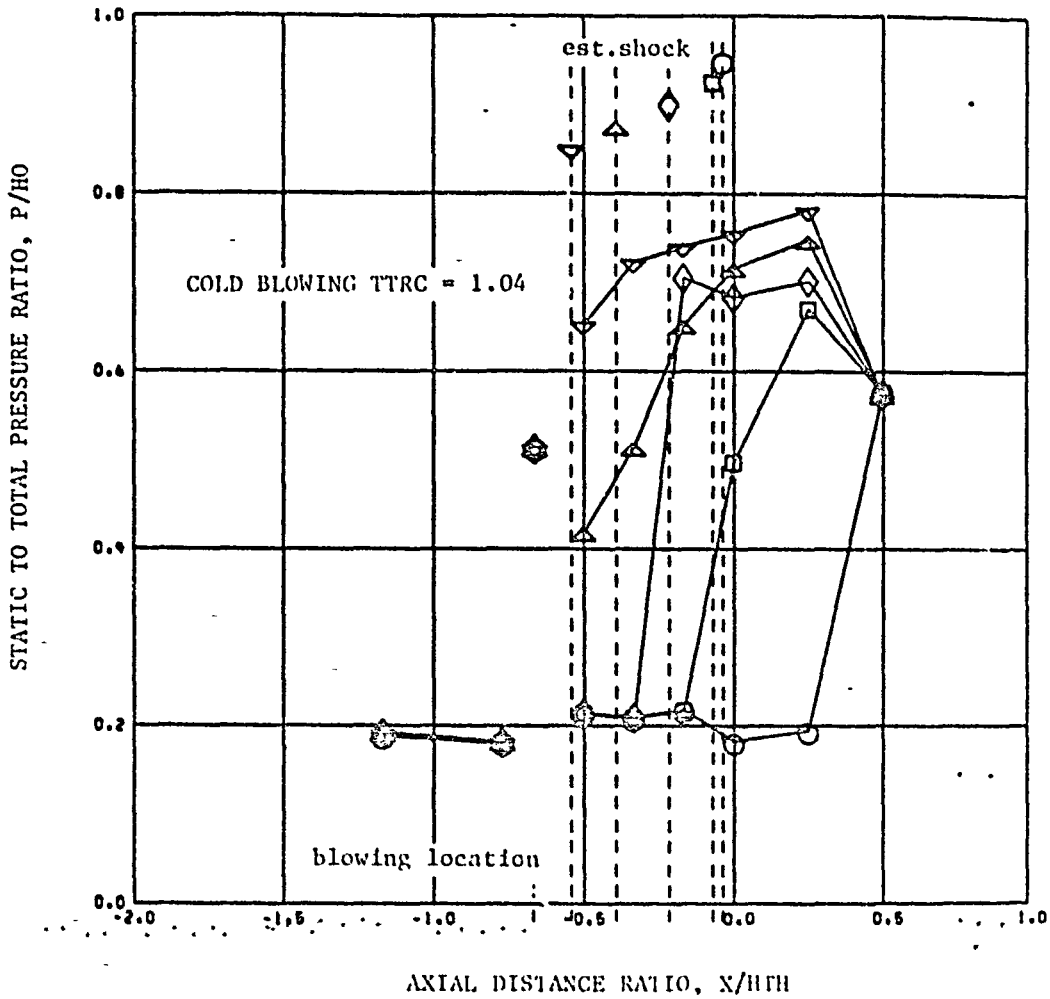

FIGURE 43. EFFECT OF BLOWING AIR TEMPERATURE ON RAMP PRESSURE DISTRIBUTION FOR CONFIGURATION 22, 1.76M, CMMCD = 26.2

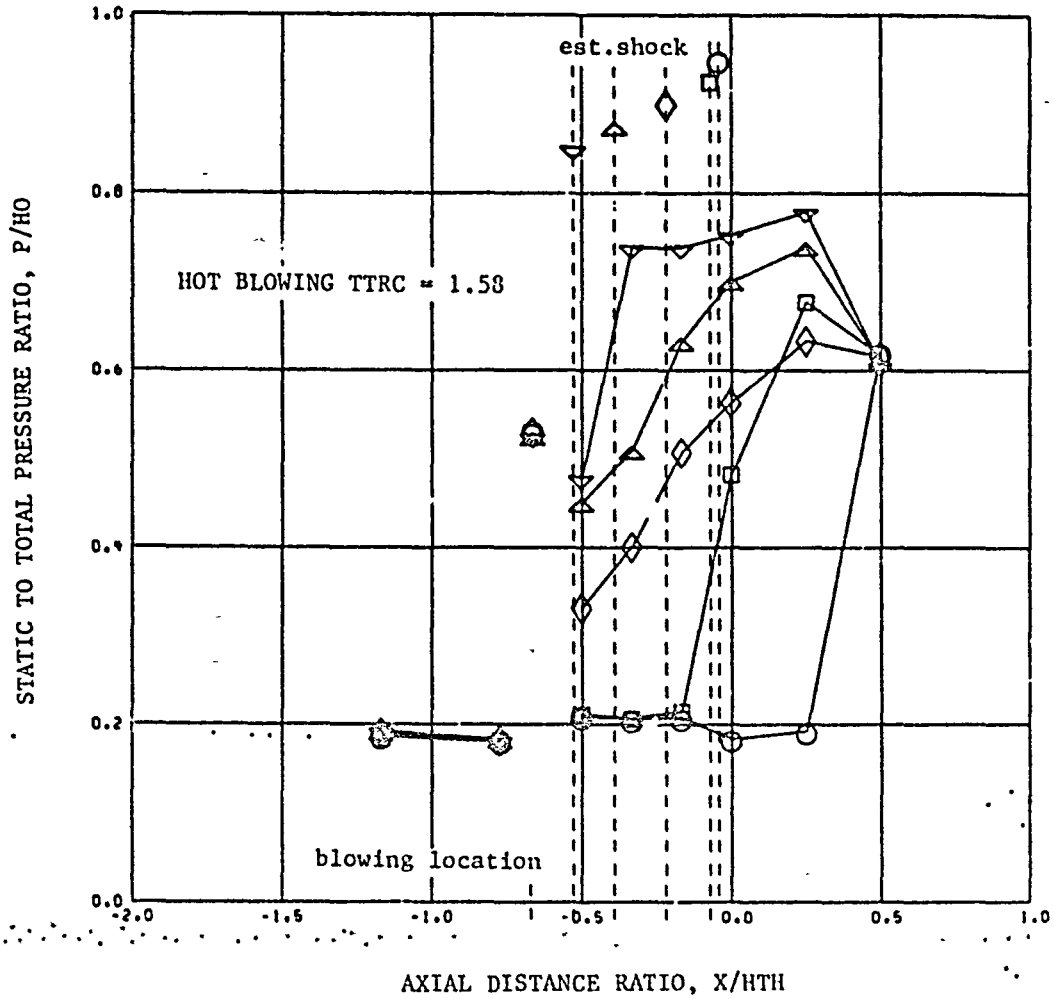

SYM	MFRX
○	1.000
□	0.974
◇	0.835
△	0.666
▽	0.526

FIGURE 43 CONCLUDED. CONFIGURATION 22, 1.76M, CMMCD = 26.2

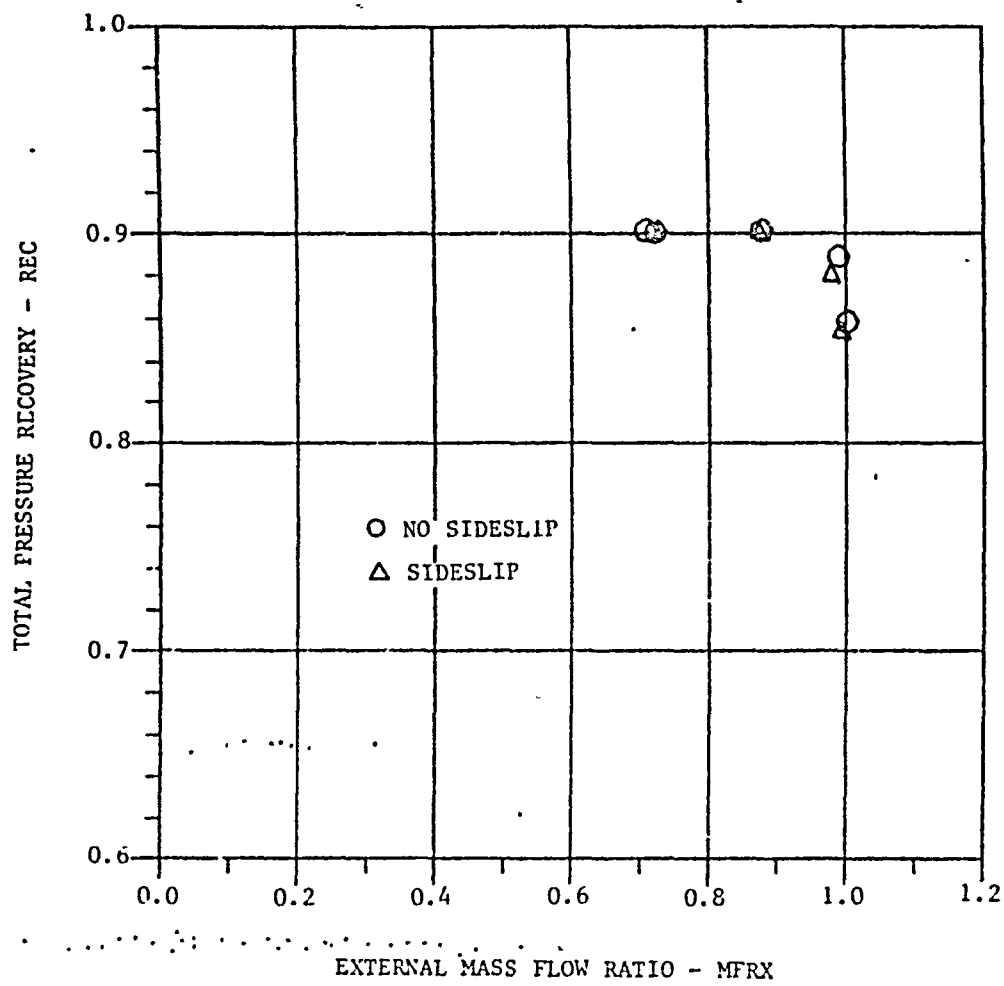

MACH • 1.56 CONF • 24

SYM	CMMCD	CMMCRD	BMFR	PPB	TTRC
O	14.7	1.56	0.027	3.15	1.050
Δ	14.7	1.52	0.037	3.13	1.030

FIGURE 44. TYPICAL EFFECT OF FIVE DEGREES SIDESLIP ON INLET PERFORMANCE

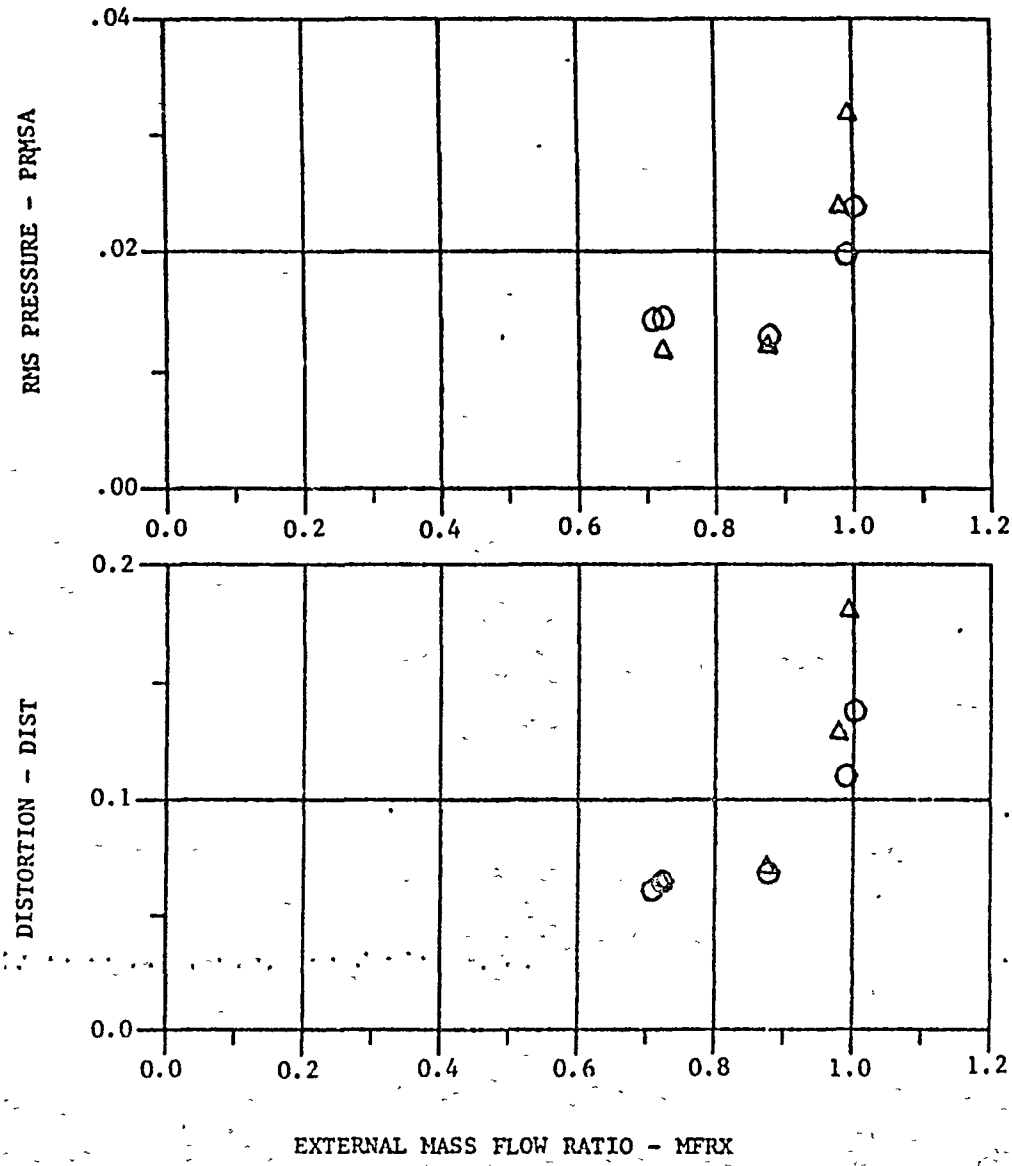

FIGURE 44 CONCLUDED. CONFIGURATION 24, 1.56M, CYMCD = 14.7, COLD FLOW.

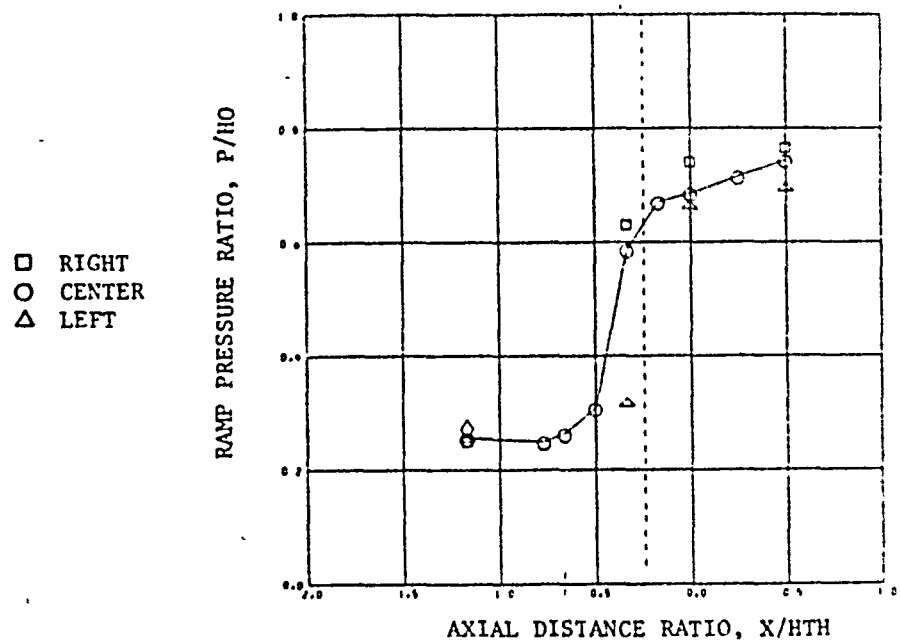

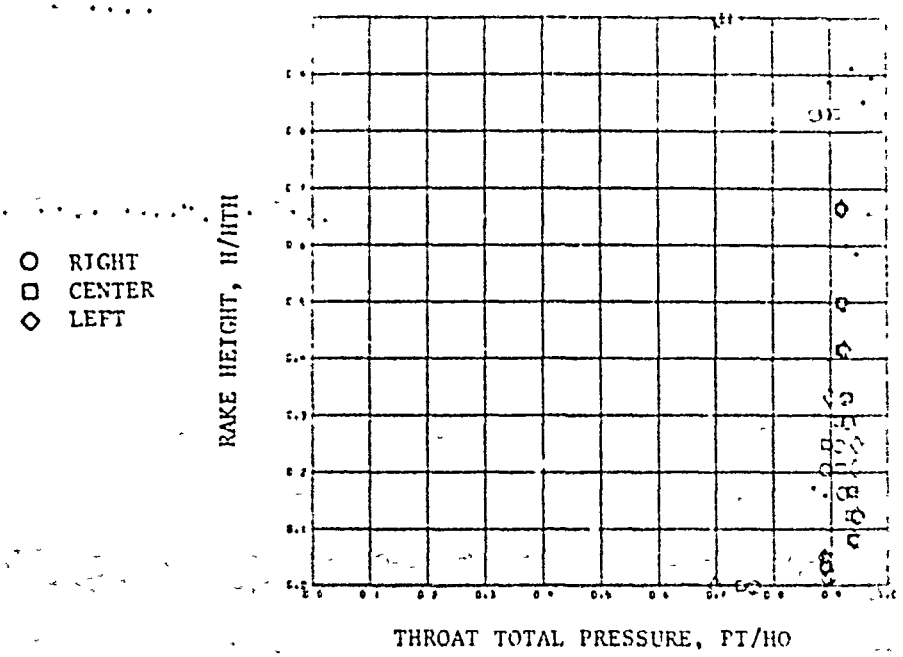

FIGURE 45. EFFECT OF FIVE DEGREES OF SIDESLIP ON INLET PRESSURES CONFIGURATION 24, CYNCD = 14.7, COLD FLOW, MFRX = 0.875

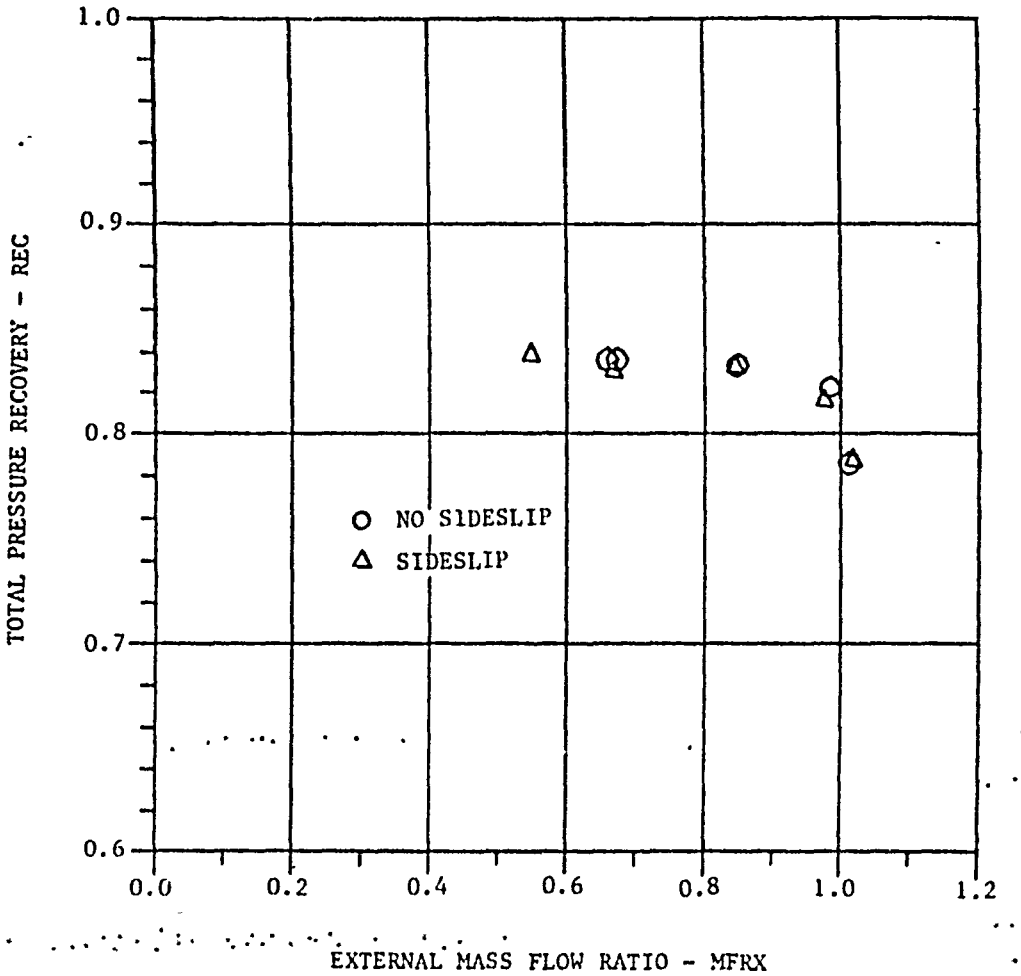

SYM	CMMCD	CMMCRD	EMFR	PPB	TTRC
○	17.3	1.78	0.038	5.40	1.043
△	17.4	1.87	0.038	6.44	1.025

FIGURE 46. ANOMALOUS BEHAVIOR OF CONFIGURATION 21 AT SIDESLIP, 1.77M, CMMCD = 17.4, COLD FLOW

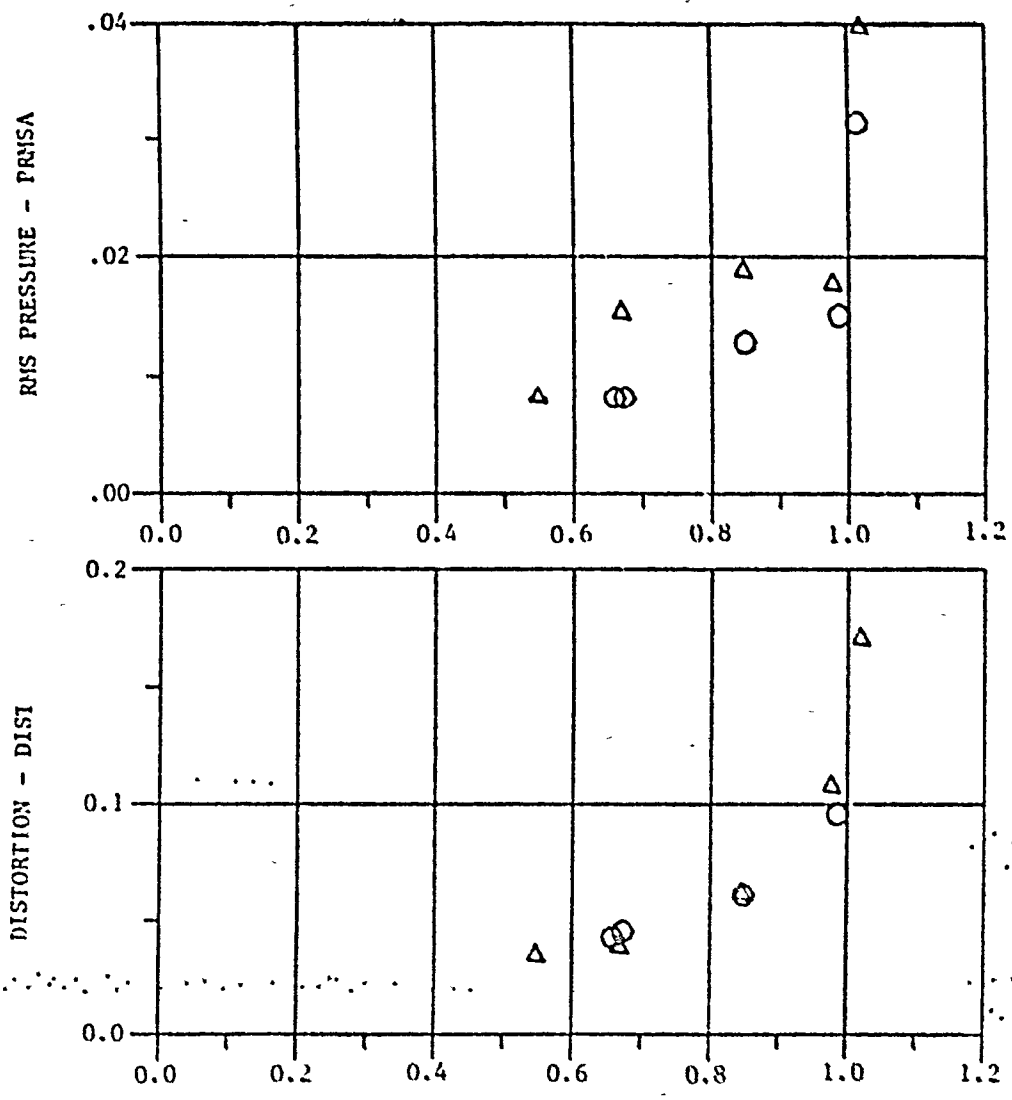

FIGURE 46. CONCLUDED

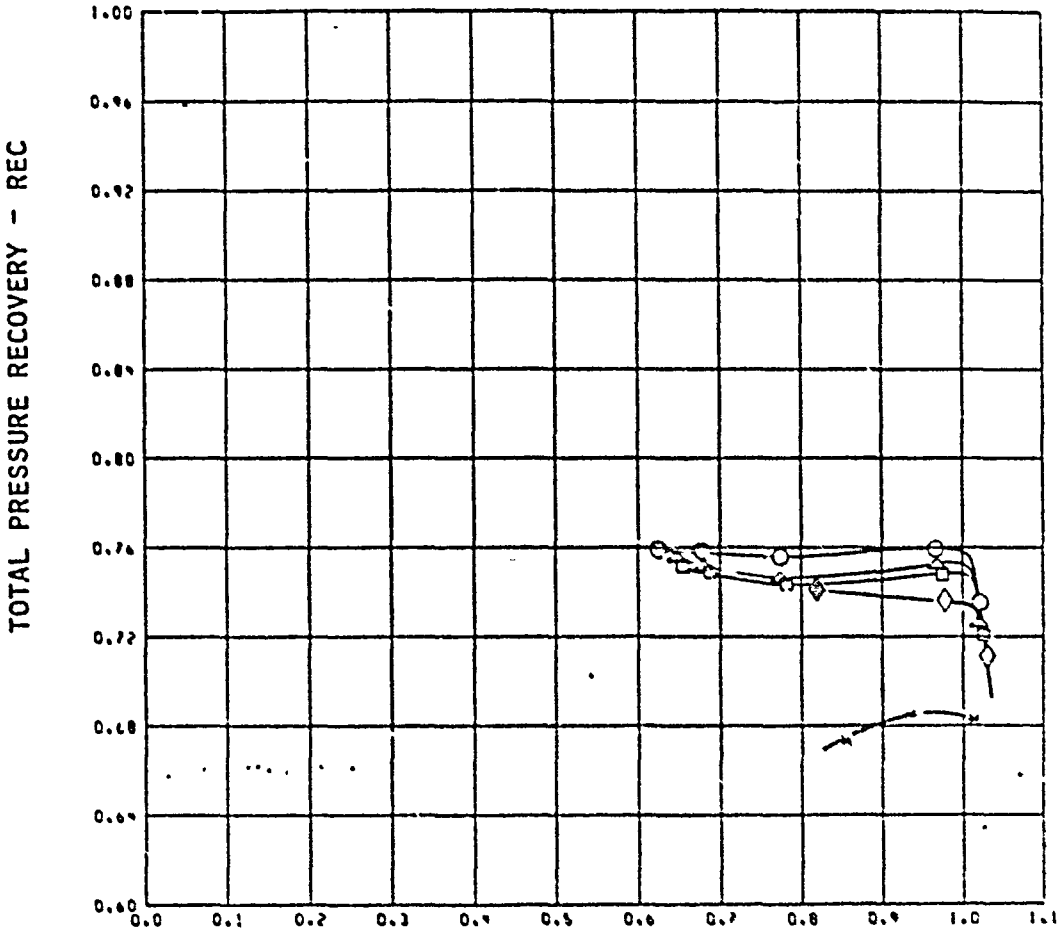

MACH = 1.96 CONF = 21

SYM	CRTCD	CRMCRD	DMFR	PPB	TTRC
○	33.7	2.53	0.061	0.91	1.067
△	32.6	1.90	0.060	0.73	1.032
□	24.9	1.39	0.046	0.72	1.035
◇	14.8	0.59	0.028	4.00	1.027
✳	0.6	-0.44	0.002	0.34	0.995

FIGURE 47. INLET PERFORMANCE AT 1.96 M, COLD FLOW

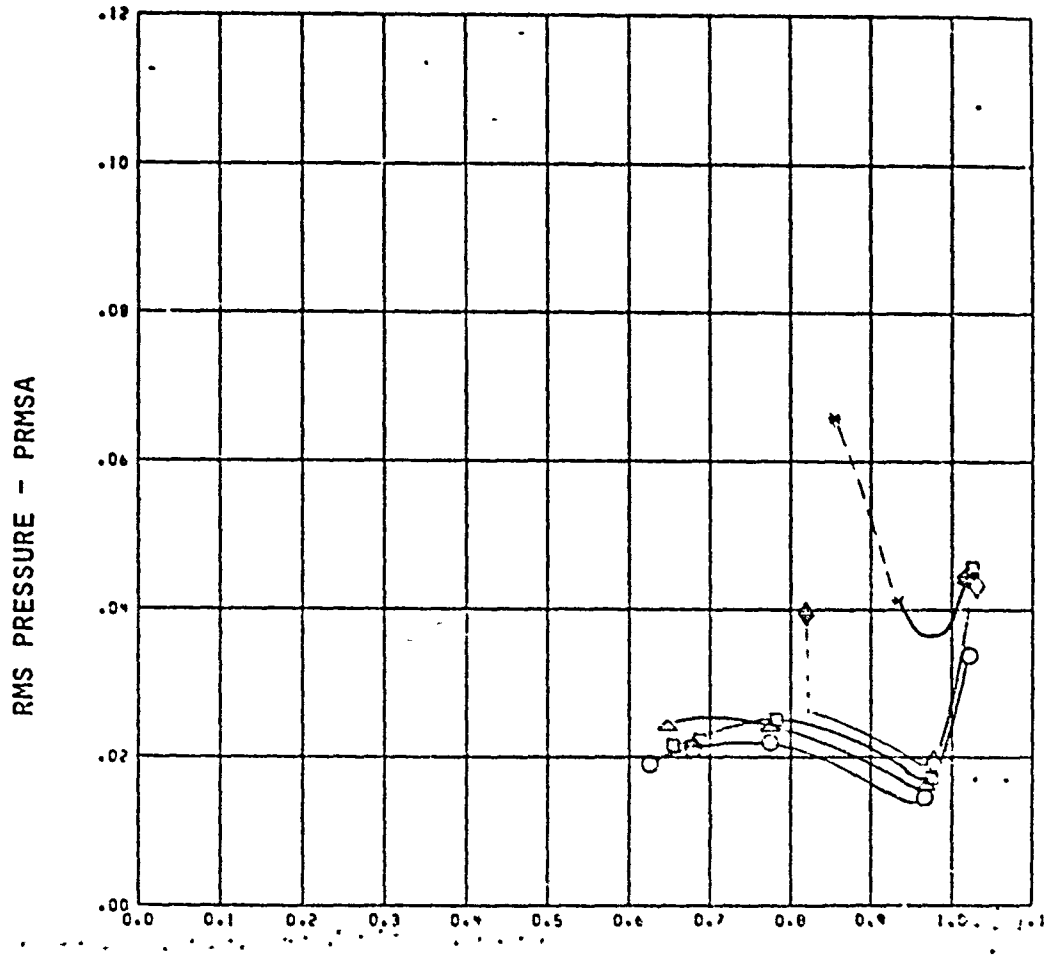

MACH • 1.96 CONF • 21

SYM	CMICD	CMNORD	DMFR	PPB	TTRC
○	33.7	2.53	0.061	8.91	1.057
△	32.6	1.98	0.060	8.73	1.032
□	24.9	1.39	0.046	6.72	1.036
◇	14.9	0.59	0.028	4.09	1.027
✳	0.6	-0.44	0.002	0.34	0.996

FIGURE 47 CONTINUED. INLET PERFORMANCE AT 1.96 M, COLD FLOW

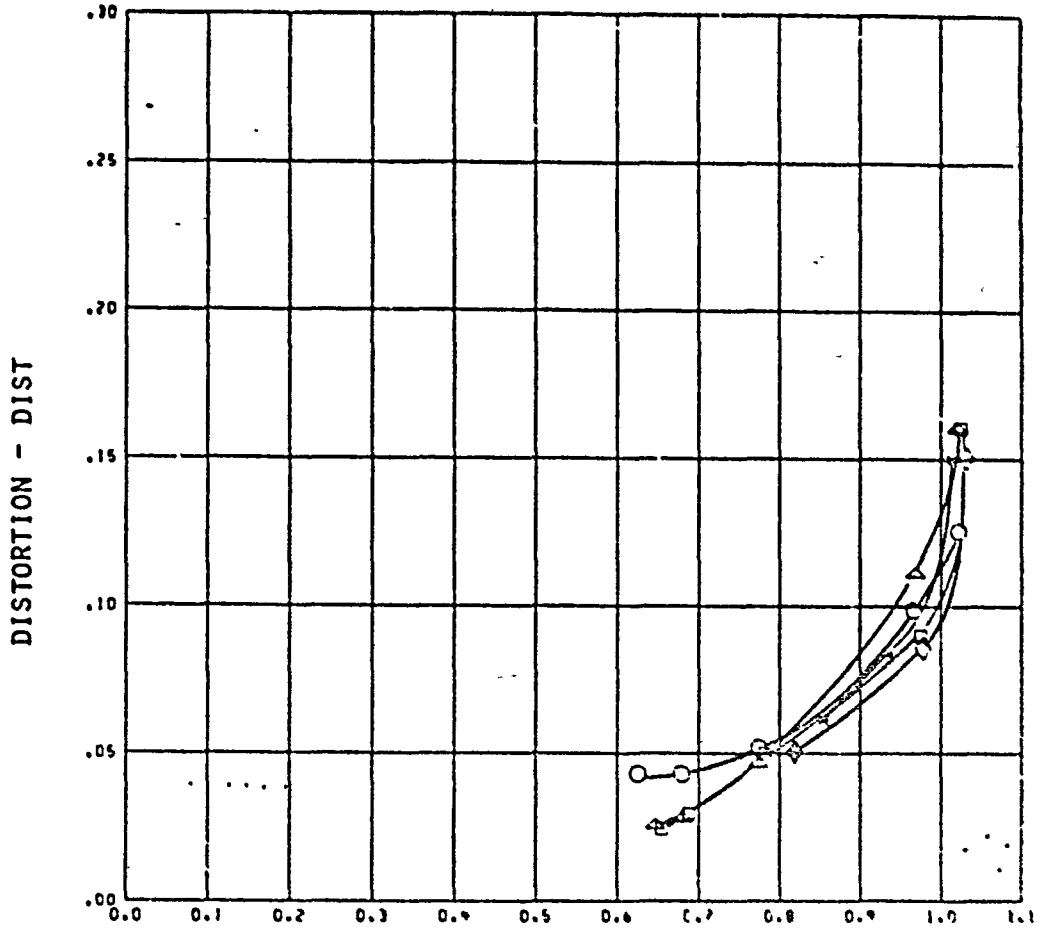

MACH = 1.96 CONF = 21

SYM	CRTCD	CRRCRD	ERFR	PPB	TTRC
○	33.7	2.53	0.061	8.91	1.057
△	32.6	1.50	0.050	8.73	1.032
□	24.9	1.39	0.046	6.72	1.035
◇	14.9	0.59	0.023	4.09	1.027
✳	0.6	-0.44	0.002	0.34	0.996

FIGURE 47 CONTINUED. INLET PERFORMANCE AT 1.96 M, COLD FLOW

ORIGINAL PAGE IS
OF POOR QUALITY

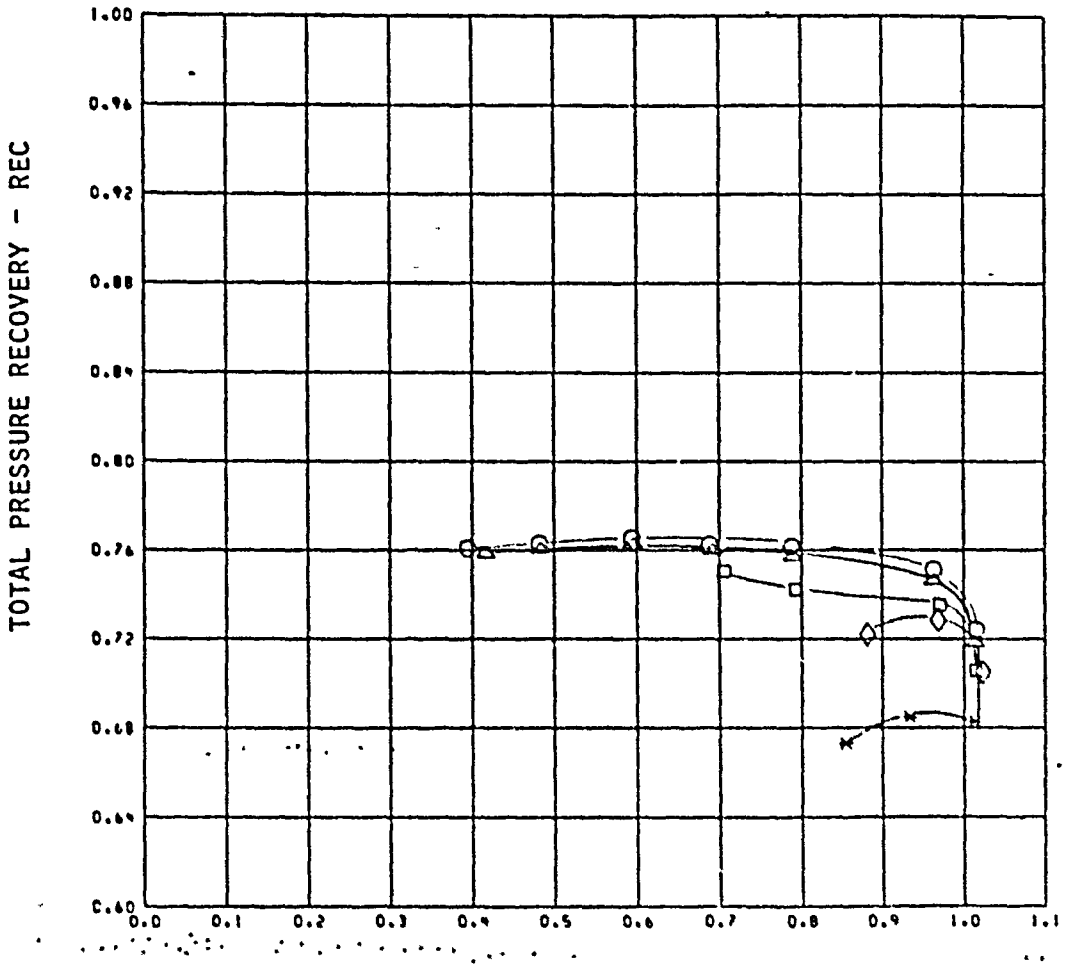

MACH = 1.96 CONF = 23

SYM	CMNCD	CMNCRD	DMFR	PPB	TTRC
○	34.2	2.19	0.052	8.64	1.043
△	33.8	2.13	0.056	7.82	1.057
□	23.8	1.34	0.044	6.08	1.039
◇	14.2	0.57	0.027	3.71	1.031
✳	0.6	-0.44	0.002	0.34	0.996

FIGURE 47 CONTINUED. INLET PERFORMANCE AT 1.96 M, COLD FLOW.

ORIGINAL PAGE IS
OF POOR QUALITY

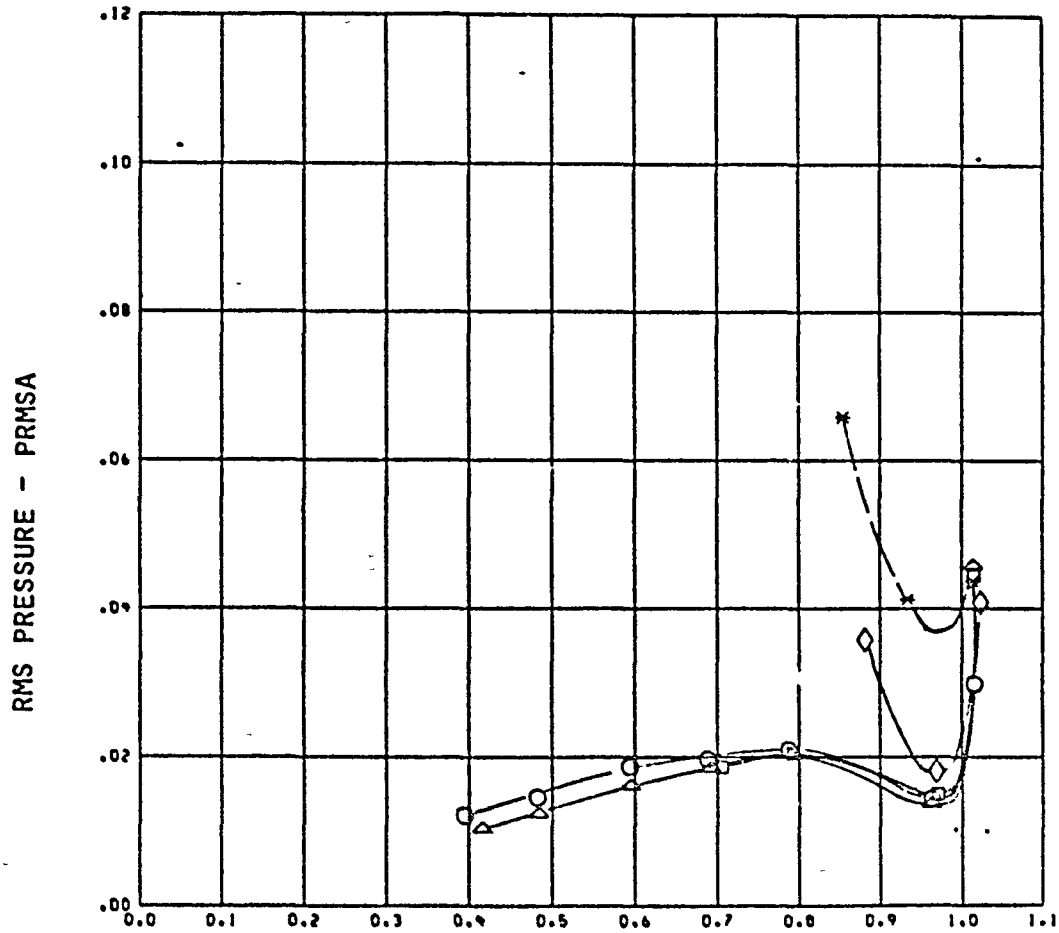

MACH • 1.95 CONF • 23

SYM	CMSCD	CMSCRD	DMFR	PPB	TTRC
○	34.2	2.19	0.062	8.64	1.043
△	30.8	2.13	0.056	7.82	1.057
□	23.8	1.34	0.044	6.03	1.039
◇	14.2	0.57	0.027	3.71	1.031
✳	0.6	-0.44	0.002	0.34	0.996

FIGURE 47 CONTINUED. INLET PERFORMANCE AT 1.96 M, COLD FLOW

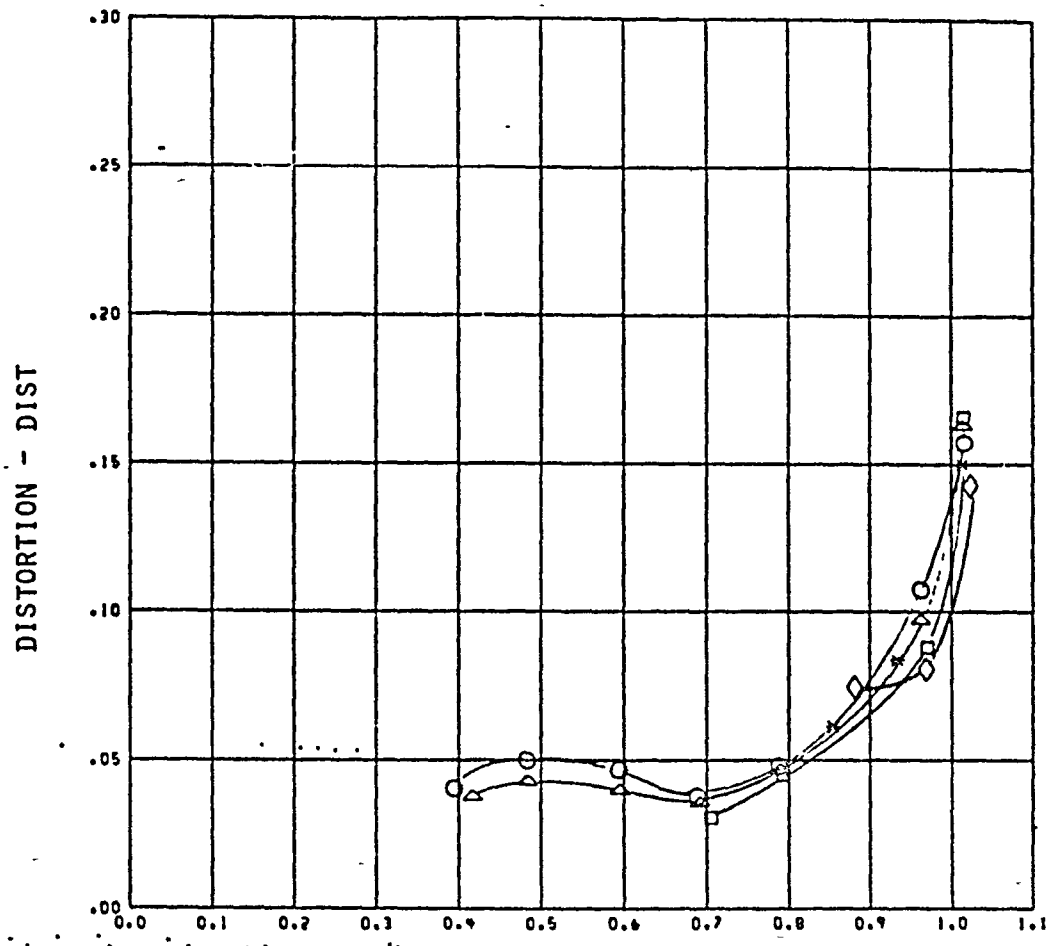

MACH = 1.95 CONF = 23

SYM	CMICD	CMICRD	BMFR	PPB	TTRC
○	34.2	2.19	0.052	8.64	1.043
△	30.8	2.13	0.056	7.82	1.057
□	23.8	1.34	0.044	6.08	1.039
◇	14.2	0.57	0.027	3.71	1.031
✳	0.6	-0.44	0.002	0.34	0.996

FIGURE 47 CONTINUED. INLET PERFORMANCE AT 1.96 M, COLD FLOW

ORIGINAL PAGE IS
OF POOR QUALITY

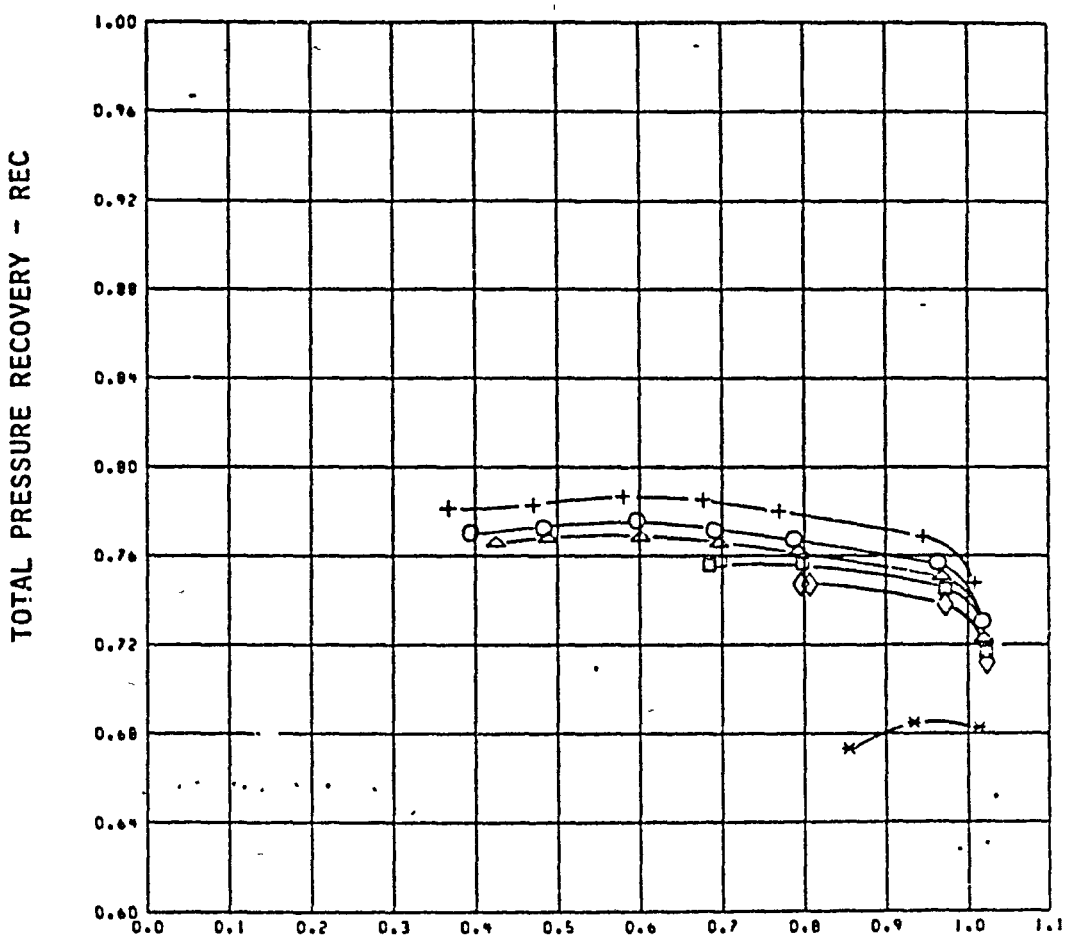

MACH = 1.96 CONF = 24

SYM	CMMCD	CMMCRD	DMFR	PPD	TTRC
+	52.7	3.22	0.097	8.34	1.038
○	35.4	2.11	0.067	5.02	1.047
△	28.9	1.59	0.053	4.06	1.045
□	22.9	0.77	0.042	3.61	1.027
◇	17.4	0.77	0.032	2.69	1.069
✳	0.6	-0.44	0.002	0.34	0.995

FIGURE 47 CONTINUED. INLET PERFORMANCE AT 1.96M, COLD FLOW.

ORIGINAL PAGE IS
OF POOR QUALITY

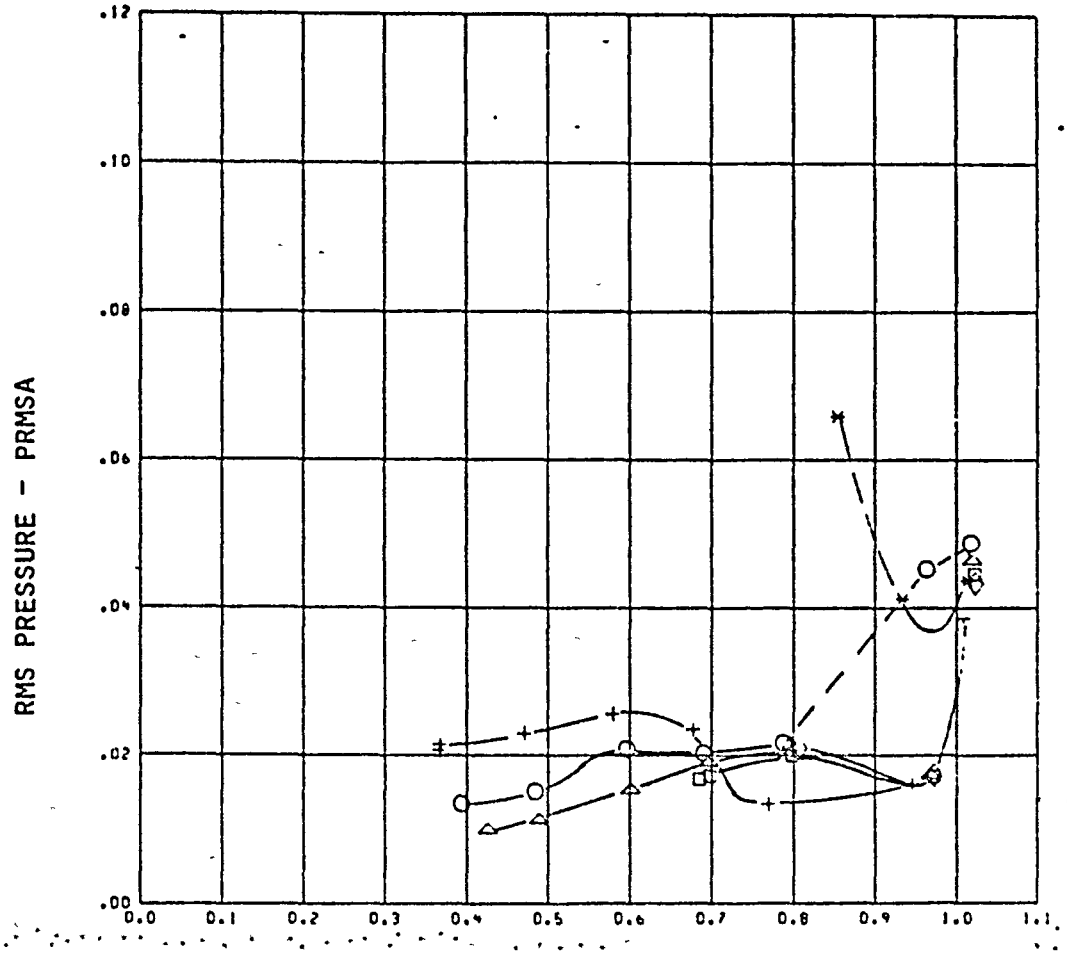

MACH = 1.96 CONF = 24

SYM	CRMCD	CRMCRD	DMFR	PPB	TTRC
+	52.7	3.22	0.097	8.34	1.038
○	36.4	2.11	0.067	5.82	1.047
△	28.9	1.50	0.053	4.66	1.045
□	22.0	0.77	0.042	3.61	1.027
◇	17.4	0.77	0.032	2.90	1.069
✳	0.6	-0.44	0.002	0.34	0.996

FIGURE 47 CONTINUED. INLET PERFORMANCE AT 1.96 M, COLD FLOW

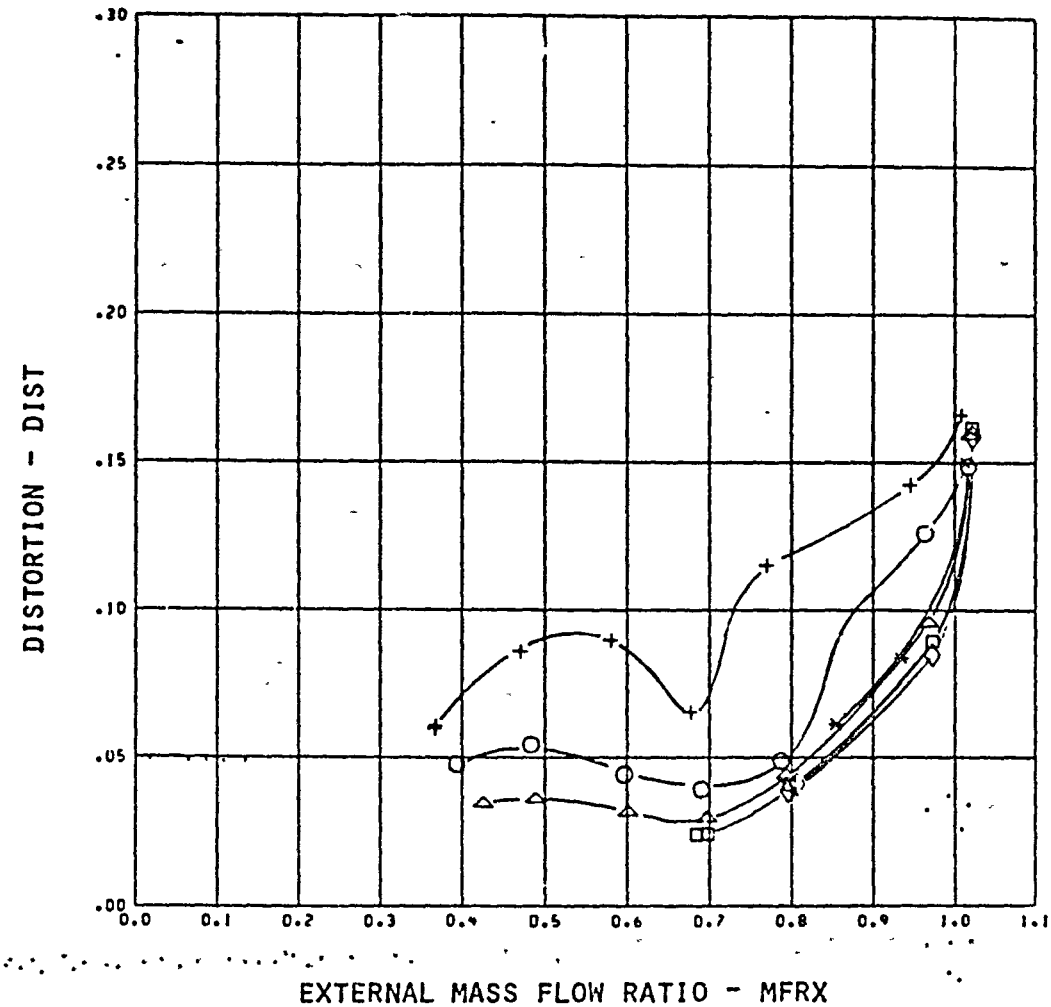

MACH = 1.96 CONF = 24

SYM	CFRNCD	CFRNCRD	RMFR	PPD	TTRC
+	52.7	3.22	0.697	8.34	1.033
○	33.4	2.11	0.667	5.82	1.047
△	28.9	1.59	0.653	4.66	1.045
□	22.0	0.77	0.642	3.61	1.027
◇	17.4	0.77	0.632	2.99	1.039
✳	0.6	-0.44	0.602	0.34	0.996

FIGURE 47 CONCLUDED, INLET PERFORMANCE AT 1.96 M, COLD FLOW

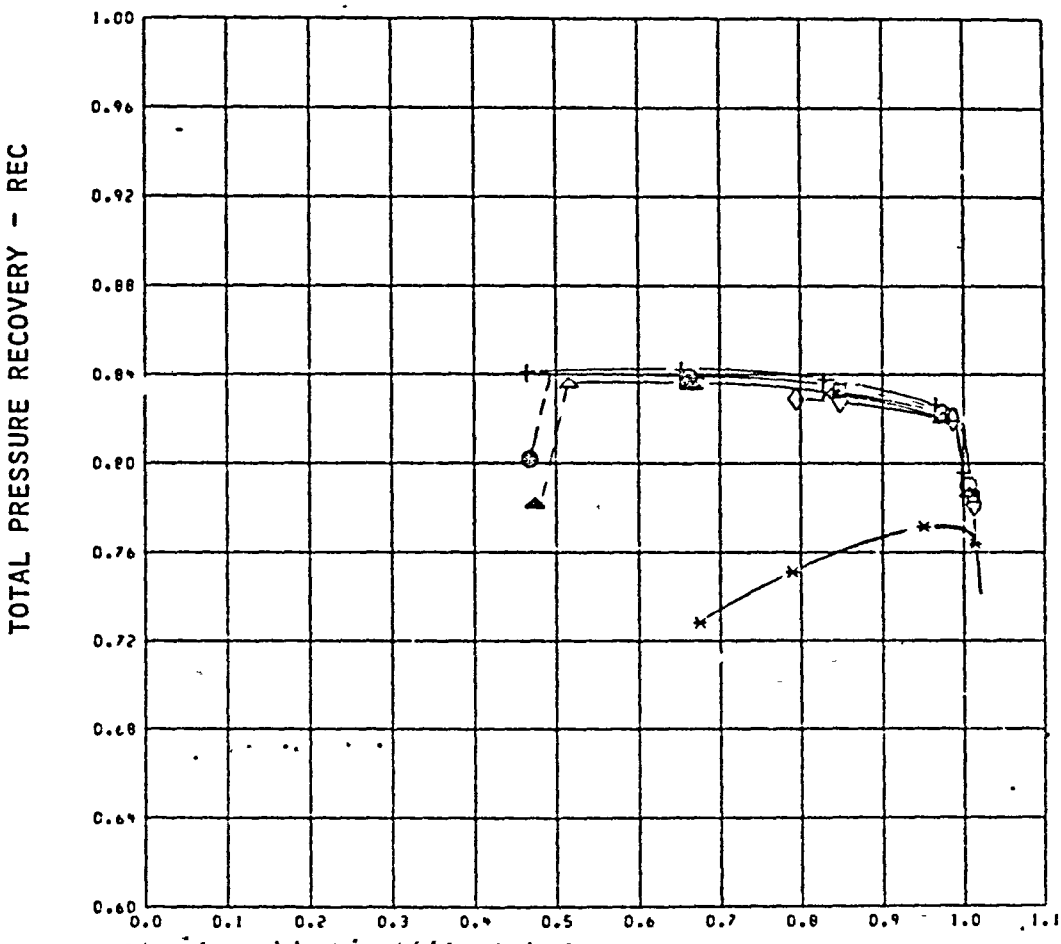

MACH • 1.77 CONF • 21

SYM	CRMCD	CRMCRD	BMFR	PPB	TTRC
+	32.1	4.81	0.056	9.60	1.065
○	24.7	2.94	0.044	7.42	1.058
△	21.4	1.81	0.040	6.73	0.987
□	17.3	1.78	0.032	5.40	1.043
◇	14.0	1.33	0.026	4.42	1.041
✳	0.4	-0.48	0.002	0.44	0.992

FIGURE 48. INLET PERFORMANCE AT 1.76 M, COLD FLOW

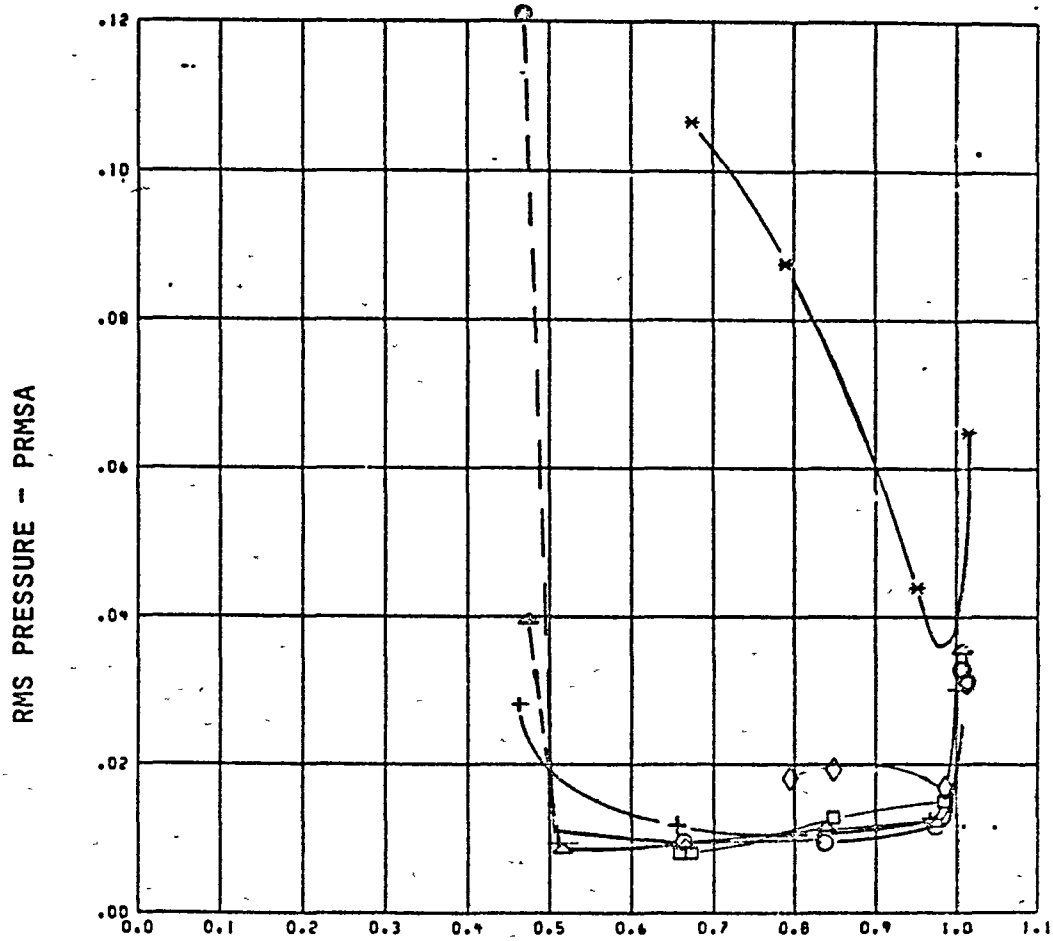

MACH = 1.77 CONF = 21

SYM	CRSCD	CRMCRD	BMFR	PPB	TTRC
+	32.1	4.01	0.056	9.69	1.085
O	24.7	2.84	0.044	7.42	1.059
△	21.4	1.81	0.040	6.73	0.937
□	17.3	1.78	0.022	5.40	1.043
◇	14.0	1.33	0.026	4.42	1.041
✳	0.4	-0.48	0.002	0.14	0.992

FIGURE 48 CONTINUED. INLET PERFORMANCE AT 1.76 M, COLD FLOW

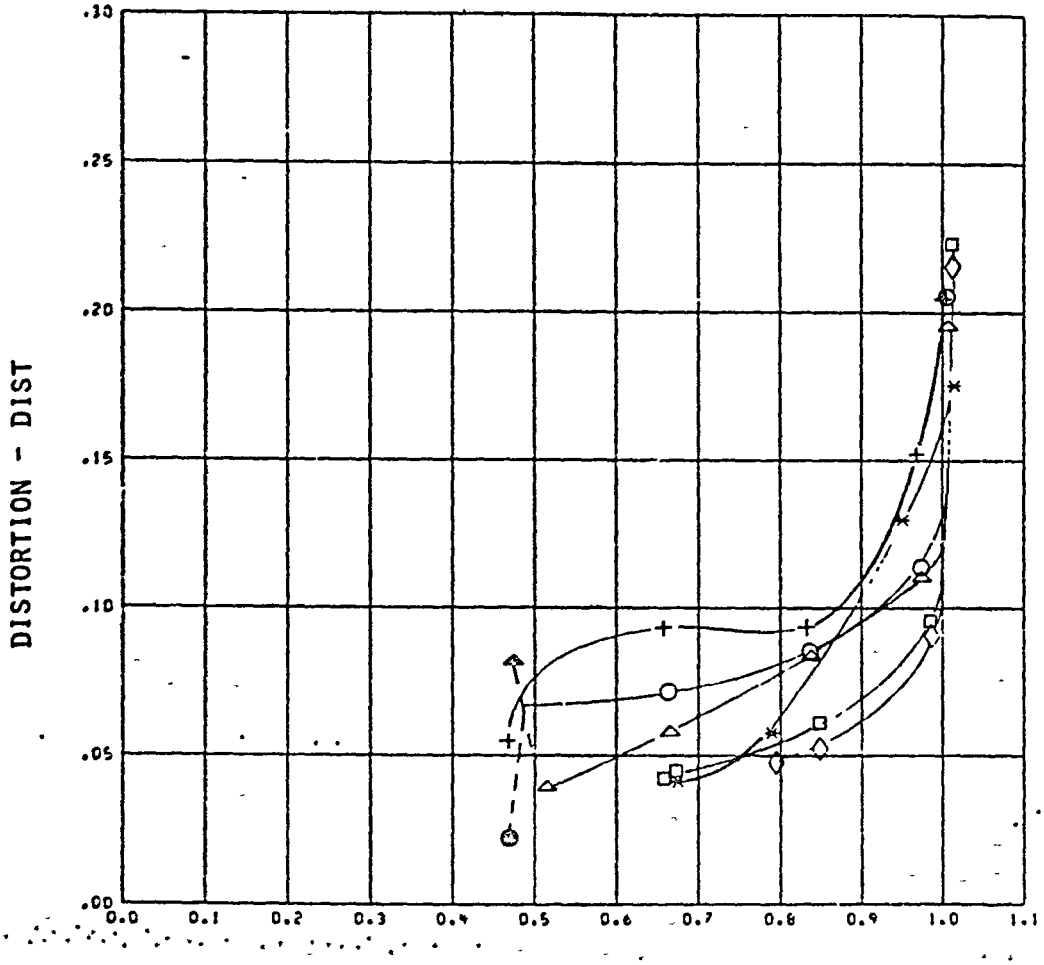

MACH = 1.77 CONF = 21

SYM	CPMCD	CPMCRD	BMFR	FPB	TTRC
+	32.1	4.01	0.056	9.60	1.065
○	24.7	2.94	0.044	7.42	1.058
△	21.4	1.81	0.040	6.73	0.987
□	17.3	1.78	0.032	5.40	1.043
◇	14.0	1.33	0.026	4.42	1.041
✳	0.4	-0.48	0.002	0.44	0.992

FIGURE 48 CONTINUED. INLET PERFORMANCE AT 1.76 M, COLD FLOW

ORIGINAL PAGE IS
OF POOR QUALITY

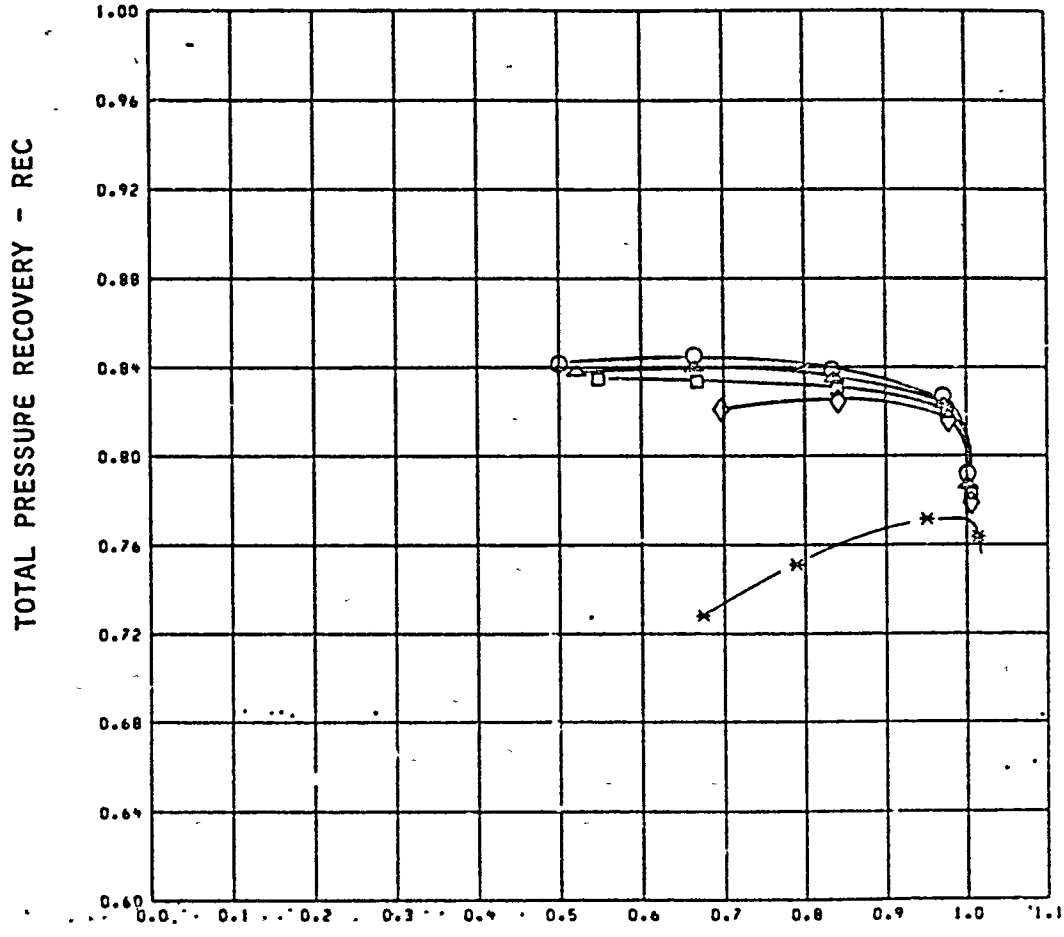

MACH = 1.77 CONF = 22

SYM	CMMCD	CMMCRD	DMFR	PPD	TTRC
○	28.5	3.05	0.051	8.39	1.024
△	24.3	2.42	0.044	7.19	1.013
□	18.6	1.83	0.034	5.55	1.025
◇	14.9	1.40	0.027	4.47	1.033
✳	0.4	-0.48	0.002	0.44	0.992

FIGURE 48 CONTINUED. INLET PERFORMANCE AT 1.76M, COLD FLOW.

ORIGINAL PAGE IS
OF POOR QUALITY

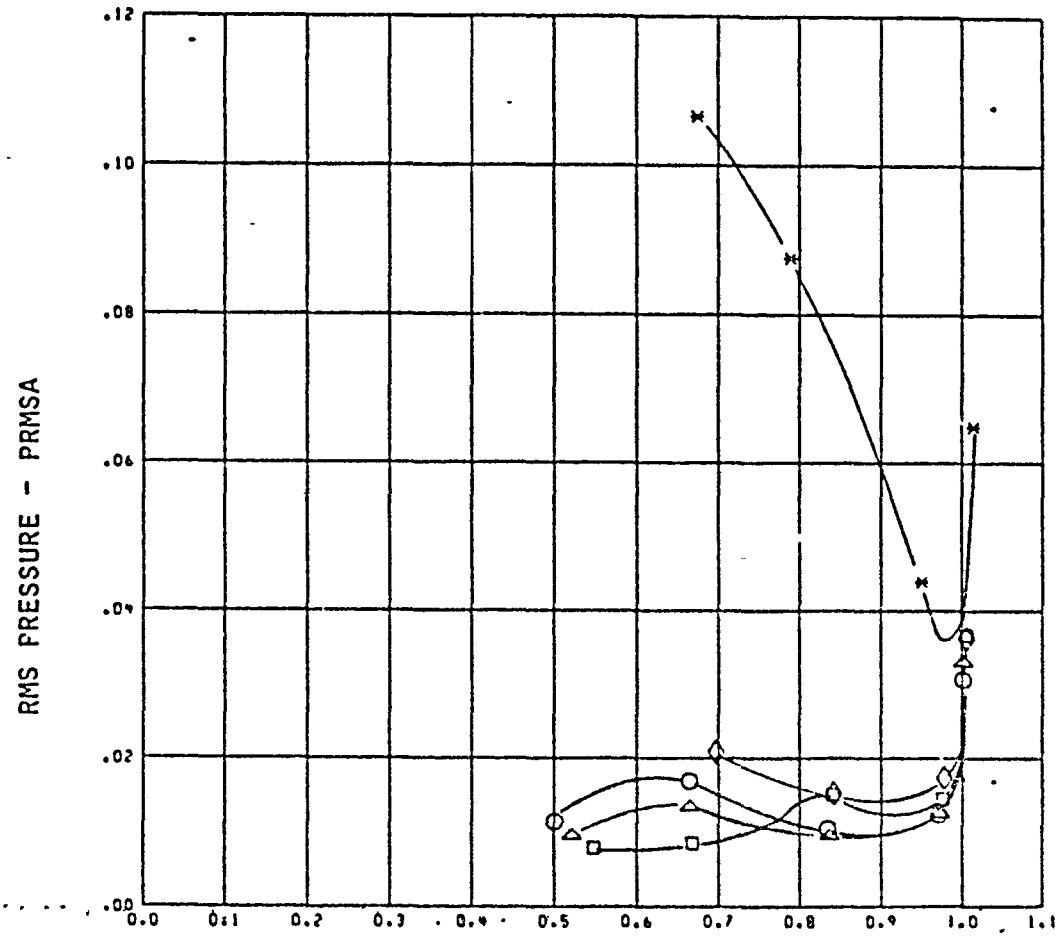

MACH = 1.77 CONF = 22

SYM	CMMCD	CMMCRD	BMFR	PPB	TTRC
○	28.5	3.05	0.051	8.39	1.024
△	24.3	2.42	0.044	7.19	1.013
□	18.6	1.83	0.034	5.55	1.025
◇	14.9	1.49	0.027	4.47	1.033
✳	0.4	-0.49	0.002	0.44	0.992

FIGURE 48 CONTINUED. INLET PERFORMANCE AT 1.76 M, COLD FLOW

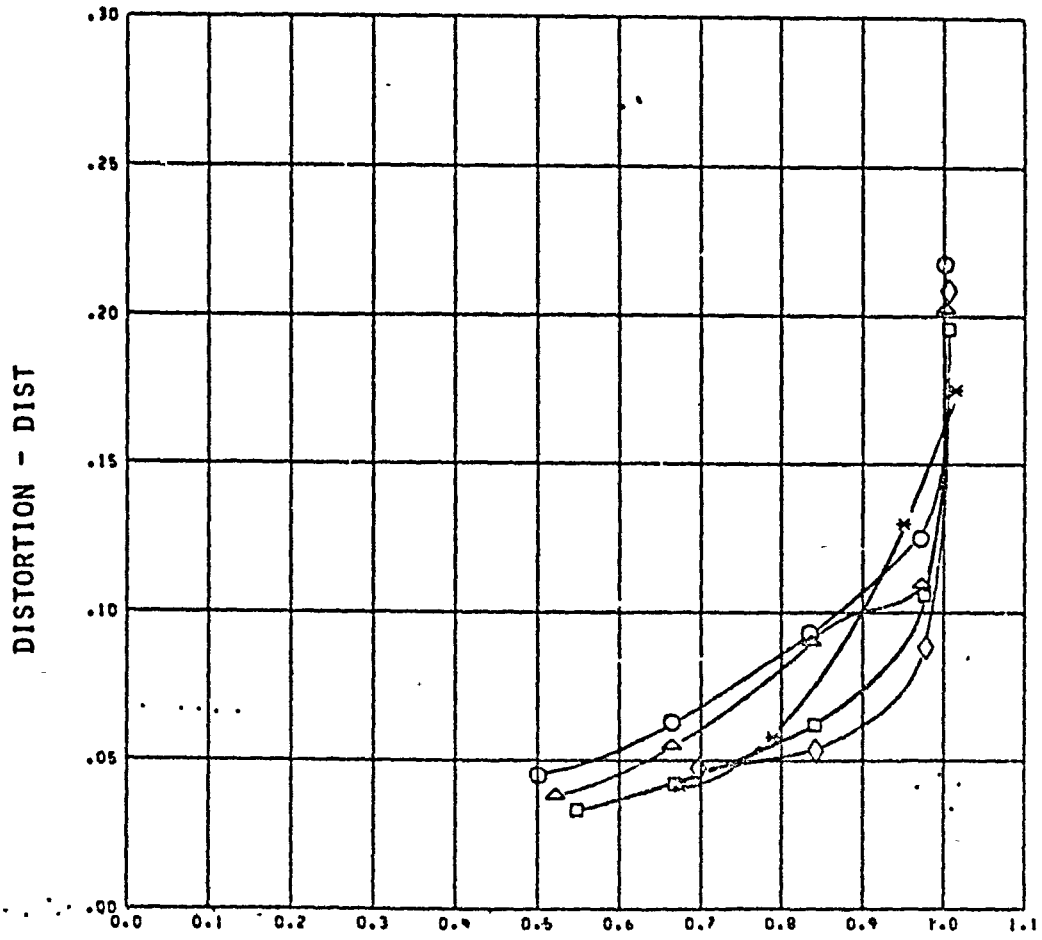

MACH • 1.77 CONF • 22

SYM	CIRCD	CIRCRD	DWFR	PPB	TTRC
○	20.5	3.65	0.051	8.39	1.024
△	24.3	2.42	0.044	7.19	1.013
□	18.6	1.83	0.034	5.55	1.025
◇	14.9	1.40	0.027	4.47	1.030
✳	0.4	-0.49	0.002	0.44	0.992

FIGURE 48 CONTINUED. INLET PERFORMANCE AT 1.76 M, COLD FLOW

ORIGINAL PAGE IS
OF POOR QUALITY

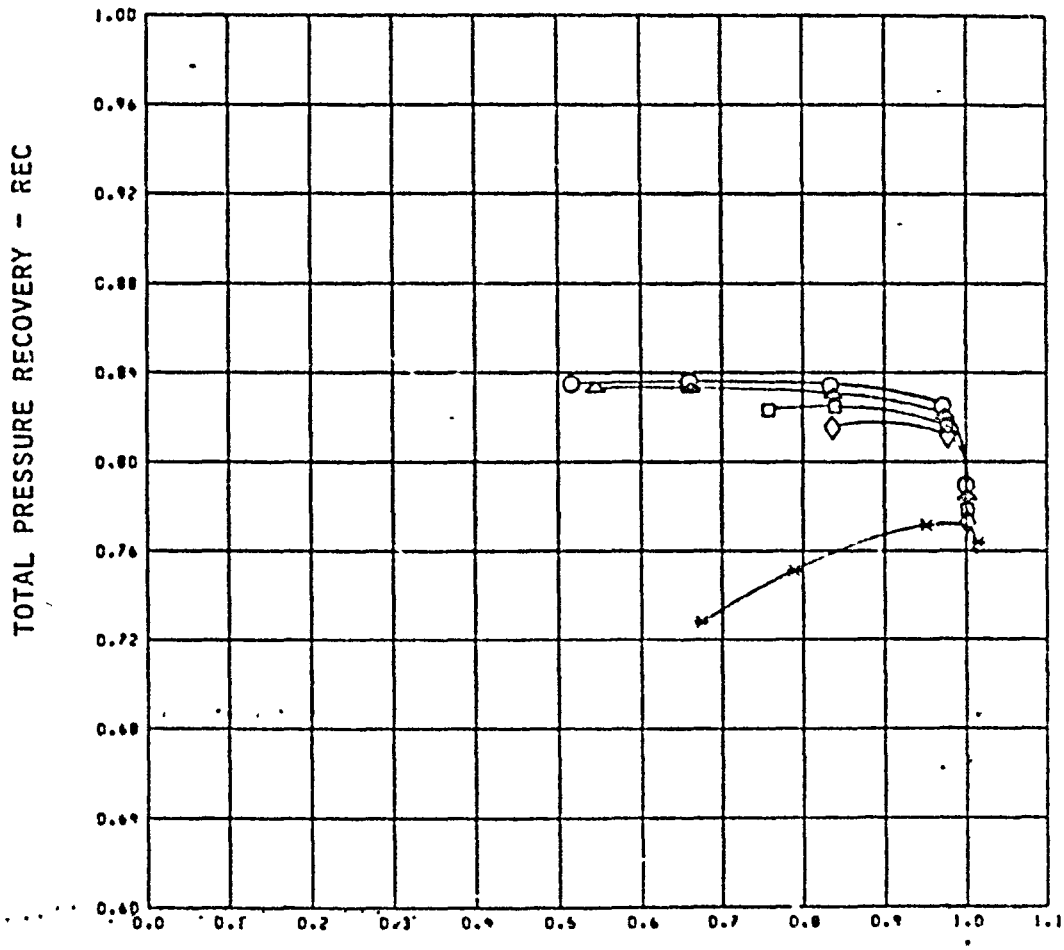

MACH • 1.77 CONF • 23

SYM	CMMCD	CMMCRD	BMFR	FPB	TTRC
○	26.8	3.01	0.048	7.76	1.040
△	22.7	3.32	0.041	6.62	1.024
□	16.7	1.68	0.030	4.84	1.037
◇	13.6	1.28	0.025	4.04	1.040
✳	0.4	-0.48	0.002	0.44	0.992

FIGURE 48 CONTINUED. INLET PERFORMANCE AT 1.76M, COLD FLOW.

ORIGINAL PAGE IS
OF POOR QUALITY

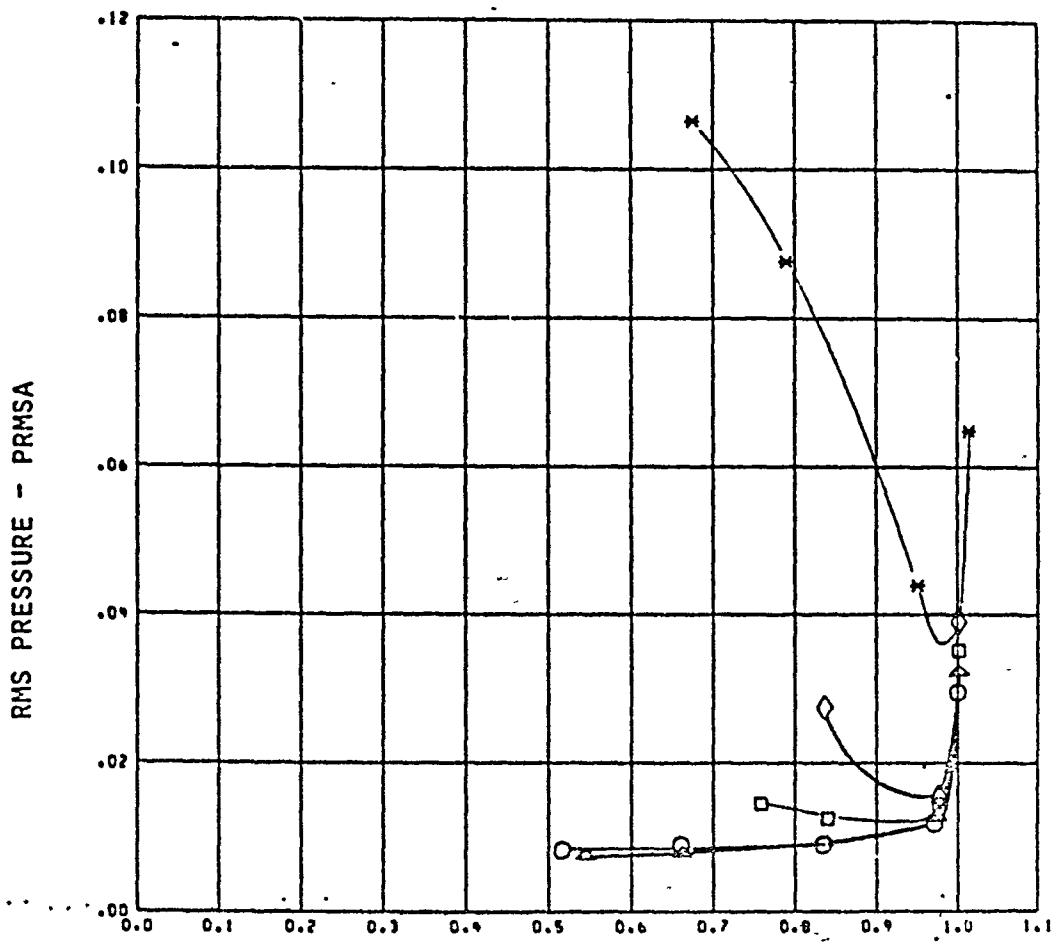

MACH = 1.77 CONF = 23

SYM	CRMCD	CRMCRD	BMFR	PPD	TTRC
○	26.8	3.01	0.048	7.76	1.049
△	22.7	2.32	0.041	6.62	1.024
□	16.7	1.68	0.030	4.94	1.037
◇	13.6	1.28	0.025	4.04	1.040
✳	0.4	-0.48	0.002	0.44	0.992

FIGURE 48 CONTINUED. INLET PERFORMANCE AT 1.76M, COLD FLOW

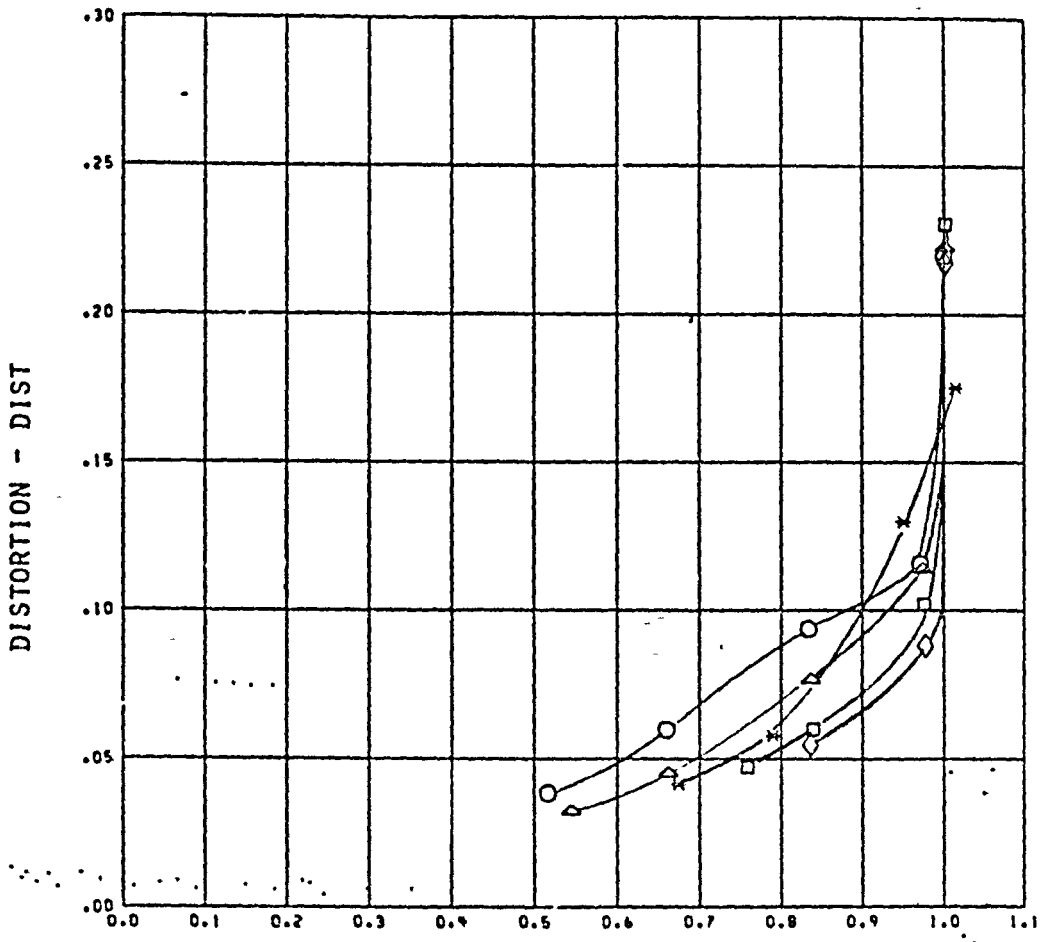

MACH = 1.77 CONF = 23

SYM	CRMCD	CRMCRD	DMFR	PPB	TTRC
○	26.8	3.01	0.048	7.76	1.040
△	22.7	2.32	0.041	6.62	1.024
□	16.7	1.68	0.030	4.04	1.037
◇	13.6	1.28	0.025	4.04	1.040
✳	0.4	-0.48	0.002	0.44	0.992

FIGURE 48 CONTINUED. INLET PERFORMANCE AT 1.76 M, COLD FLOW

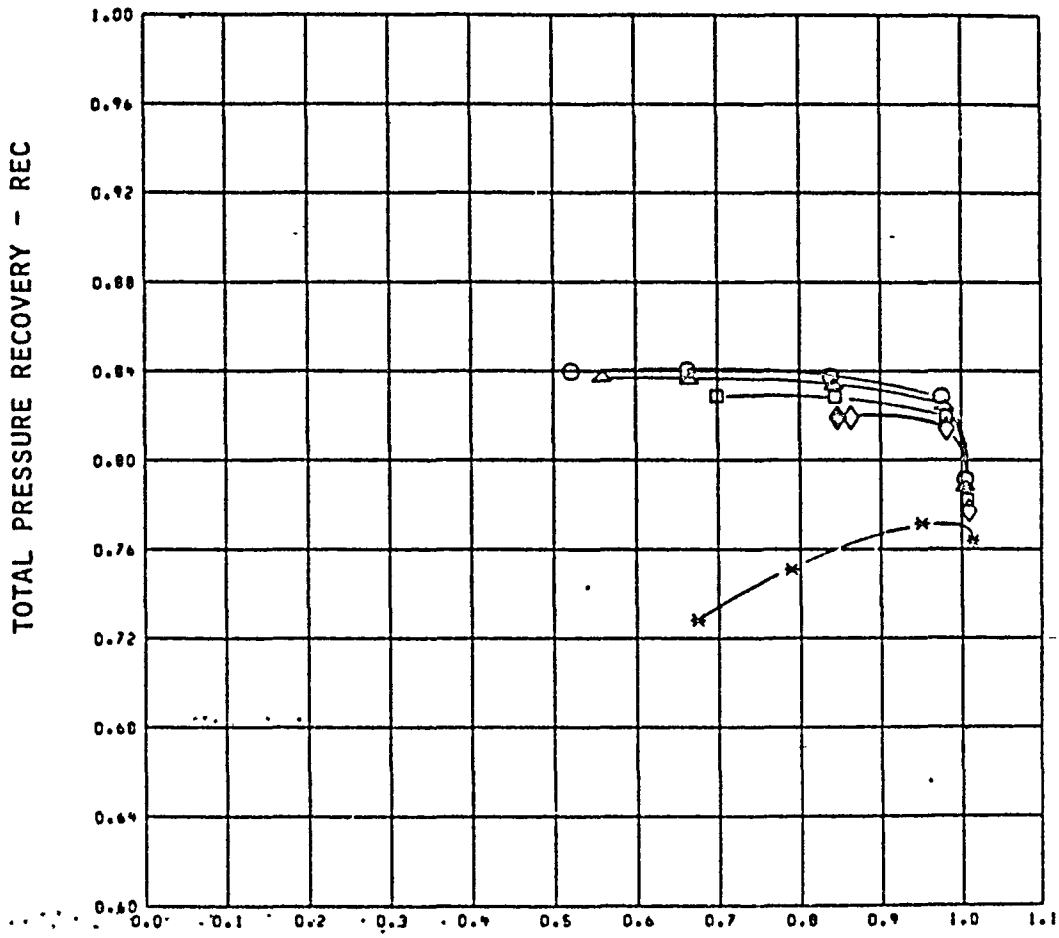

MACH • 1.77 CONF • 24

SYM	CRRCD	CRMCRD	DMFR	FPB	TTRC
○	25.6	2.36	0.047	4.74	1.029
△	21.2	1.73	0.039	3.97	1.021
□	15.6	1.22	0.028	3.01	1.047
◇	11.9	0.50	0.023	2.34	1.097
✳	0.4	-0.48	0.002	0.44	0.992

FIGURE 48 CONTINUED. INLET PERFORMANCE AT 1.76M, COLD FLOW.

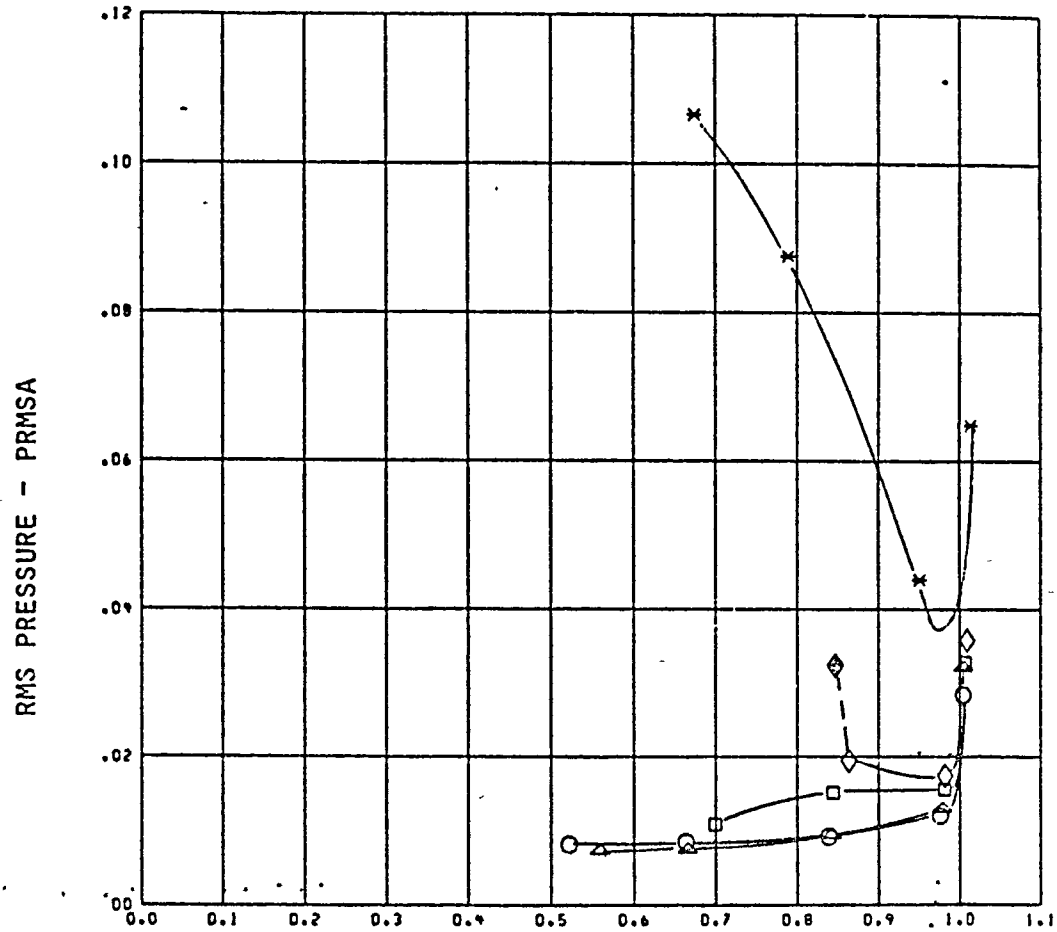

MACH = 1.77 CONF = 24

SYM	CPMCD	CPMCRD	BNFR	PPD	TTRC
○	25.6	2.36	0.047	4.74	1.029
△	21.2	1.73	0.039	3.97	1.021
□	15.6	1.22	0.029	3.01	1.047
◇	11.9	0.50	0.023	2.34	1.007
✳	0.4	-0.48	0.002	0.44	0.992

FIGURE 48 CONTINUED. INLET PERFORMANCE AT 1.76 M, COLD FLOW

ORIGINAL PAGE IS
OF POOR QUALITY

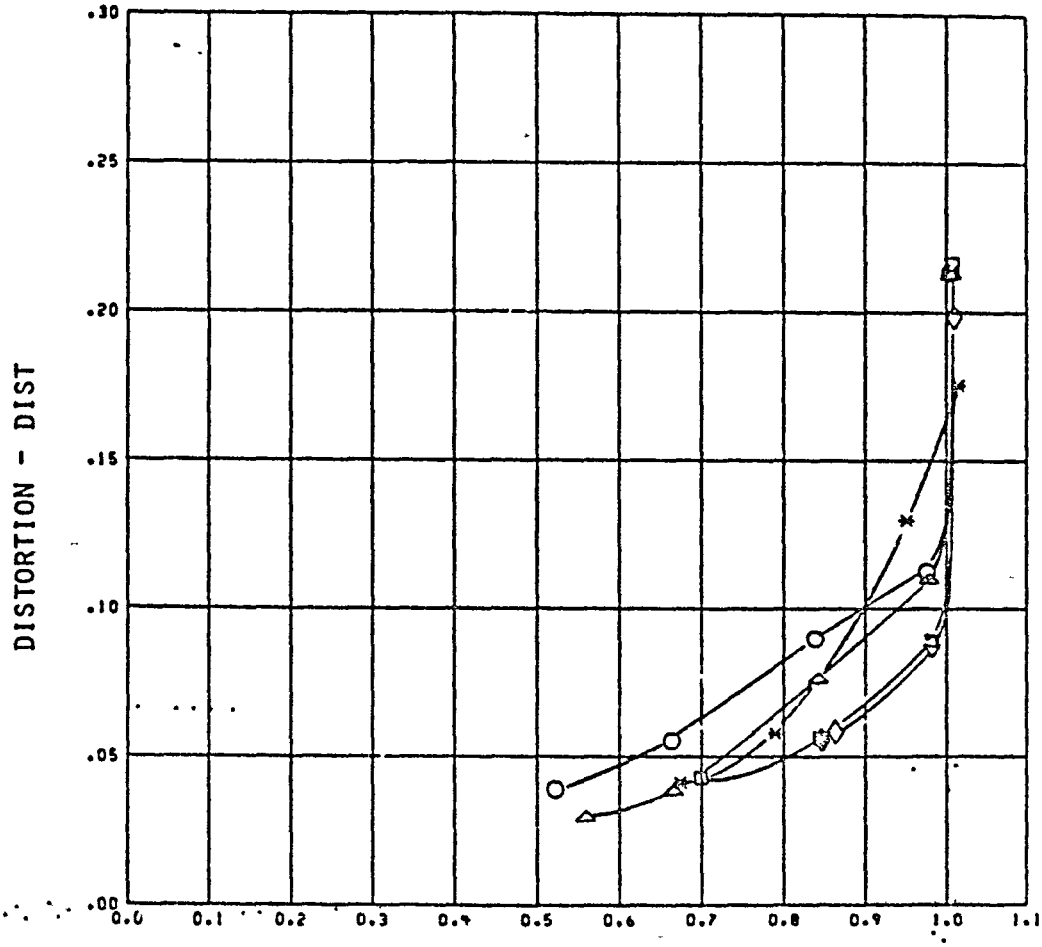

MACH = 1.77 CONF = 24

SYM	CPMCD	CPMCRD	BNFR	PPB	YTRC
○	25.6	2.36	0.047	4.74	1.029
△	21.2	1.73	0.039	3.97	1.031
□	15.6	1.22	0.029	3.01	1.047
◇	11.9	0.59	0.023	2.34	1.037
✳	0.4	-0.43	0.002	0.44	0.992

FIGURE 48 CONCLUDED. INLET PERFORMANCE AT 1.76 M, COLD FLOW

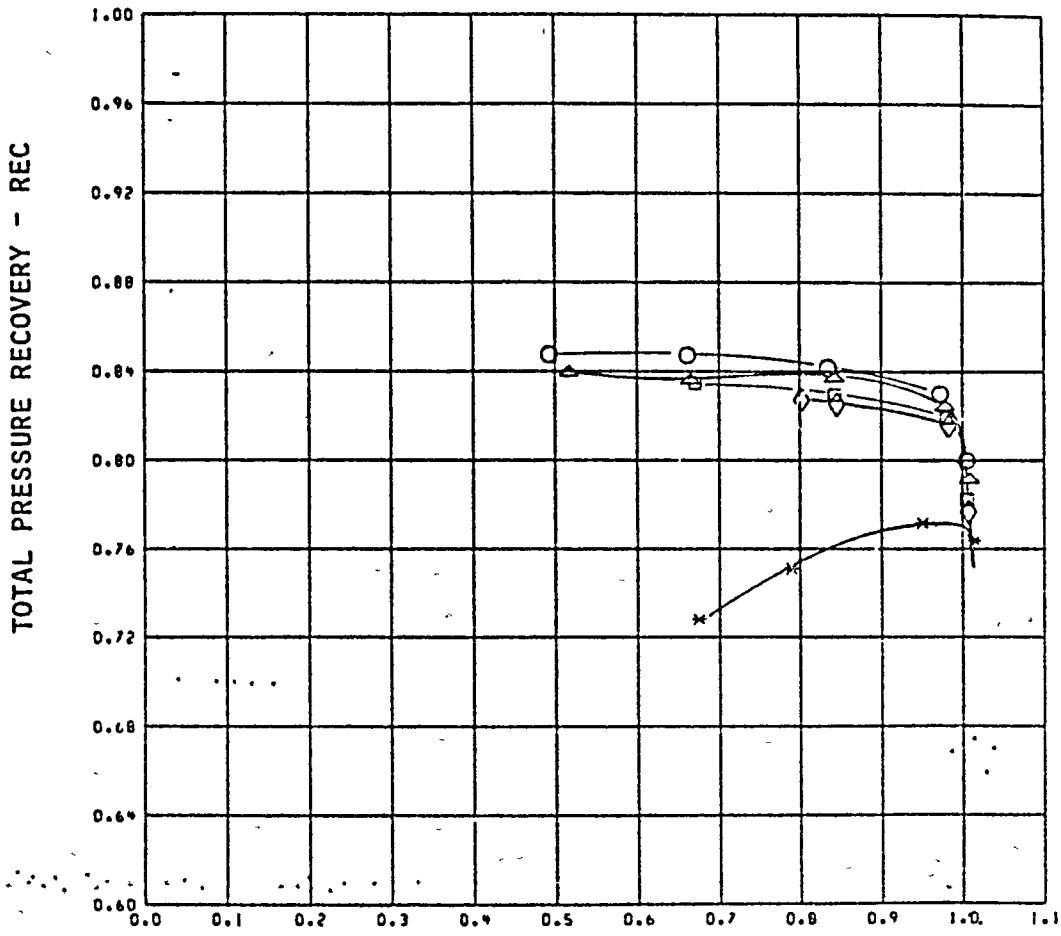

MACH = 1.77 CONF = 21

SYM	CMFCD	CMFCOD	DMFR	PPB	TTRC
○	33.6	8.27	0.046	9.33	1.530
△	23.5	6.32	0.035	7.28	1.543
□	17.9	4.65	0.027	5.69	1.529
◇	13.6	3.33	0.021	4.33	1.494
✳	0.4	-0.45	0.002	0.44	0.932

FIGURE 49. INLET PERFORMANCE AT 1.76 M, HOT FLOW

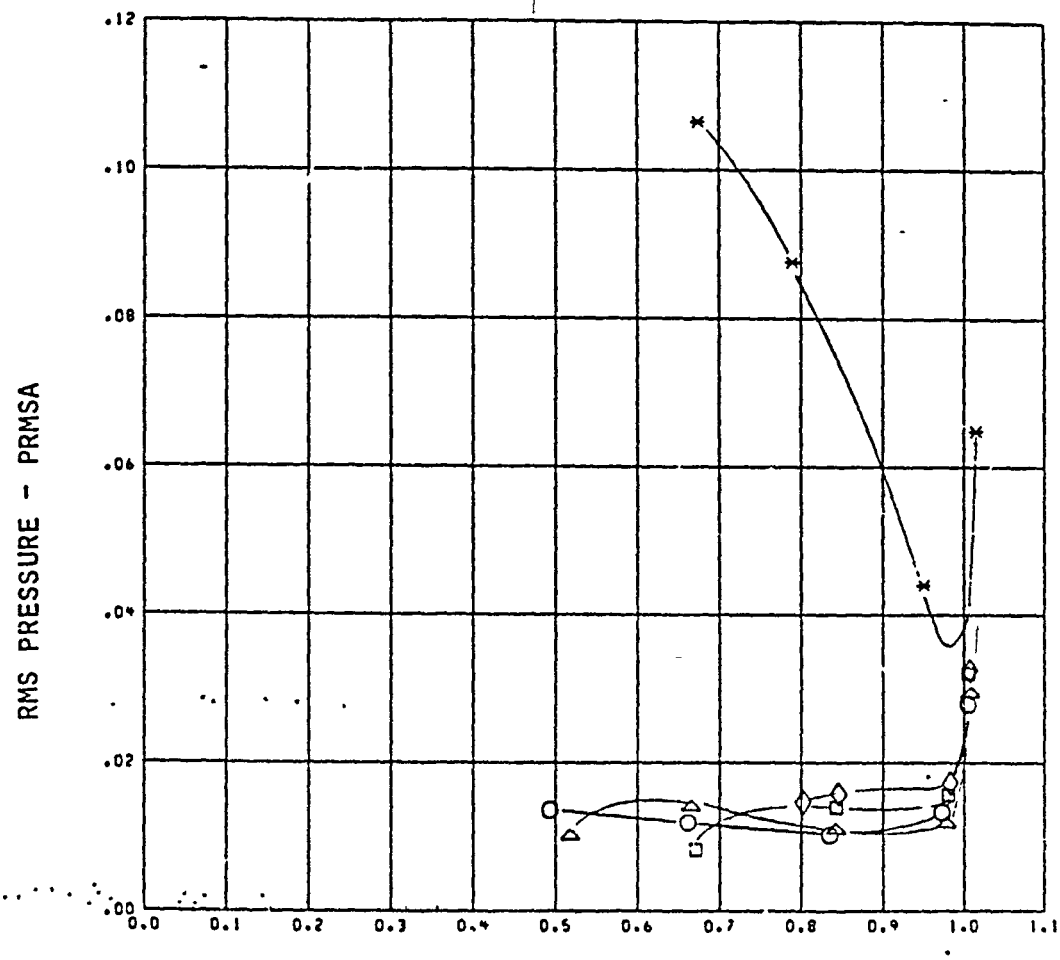

MACH = 1.77 CONF = 21

SYM	CMRCD	CMRCRD	DMFR	PPB	TTRC
○	39.6	8.27	0.046	9.39	1.539
△	23.5	6.32	0.035	7.28	1.543
□	17.9	4.65	0.027	5.65	1.529
◇	13.6	3.33	0.021	4.33	1.494
✳	0.4	-0.48	0.002	0.44	0.992

FIGURE 49 CONTINUED. INLET PERFORMANCE AT 1.76 M, HOT FLOW

ORIGINAL PAGE IS
OF POOR QUALITY

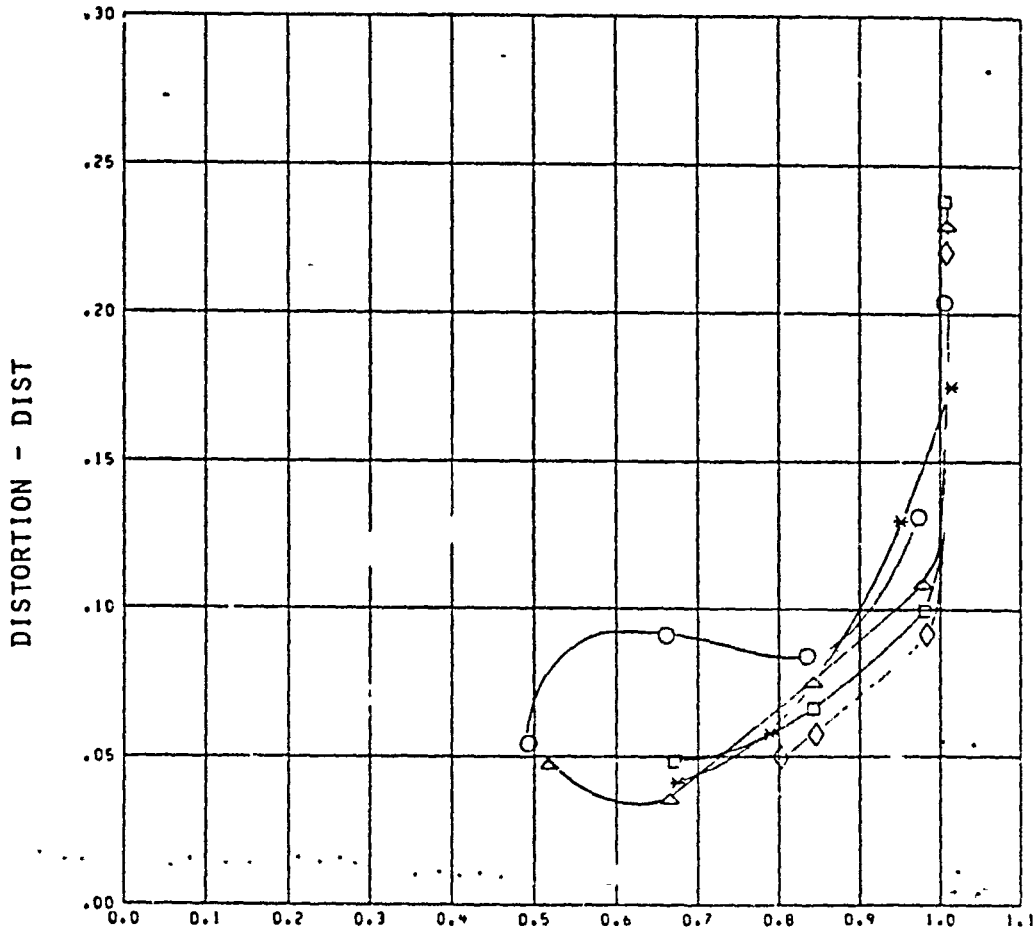

MACH • 1.77 CONF • 21

SYM	CNTCD	CNTCDD	BMFR	PPB	TTRC
○	28.6	8.27	0.048	9.39	1.530
△	23.5	6.32	0.035	7.28	1.543
□	17.9	4.65	0.027	5.68	1.529
◇	13.6	3.33	0.021	4.33	1.494
✳	0.4	-0.48	0.002	0.44	0.992

FIGURE 49 CONTINUED. INLET PERFORMANCE AT 1.76 M, HOT FLOW

ORIGINAL PAGE IS
OF POOR QUALITY

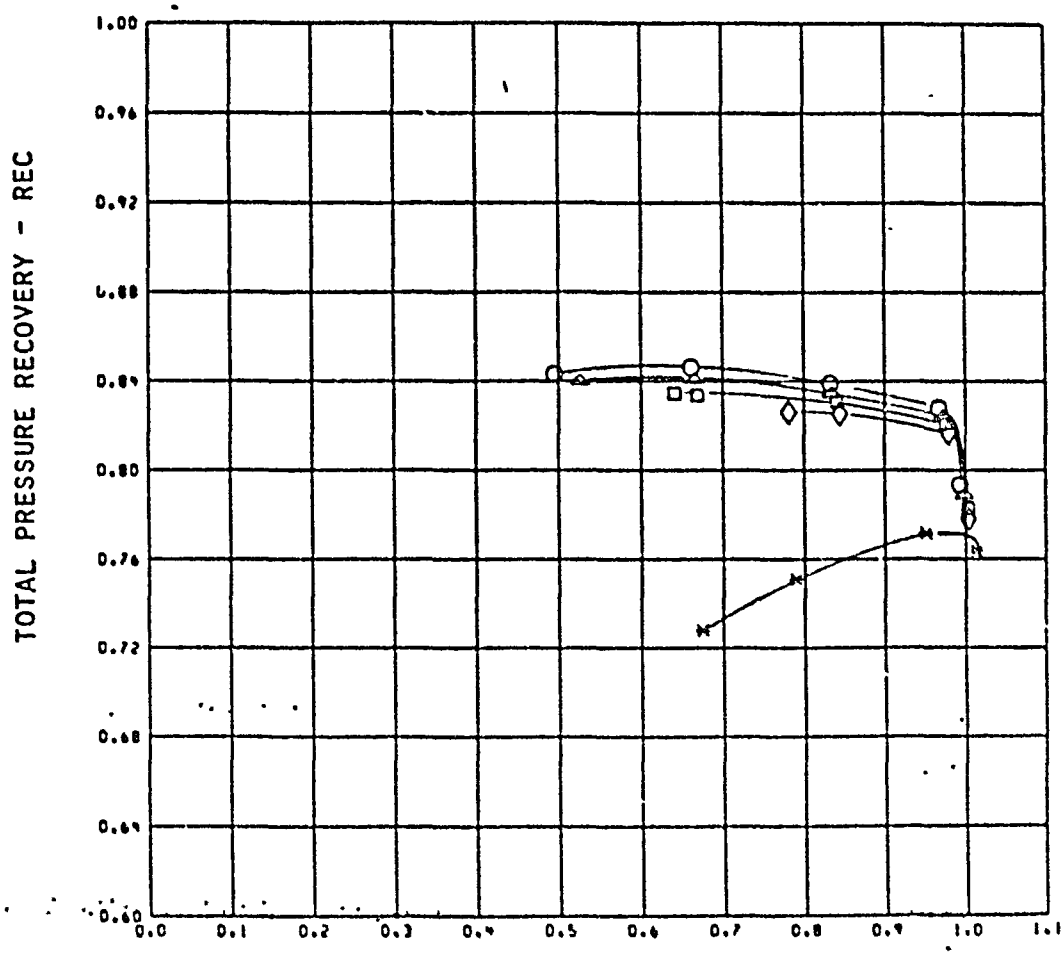

MACH = 1.7? CONF = 22

SYM	CRMCD	CRRCRD	BRFR	PPD	TTRC
○	39.8	8.68	0.048	9.13	1.495
△	25.2	7.32	0.038	7.77	1.579
□	10.5	5.35	0.028	5.82	1.630
◇	14.8	3.88	0.022	4.46	1.650
✳	0.4	-0.49	0.002	0.44	0.098

FIGURE 49 CONTINUED. INLET PERFORMANCE AT 1.76 M, HOT FLOW

ORIGINAL PAGE IS
OF POOR QUALITY

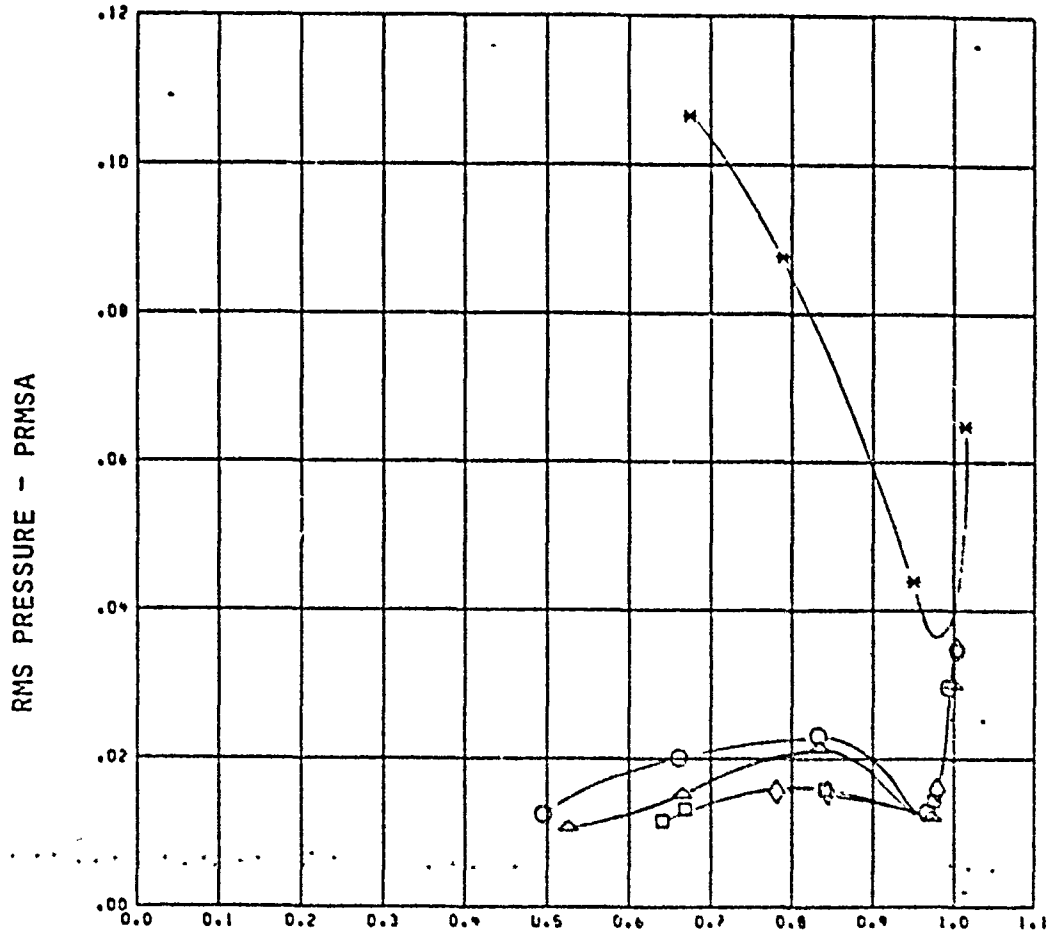

MACH = 1.77 CONF - 22

SYM	CNMCD	CNMCRD	INFR	PPB	TTRC
○	33.8	8.03	0.046	9.13	1.486
△	28.2	7.33	0.038	7.77	1.578
□	19.5	5.35	0.028	5.82	1.580
◇	14.8	3.85	0.022	4.46	1.058
✳	0.4	-0.48	0.032	0.44	0.992

FIGURE 49 CONTINUED. INLET PERFORMANCE AT 1.76 M, HOT FLOW

ORIGINAL PAGE IS
OF POOR QUALITY

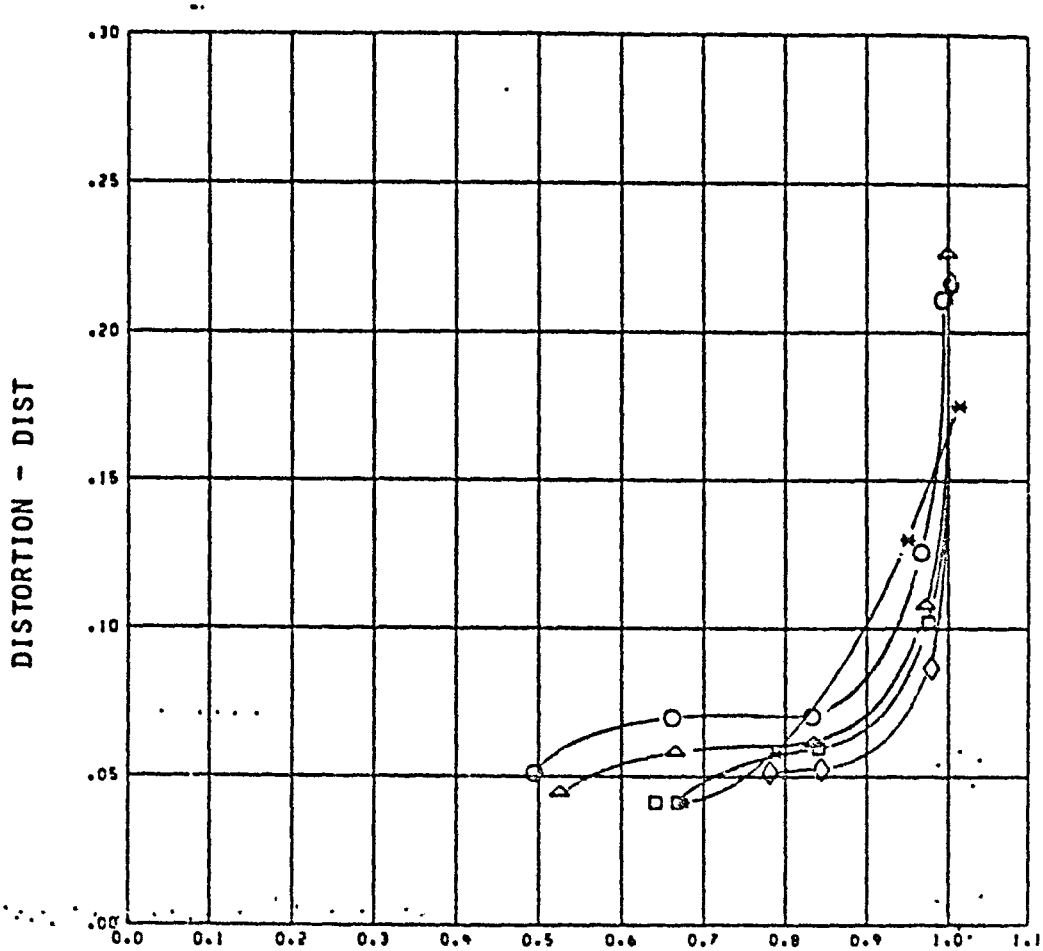

MACH • 1.77 CONF • 22

SYM	CIRCD	CRRCRD	DIFR	PFB	TTRC
○	20.8	8.05	0.040	9.13	1.485
△	08.2	7.33	0.038	7.77	1.070
□	10.5	5.35	0.029	5.82	1.080
◇	14.0	3.08	0.022	4.43	1.050
✳	0.4	-0.40	0.002	0.44	0.000

FIGURE 49 CONTINUED. INLET PERFORMANCE AT 1.76M, HOT FLOW

ORIGINAL PAGE IS
OF POOR QUALITY

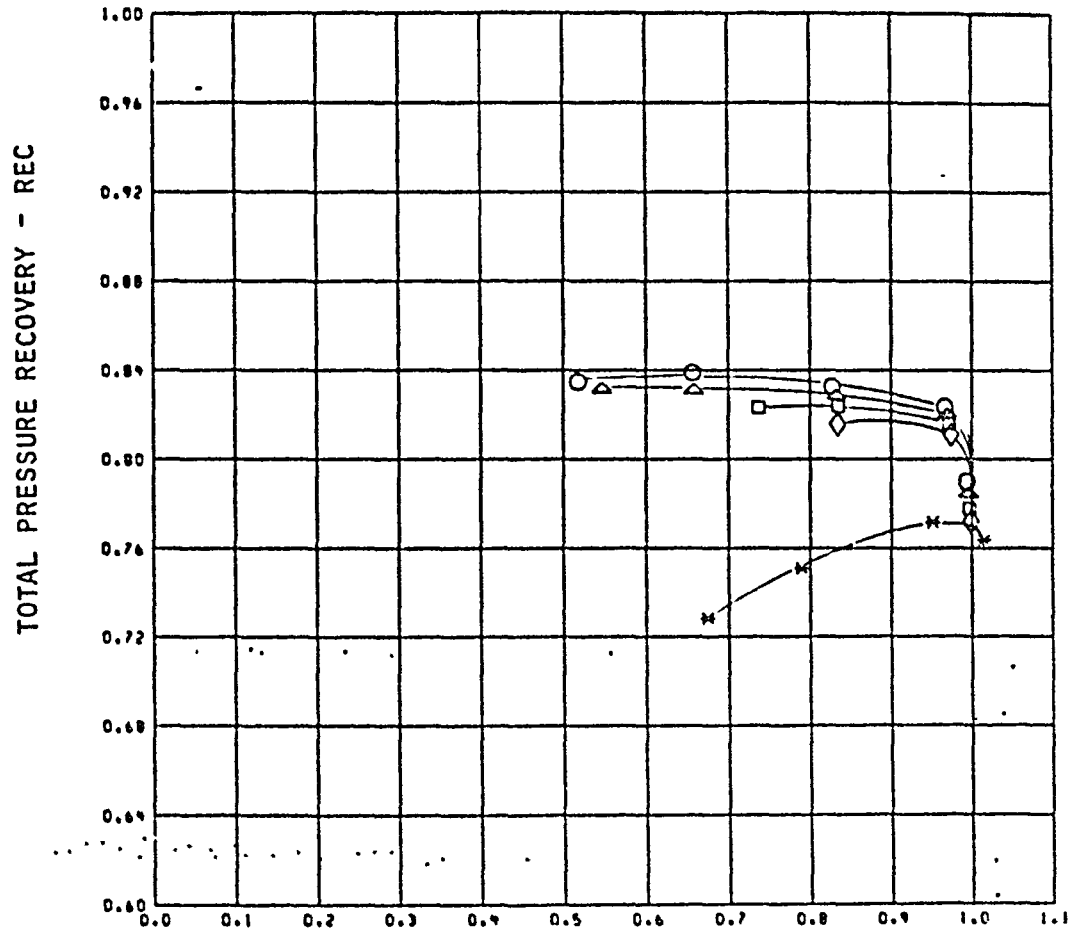

MACH • 1.77 CONF • 23

SYM	CRMOD	CHMCRD	DRFR	PPD	TTRC
○	29.4	8.49	0.042	8.56	1.597
△	24.6	6.99	0.035	7.20	1.602
□	18.3	5.84	0.027	5.42	1.588
◇	14.7	3.89	0.022	4.40	1.586
✳	0.4	-0.48	0.002	0.44	0.992

FIGURE 49 CONTINUED. INLET PERFORMANCE AT 1.76 M, HOT FLOW

ORIGINAL PAGE IS
OF POOR QUALITY

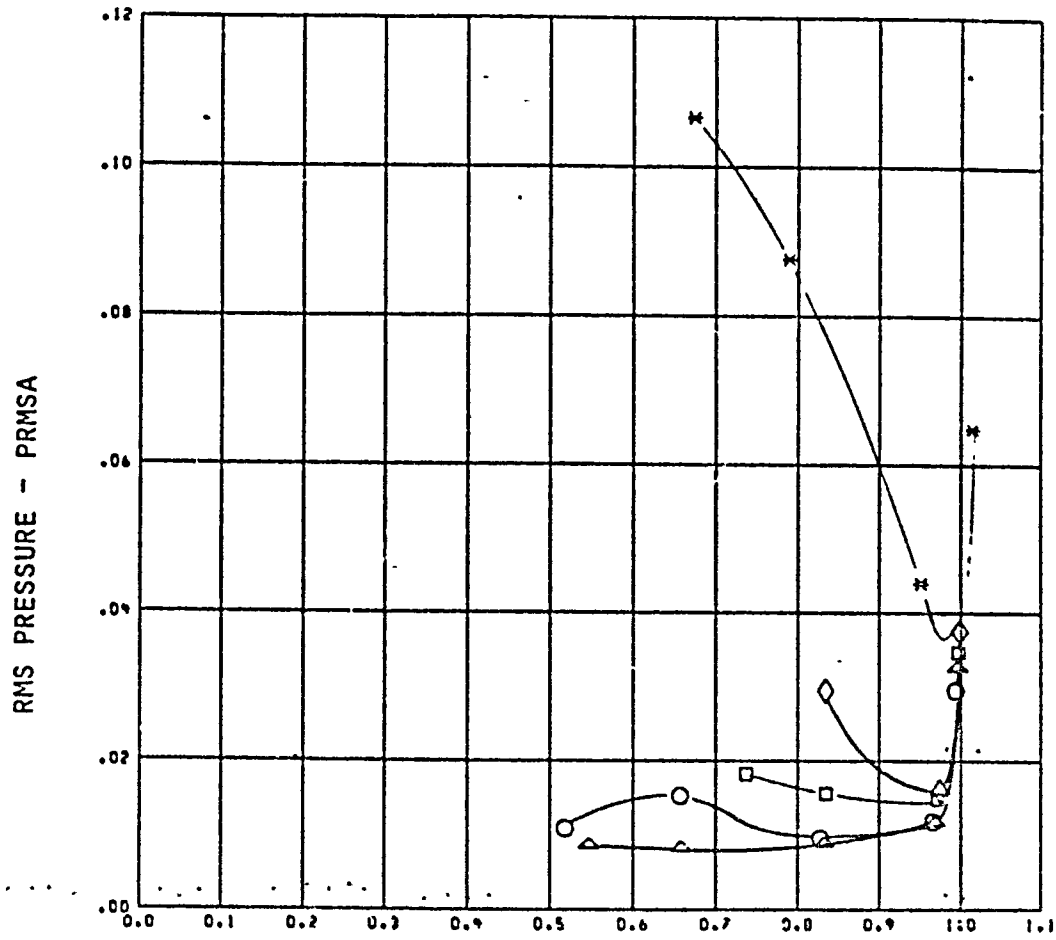

MACH = 1.77 CONF = 23

SYM	CRMCD	CRMCRD	DMFR	PPB	TTRC
○	29.4	8.49	0.042	8.56	1.597
△	24.6	6.93	0.035	7.20	1.602
□	18.3	5.04	0.027	5.42	1.588
◇	14.7	3.69	0.022	4.49	1.586
✳	0.4	-0.48	0.002	0.44	0.592

FIGURE 49 CONTINUED. INLET PERFORMANCE AT 1.76 M, HOT FLOW

ORIGINAL PAGE IS
OF POOR QUALITY

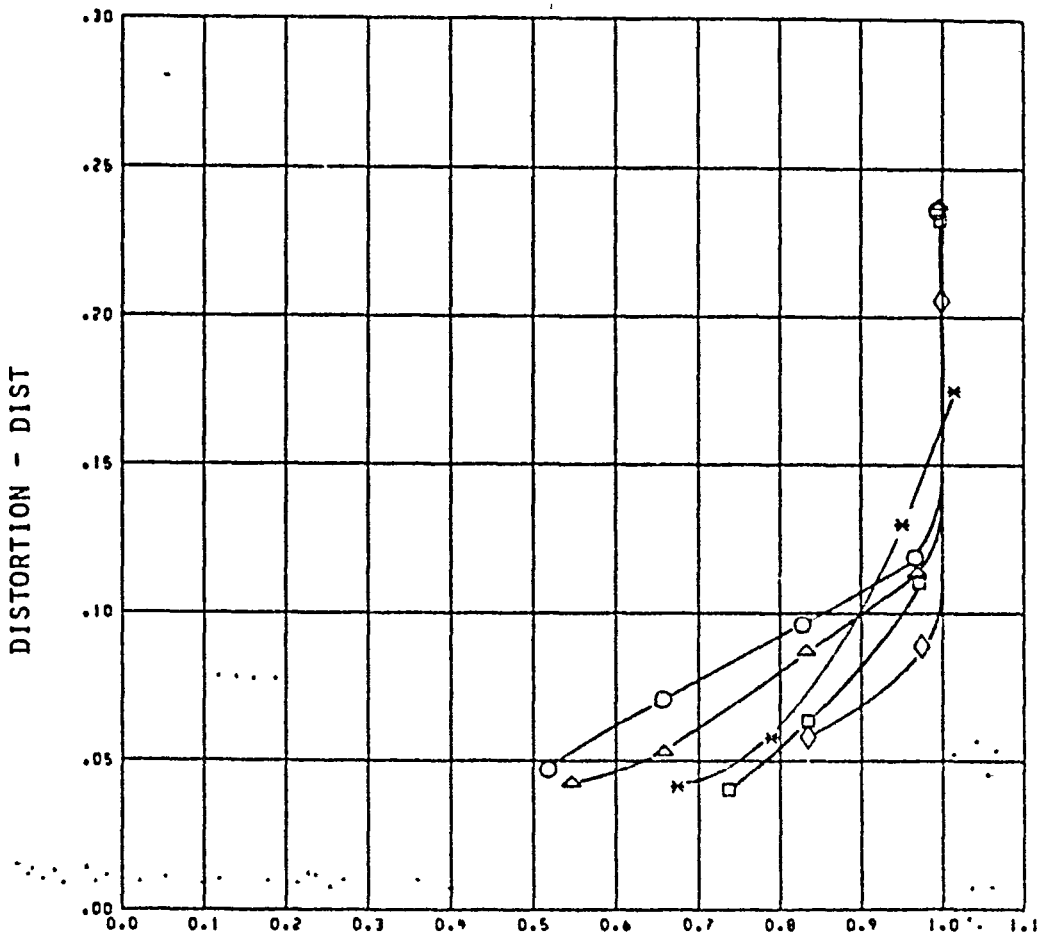

MACH • 1.77 CONF • 23

SYM	CMMCD	CMMCRD	EMFR	PPB	TTRC
○	29.4	8.40	0.042	8.56	1.597
△	24.6	6.99	0.035	7.20	1.602
□	18.3	5.04	0.027	5.42	1.588
◇	14.7	3.89	0.022	4.46	1.566
✳	0.4	-0.48	0.002	0.44	0.992

FIGURE 49 CONTINUED. INLET PERFORMANCE AT 1.76M, HOT FLOW

ORIGINAL PAGE IS
OF POOR QUALITY

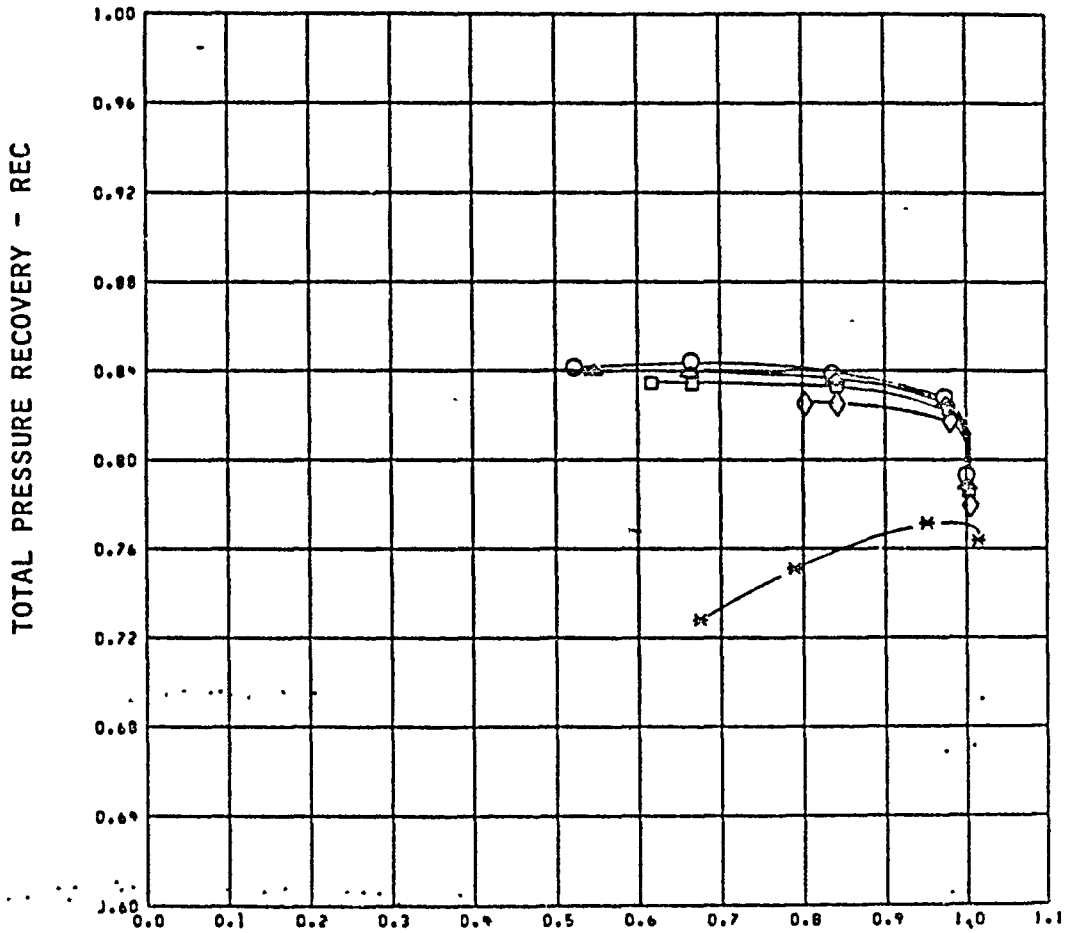

MACH = 1.77 CONF = 24

SYM	CRMCD	CRMCRD	DMFR	PPB	TTRC
○	27.8	7.63	0.041	5.17	1.602
△	24.1	6.52	0.036	4.92	1.599
□	18.7	4.78	0.028	3.96	1.571
◇	14.1	3.39	0.022	2.74	1.538
✳	0.4	-0.48	0.002	0.44	0.992

FIGURE 49 CONTINUED. INLET PERFORMANCE AT 1.76 M, HOT FLOW

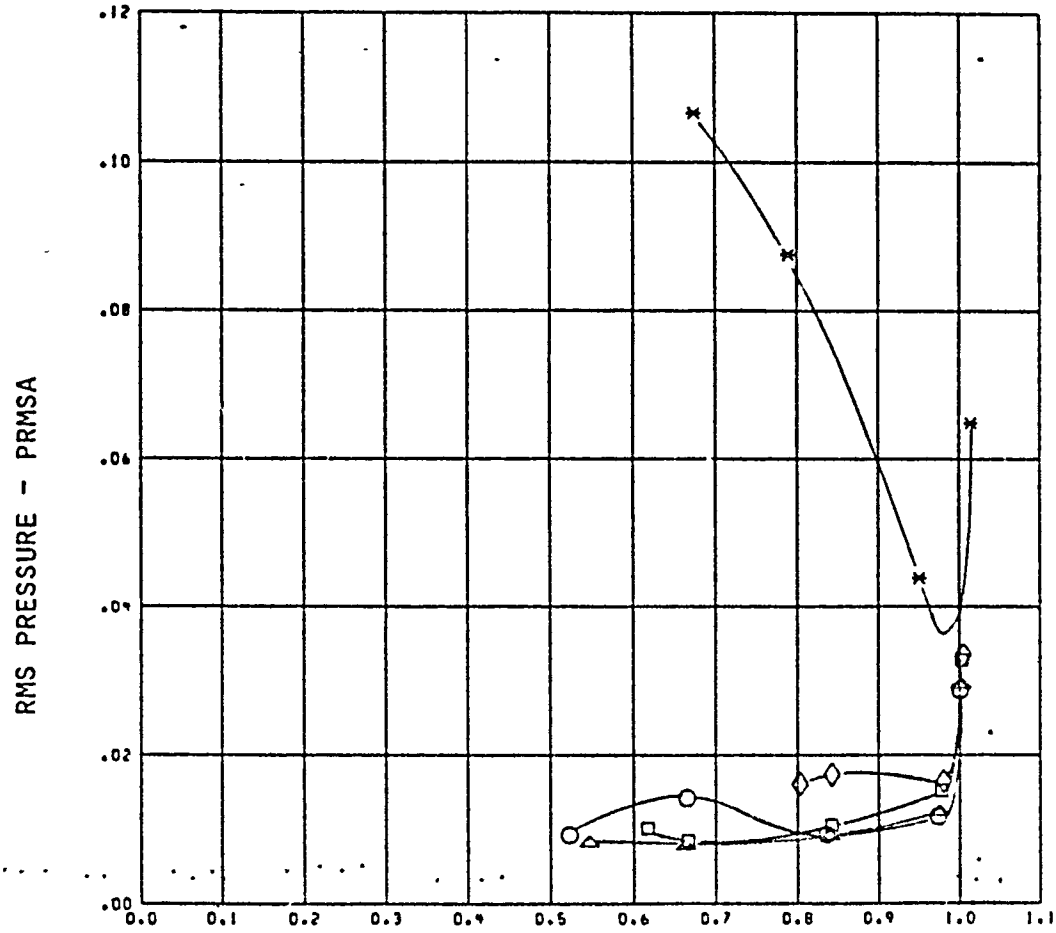

MACH = 1.77 CONF = 24

SYM	CFRCD	CRRCRD	ERFR	PPB	TTRC
○	27.8	7.63	0.041	5.17	1.002
△	24.1	6.52	0.035	4.52	1.599
□	18.7	4.78	0.028	3.56	1.571
◇	14.1	3.39	0.022	2.74	1.538
✳	0.4	-0.48	0.002	0.44	0.992

FIGURE 49 CONTINUED. INLET PERFORMANCE AT 1.76 M, HOT FLOW

ORIGINAL PAGE IS
OF POOR QUALITY

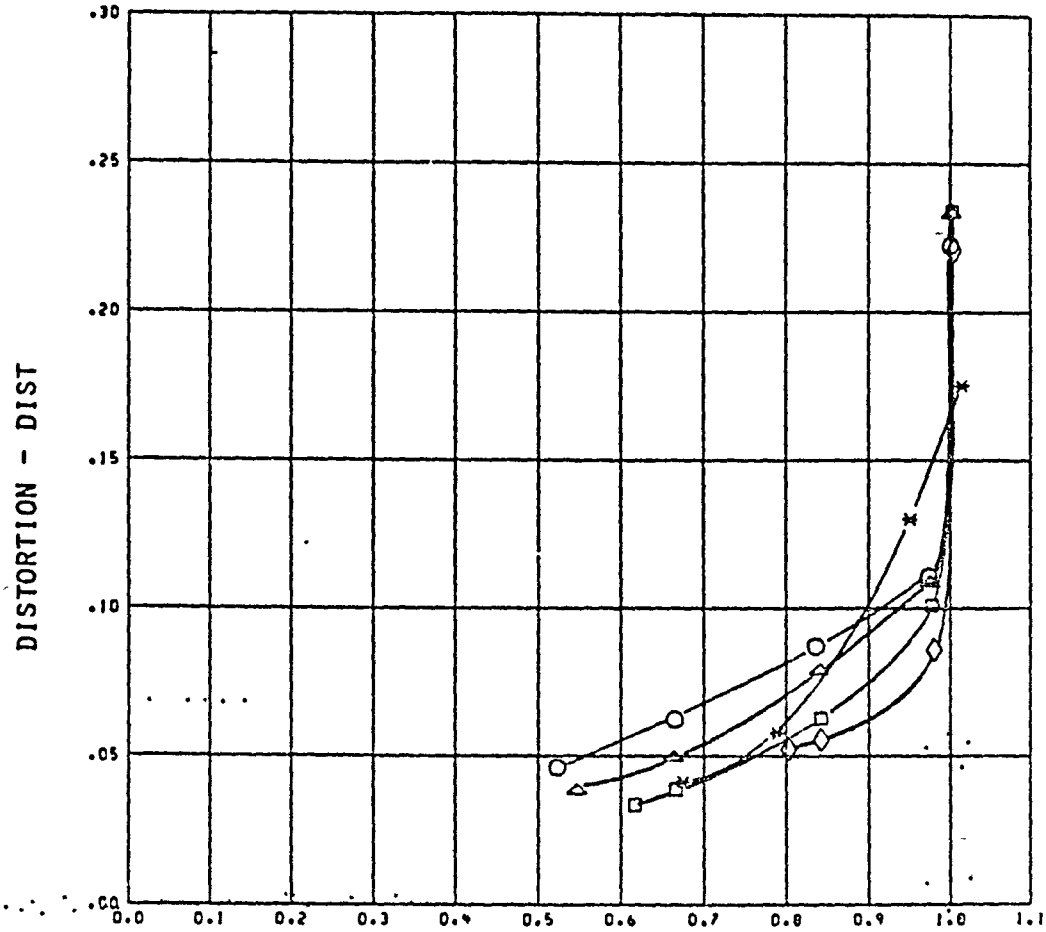

MACH = 1.77 CONF = 24

SYM	CTRCD	CRRCRD	DMFR	PPB	TTRC
○	27.8	7.63	0.041	5.17	1.602
△	24.1	6.52	0.035	4.52	1.559
□	18.7	4.78	0.033	3.56	1.571
◇	14.1	3.39	0.022	2.74	1.533
✳	0.4	-0.48	0.002	0.44	0.992

FIGURE 49 CONCLUDED. INLET PERFORMANCE AT 1.76 M, HOT FLOW

ORIGINAL PAGE IS
OF POOR QUALITY

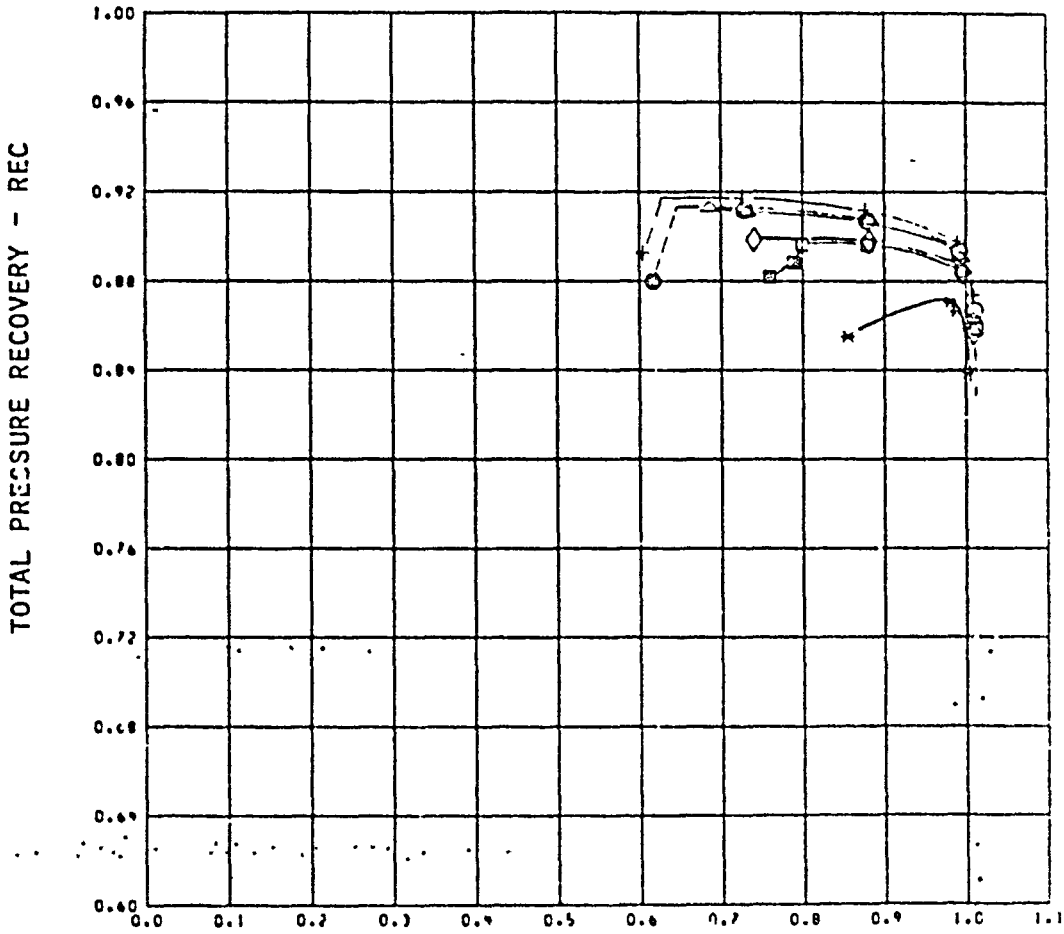

MACH • 1.56 CONF • 21

SYM	CPRCD	CMRCRD	DPFR	PPB	TTRC
+	22.0	3.42	0.033	7.40	1.031
○	17.1	2.61	0.030	5.89	1.014
△	14.9	2.26	0.027	5.23	1.023
□	9.7	1.23	0.010	3.41	1.015
◇	9.0	1.20	0.017	3.30	1.041
✳	0.3	-0.54	0.002	0.51	0.996

FIGURE 50. INLET PERFORMANCE AT 1.56 M, COLD FLOW

ORIGINAL PAGE IS
OF POOR QUALITY

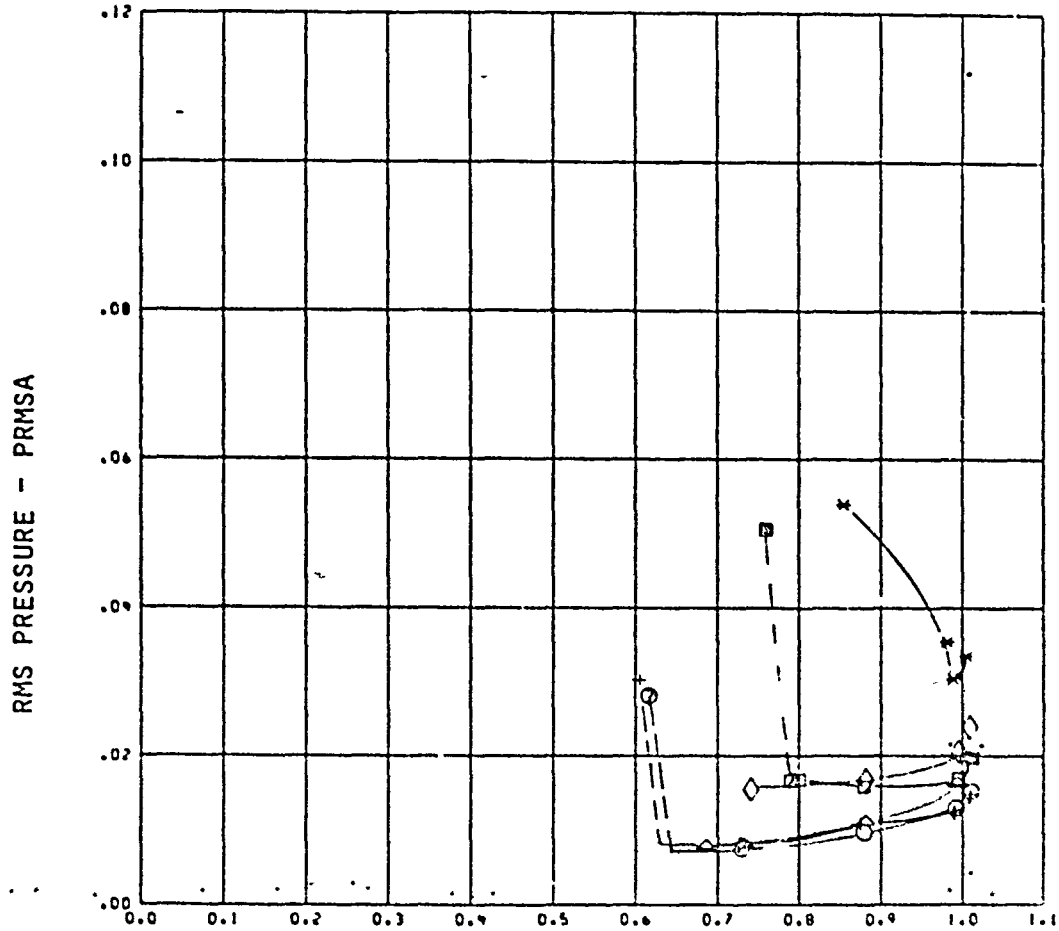

MACH = 1.56 CONF = 21

SYM	CNTCD	CNTCRD	BNFR	PPB	TTRC
+	22.0	3.42	0.039	7.49	1.031
○	17.1	2.61	0.039	5.63	1.014
△	14.9	2.26	0.027	5.23	1.023
□	9.7	1.23	0.018	3.41	1.015
◇	9.0	1.20	0.017	3.39	1.041
✳	0.3	-0.54	0.002	0.51	0.995

FIGURE 50 CONTINUED. INLET PERFORMANCE AT 1.56M, COLD FLOW

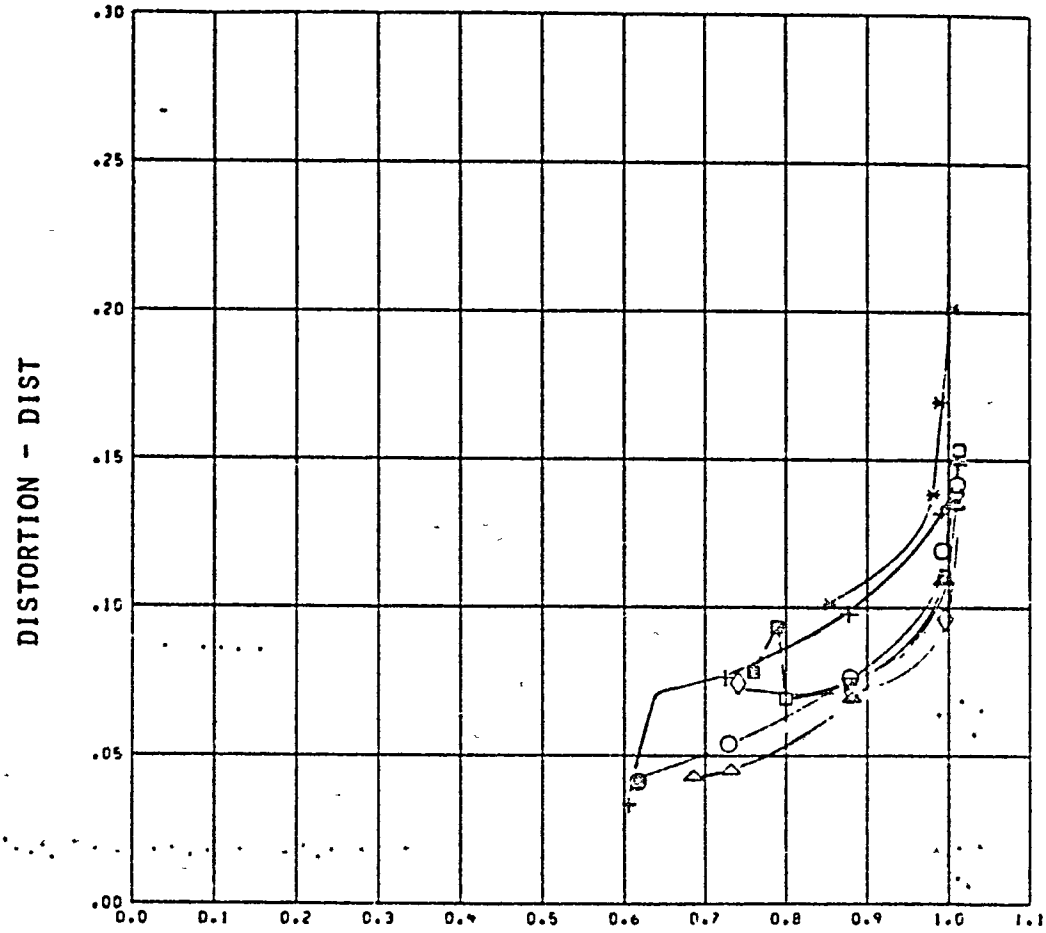

MACH = 1.56 CONF = 21

SYM	CIRCD	CIRCRD	DIFR	PPB	TTRC
+	22.0	3.42	0.039	7.40	1.031
○	17.1	2.61	0.030	5.09	1.014
△	14.9	2.26	0.027	5.23	1.023
□	9.7	1.23	0.018	3.41	1.015
◇	9.0	1.20	0.017	3.30	1.041
✳	0.3	-0.54	0.002	0.51	0.995

FIGURE 50 CONTINUED. INLET PERFORMANCE AT 1.56 M, COLD FLOW

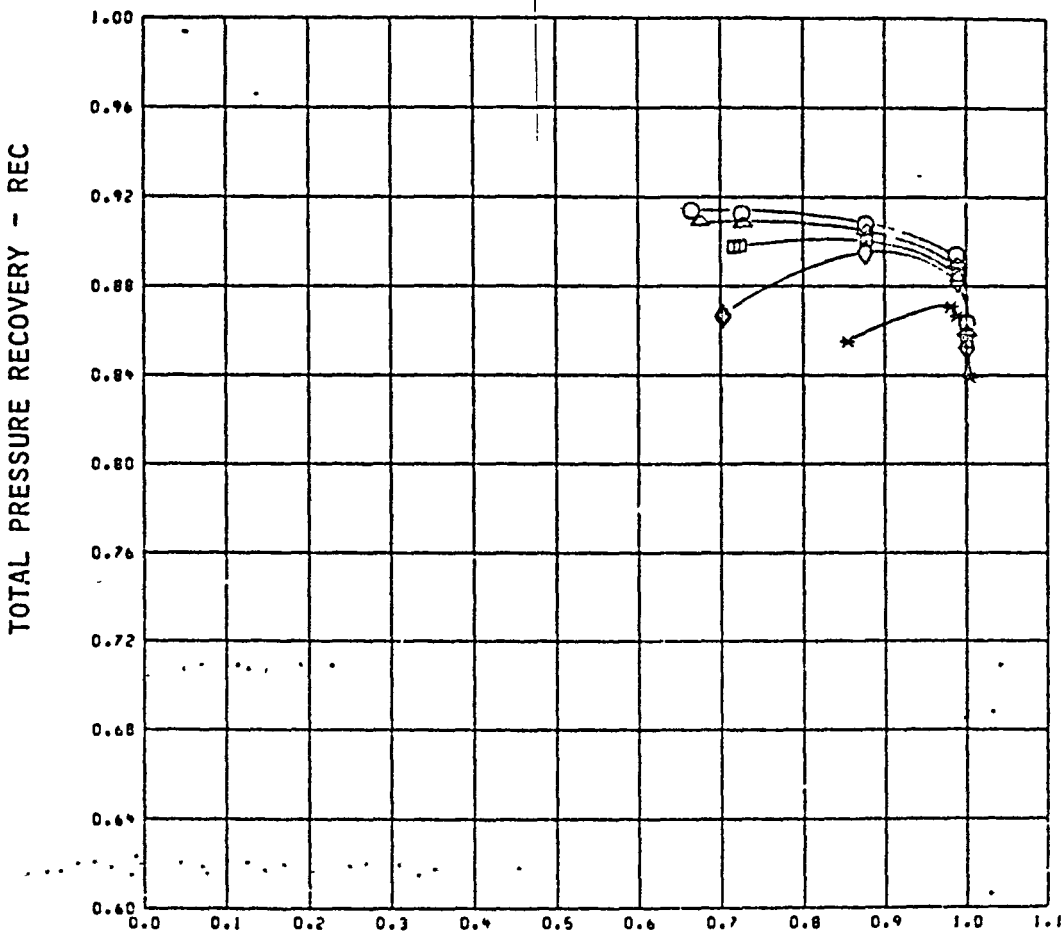

MACH • 1.56 CONF • 22

SYM	CMMCD	CMMCRD	EMFR	PPD	TTRC
○	18.9	3.03	0.033	6.28	1.022
△	16.0	2.44	0.028	5.35	1.018
□	11.6	1.61	0.021	3.96	1.017
◇	9.2	1.23	0.017	3.21	1.034
✳	0.3	-0.54	0.002	0.51	0.996

FIGURE 50 CONTINUED. INLET PERFORMANCE AT 1.56M, COLD FLOW.

ORIGINAL PAGE IS
OF POOR QUALITY

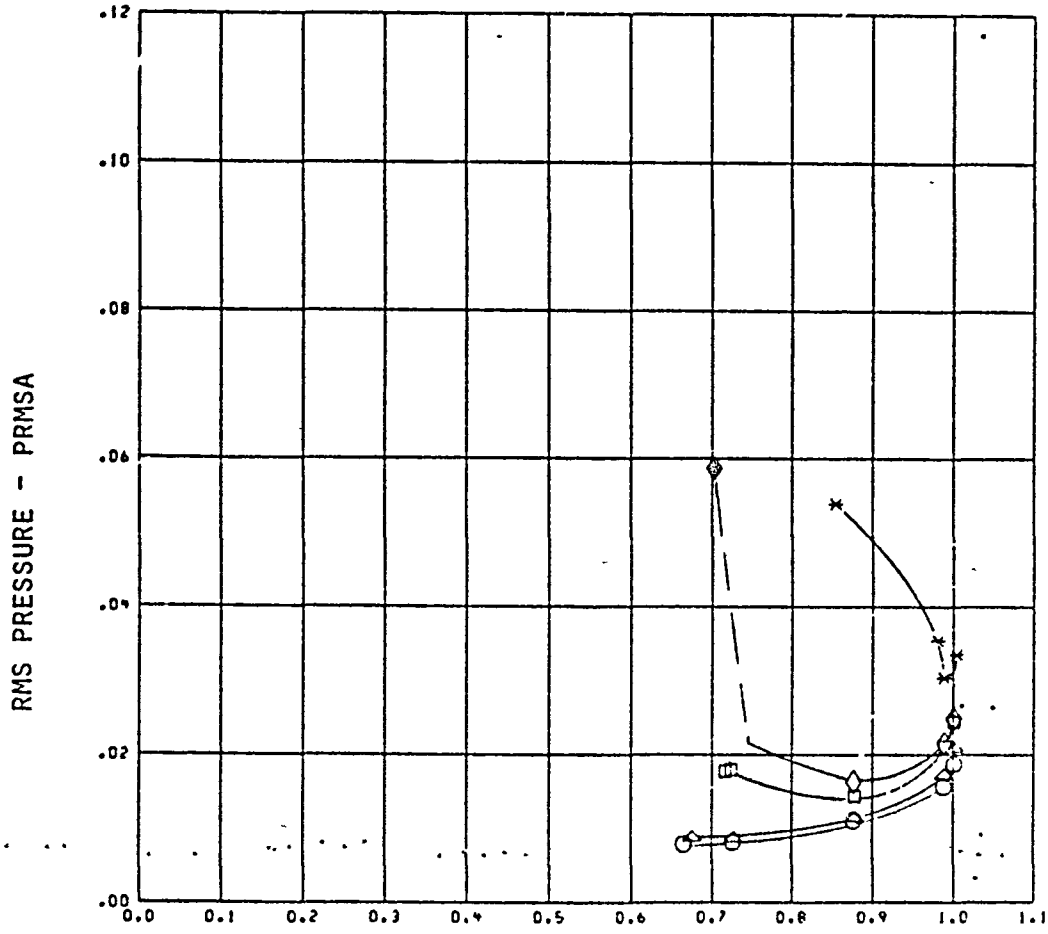

MACH = 1.56 CONF = 22

SYM	CMXCD	CMXCRD	BMFR	PPB	TTRC
○	18.9	3.03	0.033	6.28	1.022
△	16.0	2.44	0.028	5.35	1.018
□	11.6	1.61	0.021	3.9[illegible]	1.017
◇	9.2	1.23	0.017	3.21	1.034
✳	0.3	-0.54	0.002	0.51	0.996

FIGURE 50 CONTINUED. INLET PERFORMANCE AT 1.56M, COLD FLOW

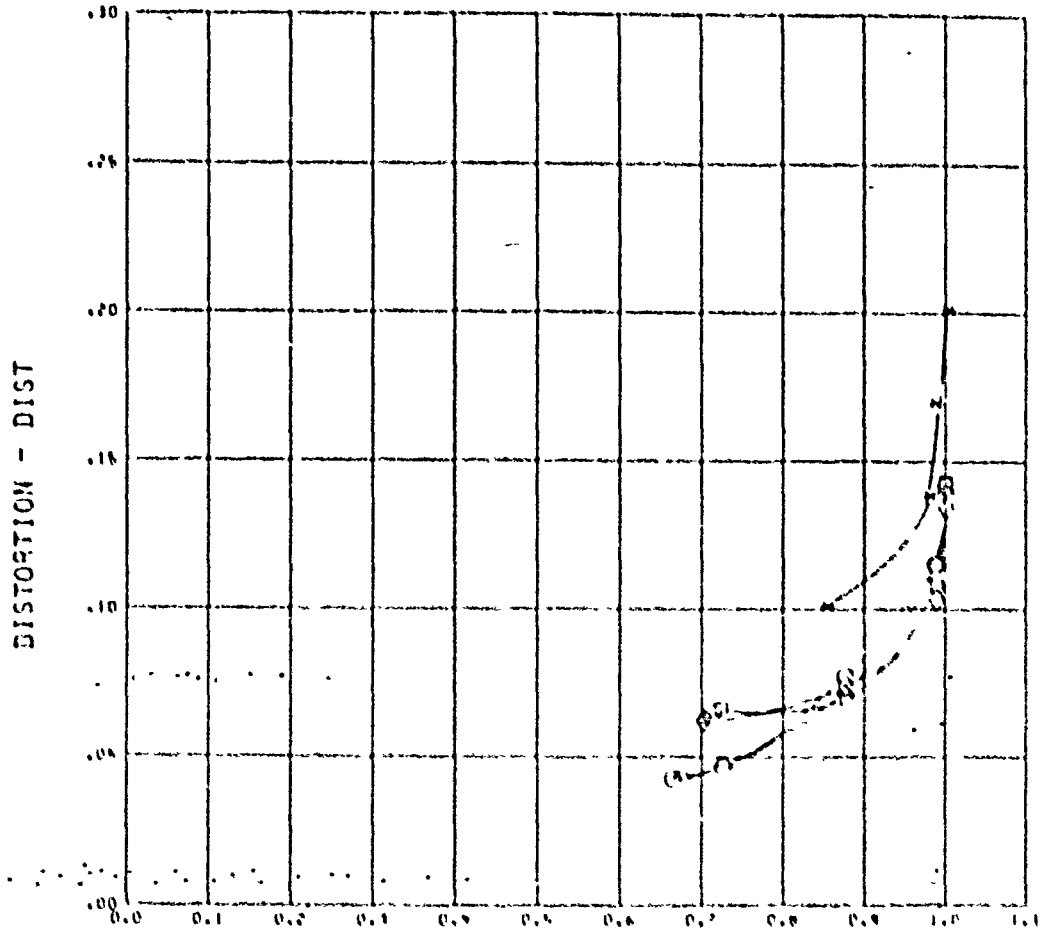

MACH • 1.56 CONF • 22

SYM	CMNCD	CMNCRD	BMFR	PPD	TTRC
○	18.0	3.03	0.031	6.28	1.022
△	10.0	2.44	0.028	5.35	1.018
□	11.6	1.61	0.021	3.96	1.017
◇	0.2	1.23	0.017	3.21	1.014
✳	0.3	-0.54	0.002	0.51	0.996

FIGURE 50 CONTINUED. INLET PERFORMANCE AT 1.56 M, COLD FLOW

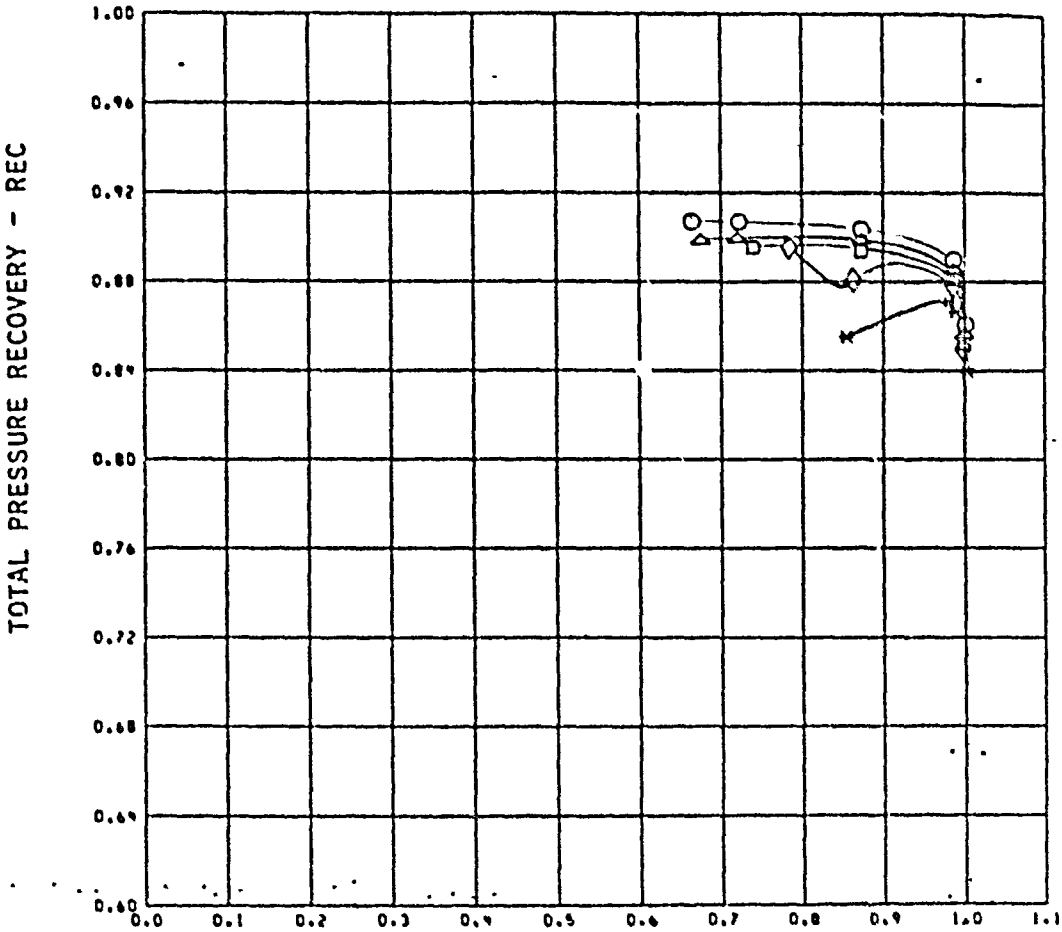

MACH • 1.56 CONF • 23

SYM	CMRCD	CMRCRD	DMFR	PPB	TTRC
○	18.7	2.81	0.033	6.09	1.091
△	15.6	2.26	0.020	5.14	1.034
□	11.5	1.69	0.021	3.87	1.019
◇	9.5	1.21	0.017	3.25	1.014
✳	0.3	-0.54	0.002	0.51	0.996

FIGURE 50 CONTINUED. INLET PERFORMANCE AT 1.56M, COLD FLOW.

ORIGINAL PAGE IS
OF POOR QUALITY

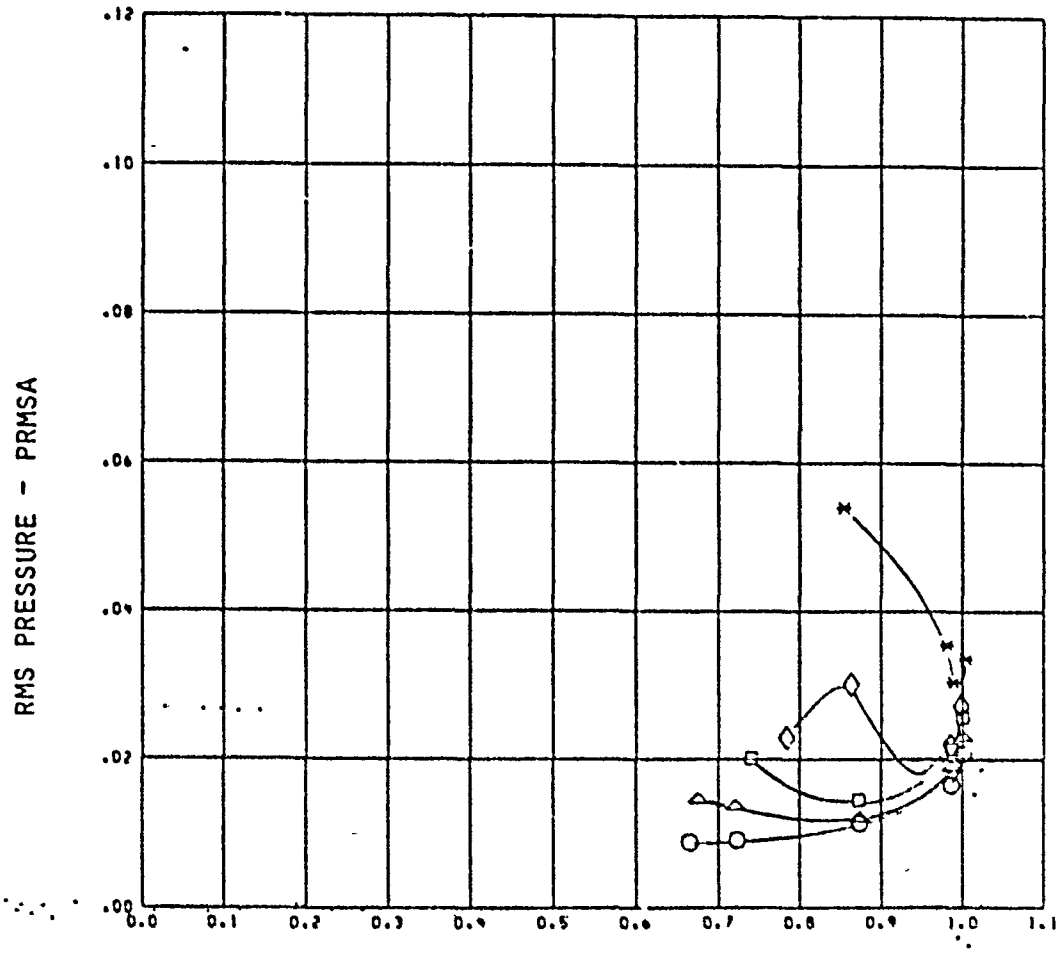

MACH = 1.56 CONF = 23

SYM	CMMCD	CMMCRD	BMFR	PPB	TTRC
○	18.7	2.81	0.033	6.09	1.031
△	15.6	2.28	0.028	5.14	1.034
□	11.5	1.60	0.021	3.87	1.019
◇	9.5	1.21	0.017	3.25	1.014
✳	0.3	-0.54	0.002	0.51	0.996

FIGURE 50 CONTINUED. INLET PERFORMANCE AT 1.56M, COLD FLOW

ORIGINAL PAGE IS
OF POOR QUALITY

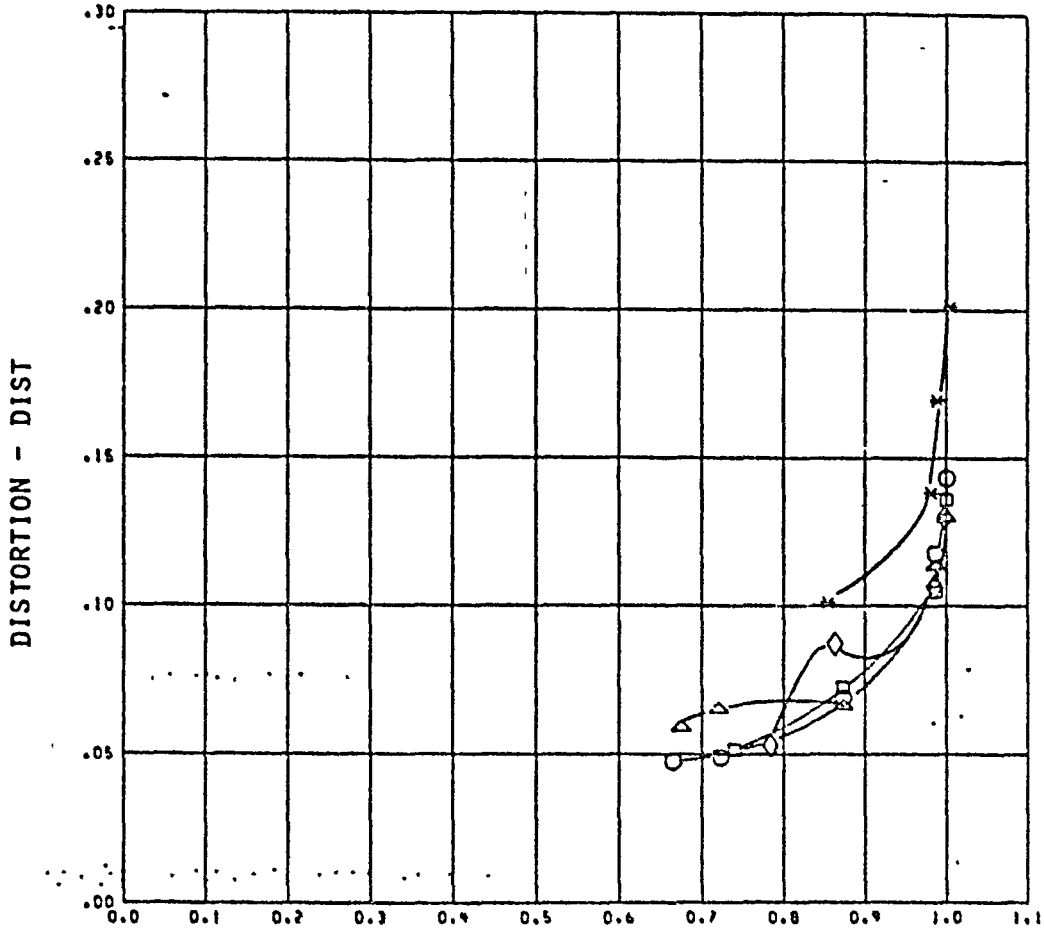

MACH • 1.56 CONF • 23

SYM	CRITCD	CRITCRD	BKFR	PPD	TTRC
○	18.7	2.81	0.033	6.09	1.031
△	15.6	2.26	0.028	5.14	1.024
□	11.5	1.60	0.021	3.87	1.019
◇	9.5	1.21	0.017	3.25	1.014
✳	0.3	-0.54	0.002	0.51	0.996

FIGURE 50 CONTINUED. INLET PERFORMANCE AT 1.56 M, COLD FLOW

ORIGINAL PAGE IS
OF POOR QUALITY

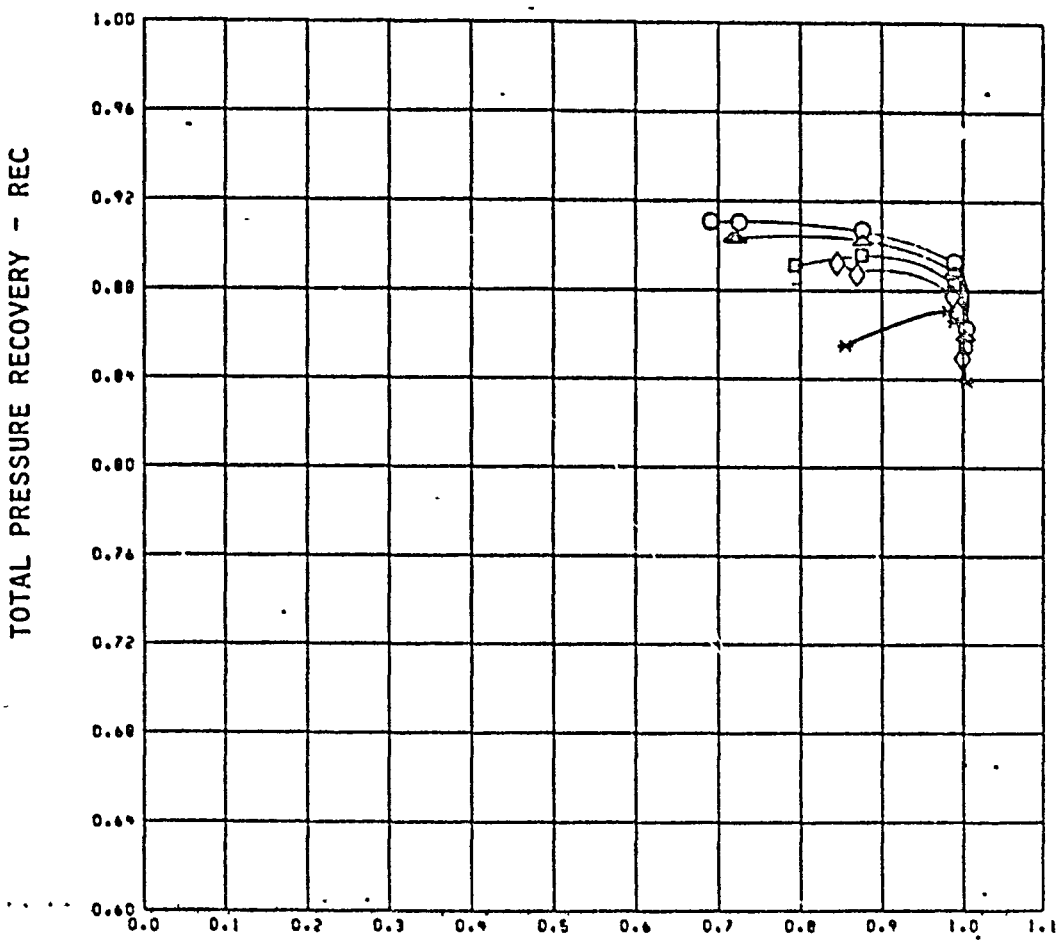

MACH = 1.56 CONF = 24

SYM	CRMCD	CRMCRD	BMFR	PPD	TTRC
○	17.6	2.31	0.032	3.76	1.018
△	14.7	1.69	0.027	3.20	1.017
□	10.3	0.93	0.020	2.34	1.010
◇	8.0	0.52	0.016	1.89	1.023
✳	0.3	-0.54	0.002	0.51	0.996

FIGURE 50 CONTINUED. INLET PERFORMANCE AT 1.56M, COLD FLOW.

ORIGINAL PAGE IS
OF POOR QUALITY

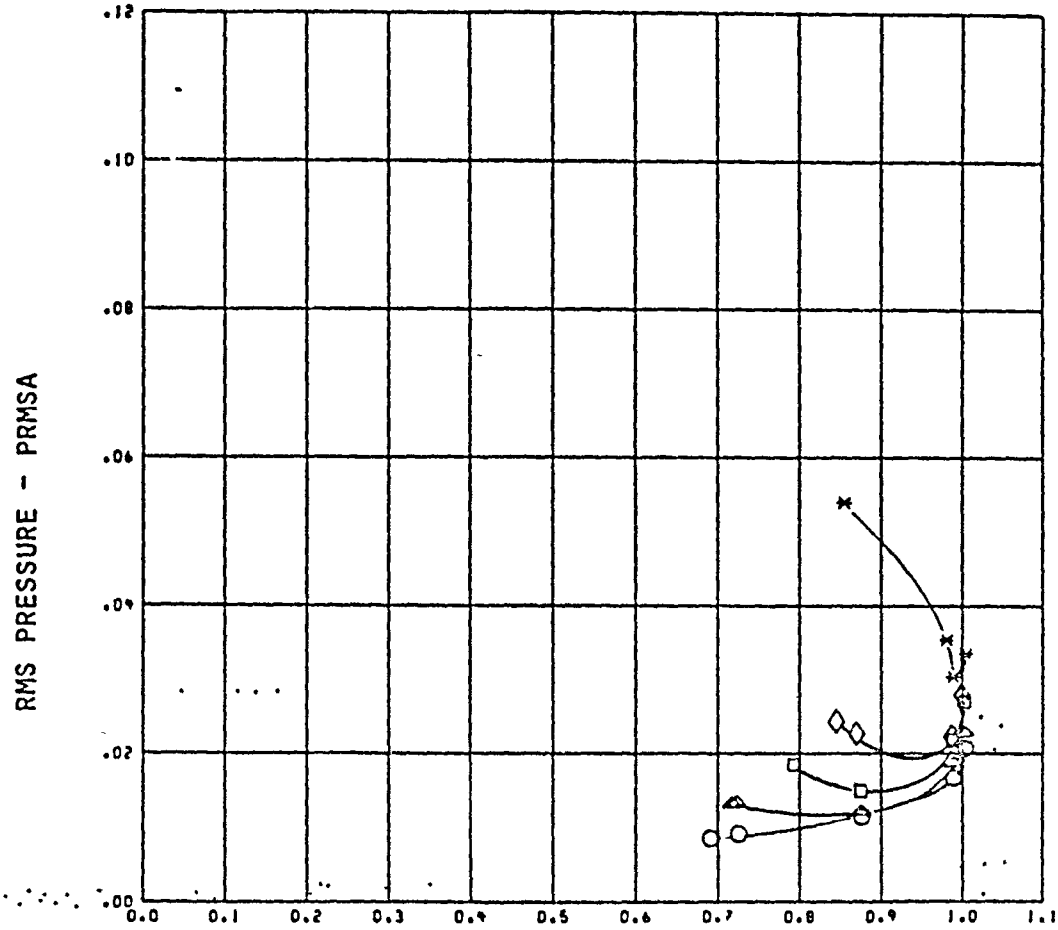

MACH = 1.56 CONF = 24

SYM	CMMCD	CMMCRD	BMFR	PPB	TTRC
○	17.6	2.31	0.032	3.76	1.010
△	14.7	1.69	0.027	3.20	1.007
□	10.3	0.99	0.020	2.34	1.009
◇	8.0	0.52	0.016	1.89	1.023
✳	0.3	-0.54	0.002	0.51	0.996

FIGURE 50 CONTINUED. INLET PERFORMANCE AT 1.56M, COLD FLOW

ORIGINAL PAGE IS
OF POOR QUALITY

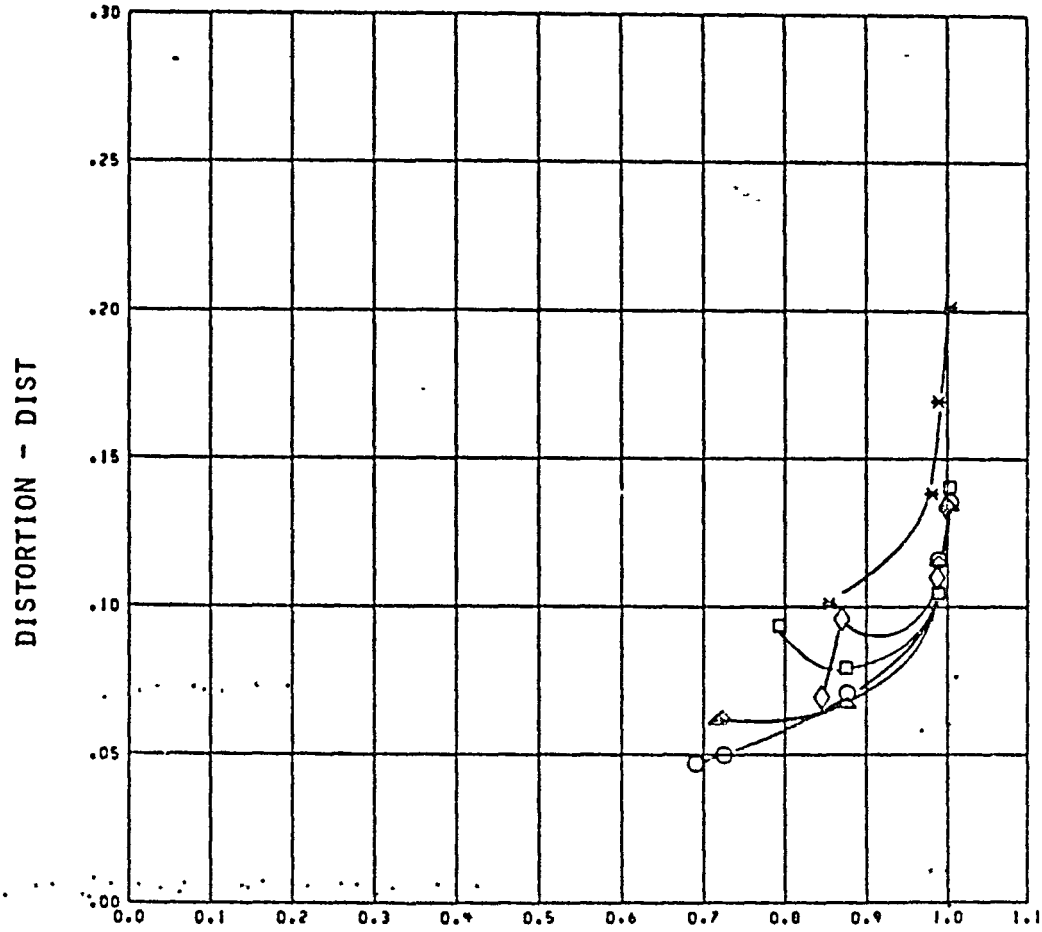

MACH • 1.56 CORE • 24

SYM	CRITCD	CRITCRD	BTER	PPD	TTRC
○	17.6	2.31	0.032	3.76	1.018
△	14.7	1.69	0.027	3.20	1.007
□	10.3	0.99	0.020	2.34	1.030
◇	8.0	0.52	0.016	1.89	1.023
✳	0.3	-0.54	0.002	0.51	0.996

FIGURE 50 CONCLUDED. INLET PERFORMANCE AT 1.56 M, COLD FLOW

ORIGINAL PAGE IS
OF POOR QUALITY

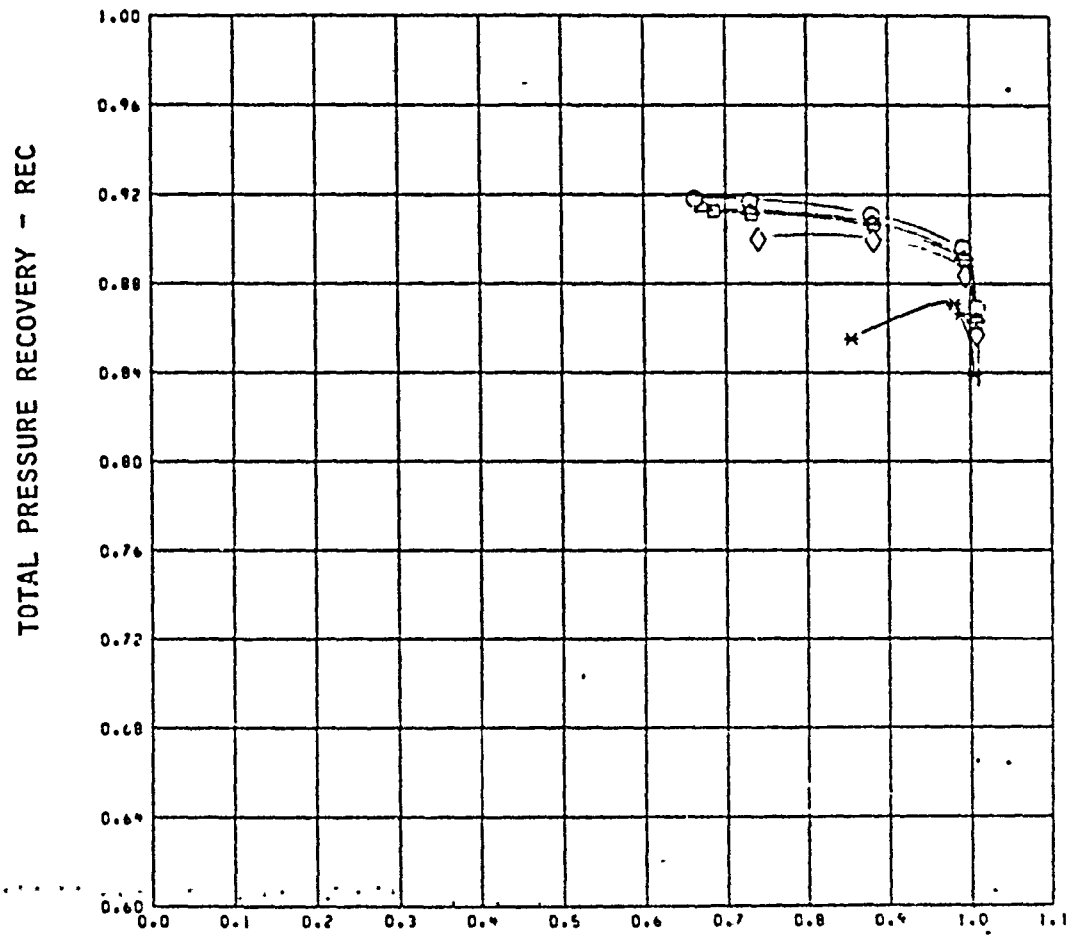

MACH = 1.56 CONF = 21

SYM	CRWCD	CRWCRD	BRFR	PPB	TTRC
○	19.6	6.42	0.028	6.79	1.597
△	16.5	5.29	0.024	5.78	1.590
□	14.2	4.43	0.021	5.02	1.561
◇	9.8	2.80	0.015	3.50	1.507
✳	0.3	-0.54	0.002	0.51	0.996

FIGURE 51. INLET PERFORMANCE AT 1.56 M, HOT FLOW

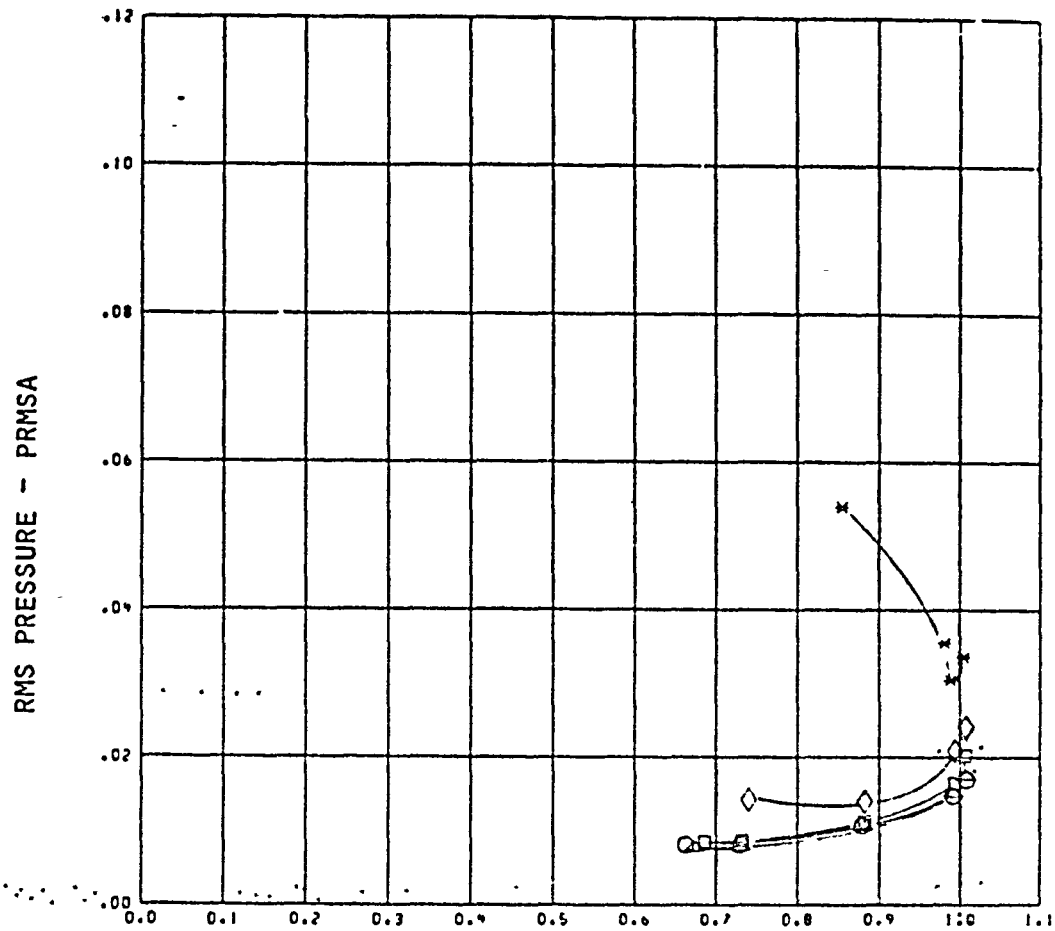

MACH = 1.56 CONF = 21

SYM	CRMCD	CRRCRD	DMFR	PPB	TTRC
○	19.6	6.42	0.028	6.79	1.597
△	16.5	5.29	0.024	5.78	1.589
□	14.2	4.43	0.021	5.02	1.561
◇	9.8	2.80	0.015	3.58	1.597
✳	0.3	-0.54	0.002	0.51	0.996

FIGURE 51 CONTINUED. INLET PERFORMANCE AT 1.56M, HOT FLOW

ORIGINAL PAGE IS
OF POOR QUALITY

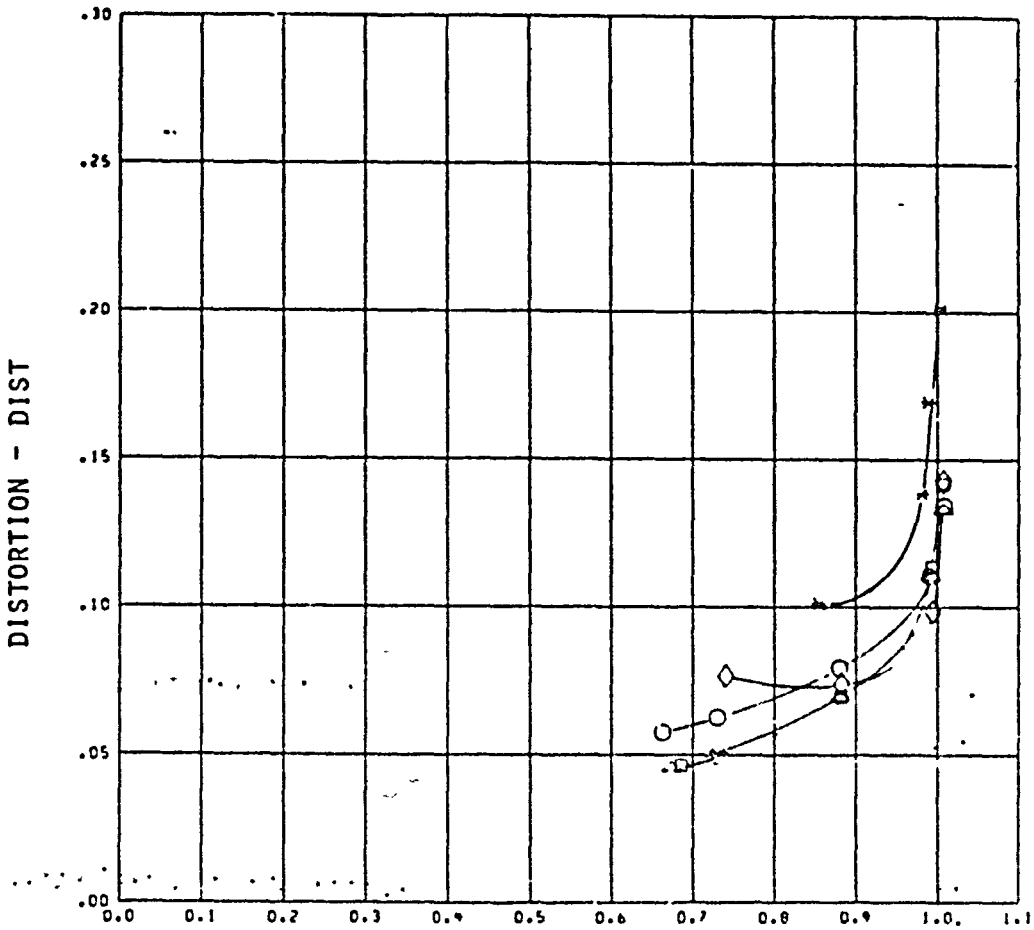

MACH = 1.56 CONF = 21

SYM	CRMCD	CRMCRD	ERFR	PPB	TTRC
○	19.6	6.42	0.020	6.79	1.597
△	16.5	5.29	0.024	5.78	1.589
□	14.2	4.43	0.021	5.02	1.561
◇	9.8	2.89	0.015	3.58	1.587
✳	0.3	-0.54	0.002	0.51	0.996

FIGURE 51 CONTINUED. INLET PERFORMANCE AT 1.56M, HOT FLOW

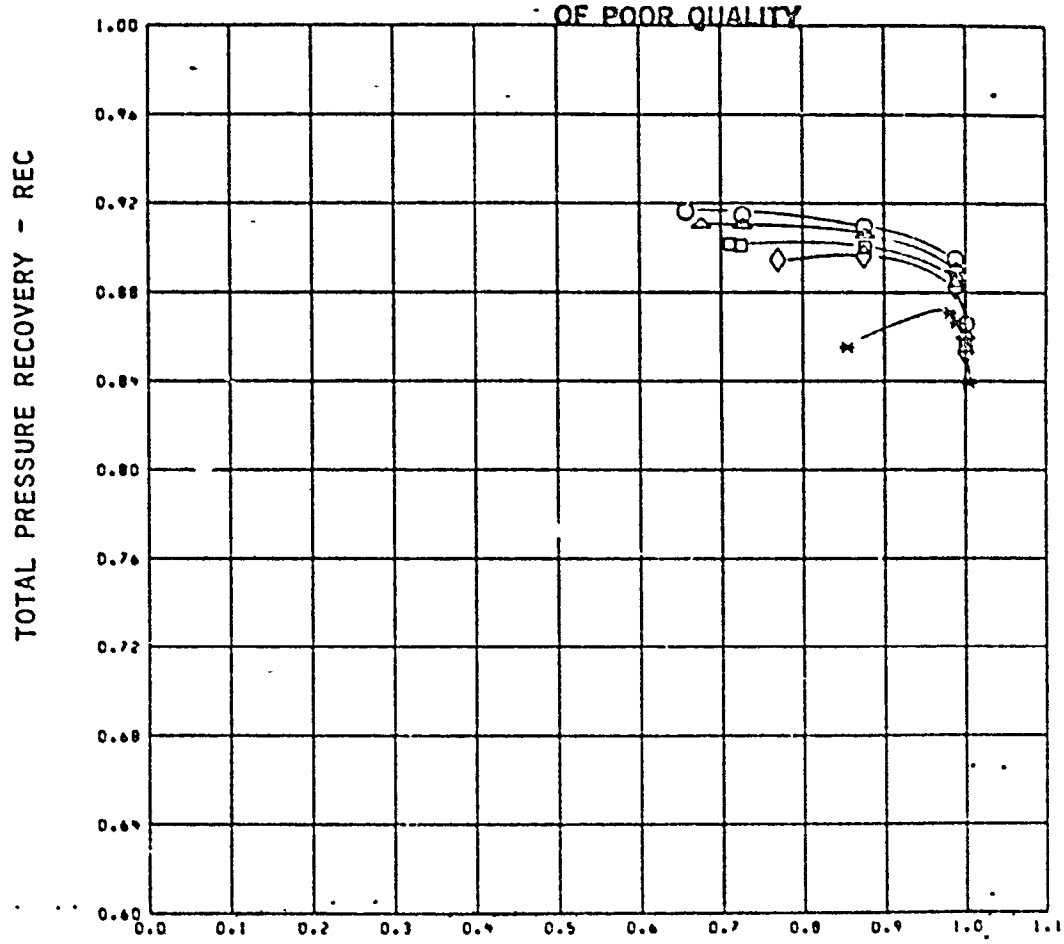

MACH = 1.56 CONF = 22

SYM	CMTCD	CMTCRD	BMFR	PPB	TTRC
○	21.1	7.33	0.020	7.01	1.694
△	17.6	5.99	0.024	5.91	1.666
□	13.1	4.33	0.018	4.45	1.646
◇	10.4	3.21	0.015	3.56	1.695
✳	0.3	-0.54	0.092	0.51	0.995

FIGURE 51 CONTINUED. INLET PERFORMANCE AT 1.56 M, HOT FLOW

ORIGINAL PAGE IS
OF POOR QUALITY

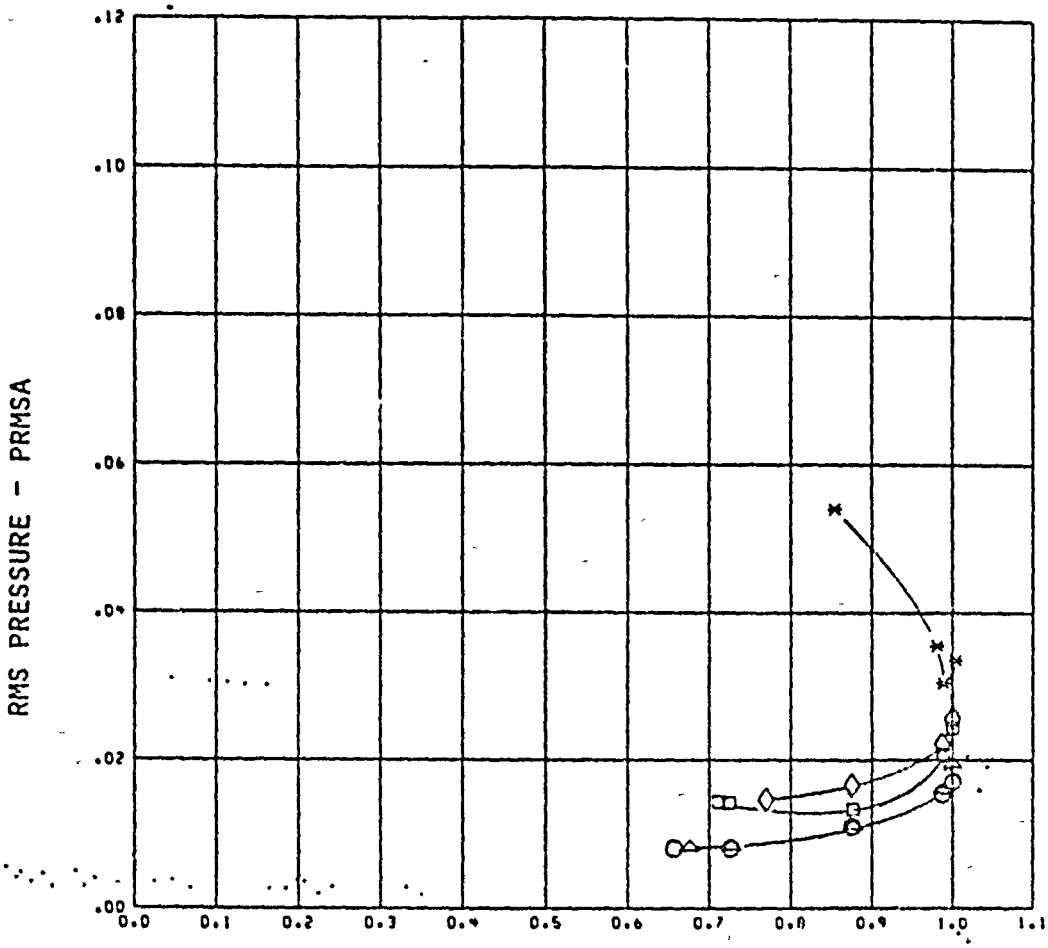

MACH = 1.56 CONF = 22

SYM	CMPCD	CORCRD	BMFR	FPB	TTRC
○	21.1	7.33	0.020	7.01	1.694
△	17.6	5.93	0.024	5.91	1.686
□	13.1	4.39	0.018	4.45	1.646
◇	10.4	3.21	0.015	3.56	1.606
✳	0.3	-0.54	0.002	0.51	0.995

FIGURE 51 CONTINUED. INLET PERFORMANCE AT 1.56M, HOT FLOW

ORIGINAL PAGE IS
OF POOR QUALITY

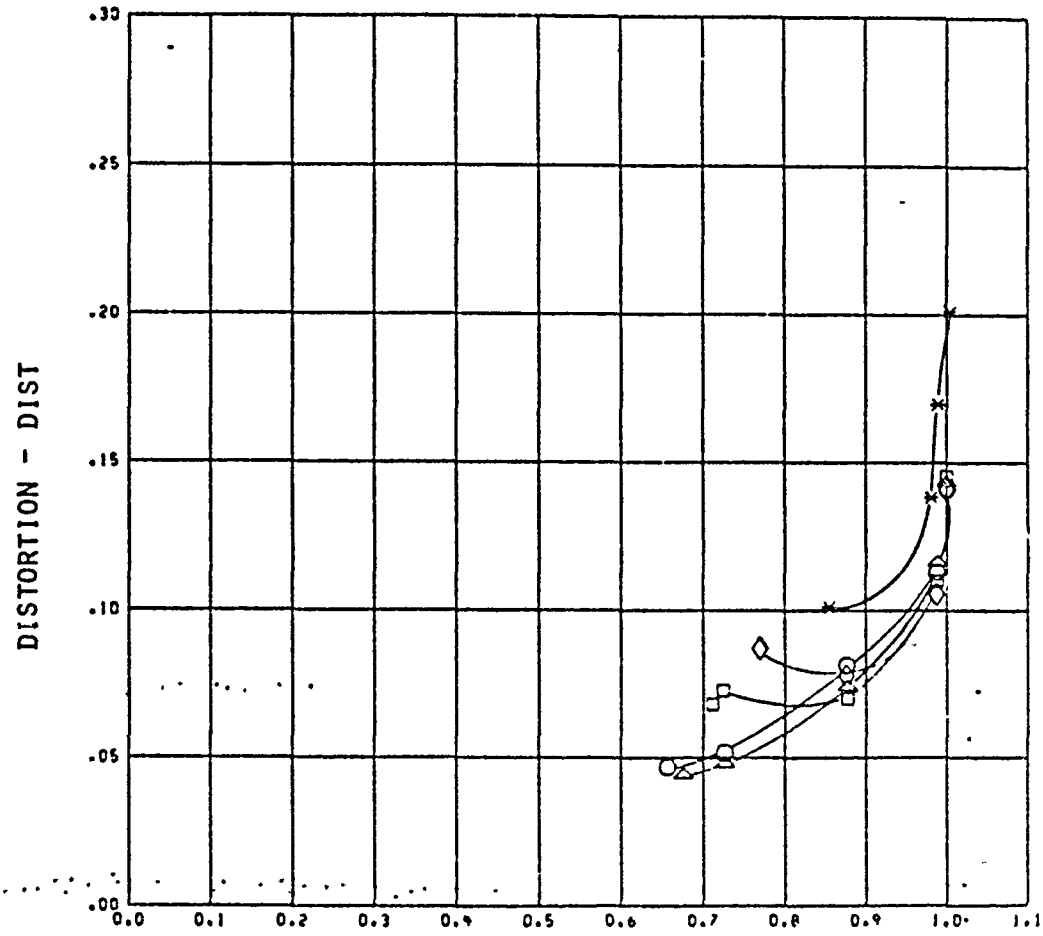

MACH = 1.56 CONF = 22

SYM	CNTCD	CNTCPD	BMFR	PPB	TTRC
○	21.1	7.30	0.029	7.01	1.004
△	17.6	5.99	0.024	5.81	1.006
□	13.1	4.30	0.018	4.45	1.006
◇	10.4	3.21	0.015	3.56	1.006
✳	0.3	-0.54	0.002	0.51	0.995

FIGURE 51 CONTINUED. INLET PERFORMANCE AT 1.56M, HOT FLOW

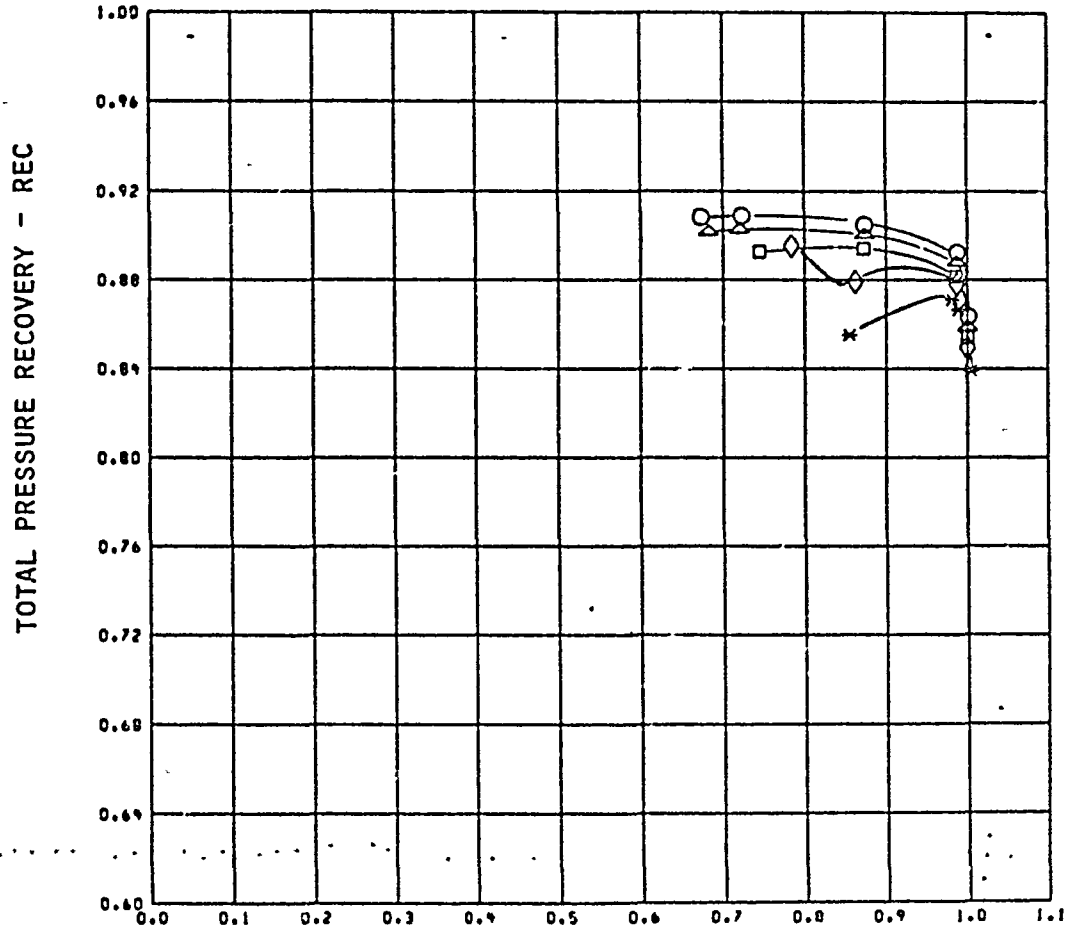

MACH = 1.56 CONF = 23

SYM	CIRCD	CIRCRD	DIFR	PPB	TTRC
○	20.2	6.90	0.028	6.60	1.657
△	17.4	5.79	0.024	5.72	1.636
□	12.3	3.86	0.018	4.15	1.591
◇	9.8	2.92	0.015	3.36	1.557
✳	0.3	-0.54	0.002	0.51	0.996

FIGURE 51 CONTINUED. INLET PERFORMANCE AT 1.56 M, HOT FLOW

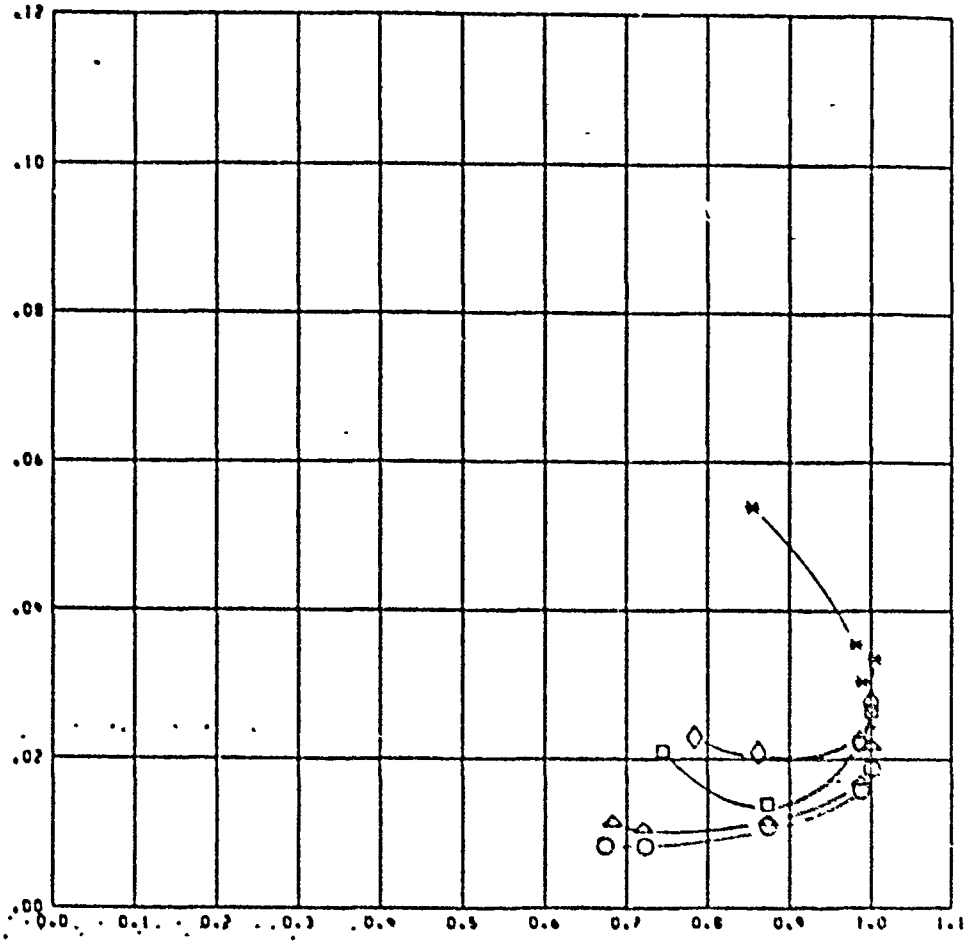

MACH = 1.56 CONF = 20

SYM	CNTCD	CNTCRD	DMFR	PPB	TTRC
○	20.2	6.90	0.020	6.69	1.657
△	17.4	5.70	0.024	5.72	1.635
□	12.3	3.86	0.018	4.15	1.591
◇	9.0	2.92	0.015	3.36	1.557
✳	0.3	-0.54	0.002	0.51	0.006

FIGURE 51 CONTINUED. INLET PERFORMANCE AT 1.56M, HOT FLOW

ORIGINAL PAGE IS
OF POOR QUALITY

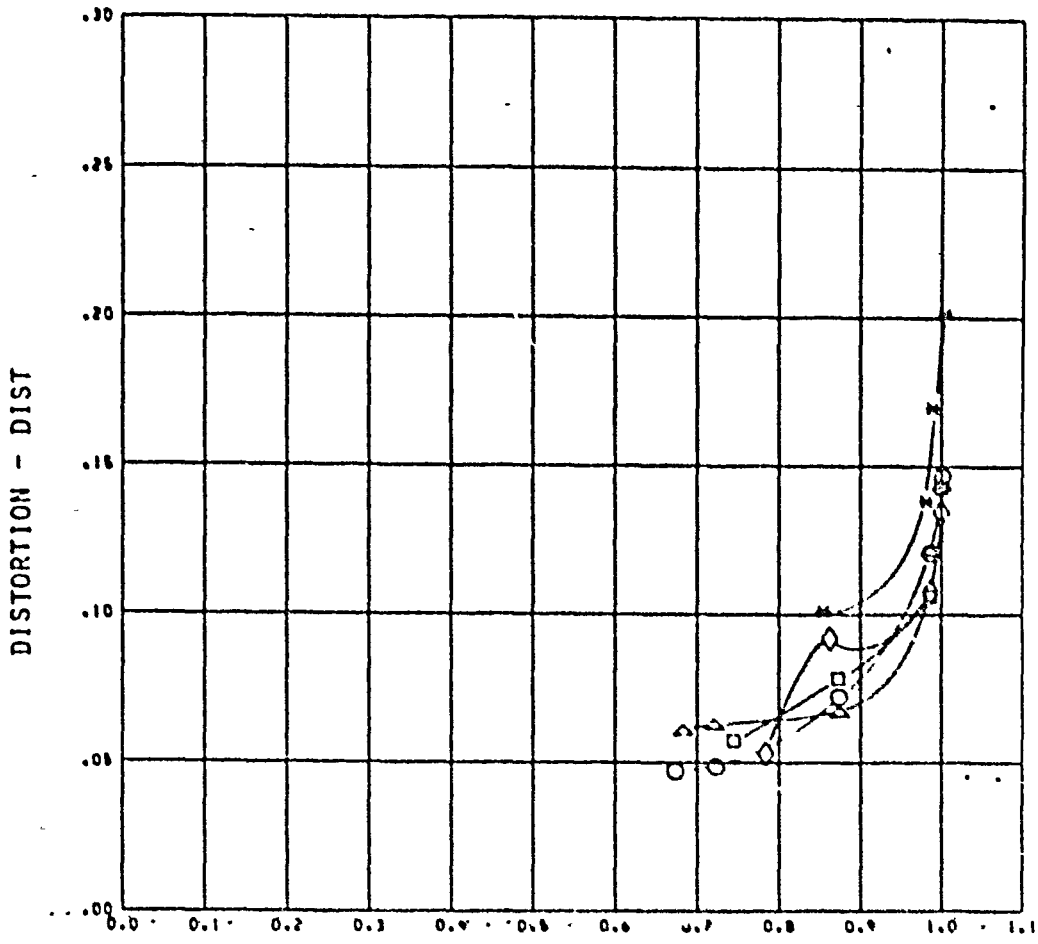

EXTERNAL MASS FLOW RATIO - MFRX

MACH = 1.56 CONF = 23

SYM	CIRCD	CIRCRD	BMFR	PPB	TTRC
○	20.2	6.00	0.023	6.60	1.657
△	17.4	5.79	0.024	5.72	1.635
□	12.3	3.06	0.018	4.15	1.591
◇	9.0	2.02	0.015	3.36	1.557
✳	0.3	-0.54	0.002	0.51	0.996

FIGURE 51 CONTINUED. INLET PERFORMANCE AT 1.56M, HOT FLOW

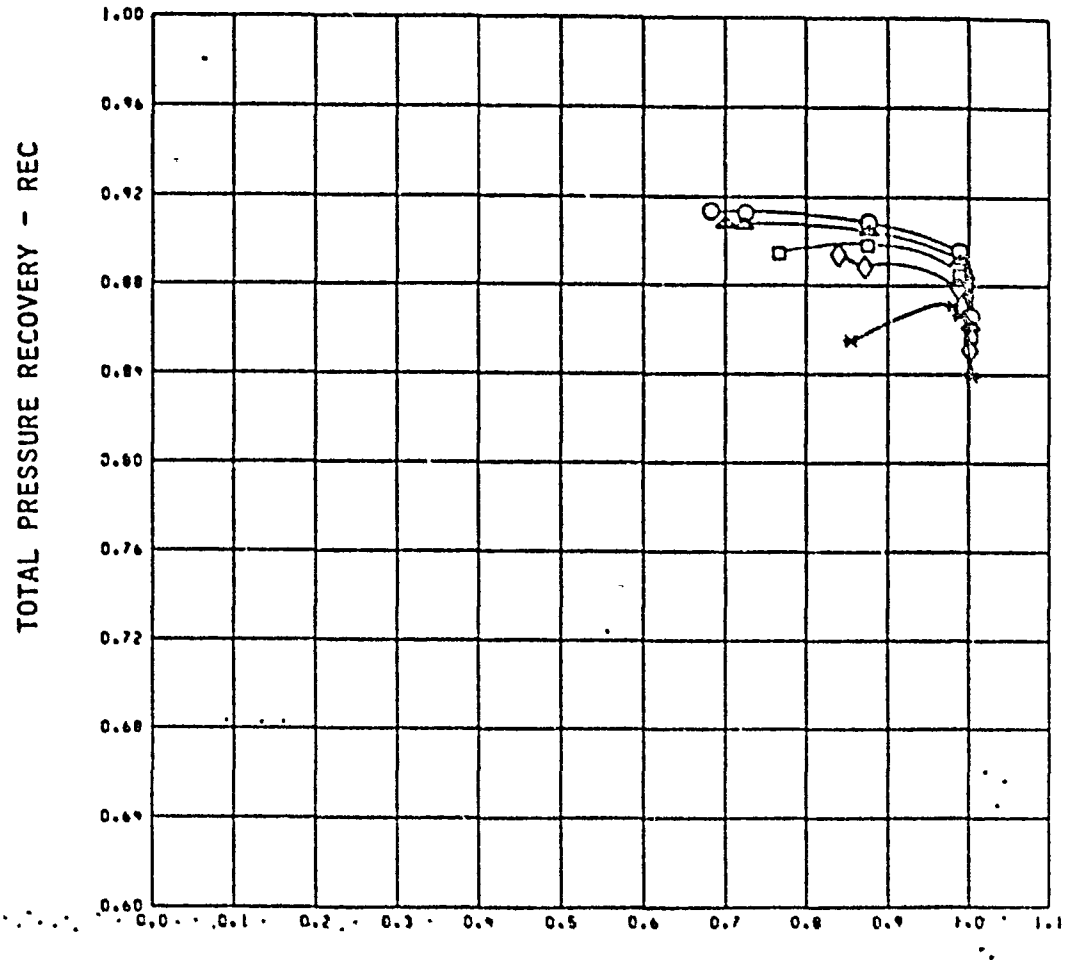

MACH = 1.56 CONF = 24

SYM	CMNCD	CMNCRD	BMFR	PPB	TTRC
○	20.1	6.44	0.029	4.27	1.633
△	17.3	5.36	0.025	3.71	1.616
□	12.3	3.45	0.019	2.72	1.573
◇	8.5	2.02	0.014	1.89	1.569
✳	0.3	-0.54	0.002	0.51	0.006

FIGURE 51 CONTINUED. INLET PERFORMANCE AT 1.56 M, HOT FLOW

ORIGINAL PAGE IS
OF POOR QUALITY

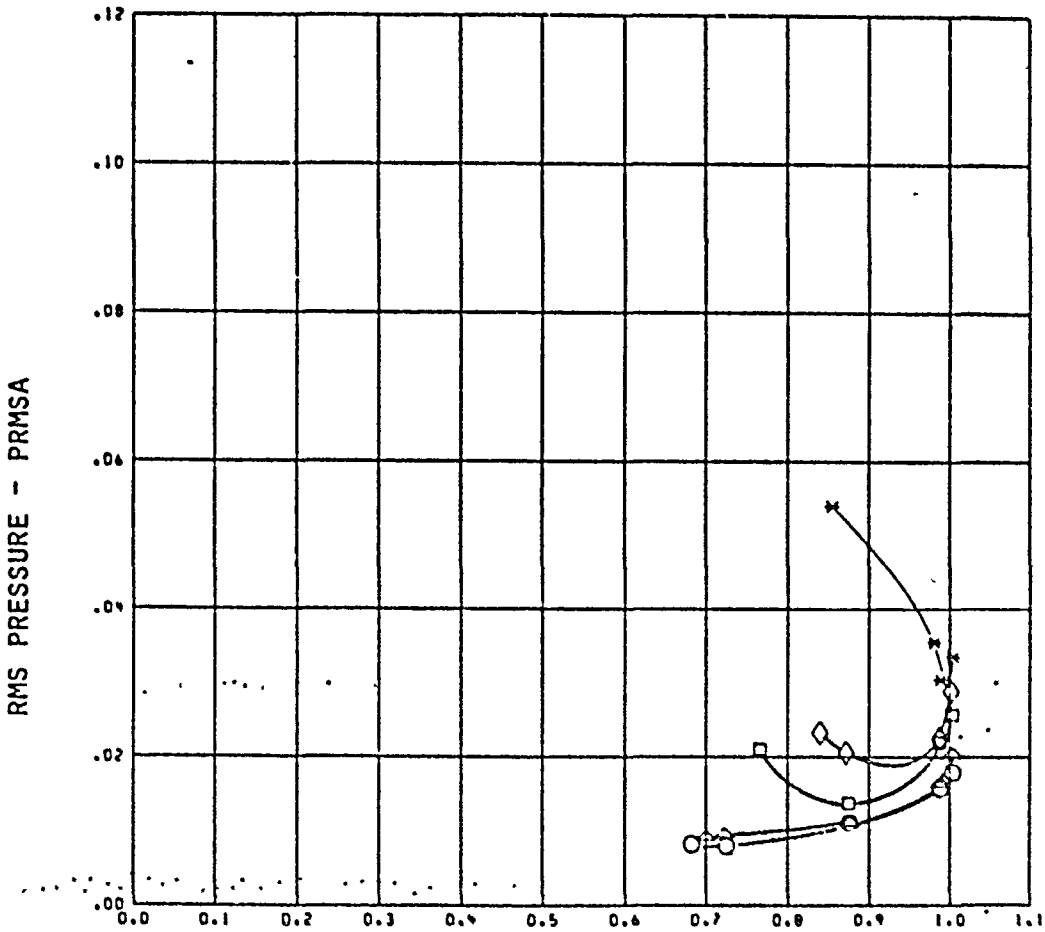

MACH = 1.56 CONF = 24

SYM	CMRCD	CMNCRD	BMFR	PPB	TTRC
○	20.1	6.44	0.020	4.27	1.633
△	17.3	5.36	0.025	3.71	1.616
□	12.3	3.45	0.019	2.72	1.573
◇	8.5	2.02	0.014	1.99	1.593
✳	0.3	-0.54	0.002	0.51	0.996

FIGURE 51 CONTINUED. INLET PERFORMANCE AT 1.56M, HOT FLOW

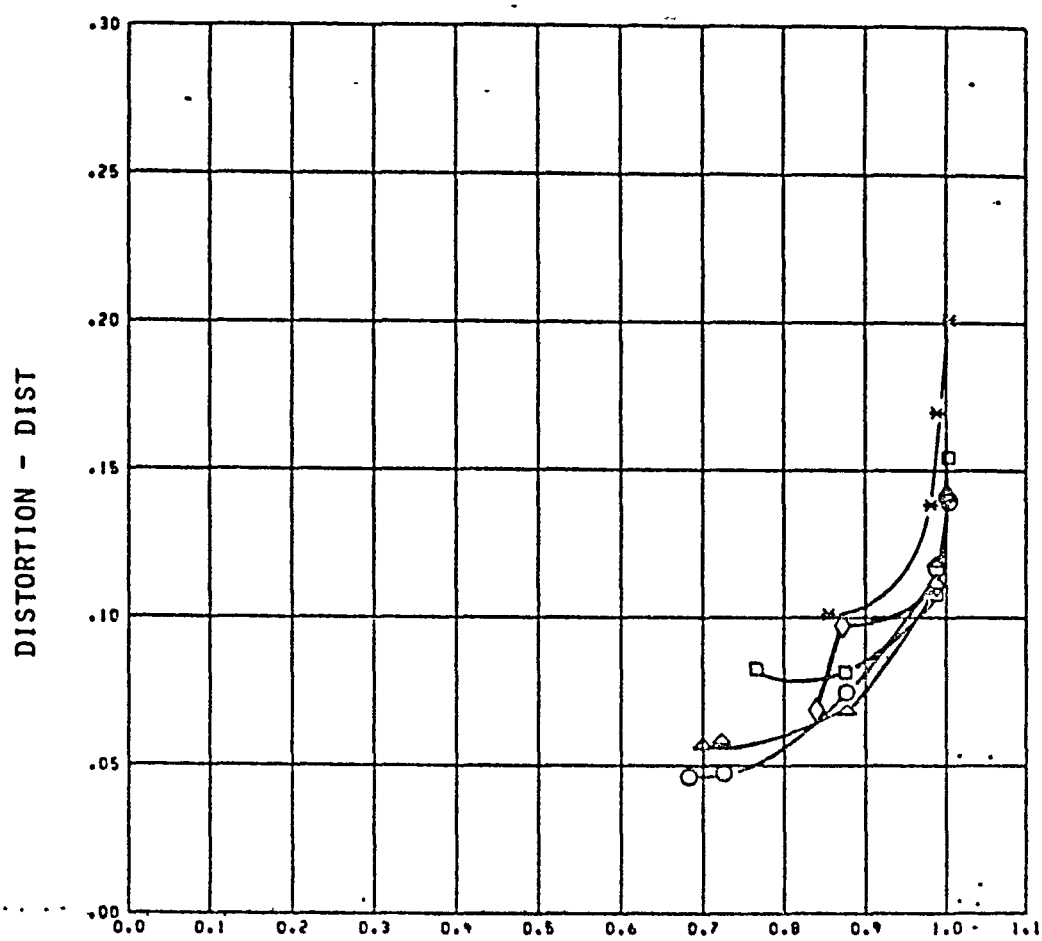

MACH • 1.56 CONF • 24

SYM	CRTCD	CRTCRD	BMFR	PPB	TTRC
○	20.1	6.44	0.029	4.27	1.633
△	17.3	5.36	0.025	3.71	1.616
□	12.3	3.45	0.019	2.72	1.573
◇	8.5	2.02	0.014	1.99	1.509
✳	0.3	-0.54	0.002	0.51	0.996

FIGURE 51 CONCLUDED. INLET PERFORMANCE AT 1.56M, HOT FLOW

ORIGINAL PAGE IS
OF POOR QUALITY

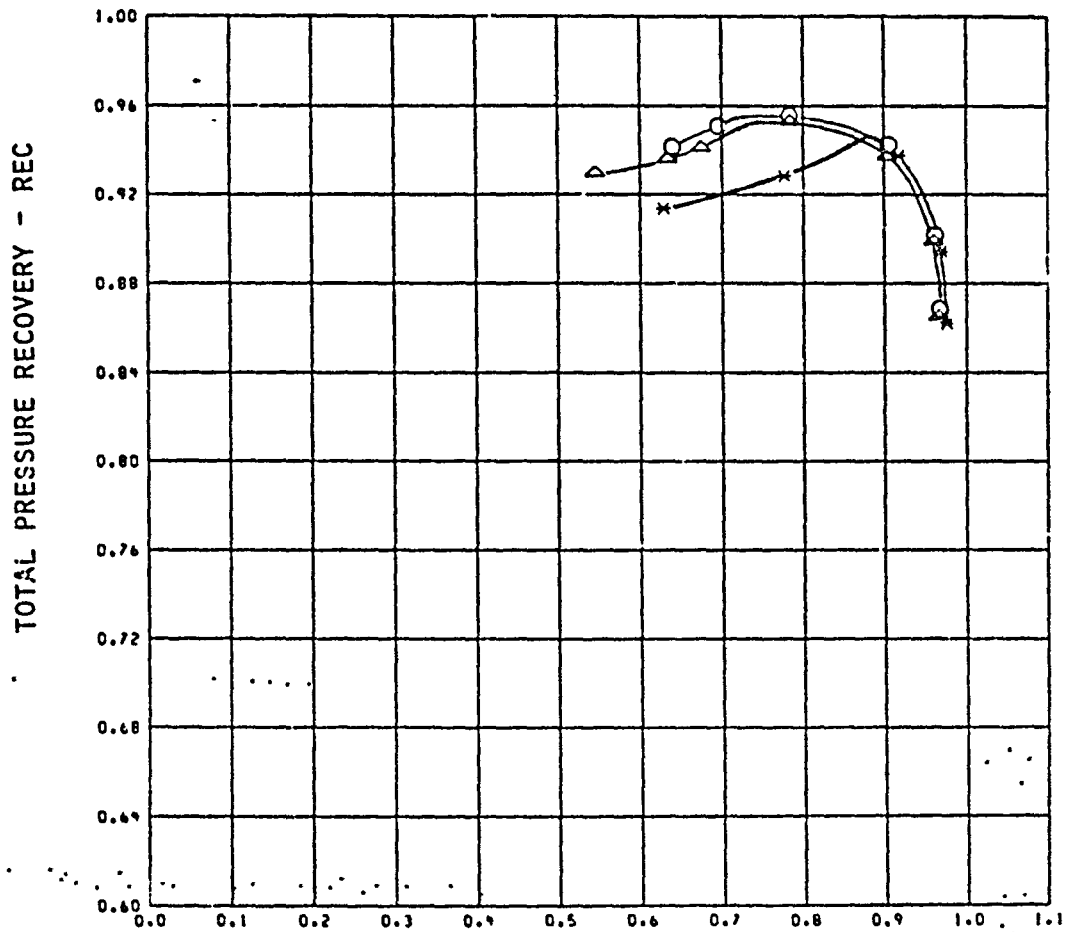

MACH = 1.36 CONF = 21

SYM	CMICD	CMRCRD	BRFR	PPB	TTRC
○	10.9	2.29	0.019	4.68	1.042
△	8.8	1.67	0.015	3.35	1.031
✳	0.2	-0.63	0.002	0.68	1.004

FIGURE 52. INLET PERFORMANCE AT 1.36 M, COLD FLOW

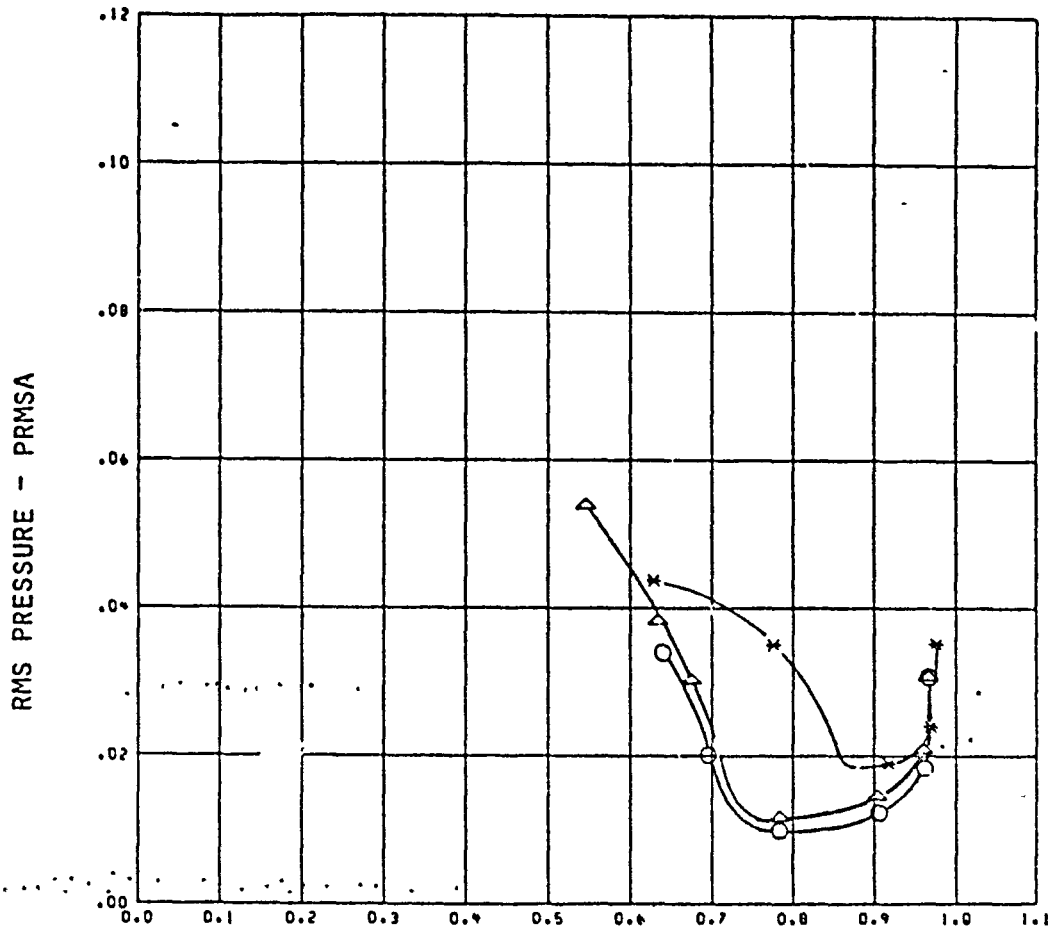

MACH = 1.36 CONF = 21

SYM	CPRCD	CORCRD	BNDR	PPB	TTRC
○	10.9	2.29	0.019	4.68	1.042
△	8.8	1.67	0.015	3.35	1.031
✳	0.2	-0.63	0.002	0.69	1.004

FIGURE 52 CONTINUED. INLET PERFORMANCE AT 1.36M, COLD FLOW

ORIGINAL PAGE IS
OF POOR QUALITY

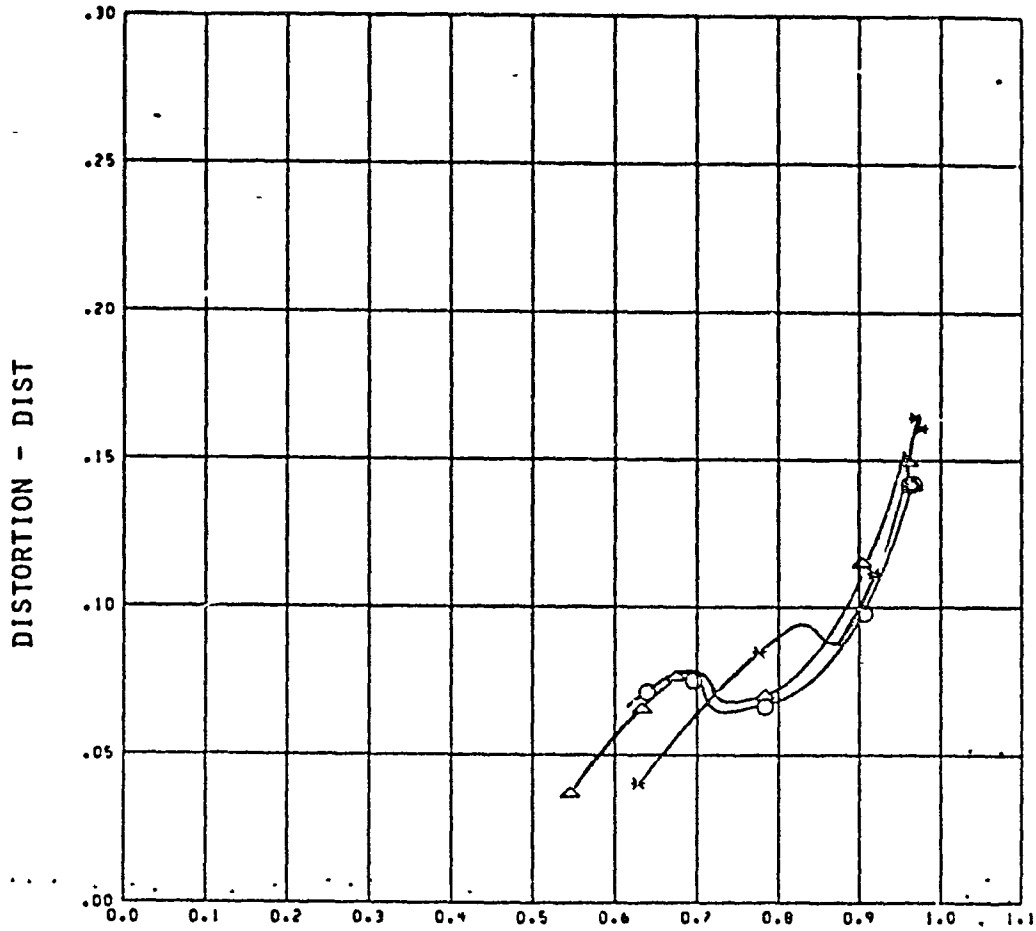

MACH • 1.35 CONF • 21

SYM	CPCCD	CPCRD	DMFR	PPB	TTRC
○	10.9	2.29	0.019	4.68	1.042
△	8.8	1.67	0.015	3.35	1.031
✳	0.2	-0.63	0.002	0.68	1.004

FIGURE 52 CONTINUED. INLET PERFORMANCE AT 1.36 M, COLD FLOW

ORIGINAL PAGE IS
OF POOR QUALITY

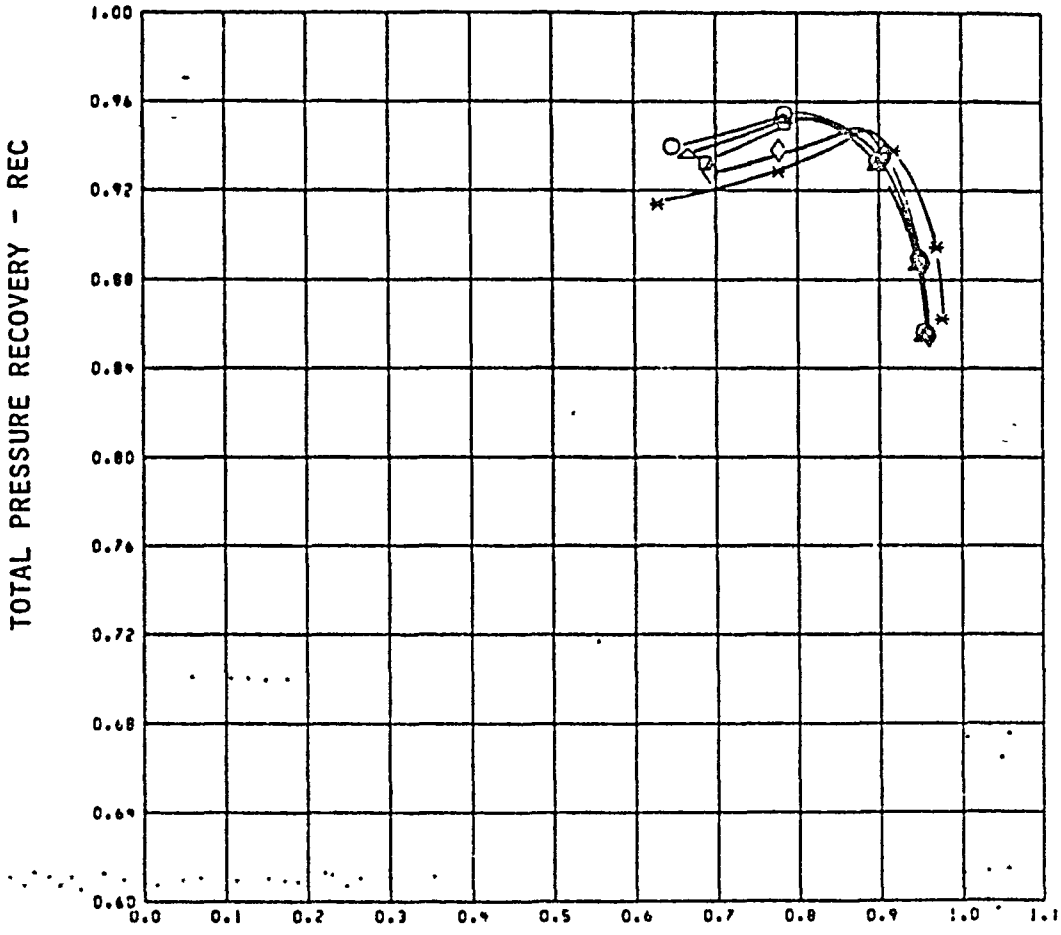

MACH = 1.35 CONF = 22

SYM	CMPCD	CMPCRD	BMFR	PP3	TTRC
○	9.2	1.87	0.016	3.43	1.059
△	7.8	1.45	0.014	2.96	1.039
□	5.2	0.78	0.010	2.10	1.048
◇	4.0	0.40	0.003	1.68	1.022
✳	0.2	-0.63	0.002	0.60	1.004

FIGURE 52 CONTINUED. INLET PERFORMANCE AT 1.36M, COLD FLOW.

ORIGINAL PAGE IS
OF POOR QUALITY

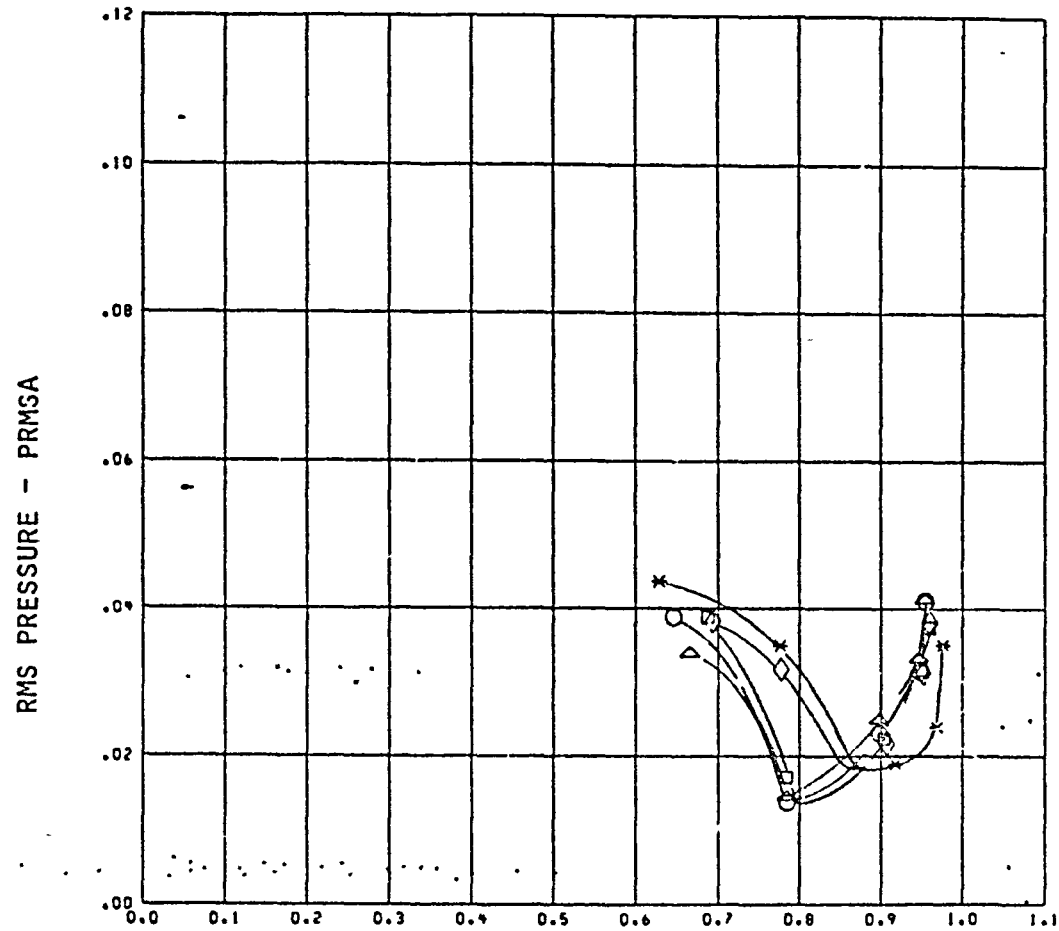

MACH = 1.33 CONF = 22

SYM	CMACD	CMACRD	DMFR	PPB	TTRC
○	9.2	1.87	0.016	3.43	1.035
△	7.8	1.45	0.014	2.56	1.029
□	5.2	0.78	0.010	2.10	1.048
◇	4.0	0.40	0.008	1.68	1.022
✳	0.2	-0.63	0.002	0.68	1.004

FIGURE 52 CONTINUED. INLET PERFORMANCE AT 1.36M, COLD FLOW

ORIGINAL PAGE IS
OF POOR QUALITY

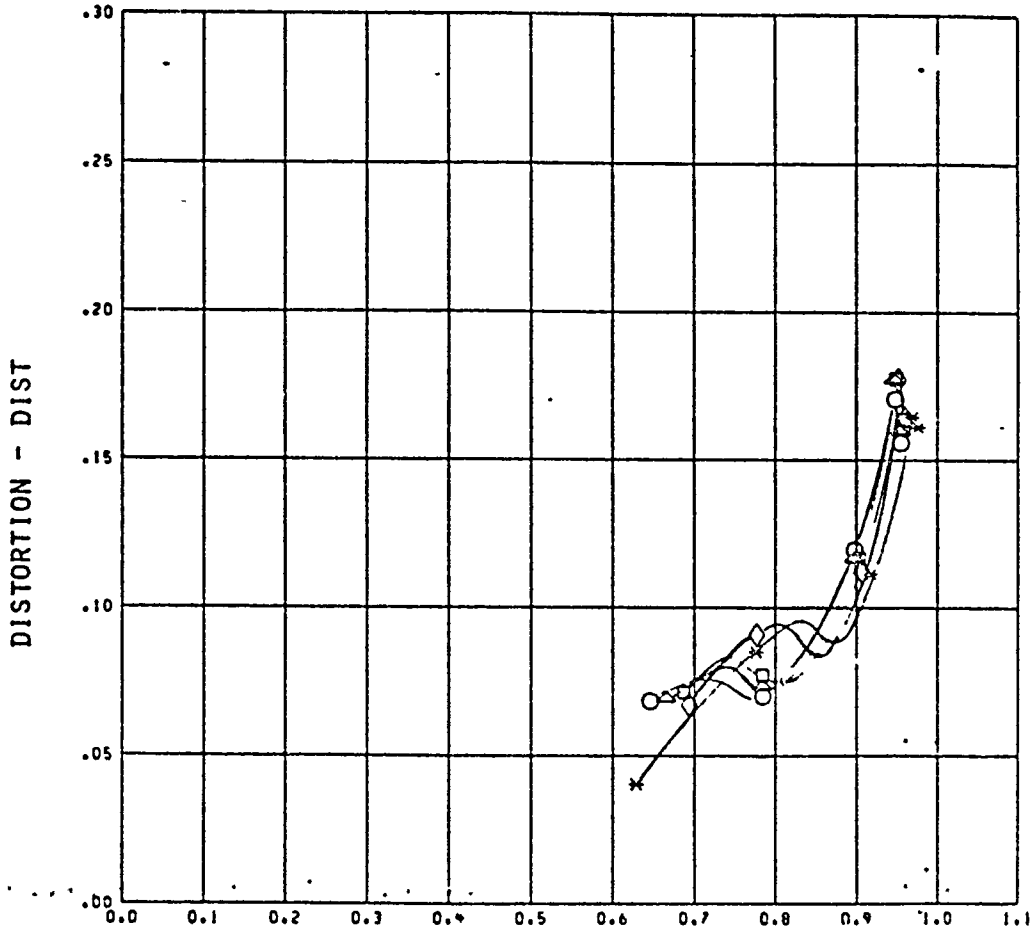

MACH • 1.36 CONF • 22

SYM	CMRCD	CMRCRD	BMFR	PPB	TTRC
○	9.2	1.87	0.016	3.43	1.059
△	7.8	1.45	0.014	2.96	1.039
□	5.2	0.78	0.010	2.10	1.048
◇	4.0	0.40	0.008	1.68	1.022
✳	0.2	-0.63	0.002	0.68	1.004

FIGURE 52 CONTINUED, INLET PERFORMANCE AT 1.36 M, COLD FLOW

ORIGINAL PAGE IS
OF POOR QUALITY

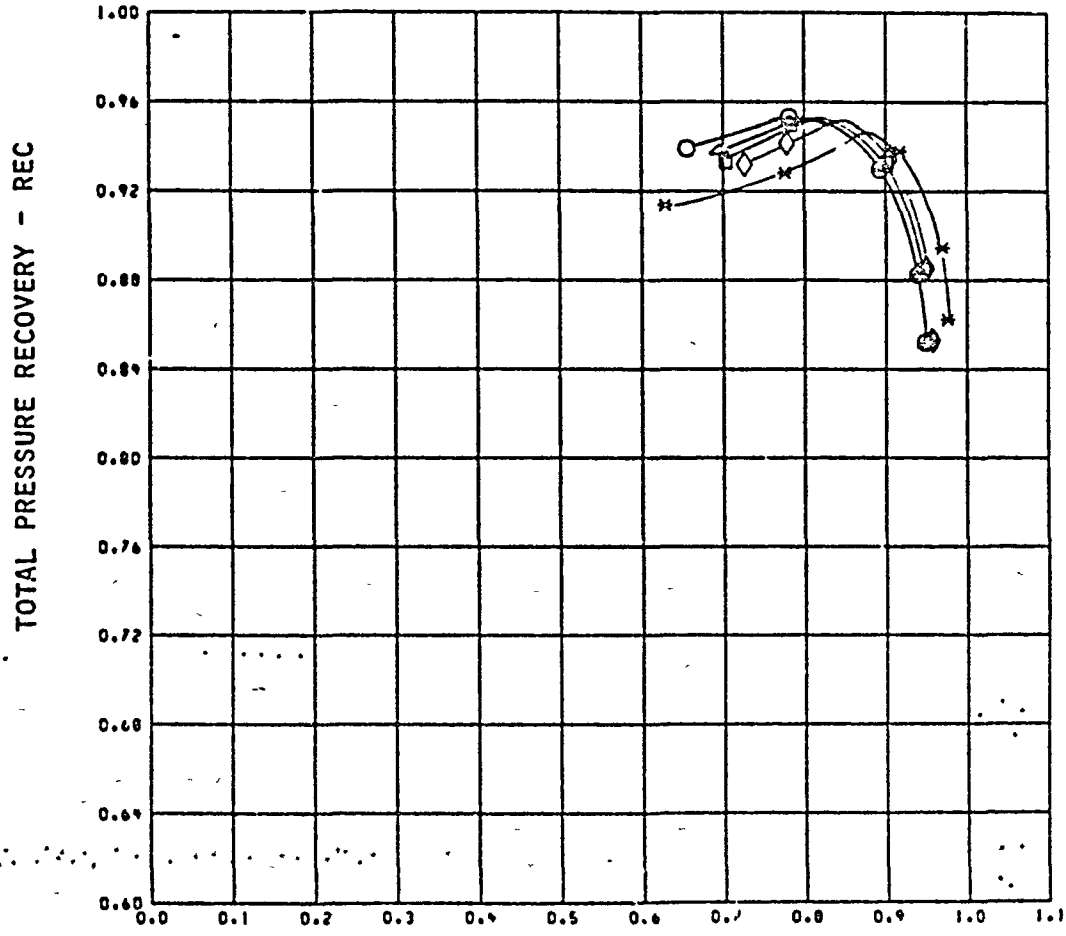

MACH = 1.36 CONF = 23

SYM	CRITCD	CRITCRD	DIFR	PPD	TTRC
○	9.7	1.04	0.017	3.56	1.002
△	8.3	1.49	0.015	3.08	1.011
□	6.2	0.95	0.011	2.39	1.010
◇	4.9	0.63	0.009	1.85	1.021
✳	0.2	-0.63	0.002	0.68	1.034

FIGURE 52 CONTINUED. INLET PERFORMANCE AT 1.36M, COLD FLOW.

ORIGINAL PAGE IS
OF POOR QUALITY

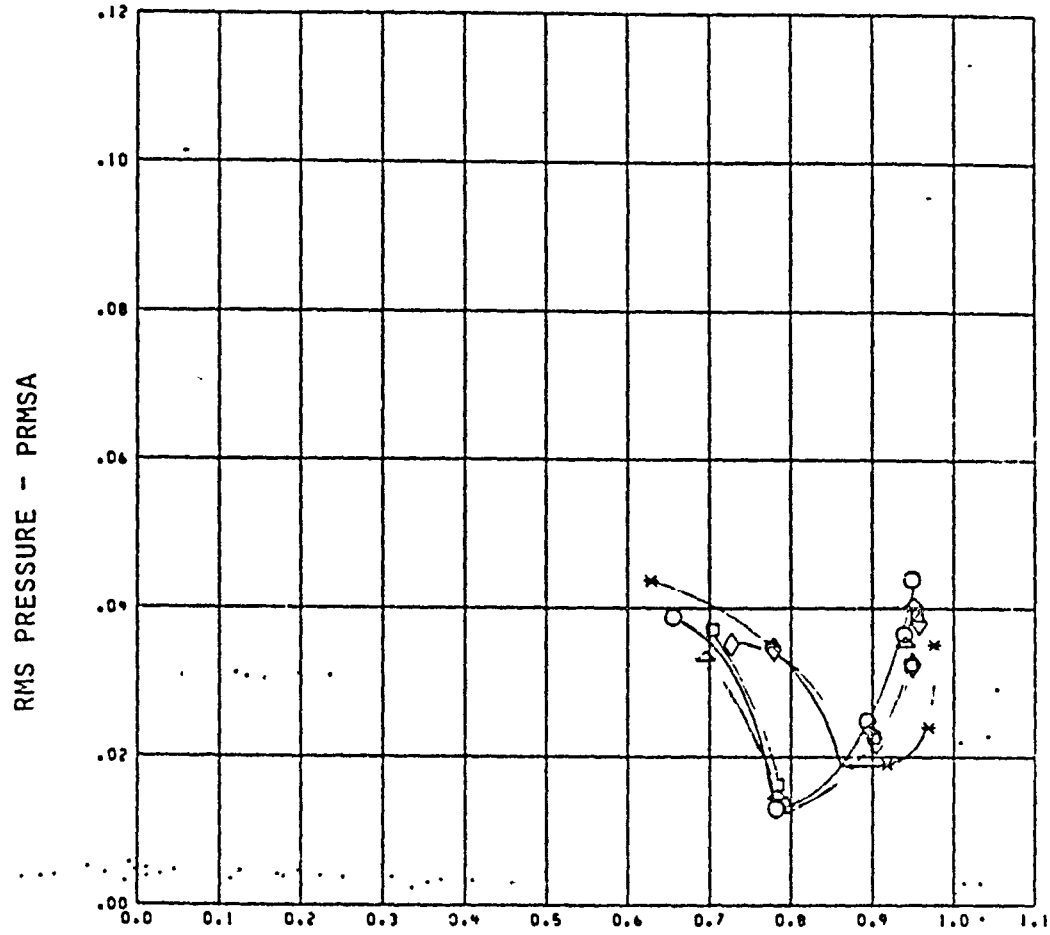

MACH = 1.36 CONF = 23

SYM	CFGCD	CMGCRD	DMFR	PPB	TTRC
○	9.7	1.04	0.017	3.56	1.002
△	8.3	1.49	0.015	3.06	1.011
□	6.2	0.95	0.011	2.39	1.010
◇	4.9	0.63	0.009	1.95	1.021
✳	0.2	-0.63	0.002	0.68	1.004

FIGURE 52 CONTINUED, INLET PERFORMANCE AT 1.36M, COLD FLOW

ORIGINAL PAGE IS
OF POOR QUALITY

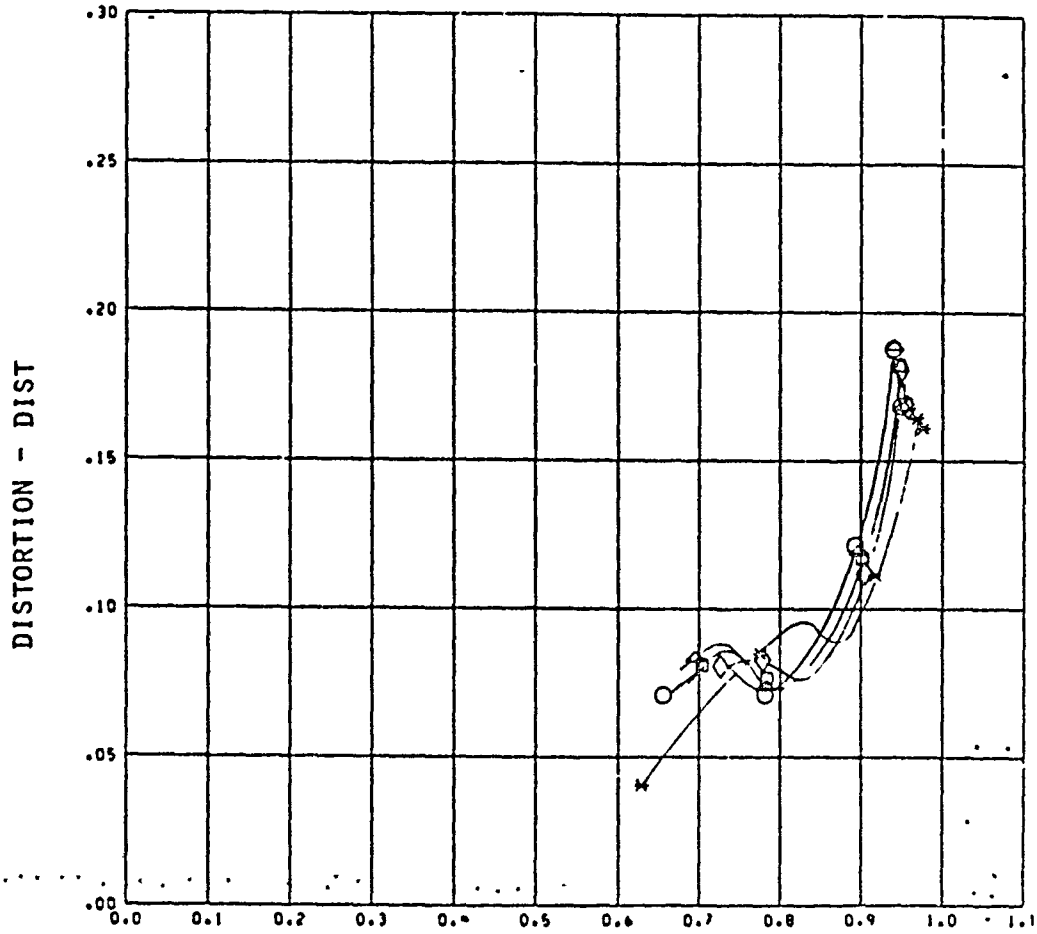

MACH = 1.36 CONF = 23

SYM	CNTCD	CNTCRD	DNFR	PPB	TTRC
○	9.7	1.84	0.017	3.56	1.002
△	8.3	1.49	0.015	3.08	1.011
□	6.2	0.95	0.011	2.39	1.010
◇	4.9	0.63	0.009	1.95	1.021
✳	0.2	-0.63	0.002	0.68	1.004

FIGURE 52 CONTINUED. INLET PERFORMANCE AT 1.36 M, COLD FLOW

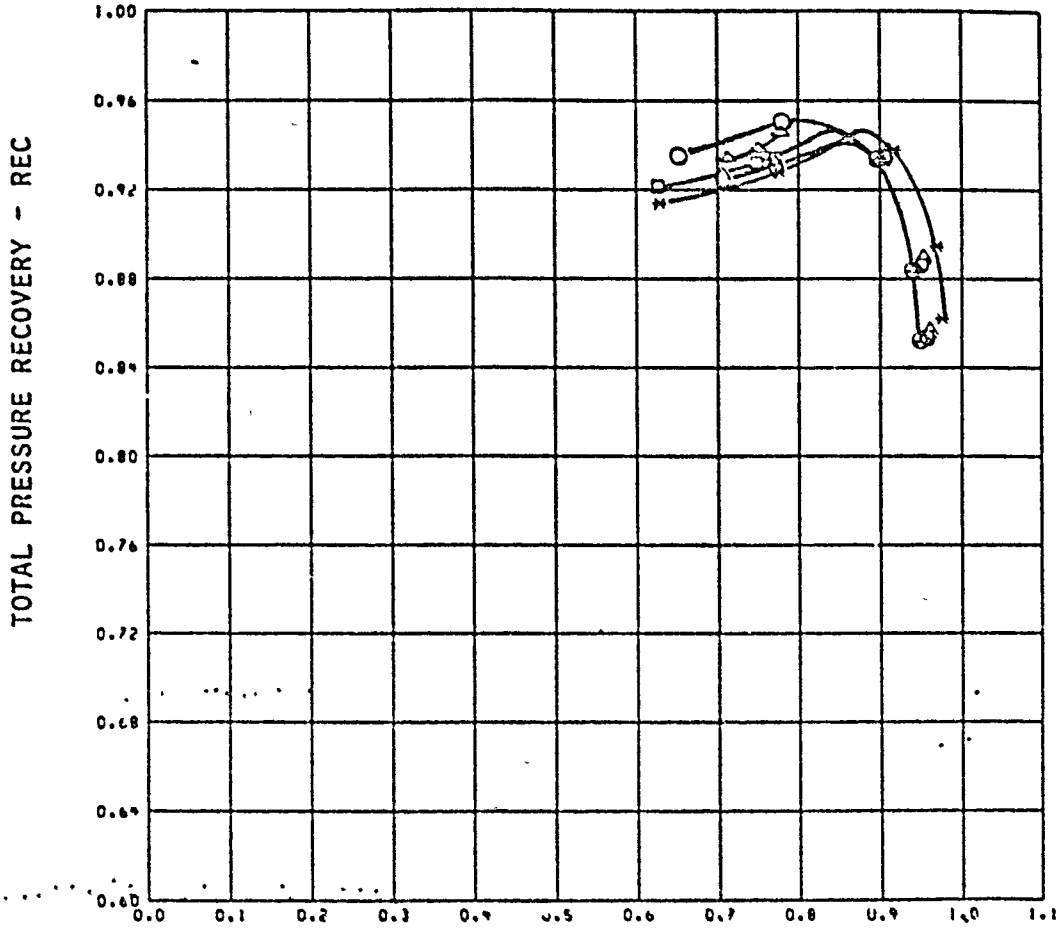

MACH = 1.36 CONF = 24

SYM	CYMCD	CMMCRD	BMFR	PPB	TTRC
○	8.7	1.12	0.017	2.19	1.019
△	6.5	0.49	0.013	1.75	0.995
□	4.4	-0.06	0.010	1.38	0.989
◇	2.9	-0.45	0.007	1.00	0.997
✳	0.2	-0.63	0.002	0.68	1.004

FIGURE 52 CONTINUED. INLET PERFORMANCE AT 1.36M, COLD FLOW.

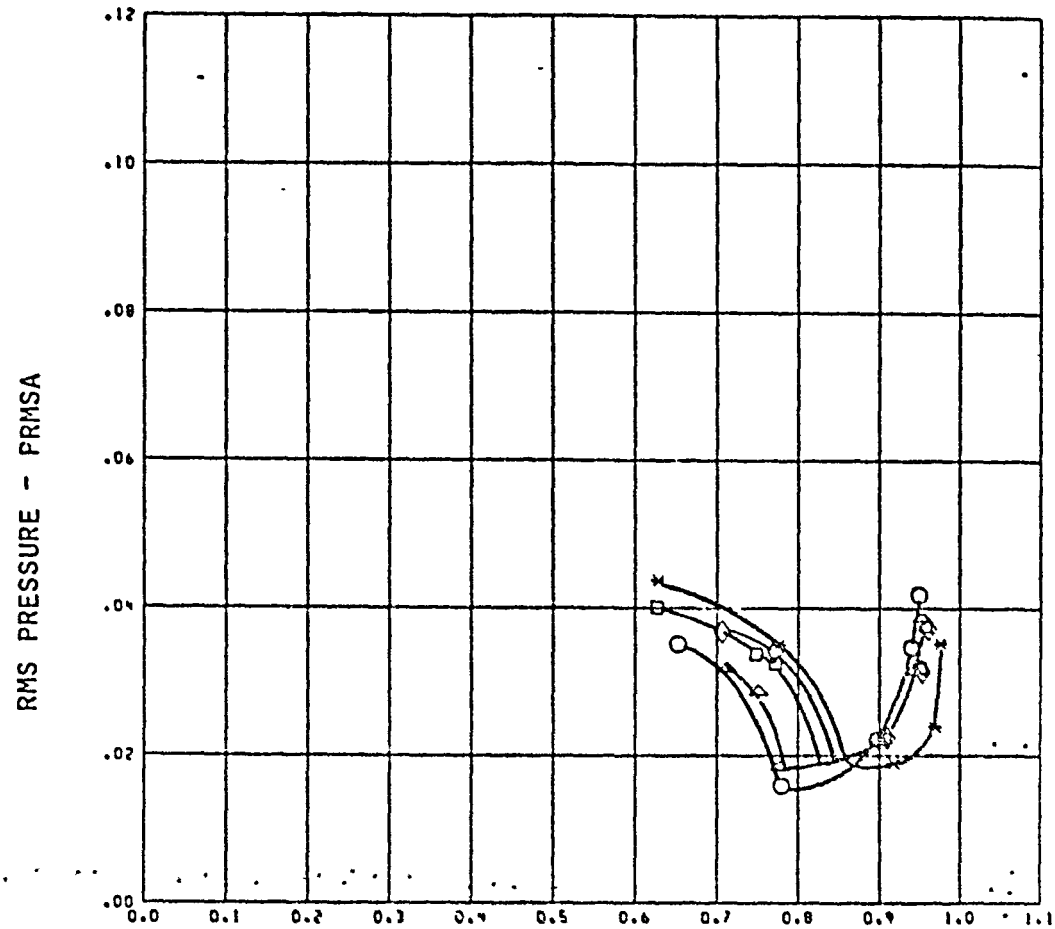

MACH = 1.36 CONF = 24

SYM	CYCCD	CHRCRD	DMFR	PPB	TTRC
○	8.7	1.12	0.017	2.19	1.018
△	6.5	0.49	0.013	1.75	0.995
□	4.4	-0.06	0.010	1.30	0.989
◇	2.9	-0.45	0.007	1.00	0.997
✳	0.2	-0.63	0.002	0.68	1.004

FIGURE 52 CONTINUED. INLET PERFORMANCE AT 1.36M, COLD FLOW

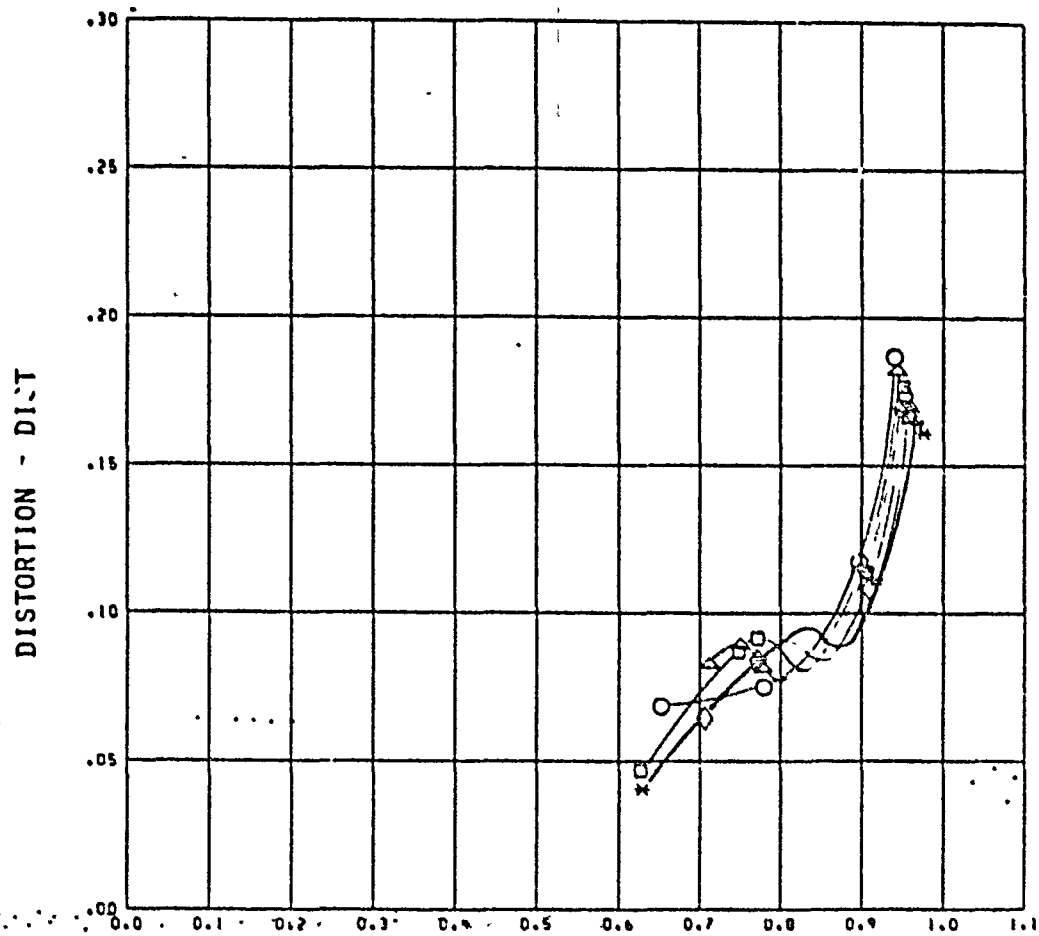

MACH • 1.36 CONF • 24

SYM	CRITCD	CRITCRD	ERFR	PPB	TTRC
○	8.7	1.12	0.017	2.19	1.018
△	6.5	0.49	0.013	1.75	0.995
□	4.4	-0.06	0.010	1.33	0.989
◇	2.9	-0.45	0.007	1.03	0.997
✳	0.2	-0.63	0.002	0.68	1.004

FIGURE 52 CONCLUDED. INLET PERFORMANCE AT 1.36M, COLD FLOW

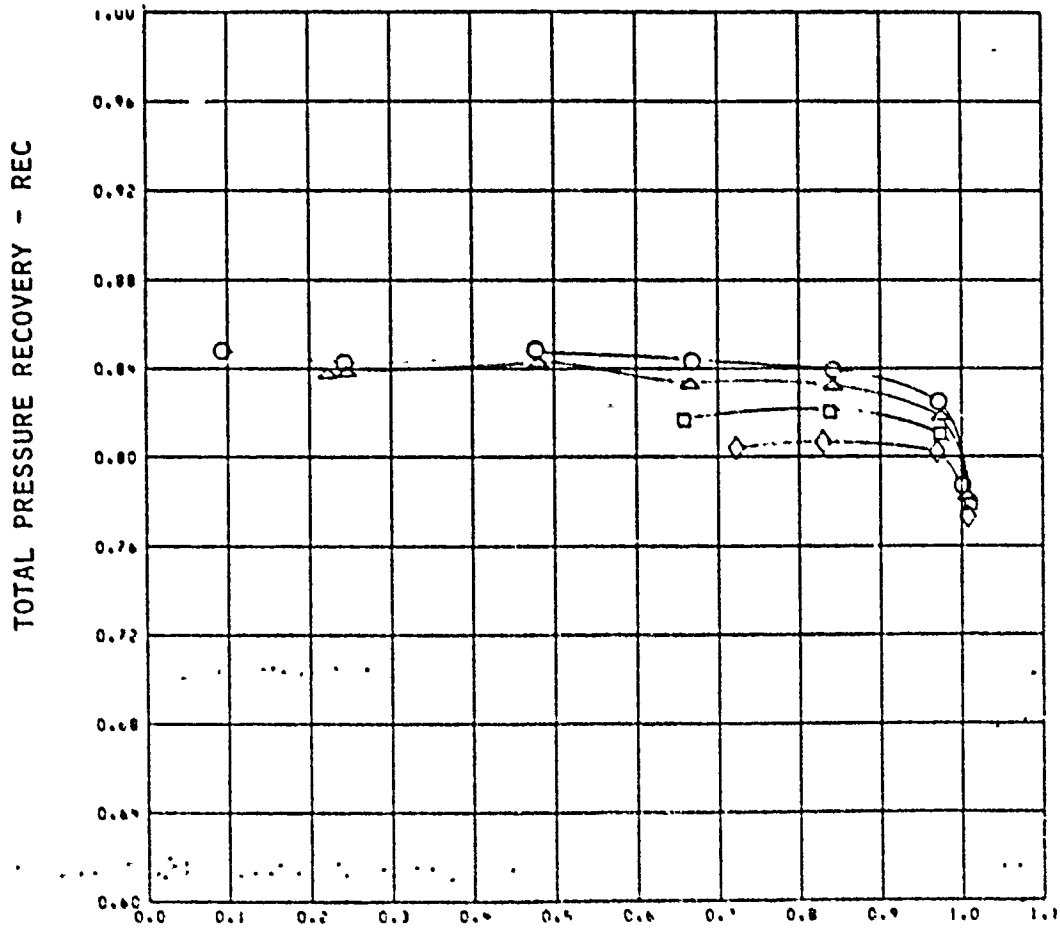

MACH = 1.77 CONF = 26

SYM	CMRCD	CMRCRD	DMFR	PPB	TTRC
○	25.1	0.37	0.048	4.81	1.037
△	81.8	1.77	0.038	3.01	1.025
□	15.5	1.02	0.029	2.03	1.023
◇	12.8	0.67	0.023	2.37	1.032

FIGURE 53. INLET PERFORMANCE WITH SHORT COWL AT 1.76 M, COLD FLOW

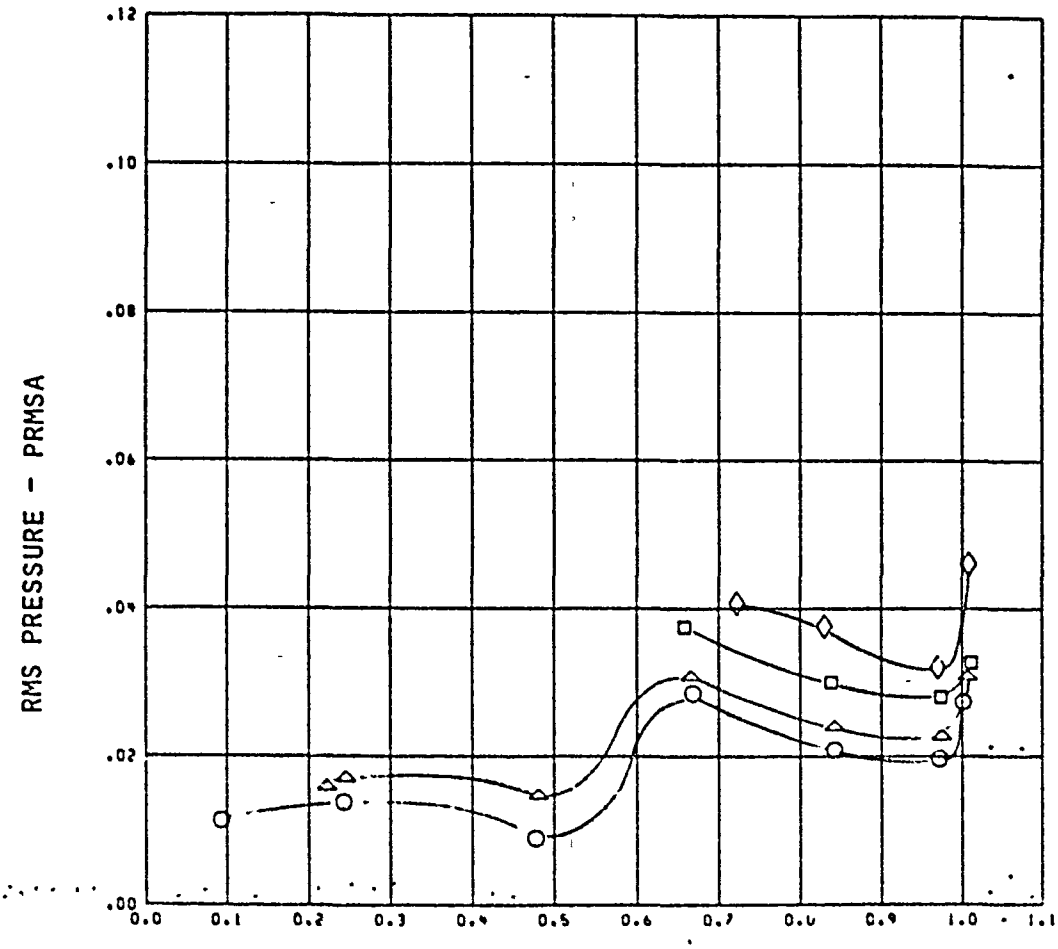

MACH • 1.77 CONF • 26

SYM	CMACD	CMACRD	EMFR	PPB	TTRC
○	25.1	2.37	0.040	4.01	1.037
△	21.8	1.77	0.030	3.01	1.028
□	15.6	1.02	0.020	2.03	1.023
◇	12.8	0.67	0.023	2.37	1.032

FIGURE 53 CONTINUED

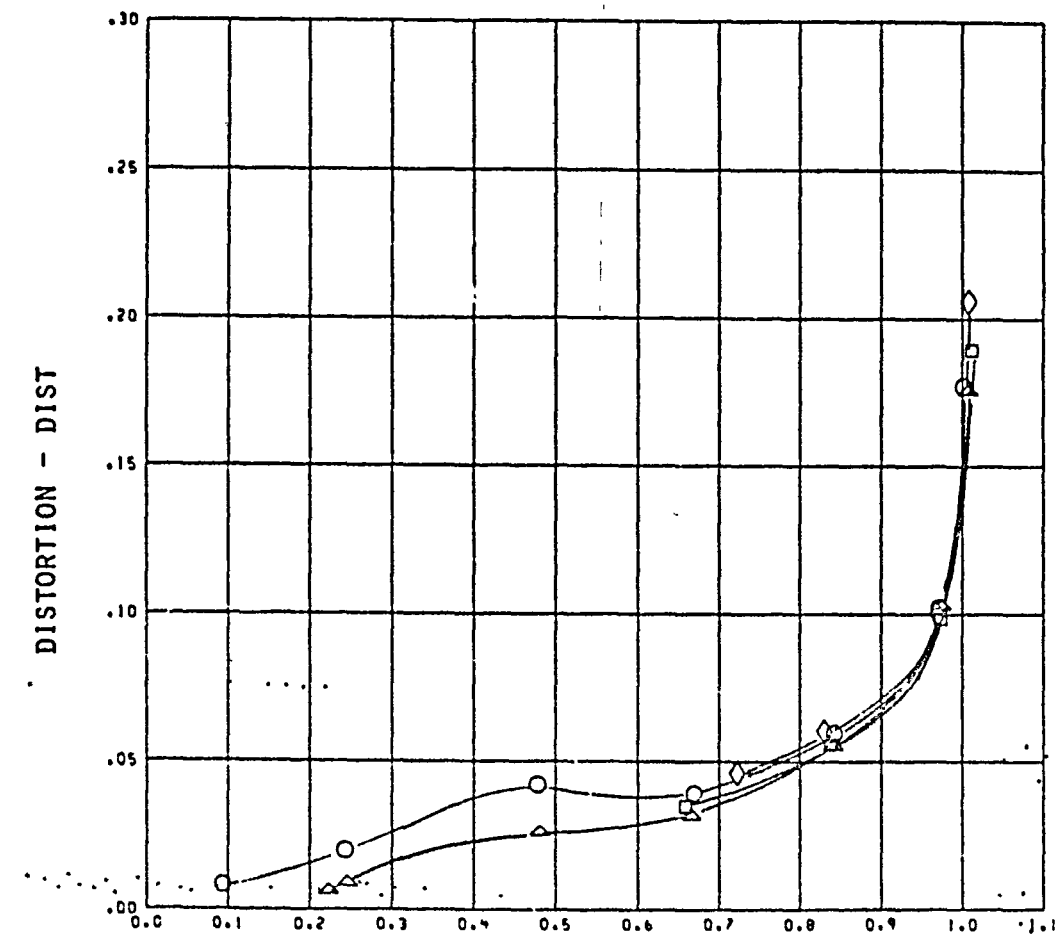

EXTERNAL MASS FLOW RATIO - MFRX

MACH = 1.77 CONF = 26

SYM	CRMCD	CRMCRD	DRFR	PPB	TTRC
○	85.1	2.37	0.043	4.81	1.037
△	81.2	1.77	0.039	3.81	1.028
□	15.5	1.62	0.029	2.93	1.023
◇	12.8	0.67	0.023	2.37	1.032

FIGURE 53 CONCLUDED

ORIGINAL PAGE IS
OF POOR QUALITY

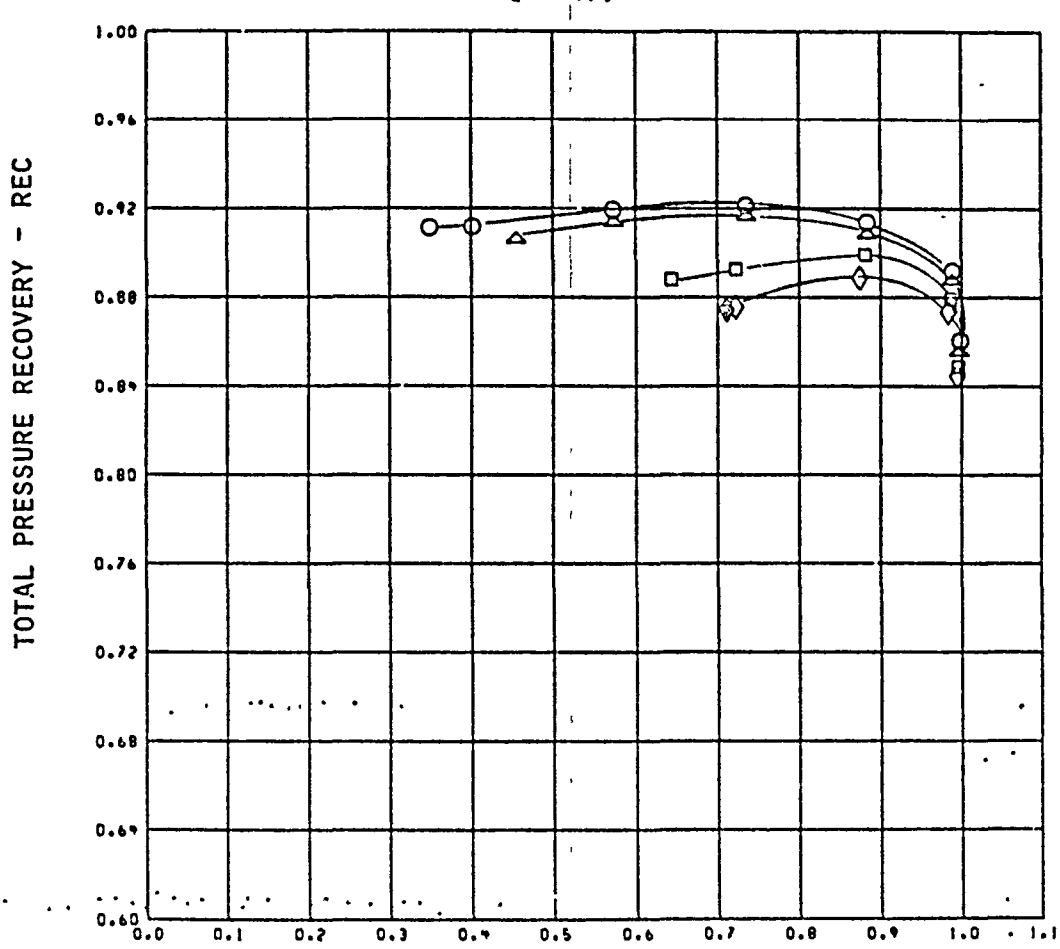

MACH • 1.56 CONF • 2G

SYM	CPMCD	CPMCRD	DMFR	FPB	TTRC
○	17.0	0.69	0.033	3.71	1.045
△	14.7	1.88	0.027	3.14	1.039
□	10.2	0.09	0.019	2.20	1.026
◇	8.1	0.03	0.016	1.87	1.033

FIGURE 54 . INLET PERFORMANCE WITH SHORT COWL AT 1.56 M, COLD FLOW

ORIGINAL PAGE IS
OF POOR QUALITY

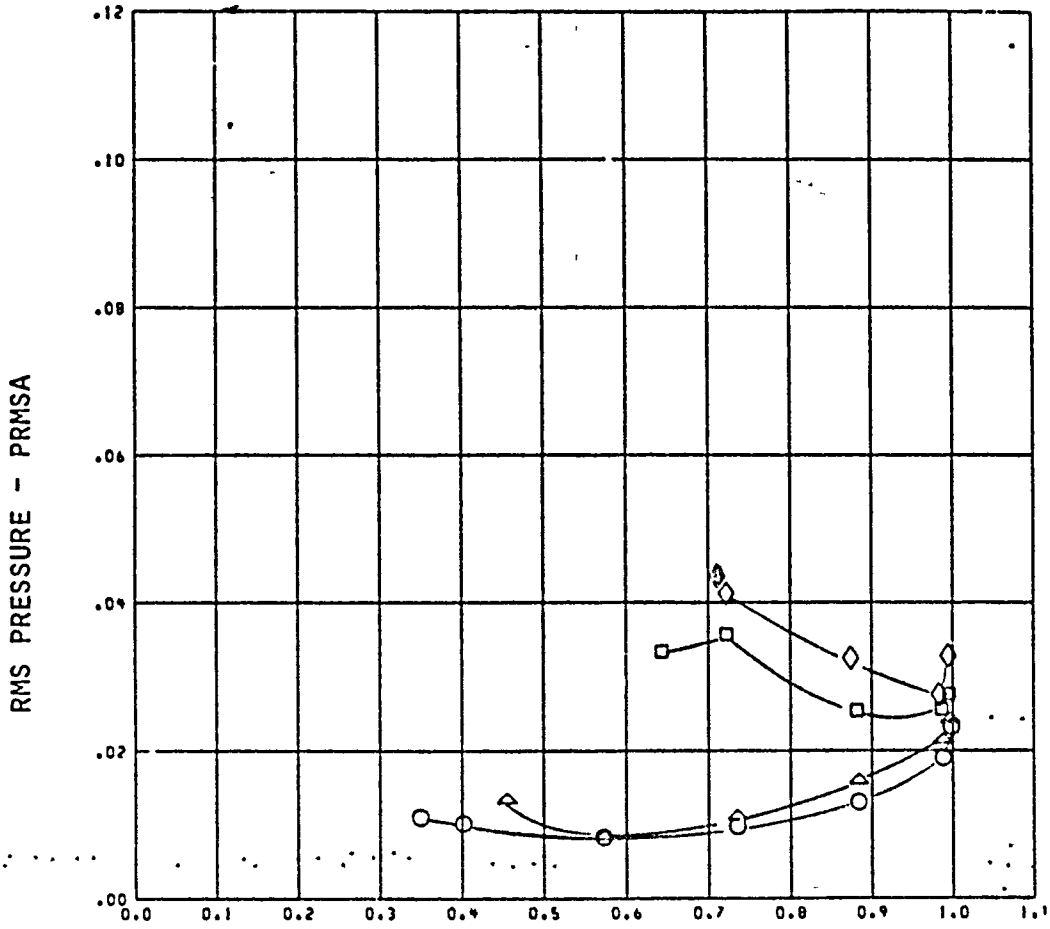

MACH = 1.56 , CONF = 26

SYM	CRRCD	CRRCRD	BMFR	PPB	TTRC
○	17.8	8.69	0.032	3.71	1.045
△	14.7	1.88	0.027	1.14	1.039
□	10.2	0.00	0.010	0.38	1.034
◇	8.1	0.58	0.016	1.87	1.038

FIGURE 54 CONTINUED

ORIGINAL PAGE IS
OF POOR QUALITY

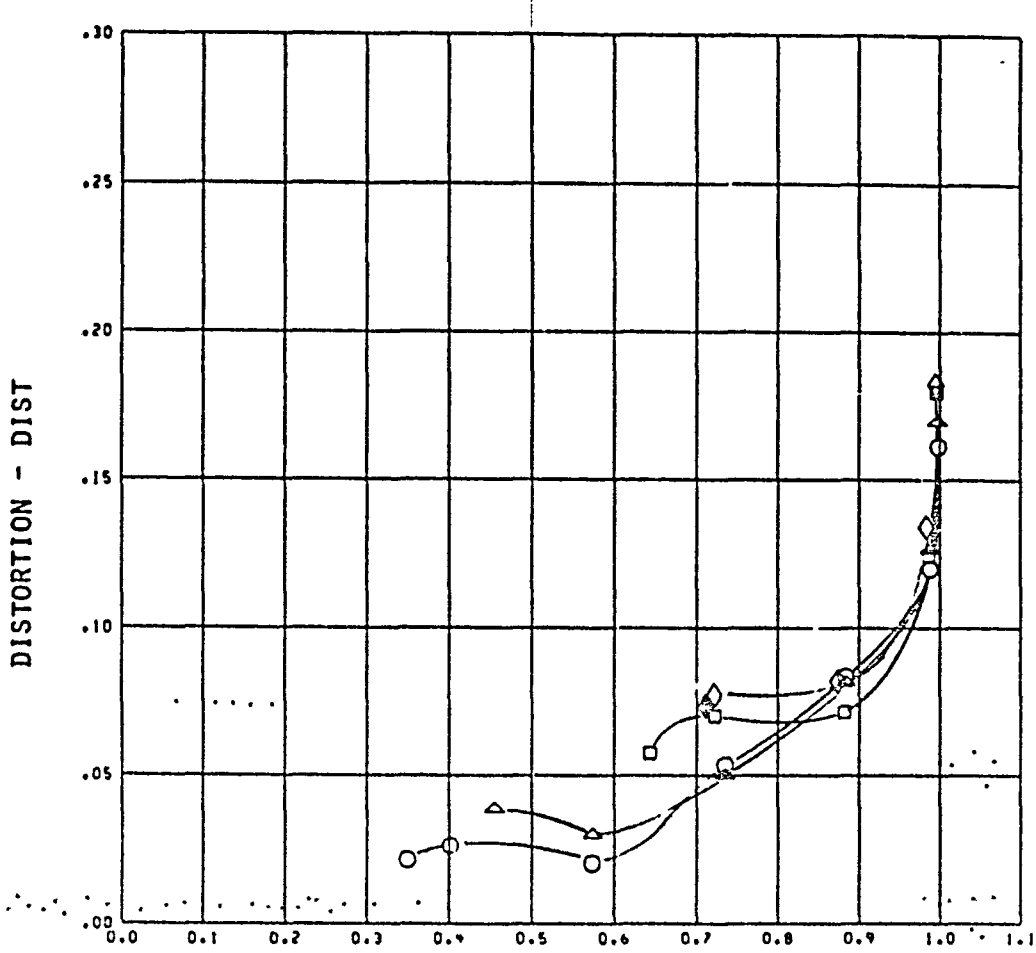

EXTERNAL MASS FLOW RATIO - MFRX

MACH • 1.56 CONF • 20

SYM	CMACD	CMACRD	BMFR	PPB	TTRC
○	17.0	0.00	0.032	3.71	1.045
△	14.7	1.00	0.027	3.14	1.039
□	10.2	0.00	0.010	0.30	1.035
◇	8.1	0.00	0.016	1.07	1.038

FIGURE 54 CONCLUDED

APPENDIX A

CORRECTION TO MEASURED PLENUM TEMPERATURE

As part of the test procedure, static performance of the blowing system was investigated. All systems were tested using cold flow with the exception of configuration 21 which was tested with both hot and cold flow. It was found that the use of heated air had a much stronger effect on the discharge coefficients when the tunnel was in operation than under static conditions, see figure A-1. Post-test analysis showed a similar temperature effect for other configurations but no static data were available for comparison.

The lack of this effect during static operation definitely indicates that the change in Reynold's number due to temperature was not the cause of the change in blowing coefficient. Two other explanations were considered: the effect of heat transfer within the blowing holes on the flow structure, and the effect of heat transfer on the accuracy of the plenum temperature measurement. Because the measured loss in temperature between the flow meter located alongside the main duct and the blowing plenum appeared larger than expected on the basis of the short length of uninsulated line, see figure 3; and no quantitative information was found on the effect of reverse-Rayleigh flow on the flow structure, it was found to be probable that the measured plenum temperature did not reflect the true temperature of the blowing flow. The thermocouple was located to the side of the plenum where the flow rate may have been low enough that the junction temperature was strongly affected by the temperature of the metal plenum in which the thermocouple was mounted. The metal would have had a temperature more nearly that of the external flow than that of the

blowing flow because of the greater wetted area and higher flow rates over the external model surfaces than over the internal plenum surface.

Two approximate heat transfer relationships were derived relating the measured plenum temperature to the corrected blowing temperature and the measured flow meter temperature to the corrected blowing temperature. The transfer coefficients were adjusted until the wind tunnel test results closely approximated the static results where heat transfer would have had a minimal effect on the measured plenum temperature. The plenum temperature used in the calculations was an average of these two corrected values. The corrections are shown in figures A-2 and A-3. The resulting corrected discharge coefficients are shown in figure A-4.

Additional data on discharge coefficients are shown in Appendix C.

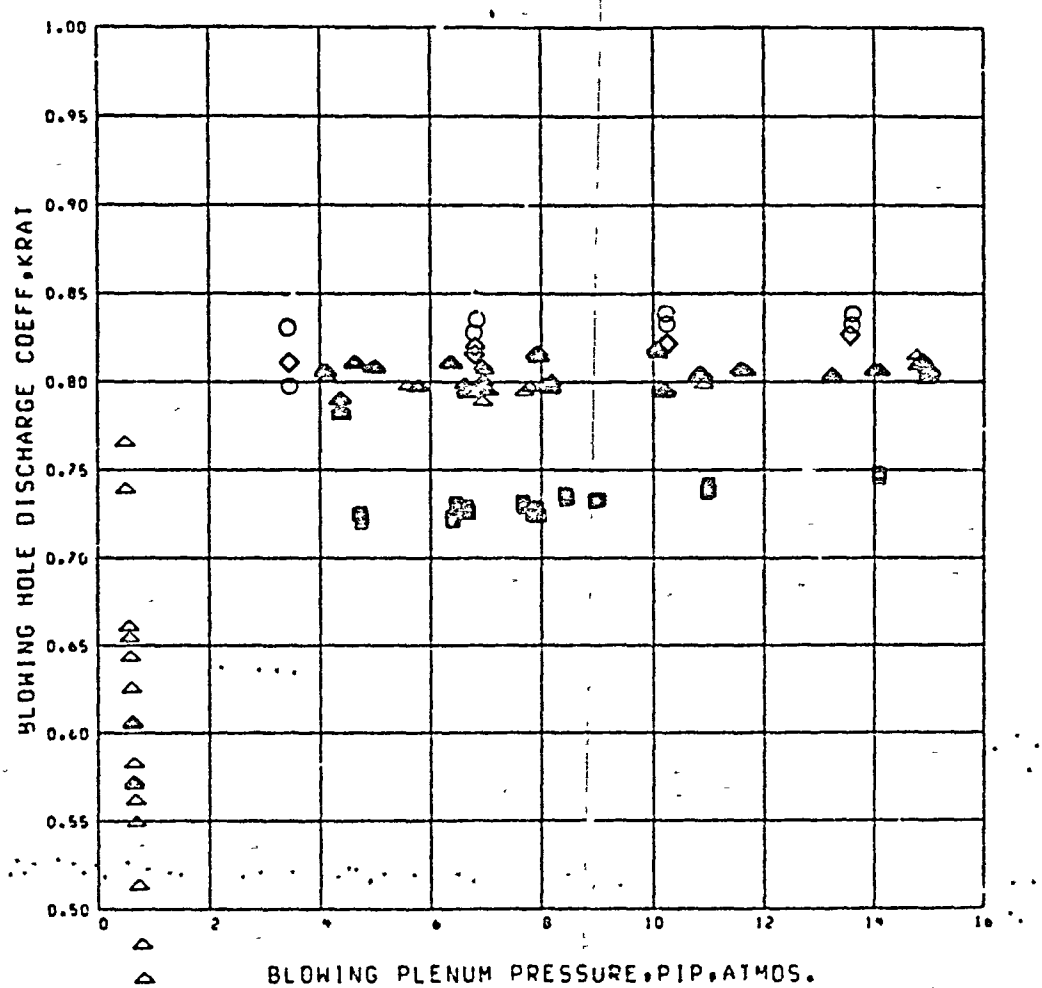

FIGURE A-1. EFFECT OF TEMPERATURE ON DISCHARGE COEFFICIENT - MEASURED PLENUM TEMPERATURE

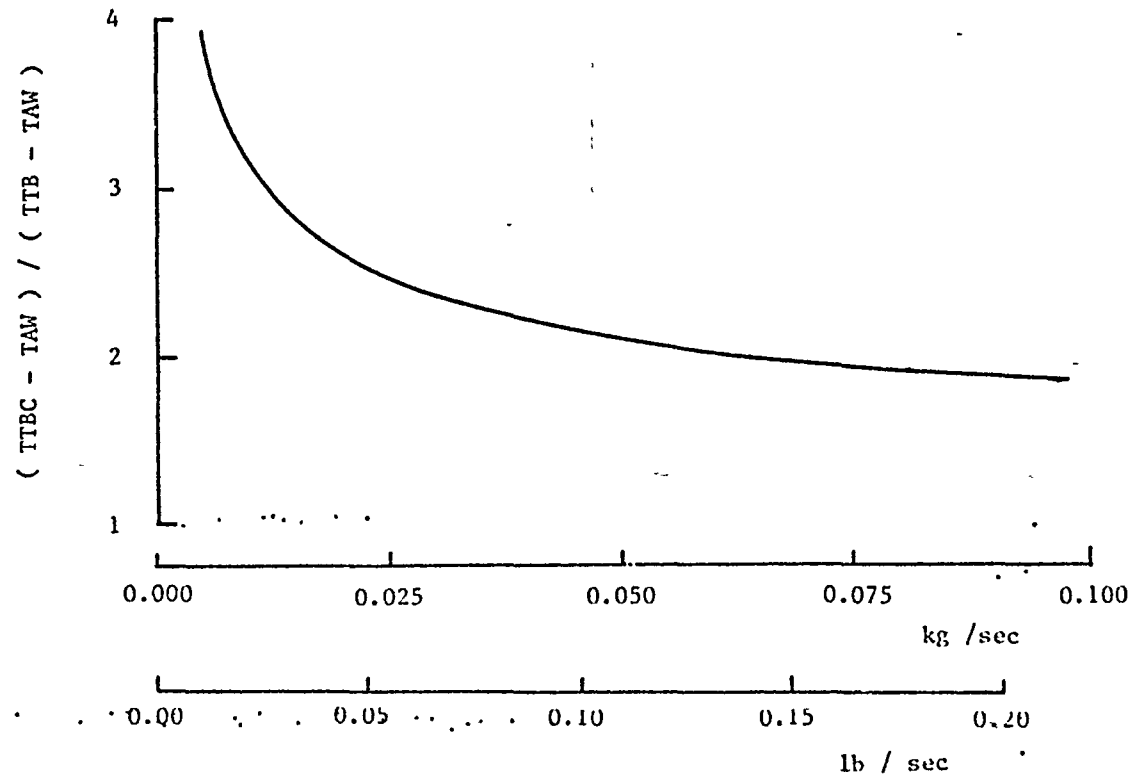

BLOWING MASS FLOW - $\dot{m}_b$

PLENUM TEMPERATURE CORRECTION DERIVED FROM THE ASSUMED HEAT TRANSFER RELATION:

heat transfer to t'cple = heat flow from t'cple

$$(TTBC - TTB) h_1 \dot{m}_b^n = h_2 (TTB - TAW)$$

WHERE: h_1, h_2 are heat transfer coefficients
n is 0.58
$\dot{m}_b$ is blowing mass flow rate
TAW is adiabatic wall temperature
TTB is measured thermocouple temperature
TTBC is true blowing plenum temperature

FIGURE A-2. CORRECTED PLENUM TEMPERATURE FROM MEASURED PLENUM TEMPERATURE

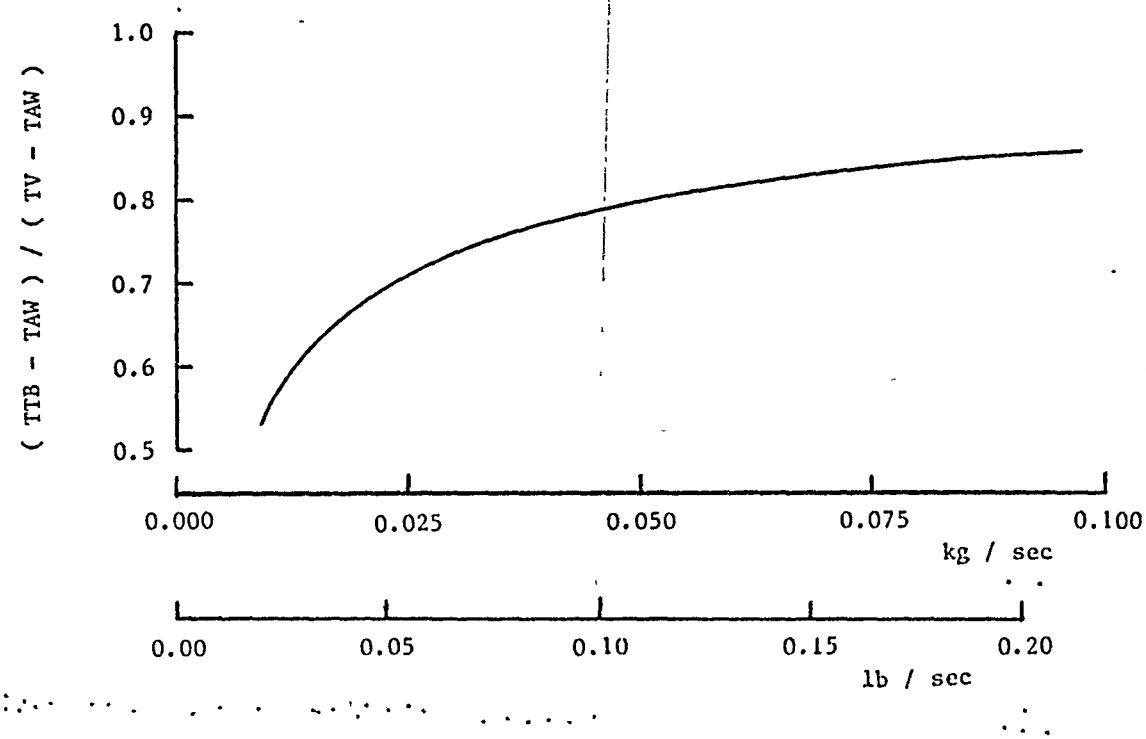

CORRECTED PLENUM TEMPERATURE DERIVED FROM THE ASSUMED HEAT TRANSFER RELATION:

heat lost from fluid = heat transfer from fluid

$$\dot{m}_b \, c_p \, dT/dx = h_3 \, \dot{m}_b^n \, (T - TAW)$$

WHERE:
- c_p is specific heat for air
- h_3 is a heat transfer coefficient
- $\dot{m}_b$ is blowing mass flow rate
- n is 0.4
- T is air temperature in line
- TAW is adiabatic wall temperature, $TO(1+0.176M0^2)$
- x is distance along the supply line

FIGURE A-3. CORRECTED PLENUM TEMPERATURE FROM FLOWMETER SUPPLY TEMPERATURE

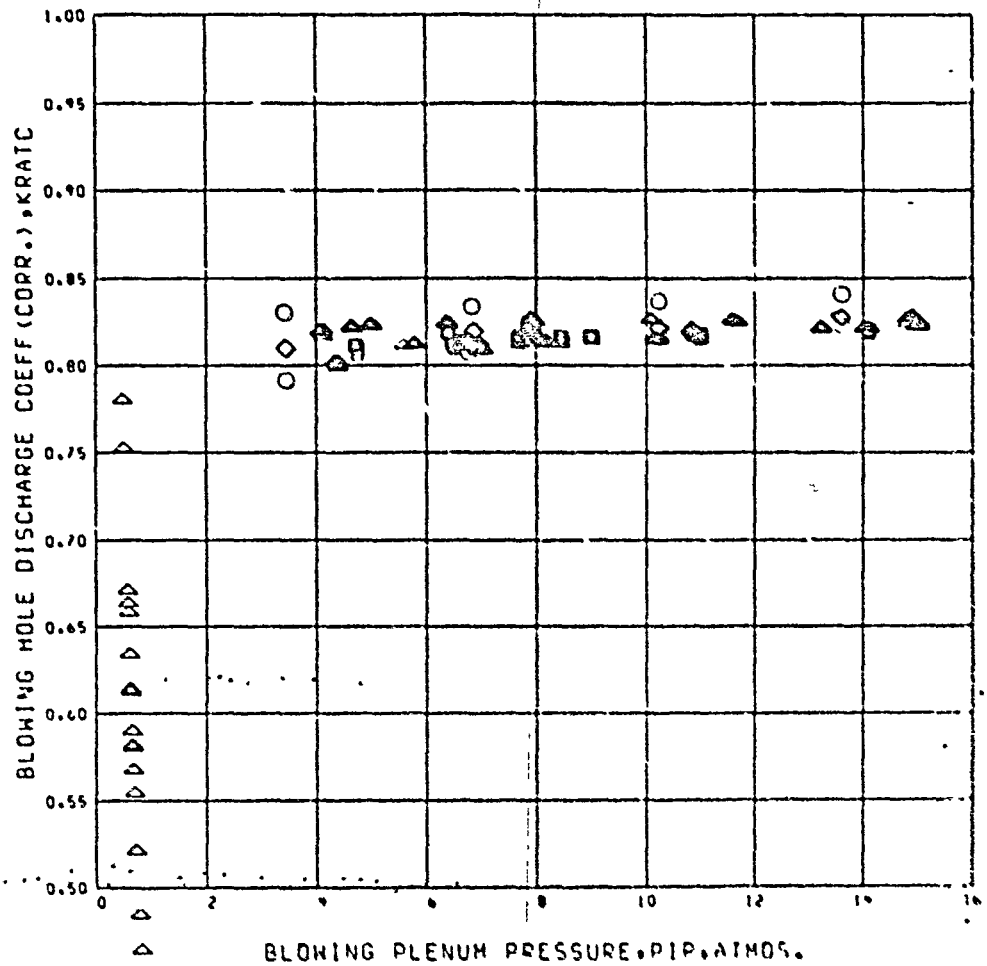

○ static -cold flow
◇ static -hot flow
△ tunnel-on -cold flow
□ tunnel-on -hot flow

FIGURE A-4. EFFECT OF CORRECTED PLENUM TEMPERATURE ON DISCHARGE COEFFICIENT

APPENDIX B

EXTERNAL MASS FLOW RATIO

The results presented in this report are given in terms of the external mass flow ratio, MFRX. It is equal to the mass flow ratio MFR, the ratio of total duct flow to capture flow, less the amount of blowing flow estimated to enter the inlet. This parameter has been chosen because the normal shock location should be a close function of MFRX regardless of the amount of blowing flow used, and thus the ideal ramp flow should be similar for like values of MFRX for different configurations and blowing levels.

The ratio of ingested blowing flow to total blowing flow was assumed to be equal to the external mass flow ratio in the ramp plane, that is the blowing flow was assumed to be spilled in the same manner as the layer of external flow just above the blowing flow. The derivation of the blowing capture ratio is shown in figure B-1. The captured stream tube is assumed to be rectangular and equidistant from the cowl roof and sides, an assumption of locally two-dimensional flow. The ratio of the area of the captured streamtube to the cowl area is then defined by the external mass flow ratio, and the ratio the blowing air captured m_{bc} to total blowing air m_b is determined by the ratio of the width of the capture streamtube to the width of the cowl. This ratio is shown in figure B-2, and the relationship of MFR to MFRX is shown in figure B-3 for various ratios of blowing flow to capture flow, BMFR.

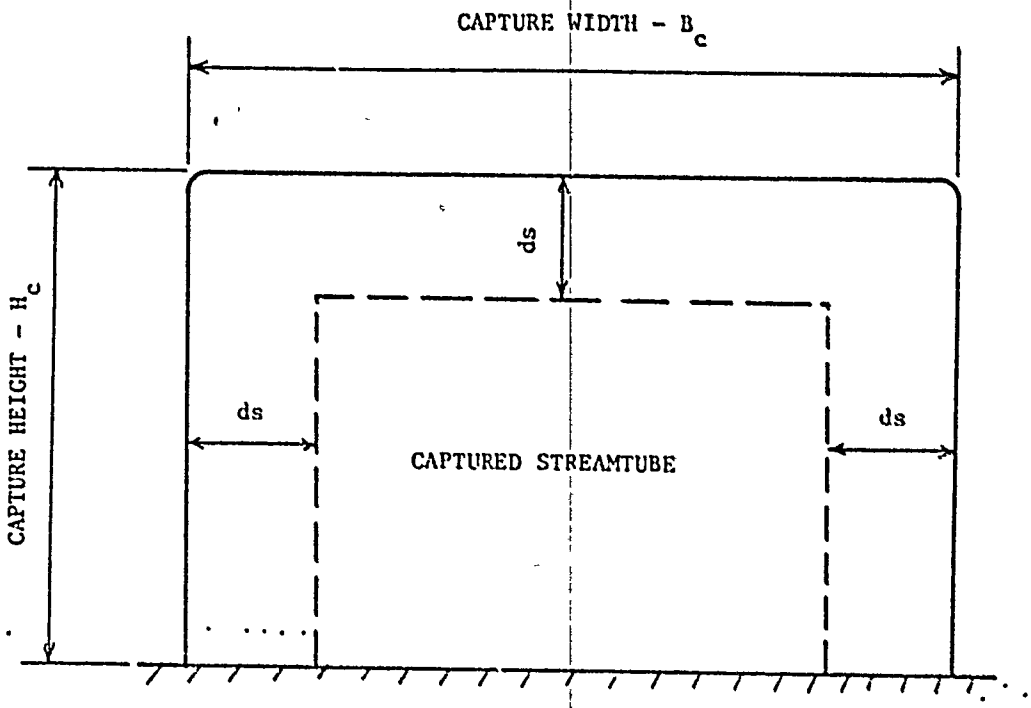

1) relation of captured streamtube area to capture area, A_c.

$$MFRX = (B_c - 2ds)(H_c - ds) / A_c$$

2) relation of ratio of blowing air captured by the inlet, R_i to spillage in the plane of the ramp.

$$R_i = (B_c - 2ds) / B_c$$

3) relation of external mass flow ratio, MFRX, to mass flow ratio, MFR, and blowing mass flow ratio, BMFR.

$$MFRX = MFR - R_i * BMFR$$

FIGURE B-1. DERIVATION OF EXTERNAL MASS FLOW RATIO - MFRX

ORIGINAL PAGE IS
OF POOR QUALITY

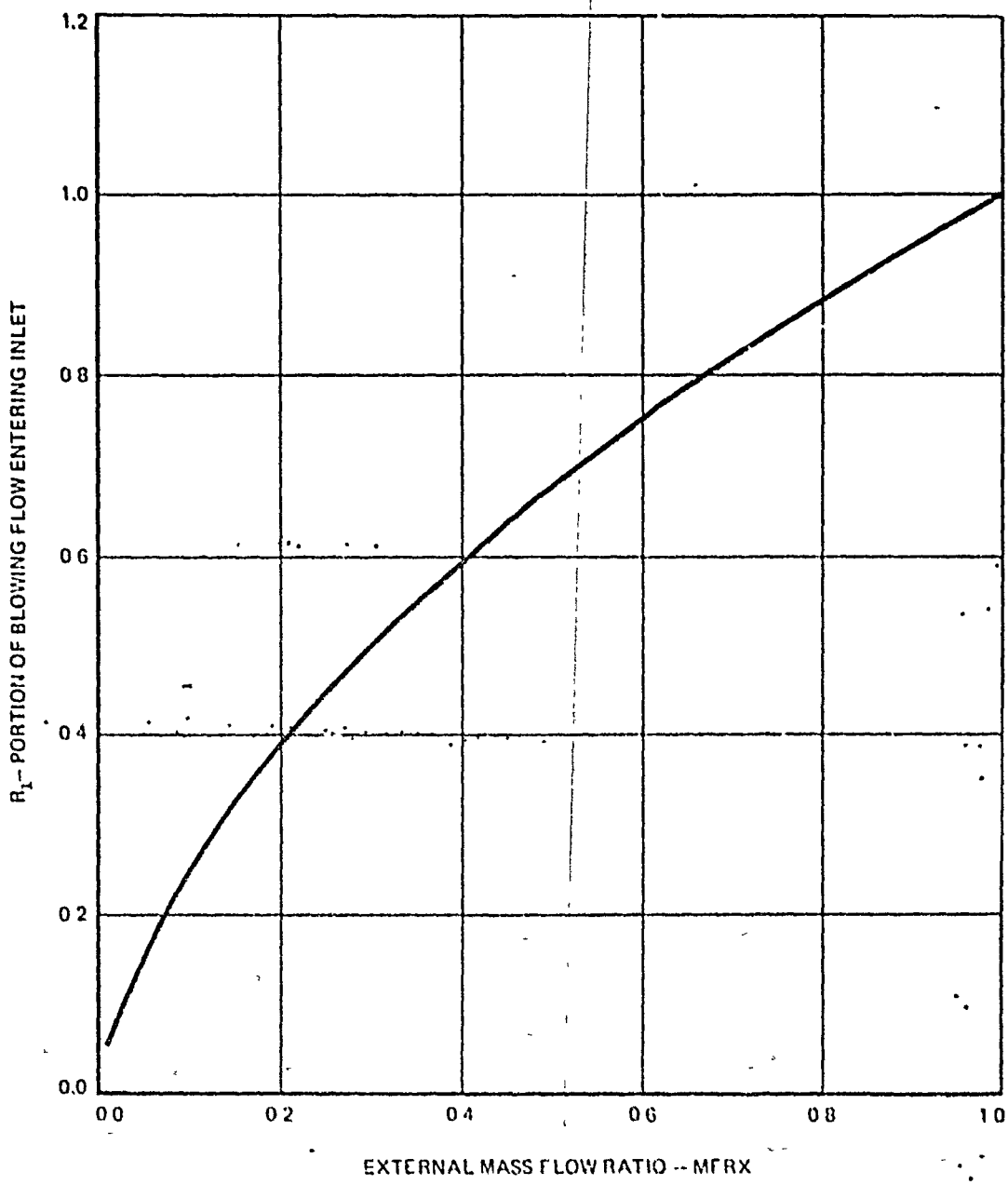

FIGURE B-2. EFFECT OF MASS FLOW RATIO ON INGESTION OF BLOWING AIR

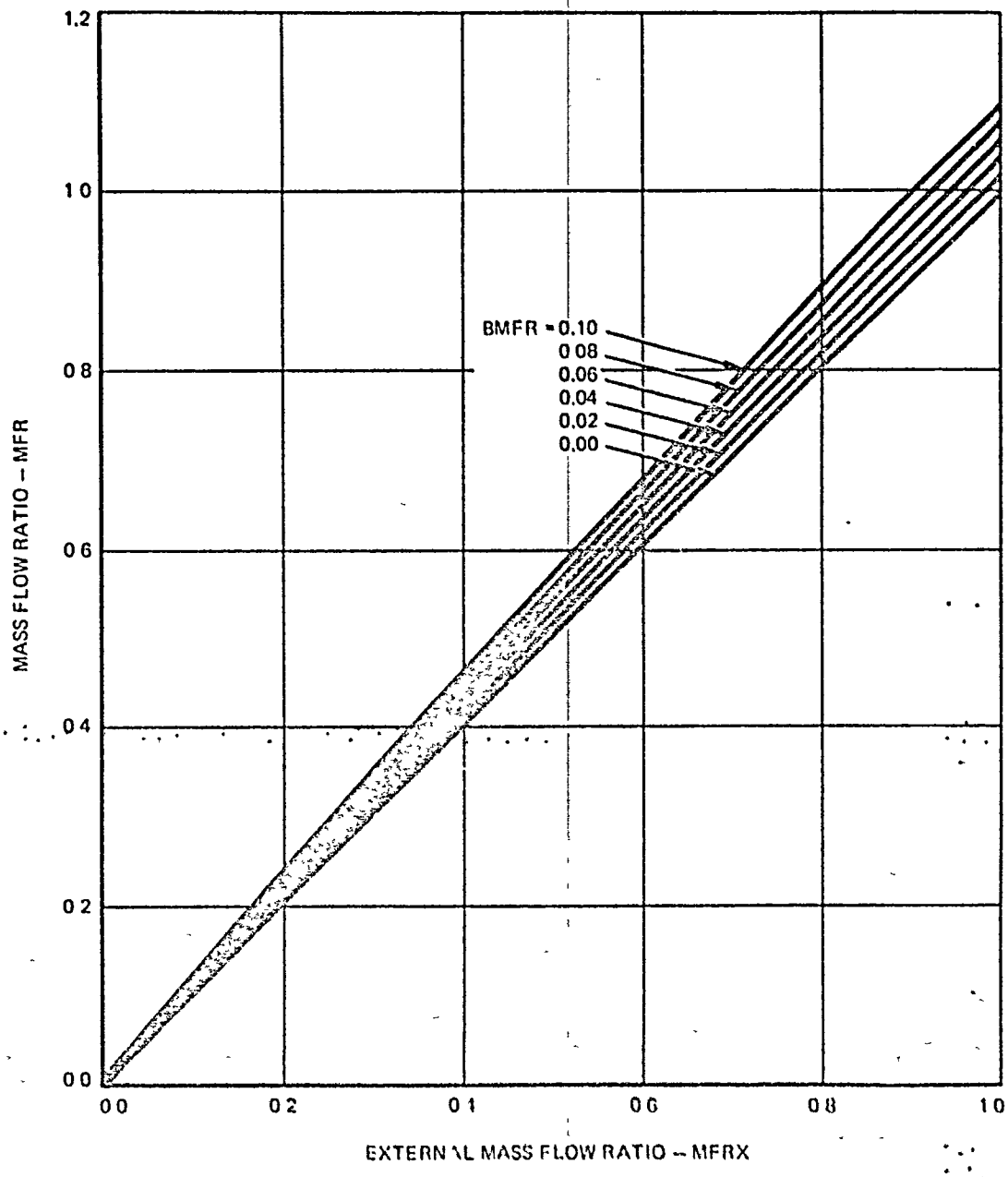

FIGURE B-3. EFFECT OF BLOWING FLOW ON MASS FLOW RATIO

APPENDIX C

BLOWING HOLE DISCHARGE COEFFICIENTS

Blowing hole discharge coefficients, the ratio of measured mass flow to ideal mass flow, calculated using perfect gas relations for air and based on blowing plenum temperature and pressure, are shown in figures C-1 to C-4. The data are presented for both corrected plenum temperature, see Appendix A, and measured plenum temperature. The corrected value of discharge coefficient is identified as KRATC and the uncorrected value as KRAT. A reduction in scatter between tunnel-on and static data is apparent due to the application of the plenum temperature correction.

The area used in computing the ideal flow was based on the nominal design area with corrections based on information contained in the builder's inspection report. Note that very small errors in hole size or spacing could produce significant changes in flow area.

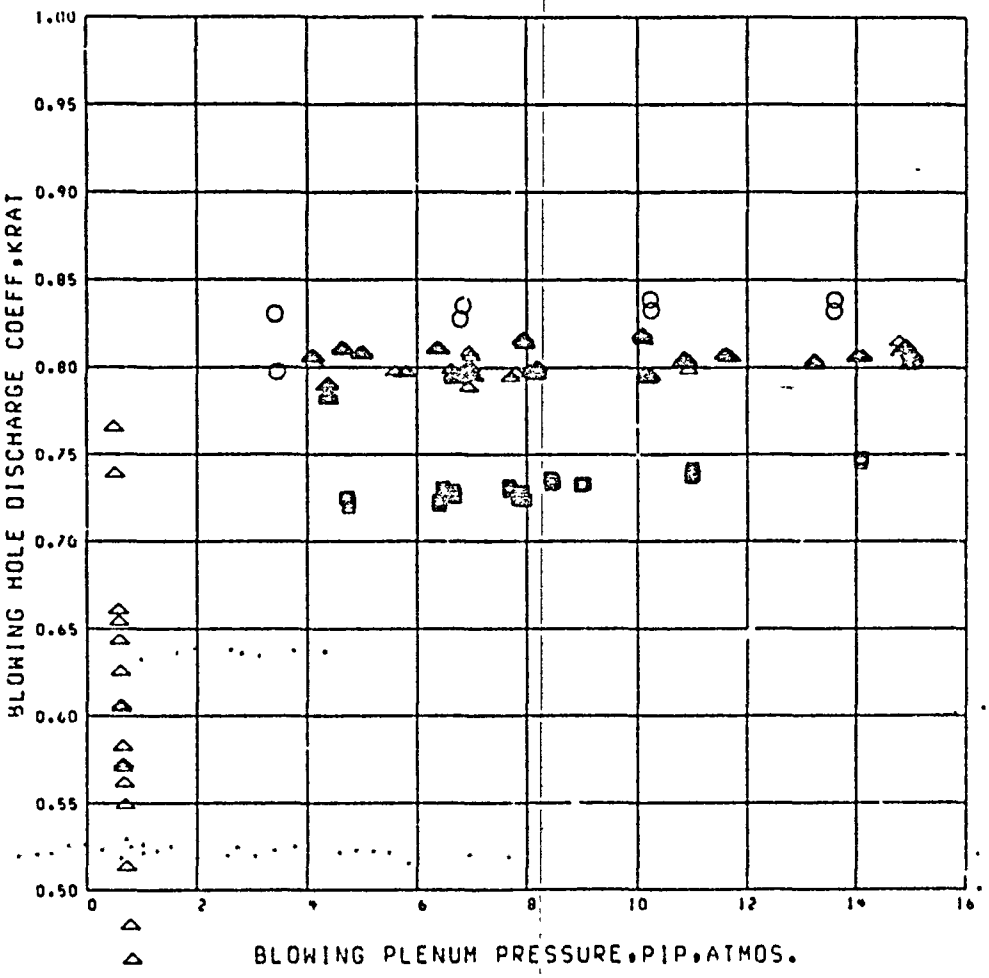

○ static -cold flow
△ tunnel-on -cold flow
□ tunnel-on -hot flow

FIGURE C-1. DISCHARGE COEFFICIENT FOR CONFIGURATION 21

ORIGINAL PAGE IS
OF POOR QUALITY

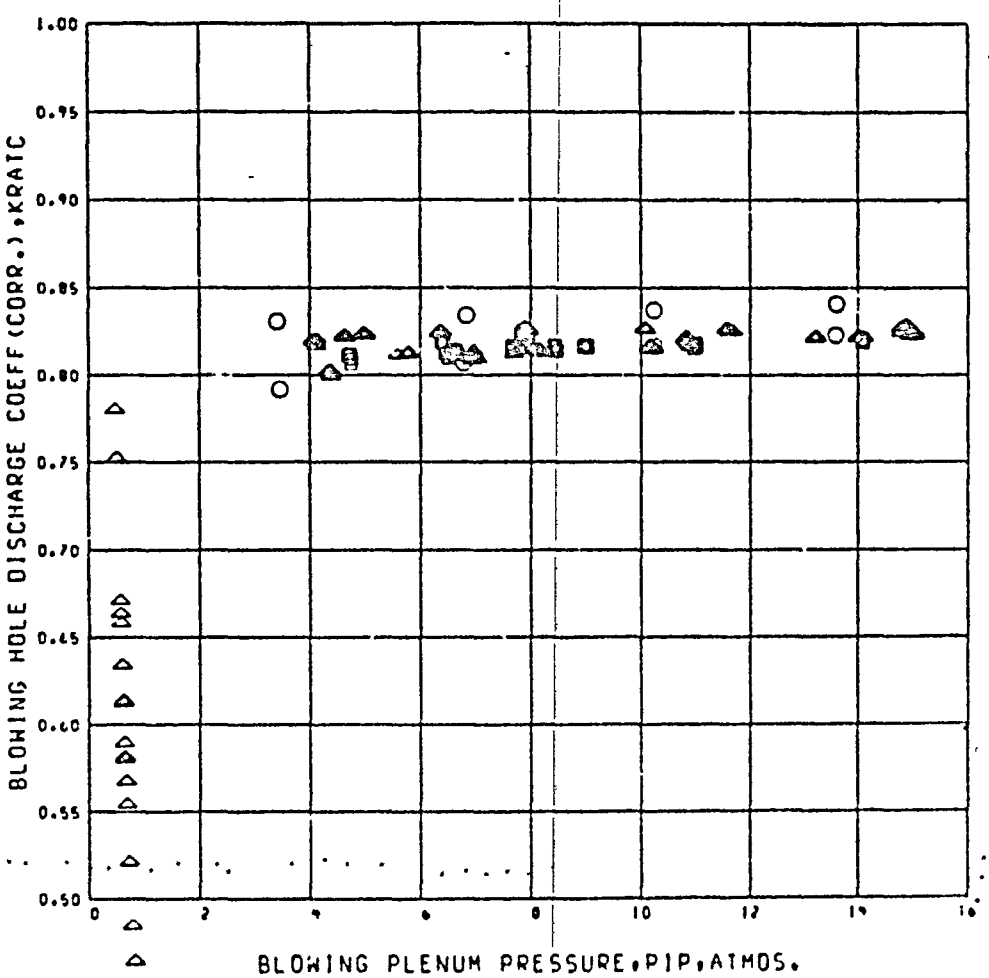

○ static -cold flow
△ tunnel-on -cold flow
□ tunnel-on -hot flow

FIGURE C-1. CONCLUDED

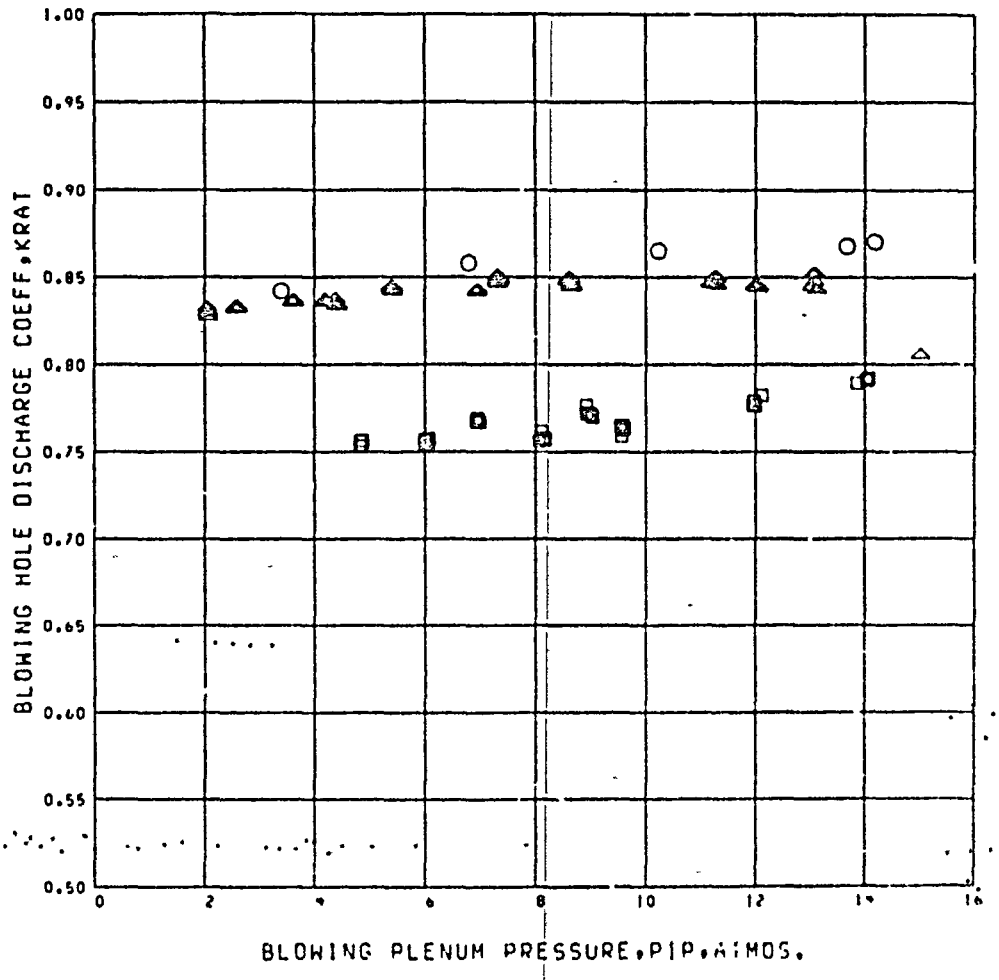

FIGURE C-2. DISCHARGE COEFFICIENT FOR CONFIGURATION 22

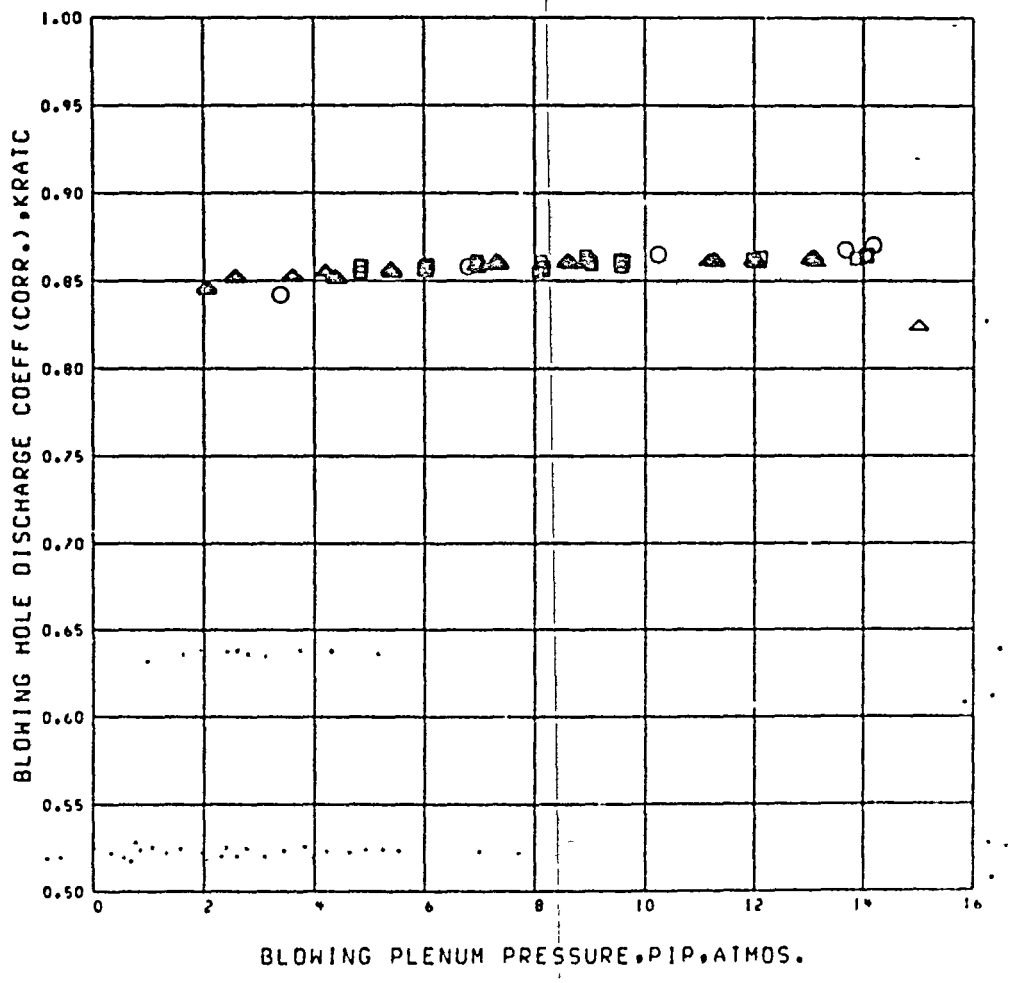

○ static -cold flow
△ tunnel-on -cold flow
□ tunnel-on -hot flow

FIGURE C-2. CONCLUDED

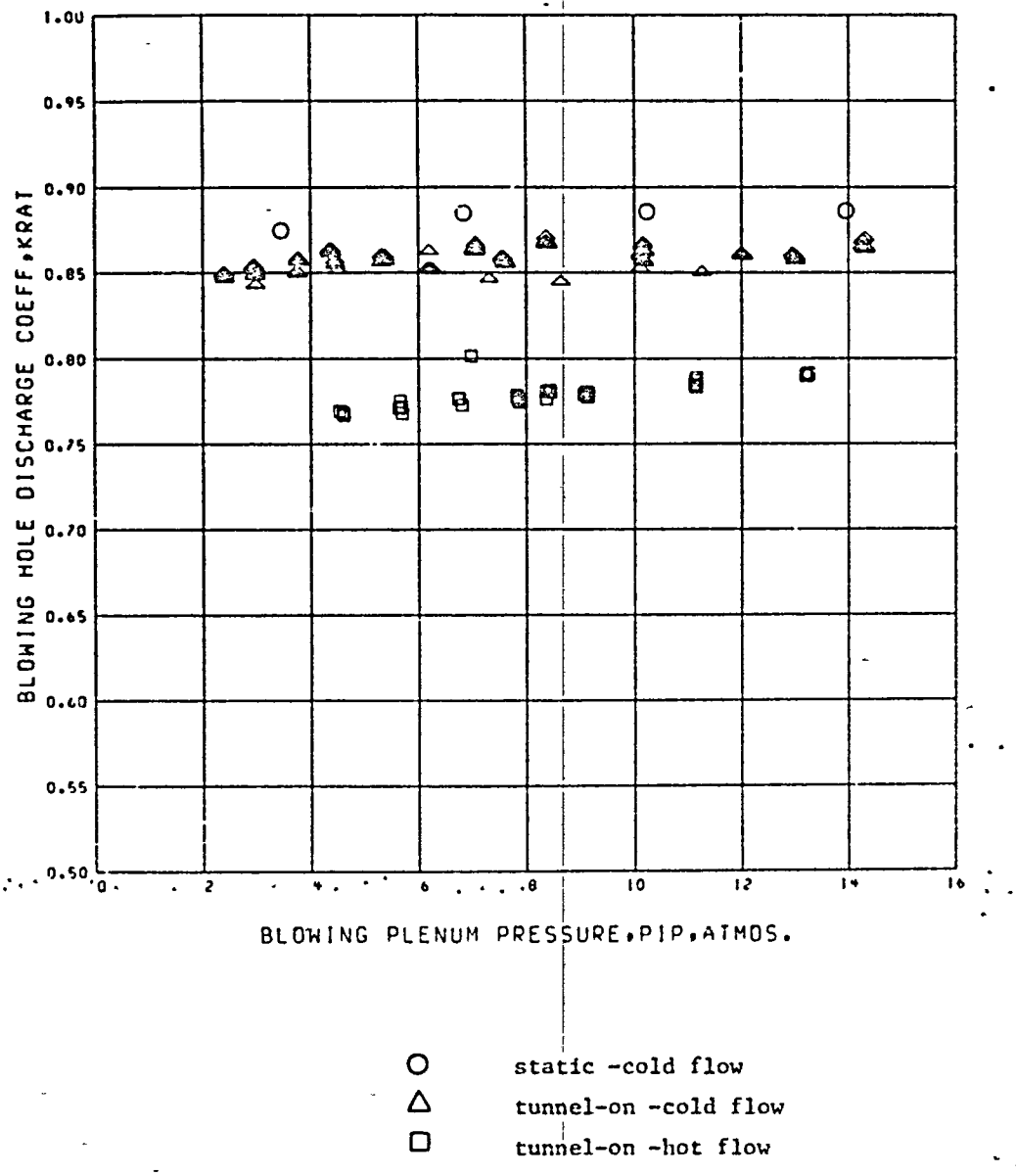

FIGURE C-3. DISCHARGE COEFFICIENT FOR CONFIGURATION 23

ORIGINAL PAGE IS
OF POOR QUALITY

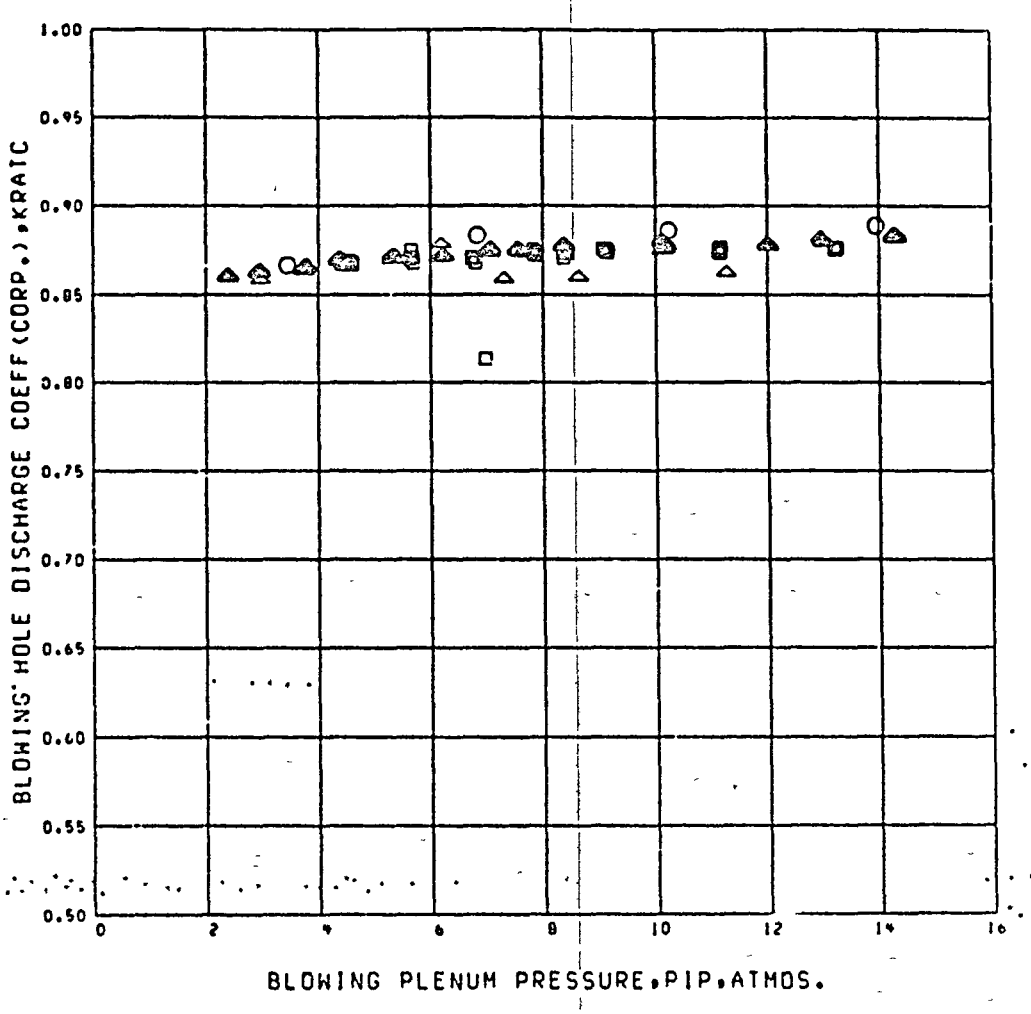

FIGURE C-3. CONCLUDED

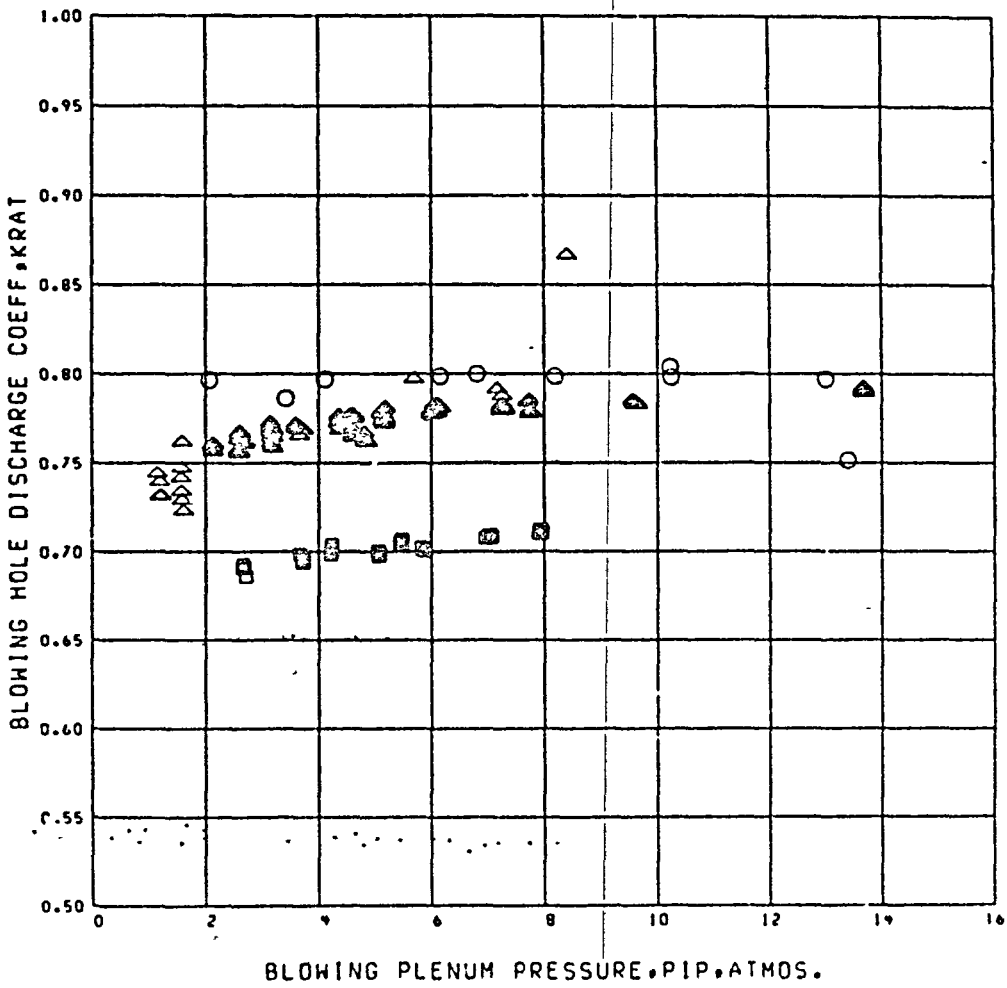

FIGURE C-4. DISCHARGE COEFFICIENT FOR CONFIGURATION 24

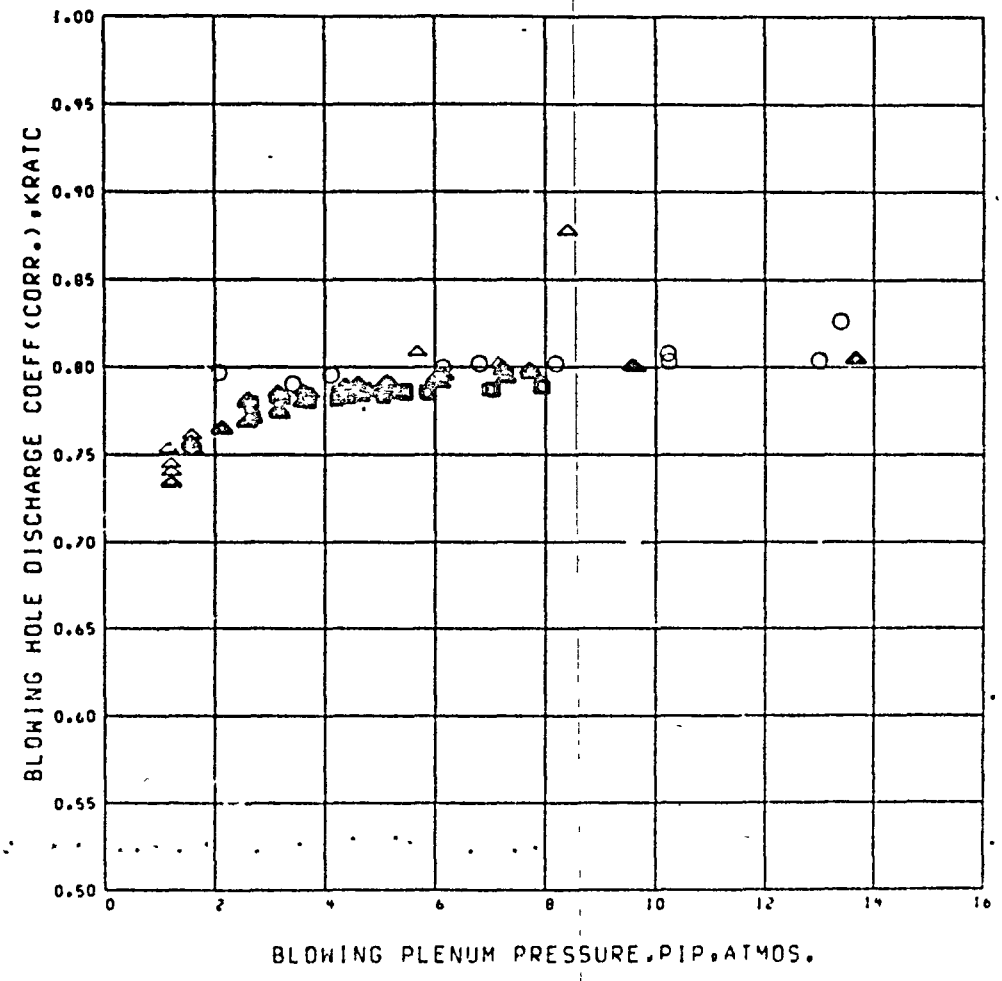

○ static -cold flow
△ tunnel-on -cold flow
□ tunnel-on -hot flow

FIGURE C-4. CONCLUDED

APPENDIX D

ANALYTICAL INVESTIGATION

An analytical investigation was carried out by W. F. Wong to further investigate the effect of blowing air temperature on control of the shock-boundary layer interaction that was reported in references 2 and 3. The computational tool utilized in this study was a version of the Kays-Patankar-Spaulding Boundary Layer Program, STAN 1, a later version of the program is documented in reference D-1. Although the results of this analysis are not directly comparable to the results of the test program because only the effect of the shock pressure rise was considered and the post-shock pre-cowl pressure rise was neglected, the analytical results clearly indicate that the absolute blowing coefficient CMMCD provides a better correlation for hot and cold blowing than the relative blowing coefficient, CMMCRD.

Several approximations to the interaction problem were made to accommodate input to the unmodified program. Because the pressure calculated by the program at the external boundary of the viscous flow region was linked to an input velocity gradient by an isentropic relation, it was not possible to simulate both the velocity gradient and pressure gradient, thus it was necessary to input a artificial velocity gradient to simulate the non-isentropic shock static pressure rise. The input velocity was varied from the pre-shock value to the post-shock artificial level using a hyperbolic tangent relationship over a distance of five boundary layer displacement thicknesses. A further approximation was introduced into the two-dimensional calculation due to the necessity of modifying

the initial profile at the blowing station because it was not possible to input a constant velocity blowing layer beneath a turbulent wall profile having zero velocity at the blowing layer. This would have required a midstream velocity discontinuity, introduced a midstream velocity null, and generated a slip velocity at the surface. The input velocity profile was modified to retain the maximum blowing velocity at the midpoint of the assumed slot blowing thickness while smoothing the velocity profile between this point and both the wall beneath and the oncoming ramp boundary layer profile above. Total momentum in the smoothed profile was maintained equal to that in the ideal profile.

The results of this analysis are summarized in figure 6-1. The computed skin friction is shown as a function of distance along the surface expressed in boundary layer height at the blowing station. The blowing slot height for this case was 0.13 boundary layer thicknesses. The temperature of the blowing jet was varied but a constant absolute blowing coefficient was maintained causing the relative blowing coefficient to vary. Although the initial skin friction varies due to differing jet exit velocities, the minimum coefficient does not vary with temperature indicating that separation and therefore inlet "buzz" characteristics are independent of blowing temperature.

References

1. Crawford, M. E. and Kays, W. M.: STAN5 A Program for Numerical Computation of Two-Dimensional Internal and External Boundary Layer Flow. NASA CR-2742, December 1976.

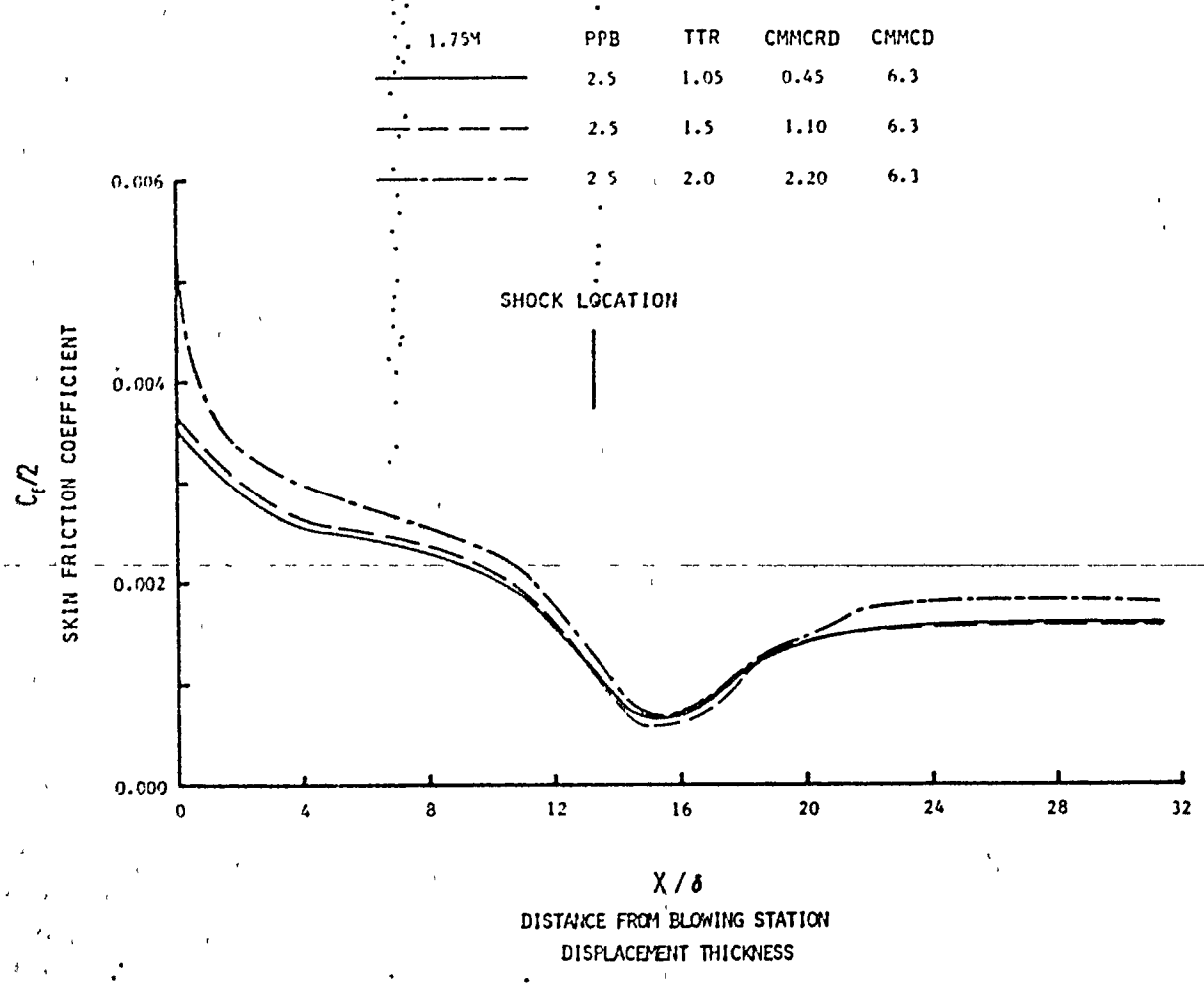

FIGURE D-1 . CALCULATED EFFECT OF TEMPERATURE ON BLOWING PERFORMANCE

APPENDIX E

SYMBOLS

A	Area
A_b	Blowing hole exit area, see figure 8
A_c	Inlet Capture area, 97.897 CM^2 (14.554 in^2)
A_{th}	Throat area, 89.654 CM^2 (13.896 in^2)
B	Blowing slot span
B_c	Inlet capture width
BMFR	Blowing mass flow ratio, $\dot{m}_b/\dot{m}_c$
C_f	Skin friction coefficient
CMMCD	Absolute blowing coefficient, see figure 2, $\dot{m}_b V_b/(2Q_1\theta_1 B)$
CMMCRD	Relative blowing coefficient, see figure 2, $\dot{m}_b(V_b-V_1)/(2Q_1\theta_1 B)$
D	Diameter
DIST	Compressor face distortion, (PTMAX-PTMIN)/PTAVG
H	Height of blowing step, pitot probe height above ramp
H_c	Inlet capture height
HO	Freestream total pressure
H_{th}	Inlet throat height, 7.62 cm (3.00 in)
KRAT	Blowing hole discharge coefficient, ratio of measured mass flow to ideal perfect gas flow
KRATC	Blowing hole discharge coefficient based on corrected plenum temperature
$\dot{m}$	Main duct mass flow
$\dot{m}_b$	Blowing mass flow

$\dot{m}_c$	Capture mass flow, $\rho_o V_o A_c$
M	Mach number
MIR	Mass flow ratio, $\dot{m}/\dot{m}_c$
MFRX	External mass flow ratio, $(\dot{m}-\dot{m}_b R_i)/\dot{m}_c$
MO	Freestream Mach number
MI	Ramp Mach number
P	Static pressure
PIP	Blowing plenum pressure
PO	Freestream static pressure
PPB	Blowing plenum pressure ratio, PIP/HO
PRMSA	Average rms pressure from compressor face dynamic transducers, normalized by freestream total pressure, area weighted
PT	Total pressure
PTAVG	Area weighted average total pressure from 40 probe compressor face array
PTMAX	Maximum pressure measured at 40 probe compressor face array
PTMIN	Minimum pressure measured at 40 probe compressor face array
PI	Ramp, static pressure (nominal)
QO	Freestream dynamic pressure, $\frac{\gamma}{2}$ (PO) $(MO)^2$
Q_I	Ramp dynamic pressure, $\frac{\gamma}{2}(PI)(MI)^2$
R	Radius, recovery factor, gas constant
R_I	Ratio of blowing flow ingested to total blowing flow
RCF	Compressor face radius, 13.716 cm (5.4 in)

REC	Compressor face total pressure recovery, PTAVG/HO
S	Blowing hole spanwise spacing, see figure 8
TAW	Adiabatic wall temperature
TO	Freestream static temperature
TS	Flowmeter temperature
TTB	Blowing plenum temperature
TTBC	Corrected blowing temperature
TTO	Freestream total temperature
TTR	Blowing temperature ratio, TTB/TTO
TTRC	Corrected blowing temperature ratio, TTBC /TTO
V_b	Blowing velocity, constant momentum expansion to P1, $\sqrt{2\gamma R(TTBC)/(\gamma+1)} + (A_b) \left[KRATC \left(\frac{2}{\gamma+1}\right)^{\frac{\gamma}{\gamma-1}} PIP-P1 \right] / \dot{m}_b$
V_o	Freestream velocity
V_1	Ramp velocity
X	Axial Distance
X_{hl}	Distance aft of highlight
Y	Lateral distance from model centerline, positive to the right
γ	Ratio of specific heats, 1.4
ρ_o	Freestream density
θ_1	Ramp boundary layer momentum thickness at blowing station

End of Document